REFERENCE ONLY

UNIVERSITY OF LONDON THESIS

Degree PhD Year 2005 Name of Author HENN, J.A.

Studies on the Human Adenosine A_1 Receptor.

Jonathan A. Hern

A thesis submitted in fulfilment of the requirements of the University of London for the degree of Doctor of Philosophy.

2005

National Institute for Medical Research. Mill Hill. London.

ProQuest LLC
789 East Eisenhower Parkway
P.O. Box 1346
Ann Arbor, MI 48106-1346

Abstract

The adenosine A_1 receptor (A_1R) is an important G protein-coupled receptor (GPCR) distributed widely throughout the human body and influences many bodily functions. The work presented here investigates in detail the complex heterogeneous nature of agonist binding to the human A_1R in order to explore receptor-receptor interactions that might be present in oligomeric receptor complexes.

The equilibrium and kinetic binding properties of two cell lines expressing the A_1R at different densities were characterised in detail. This characterisation was compared with that of a series of 47 cell lines expressing different levels of either the A_1R-GFP or A_1R-GFP-$G\alpha_i$ fusion proteins.

Equilibrium radioligand saturation and competition experiments provided evidence for a relationship between the fraction of high affinity agonist binding sites and the level of receptor expression. Cell lines expressing lower levels of the A_1R showed a greater relative ability to bind agonists with high affinity, and to promote formation of the activated agonist-receptor-G protein ternary complex.

The association of [^{3}H]agonist to the A_1R was biphasic and determined by two different molecular processes. The association rate constant of the fast component was entirely dependent on the concentration of [^{3}H]agonist, whereas dependence of the slow component on concentration was inconclusive.

The dissociation of a [^{3}H]inverse agonist from the A_1R was rapid, mono-exponential, complete, and insensitive to GTP. In contrast, the kinetics of [^{3}H]agonist dissociation were complex. Dissociation of [^{3}H]agonist from the A_1R-G protein complex was biphasic and dependent on the nature of ligand used to prevent [^{3}H]agonist rebinding. Greater [^{3}H]agonist dissociation was observed in the presence of competing agonist than competing inverse agonist, a novel finding called "agonist-induced agonist dissociation," and was dependent on agonist efficacy. The mechanism behind this is unknown, but appears to involve interactions between high affinity receptor-G protein complexes, possibly in the form of receptor oligomerisation. These interactions are absent at low expression levels and progressively increase with level of expression. Agonist-induced agonist dissociation was

observed even in the presence of a high concentration of GTP.

Separation of cell membrane fractions by their buoyant density clearly showed the A_1R-GFP and A_1R-GFP-Gα_i fusion proteins were not found in lower density caveolin-enriched "raft" fractions. These observations have implications for the nature of the immediate receptor environment and whether the A_1R and other components of the receptor signalling complex are actively concentrated in regions of the cell membrane.

The work presented here describes novel properties of agonist and antagonist binding at the human adenosine A_1 receptor and to A_1R-GFP and A_1R-GFP-Gα_i fusion proteins. The ligand dependence of the kinetics of agonist dissociation provides direct evidence for receptor-receptor interactions, such as receptor oligomerisation.

Abbreviations

A_1R	The adenosine A_1 receptor.
A_1HE	Stable CHO cell line expressing a *high level* of the human adenosine A_1 receptor.
A_1LE	Stable CHO cell line expressing a *low level* of the human adenosine A_1 receptor.
ADA	Adenosine deaminase.
B_{max}	Ligand binding capacity measured in a radioligand binding assay.
CHA	N^6-cyclohexyladenosine (a high efficacy adenosine A_1 receptor agonist, see Figure 2.1 on page 50).
CHO	Fibroblast-like cell line originating from Chinese hamster ovary.
DMSO	Dimethylsulfoxide.
DPCPX	8-cyclopentyl-1,3-dipropylxanthine (adenosine A_1 receptor antagonist / inverse agonist, see Figure 2.1 on page 50).
EDTA	Ethylenediaminetetraacetic acid.
FACS	Fluorescence activated cell sorting.
fr_H	The fraction of high affinity agonist binding in relation to the total orthosteric antagonist binding capacity of a GPCR.
$G\alpha_{12}$	G protein alpha subunit, a member of the G_{12} class of the heterotrimeric G protein family.
$G\alpha_{13}$	G protein alpha subunit, a member of the G_{12} class of the heterotrimeric G protein family.
$G\alpha_i$	G protein alpha subunit, of the class mediating inhibition of adenylate cyclase (G_i).

GDP Guanosine-5'-diphosphate.

GFP Green fluorescent protein.

GPCR G protein-coupled receptor.

GR161144 9-[3R,4S-dihydroxy-5-[4-methyl]-1,2,4-oxadiazol-2-yl]-tetrahydrofuran-2(R)-yl]-6-[[tetrahydropyran-4-yl]amino]-9H-purine.

GR162900 (2R,3R,4S,3R)-2-[6-[(1-methylethyl)amino]-9H-purin-9-yl]-5-[4H-5-methyl-1,2,4-triazol-2-yl]tetrahydrofuran-3,4-diol.

GR190178 (2R,3R,4S,5R)-2-{6-[(3-fluoro-4-hydroxyphenyl)amino]-2-methyl-9H-purin-9-yl-5-(methoxymethyl)tetrahydrofuran-3,4-diol.

GTP Guanosine-5'-triphosphate.

HBSS Hank's balanced salt solution.

Hepes N-[2-Hydroxyethyl]piperazine-N'-[2-ethanesulfonic acid]

IC_{50} Concentration of competing ligand at the mid-point of inhibition dose response curve.

kDa Kilodalton.

K_A Affinity constant.

K_D Dissociation constant. Concentration of ligand required to reach half-maximal occupancy of the receptor population. Reciprocal of the affinity, i.e. $\frac{1}{K_A}$.

K_H Affinity constant of the *high affinity* component of agonist binding.

K_L Affinity constant of the *low affinity* component of agonist binding.

k_{off} Dissociation rate constant.

log K_A Log affinity. Used in preference to K_A due to symmetry of confidence intervals (Christopoulos 1998).

M_1R The muscarinic M_1 receptor.

MOPS 3-[N-Morpholino]propanesulfonic acid.

N0840 N^6-cyclopentyl-9-methyladenine.

NSB Non-specific binding of radioligand, determined in the presence of an excess of unlabelled competing ligand.

PAGE	Polyacrylamide gel electrophoresis.
PIA	(-)-N^6-(2-Phenylisopropyl)-adenosine (see Figure 2.1 on page 50).
pK_A	Negative log affinity constant.
RT	Room temperature, thermostatically maintained at 22 $\pm$ 1°C.
SB	Specific binding. Total bound radioligand with non-specific binding subtracted.
SDS	Sodium dodecyl sulphate.
s.e.m.	Standard error of the mean.
$t\frac{1}{2}$	Half-life for dissociation, equals $\frac{\ln(2)}{k_{off}}$.

Publications and abstracts arising from this thesis.

Birdsall NJM, Browning C, Hern J & Lazareno S (2004) Allosteric regulation of binding and function at GPCRs. *Medicinal Chemistry Research* 13: 52-62.

Hern J, Browning C, Baig A & Birdsall NJM (2004) Effect of receptor expression level on agonist dissociation from adenosine A_1 receptor-GFP-G protein complexes. *Proceedings of the British Pharmacological Society at http://www.pA2online.org/Vol2Issue2abst005P.html*

Hern J & Birdsall NJM (2004) Effect of receptor expression level on equilibrium binding to A_1 receptor-GFP and A_1 receptor-GFP-G fusion proteins. *Proceedings of the British Pharmacological Society at http://www.pA2online.org/Vol2Issue2abst004P.html*

Baig A, Hern J & Birdsall NJM (2004) Modulation of the GDP/GTP binding selectivity of G-proteins interacting with the human adenosine A_1 receptor. *Proceedings of the British Pharmacological Society at http://www.pA2online.org/Vol2Issue2abst006P.html*

Birdsall NJM, Browning C, Hern J, Baig A & Lazareno S (2004) Novel pharmacological aspects of the allosteric regulation of binding and function at GPCRs. *Drugs of the Future* 29 Suppl. A: 7.

Birdsall NJM, Lazareno S, Browning C, Hern J & Baig A (2004) Allosteric enhancers and their actions on muscarinic receptors and other GPCRs. *Fundamental and Clinical Pharmacology* 18 Suppl. 1: 5-22.

Hern J, Browning C, Baig A & Birdsall NJM (2003) Agonist-induced agonist dissociation from human adenosine A_1 receptor-G protein complexes. *Proceedings of the British Pharmacological Society at http://www.pA2online.org/Vol1Issue4abst053P.html*

Contents

List of Figures

List of Tables

Chapter 1

Introduction.

1.1 The seven-transmembrane G protein-coupled receptor superfamily.

The seven-transmembrane G protein-coupled receptor (GPCR) superfamily is an enormous collection of diverse but related cell surface receptors (for review see Pierce *et al.* 2002). In humans 367 GPCRs have been estimated to be receptors for endogenous signals such as peptides, lipids, neurotransmitters and nucleotides (Vassilatis *et al.* 2003). GPCRs respond to a vast variety of stimuli, including hormones, odorants, neurotransmitters and light. Despite such diversity in receptor stimuli, all GPCRs have a hydrophobic core of seven membrane-spanning domains, an extracellular amino terminus, intracellular carboxy terminus, and typically signal through the activation of heterotrimeric G proteins (Heuss and Gerber 2000; Pierce *et al.* 2002). To date, a high resolution crystal structure has been elucidated for only one GPCR, the vertebrate retinal photoreceptor rhodopsin (Palczewski *et al.* 2000; Teller *et al.* 2001).

Three distinct families of GPCRs can be identified on the basis of sequence similarity, and Figure 1.1 on page 20 illustrates some of the significant structural characteristics of each family. Family 1 which includes receptors for light (rhodopsin) and odorants (the large olfactory receptor subgroup) is by far the largest of the three groups. Fredriksson and Schioth (2005) estimated 87% of human GPCRs are members of the same family as rhodopsin. The adenosine A_1 receptor belongs to GPCR family 1. Family 2 is much smaller than family 1 and its members couple mainly through G_S G proteins which stimulate the activity of adenylate cyclase. Family 2 includes receptors for the gastrointestinal peptide hormone family and corticotropin-releasing hormone. Family 3 is also much smaller than family 1 and all members have a large extracellular N-terminal domain involved

in ligand binding and receptor activation. Family 3 includes the metabotropic glutamate receptor family, the $GABA_B$ receptor and the calcium-sensing receptor.

GPCRs have very important roles in physiological and pathophysiological processes and are of intense interest within the pharmaceutical industry (Schoneberg *et al.* 2002). Not only do GPCRs represent the largest class of drug targets, but it has been estimated that up to half of all modern drugs may act by either enhancing (agonists) or inhibiting (antagonists) the activation of GPCRs (Chalmers and Behan 2002).

GPCRs emerged from the general study of receptors as their molecular basis of action became apparent in the 1960s and 1970s (see Limbird 1986 and Lefkowitz 2004 for historical perspectives). The development of new technologies, especially radioligand binding, in the 1970s established fundamental principles of GPCR behaviour such as heterogeneous agonist binding (Birdsall *et al.* 1978) and the ternary complex model which remain in use today (De Lean *et al.* 1980). The purification of GPCRs from tissues where they are found at high levels, followed by the cloning and sequencing of individual GPCRs showed that receptors with very different physiological roles and stimuli could be part of the same GPCR superfamily and share key structural characteristics such as the seven membrane-spanning helical core. Biochemical, cellular, pharmacological and molecular interrogation of the rapidly expanding repertoire of GPCRs has firmly established them as the largest and most diverse family of cell surface receptors transducing extracellular stimuli into intracellular effects. Today GPCRs remain the largest receptor superfamily and researchers in academia and industry have a wide array of tools with which to investigate GPCR activation, expression, localisation and function. The sequencing of the human genome (Lander *et al.* 2001) has opened yet more avenues in GPCR research and provides more candidates for characterisation by the experimental tools developed beforehand. The interest in G protein-coupled receptors has increased immensely over the last several decades and their significance appears set to grow further.

1.1.1 Heterotrimeric G proteins.

G protein-coupled receptors, as their name suggests, transduce extracellular signals into intracellular actions through their ability to couple to and activate heterotrimeric G proteins. Heterotrimeric G proteins, typically referred to as just "G proteins," are guanine-nucleotide regulatory protein complexes composed of α and $\beta\gamma$ subunits. They are responsible for the majority of signal transduction from activated GPCRs to downstream effectors such as adenylate cyclase and phospholipases. GPCR activation is associated with formation of the high affinity agonist–receptor–G protein ternary complex and exchange of GDP for GTP on the G protein α subunit. Heterotrimeric G proteins dissociate from the activated GPCR through separation into α-GTP and $\beta\gamma$ subunits

Figure 1.1 Structural characteristics of the three G protein-coupled receptor families.

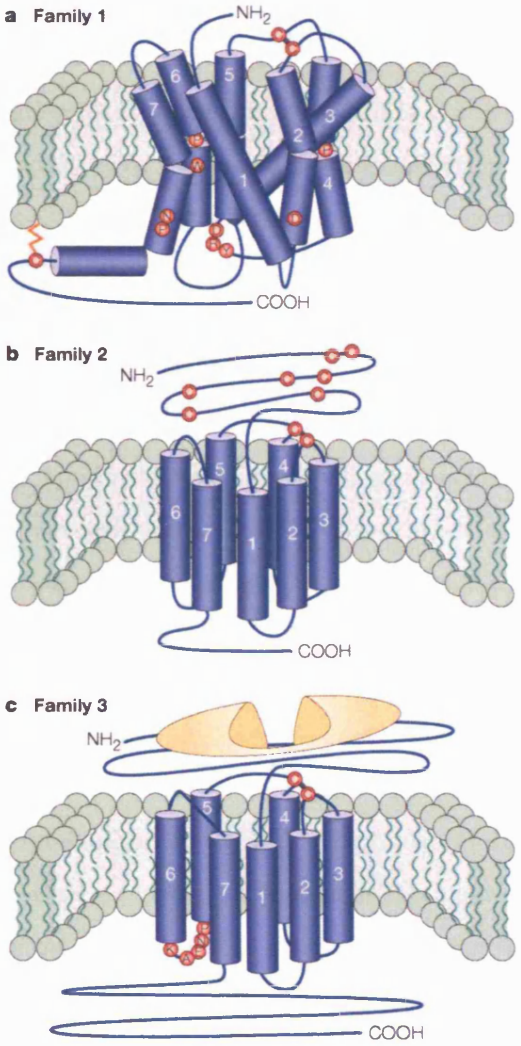

Figure 1.1: Three major families of G protein-coupled receptor can be distinguished by sequence and structural similarity. Rhodopsin, from family 1, is the only high resolution GPCR structure determined to date and the orientation of the seven transmembrane helices is illustrated for family 1, but not 2 or 3, above. Family 1 is by far the largest GPCR family and most family 1 GPCRs have a short N-terminus and a palmitoylated cysteine anchoring the C-terminus to the membrane. In general family 2 GPCRs have a longer N-terminus containing several disulphide bonds. Family 3 GPCRs have long C- and N-termini. The red circles indicate highly conserved amino acids within each family. Monomeric receptors are illustrated although some GPCRs have been shown to function as dimers or higher order oligomeric complexes. Figure is from Ellis 2004.

which can both have effects on cellular targets. Activation of G proteins is regulated by hydrolysis of GTP on the α-GTP subunit to GDP and subsequent re-association of α and $\beta\gamma$ subunits into the inactive Gα-GDP.$\beta\gamma$ heterotrimeric complex. The GTPase action of the Gα subunit is regulated by a family of proteins called regulators of G protein signalling (RGS) or GTPase activating proteins (GAP). The activation of G protein is illustrated in Figure 1.2 on the next page).

The binding of guanine nucleotides to G protein Gα subunits and their intrinsic GTPase activity have been exploited experimentally. The addition of high concentrations of GDP or GTP uncouples high affinity agonist-receptor-G protein complexes and all subsequent agonist binding is of low affinity. The mechanism by which guanine nucleotides uncouple receptor-G protein complexes is unknown, and not predicted by simple models such as the ternary complex model. A number of studies have investigated the effect of graded guanine nucleotide concentration on agonist binding at GPCRs. Some have reported reduced agonist affinity (Hoffman *et al.* 1982) while others have reported reduced availability of high affinity agonist binding sites (Lorenzen *et al.* 1993, Mahle et al. 1992). Previous work in the receptor group at NIMR provided evidence of both reduced affinity and high affinity agonist binding site availability at the adenosine A_1 receptor in the presence of GDP (Browning 2003).

At least twenty different G protein α subunits have been identified (for review see Albert and Robillard 2002). Common examples of G protein α subunits are $G\alpha_s$ (which stimulates the activation of adenylate cyclase, raising intracellular cAMP levels), $G\alpha_q$ (activates phospholipase C which generates the second messengers inositol trisphosphate and diacylglycerol), $G\alpha_i$ (inhibits the activation of adenylate cyclase, reducing the level of intracellular cAMP), and $G\alpha_t$(activated by rhodopsin in response to stimulation by light). The N-terminus of Gα subunits are attached to the cell membrane by means of N-myristoylation or palmitoylation (Wedegaertner *et al.* 1995).

Pertussis toxin (or islet activating protein) from species of bacteria of the *Bordetella* genus (of which *B. pertussis* is responsible for the majority of cases of the respiratory infection whooping cough) catalyses the ADP-ribosylation of $G\alpha_i$, $G\alpha_o$ and $G\alpha_t$ G protein subunits. This covalent modification prevents coupling of these G proteins to GPCRs. Pertussis toxin is of use when investigating the coupling of GPCRs to G proteins other than $G\alpha_{i,o,t}$ (Cordeaux *et al.* 2000) or the coupling of receptors to G proteins covalently attached their GPCR and mutated to be insensitive to pertussis toxin (Bevan *et al.* 1999).

Although fewer in number than G protein α subunits, there is still appreciable diversity in G protein β and γ subunits. Currently at least five β subunits and twelve γ subunits have been identified, most of which are distributed widely throughout the body. $\beta\gamma$ heterodimers can stimulate or inhibit the activity of a large number of downstream cellular effectors including Ca^{2+} and

Figure 1.2 The activation of G protein by agonist and GPCR.

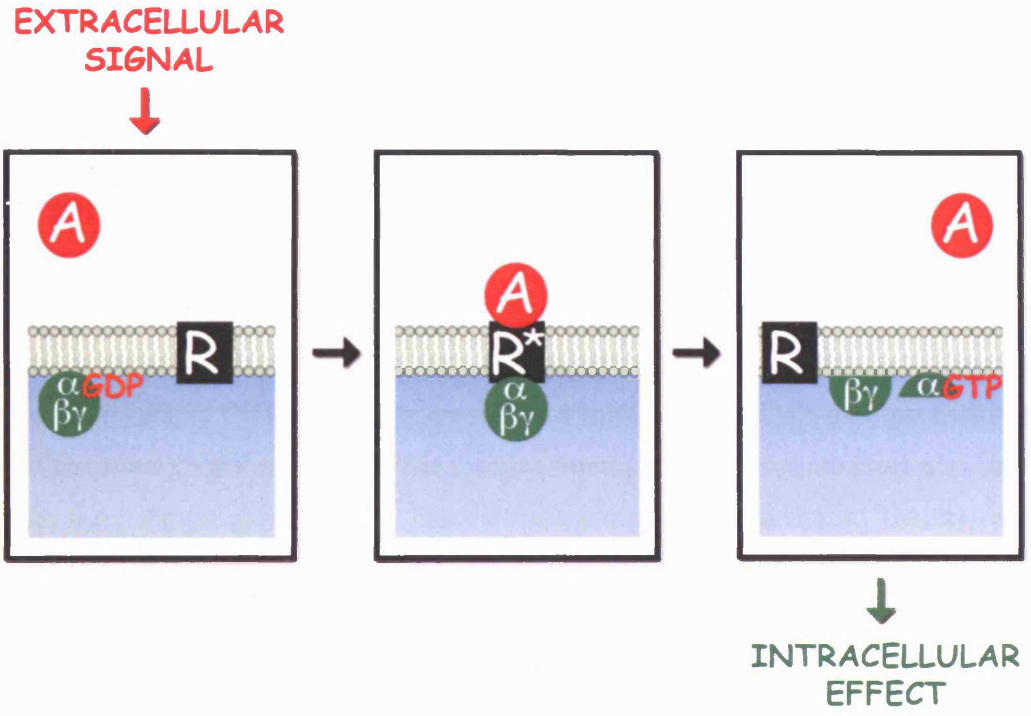

Figure 1.2: G protein coupled receptors transduce extracellular signals, such as an agonist, into intracellular effects largely through the control of G protein activation. The binding of extracellular agonist (**A**) to the GPCR (**R**) is associated with formation of the active agonist-receptor-G protein (**ARG**) ternary complex. Activation of the G protein by within the ternary complex drives the exchange of GDP for GTP on the Gα G protein subunit and dissociation of the G protein from the receptor and into separate α-GTP and $\beta\gamma$ subunits. Both the α-GTP and $\beta\gamma$ subunits can act on downstream intracellular targets. The GTPase activity of the Gα subunit hydrolyses the bound GTP to GDP and the inactive heterotrimeric Gα-GDP.$\beta\gamma$ complex reassembles.

K^- channels, kinases and subtypes of adenylate cyclase. They also appear to fulfil further roles by encouraging the binding of other proteins to the receptor, such as Gα subunits (Phillips *et al.* 1992) and receptor kinases (Inglese *et al.* 1995).

Heterotrimeric G proteins are not the only signal transduction systems that can be directly activated by GPCRs. Identification of an increasing number of proteins which interact directly with GPCRs has provided evidence for G protein-independent modulation of cellular effectors, such as ion channels (Heuss and Gerber 2000). The influence of other proteins on GPCR behaviour is discussed more in Section 1.3.

1.1.2 The molecular structure of G protein-coupled receptors.

To date, a high resolution crystal structure has been elucidated for only one GPCR, the vertebrate retinal photoreceptor rhodopsin (Palczewski *et al.* 2000; Teller *et al.* 2001). Rhodopsin is a Family 1 GPCR and a representation of its molecular structure, along with its G protein transducin, is illustrated in Figure 1.3 on the following page. Low resolution structural studies and sequence analysis strongly suggested the seven membrane-spanning helix conformation which was confirmed by the high resolution crystal structures. The inactive "resting-state" crystal structure also identified an eighth helix aligned parallel to the internal surface of the cell membrane. Despite considerable academic and industrial efforts to obtain high resolution crystal structures of other GPCRs, rhodopsin remains the only successful example. Rhodopsin is unique within GPCRs in that it can be purified in large quantities from retinae and can be locked in an inactive conformation by its covalently bound inverse agonist 11-*cis*-retinal. Exposure of the crystal to light destroyed the crystal (Palczewski *et al.* 2000) preventing the determination of the structure of the "active state" of the receptor. The main obstacle to the creation of suitable crystals appears to be difficulties in the purification of a homogeneous preparation of receptor in a uniform conformation.

The crystal structure of rhodopsin has been useful as a template from which to design structural models of other GPCRs. While the helical core of the rhodopsin crystal structure has been useful, to an extent, when modelling GPCRs who bind small molecules within that region, the crystal structure of rhodopsin is of limited use when modelling intra- and extra-cellular loops. Also, rhodopsin purified for the crystal structure was locked in its inactive conformation so there remains no high resolution structure of an activated GPCR. The high resolution structure of a GPCR in an activated conformation would provide information on the structural reorientation of the receptor and how this is influenced by ligands. GPCR homology models have been developed in order to investigate how ligands bind within the helical core of selected GPCRs. For example, a homology model of the muscarinic M_1 receptor based on the crystal structure of bovine rhodopsin has been

Figure 1.3 The molecular structure of rhodopsin and transducin.

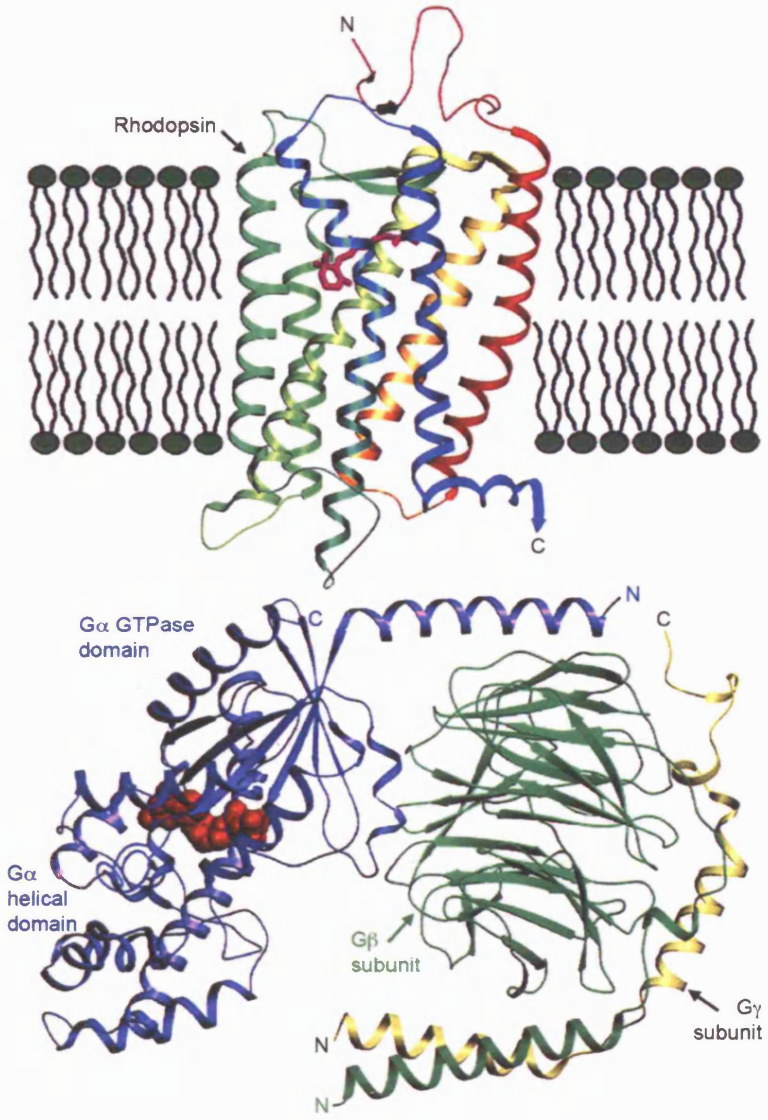

Figure 1.3: High resolution crystal structures have been determined for both rhodopsin and its G protein transducin and are shown to scale (taken from Hamm 2001). The structures were determined separately and the molecular position of the interaction between receptor and G protein is not known. The characteristic seven transmembrane domains of rhodopsin are clearly illustrated and coloured red to blue from the N-terminus to the C-terminus. The last 32 residues of the C-terminus are not shown. Retinal, rhodopsin's covalently-attached light-activated ligand, is indicated in purple buried within the transmembrane helices. The three G protein subunits (α, β and γ) are illustrated in different colours with a space-filled guanine nucleotide (in red) within the Gα GTPase domain.

used to interpret the results of mutagenesis studies on the receptor's transmembrane core, providing insights into the binding of different ligands and their control of receptor activation (Hulme *et al.* 2003). GPCR homology models are also of use in the pharmaceutical industry and have been applied to virtual screening of large chemical databases in order to identify promising compounds for experimental screening (Bissantz *et al.* 2003).

Many studies have created chimeric receptors from domains of different GPCRs in order to investigate the importance of structural motifs or features of receptor behaviour. The creation of functional chimeric GPCRs has shown that structural motifs from receptors with little sequence similarity can be fused to form a functional receptor (for review see Yin *et al.* 2004). Chimeric GPCRs have been used to investigate mechanisms of receptor oligomerisation (in the case of the $GABA_B$ receptor) and the consequences of receptor activation at GPCRs where the nature of endogenous ligands was uncertain (in the case of the Frizzled-2/β_2-adrenoceptor fusion construct; Liu *et al.* 1999).

1.1.3 The oligomerisation of G protein-coupled receptors.

Traditionally the activation of GPCRs has been considered as the functional response to formation of the high affinity agonist–receptor–G protein ternary complex. Models of receptor activation describing the binding of ligands and G protein to a GPCR have been reasonably successful in describing many aspects of GPCR behaviour. Reconstitution experiments creating functional GPCR systems in synthetic phospholipid vesicles using purified receptor and G protein have supported such simple models. However it is now apparent the formation of oligomeric receptor complexes is crucial to the function of a number of GPCRs. While there has been phenomenal interest in the study of GPCR oligomerisation over the last several years, driven in part by the emergence of new technologies, no consistent mechanism of receptor oligomerisation has appeared which is applicable to all GPCRs. As with many aspects of GPCR behaviour, the nature and mechanisms of receptor oligomerisation are entirely dependent on the receptor itself.

For many studies of GPCR oligomerisation it is difficult to determine whether the receptor is present as a dimeric complex or a higher-order oligomer. Therefore in this document the description "oligomer" is used to describe in general the association of GPCRs into complexes of two or more receptors.

An interesting account of GPCR oligomerisation reported functional rescue by co-expression of two different non-functional angiotensin receptors, demonstrating for the first time in peptide hormone receptors intermolecular complementation mediated by receptor oligomerisation (Monnot *et al.* 1996). However, arguably the "classic" example of GPCR oligomerisation is that of

the metabotropic γ-aminobutyric acid ($GABA_B$) receptor which functions as an obligate hetero-dimer. When the $GABA_B$ receptor was first cloned, which was subsequently determined to be the $GABA_{B1}$ receptor, the cloned receptor did not behave in the same manner as endogenous GABA receptors characterised in brain preparations (Kaupmann *et al.* 1997, White *et al.* 1998). Several groups later cloned a second $GABA_B$ receptor ($GABA_{B2}$) which when co-expressed with the originally-cloned receptor, $GABA_{B1}$, restored the pharmacology observed in brain membrane preparations (Jones *et al.* 1998, Kaupmann *et al.* 1998, Kuner *et al.* 1999, White *et al.* 1998, Ng *et al.* 1999, Martin *et al.* 1999). The $GABA_{B1}$ receptor when expressed alone is retained within the cell and does not reach the cell surface. The $GABA_{B2}$ receptor however is expressed at the cell surface, but does not bind GABA. $GABA_{B2}$ acts as a chaperone to mask the C-terminal ER retention signal of $GABA_{B1}$and the hetero-dimer is expressed on the cell surface and can bind GABA and activate G protein. $GABA_{B2}$ may fulfil more than just a chaperone role, and it appears to be important in the activation of G protein following agonist binding at $GABA_{B1}$. While oligomerisation of the $GABA_B$ receptor has been studied in great detail, there remain few examples of GPCRs which function similarly as obligate hetero-dimers.

A considerable number of reports have employed co-immunoprecipitation techniques to propose the existence of GPCR oligomerisation. Co-expression of differentially epitope tagged β_2-adrenergic receptors has provided evidence of β_2 receptor dimerisation (Hebert *et al.* 1996). Similar studies have proposed dimerisation of other GPCRs in both recombinant and native systems, including the δ opioid (Cvejic and Devi 1997), muscarinic M_3 receptor (Zeng and Wess 1999), dopamine D_2 receptor (Guo *et al.* 2003) and histamine H_2 receptor (Fukushima et al. 1997). Several reports have extended co-immunoprecipitation to investigate hetero-oligomerisation of GPCRs. Different opioid receptor subtypes have been proposed to form hetero-dimers (for example Jordan and Devi 1999, George *et al.* 2000) and hetero-dimerisation has been reported between the adenosine A_1 and dopamine D_1 receptors (Gines *et al.* 2000) and angiotensin and bradykinin receptors (AbdAlla et al. 2000). However, co-immunoprecipitation techniques leave concerns regarding the specificity and relevance of reported associations, and while they provide an interesting starting-point to the characterisation of GPCR oligomerisation other techniques have provided greater insights into the details and consequences of oligomerisation.

Other popular approaches used to investigate the oligomerisation of GPCRs involve the use of techniques employing resonance energy transfer. These techniques have the advantage that they can be performed in living cells, although typically cells recombinantly expressing the receptors of interest. Of considerable interest would be reports using resonance energy transfer techniques to show the presence or absence of oligomeric endogenously expressed receptors. In some cases

the energy donor and acceptor are covalently fused to the C-termini of the receptors of interest and this has provided further evidence of β_2 receptor oligomerisation (Angers *et al.* 2000), for example. Other reports have used energy donor and acceptors coupled to antibodies targeted at specific epitopes on the N-termini of GPCRs. This has the advantage of directly labelling receptor expressed only at the cell surface and has, for example, been employed to show oligomerisation of the δ opioid receptor (McVey *et al.* 2001).

Reconstitution experiments using recombinantly expressed and purified human leukotriene B_4 receptor (BLT1) showed low and high affinity agonist binding (Baneres *et al.* 2003, Baneres and Parello 2003). BLT1 is a member of the rhodopsin-like GPCR family 1. Detergent-solubilised BLT1 was observed to associate with heterotrimeric G protein, and activate $G\alpha_i$, following agonist binding at the receptor. The stoichiometry of this complex was identified as only one G protein for every two receptors and two agonist molecules ($[\text{agonist–receptor}]_2 : [\text{G protein}]_1$), providing strong evidence of a role for receptor dimerisation in receptor activation.

GPCRs can form oligomeric complexes through interaction of their C- or N-termini or transmembrane domains depending on the receptor subtype. The C-terminus has been identified as an important determinant for hetero-oligomerisation of $GABA_{B1}$ and $GABA_{B2}$ receptors (Kuner *et al.* 1999) and homo-oligomerisation of the δ opioid receptor (Cvejic and Devi 1997). A synthetic peptide of transmembrane helix 6 from the β_2 adrenergic receptor decreased dimerisation, suggesting the transmembrane helix forms an important interface between receptors (Hebert *et al.* 1996). Transmembrane helices 6 and 7 have been proposed to be important in dopamine D_2 receptor dimerisation (Ng *et al.* 1996). Family 3 GPCRs have been shown to use their large N-terminal domains to form receptor-receptor interactions important in oligomerisation. X-ray crystallography of the N-terminal domain of the metabotropic glutamate receptor observed a disulphide-linked homodimer (Kunishima *et al.* 2000). Also, the conformation of this dimeric extracellular domain was observed to change with the binding of glutamate.

1.2 The regulation of G protein-coupled receptor activation.

The most simple models developed to describe the activation of G protein by a GPCR incorporate three components; ligand, receptor and G protein. The physiological relevance of such models are supported by experiments reconstituting functional GPCR systems into phospholipid vesicles using purified receptor and purified G protein (for example using the β-adrenergic receptor see Cerione *et al.* 1984). The binding of ligands which increase the overall level of receptor activation (agonists) increases formation of the high affinity agonist–receptor–G protein "ternary complex."

Other ligands which bind at the agonist binding site regardless of the presence of G protein are generally termed antagonists and inhibit the binding of agonist in a concentration-dependent manner. Many GPCRs exhibit a level of receptor activation in the absence of agonist stimulation, termed "constitutive activity." Antagonists can be divided into two further classes of ligand. Neutral antagonists competitively inhibit the binding of agonist but do not directly alter the activation state of the receptor. Inverse agonists reduce the overall level of receptor activation by favourably binding to GPCRs not coupled to G protein, and as a result reduce constitutive activity. Figure 1.4 on page 29 illustrates the change in level of receptor activation following the binding of agonist, neutral antagonist or inverse agonist.

1.2.1 Efficacy.

The affinity of a ligand for its molecular target, such as a GPCR, is the product of thermodynamic mechanisms and can be described simply and quantitatively. The extent to which a ligand can alter the level of receptor activation is a molecular property known as "efficacy." There are many ways in which to measure the efficacy of a ligand, from immediate effects on ternary complex formation to downstream effects such as regulation of gene expression. Aspects of agonist binding at equilibrium, such as the ratio of high and low affinity constants of agonist binding ($\frac{K_H}{K_L}$), are thought to reflect agonist efficacy. Figure 1.4 represents the efficacy of a ligand as a shift along the y-axis, the level of receptor activation. Efficacy is very much more difficult than affinity to model quantitatively, although models have been proposed which link efficacy and affinity (Kenakin 2002).

1.2.2 Models of G protein-coupled receptor binding and function.

The ternary complex model (Figure 1.5A on page 30) has been used widely to describe and analyse the binding of ligands to G protein-coupled receptors (De Lean *et al.* 1980). It can be used, to an extent, to describe many aspects of GPCR behaviour including heterogeneous agonist binding (agonist binding of more than one affinity), receptor-G protein interactions, the actions of inverse agonists, allosterism and guanine nucleotide sensitivity. Figure 1.6 on page 32 shows other commonly used models of GPCR systems including those based on the ternary complex model. Below are simple descriptions for each of the models shown.

Simple binding and activation (Figure 1.6a) The most simple model of GPCR activation consists of two steps and two receptor conformations or activation states. Agonist (A) binds to the inactive receptor (R_i) to form the non-signalling complex AR_i which undergoes a change

Figure 1.4 The regulation of G protein-coupled receptor activation.

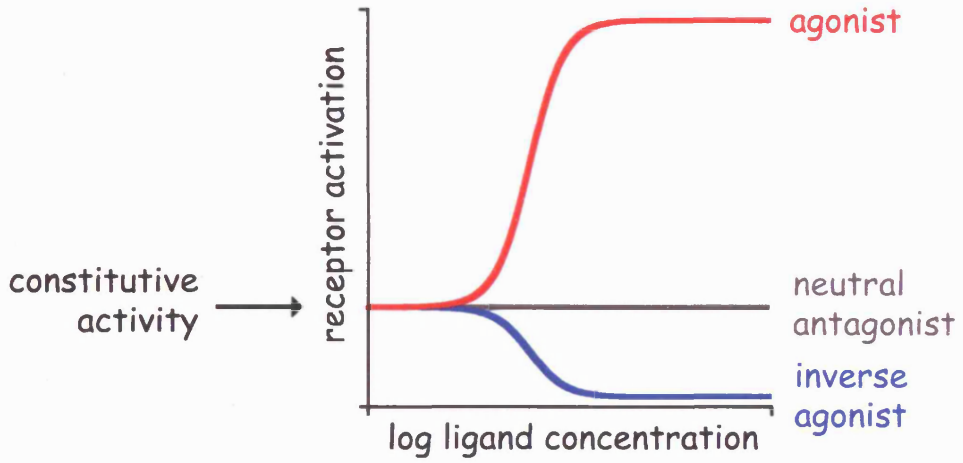

Figure 1.4: The measurement of efficacy at the level of receptor activation divides ligands into three classes. Many GPCRs show a level of activation in the absence of ligand, a behaviour termed "constitutive activity." Ligands which bind to the receptor can increase (**agonists**) or reduce (**inverse agonists**) the level of receptor activation, or indeed do neither (neutral antagonists). Ligands can show intermediate levels of efficacy, such as partial agonists which at similar levels of receptor occupancy show a reduced capacity to increase receptor activation. Neutral antagonists and inverse agonists are often generally termed "antagonists" due to their similar ability to competitively inhibit the binding and action of agonists however there are important therapeutic differences in the action of neutral antagonists and inverse agonists. The above figure illustrates three hypothetical ligands of different efficacy but equal affinity for the receptor.

Figure 1.5 The ternary complex model of G protein-coupled receptor activation.

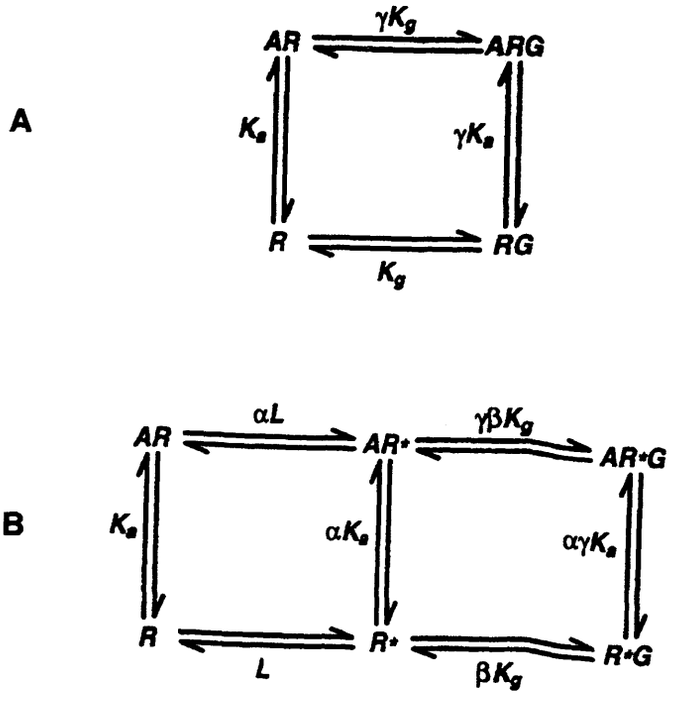

Figure 1.5: **(A)** The ternary complex model of G protein-coupled receptor activation, first proposed in 1980 (De Lean *et al.* 1980). Agonist A binds to GPCR R with affinity constant K_a. G protein G binds independently to R with affinity constant K_g. Binding of A and G to R is reciprocal, and expressed as cooperativity factor γ. Agonists (γ>1) promote formation of the active ARG ternary complex and receptor activation. Inverse agonists (γ<1) inhibit formation of the ternary complex, and neutral antagonists (γ=1) do not directly effect receptor activation but compete against agonist and inverse agonist binding. **(B)** The extended ternary complex model combines a two-state receptor model with the ternary complex model where only the activated receptor (R^*) can couple to the G protein. Isomerisation constant L represents the transition of receptor between inactive (R) and active (R^*) states. Three cooperativity factors α, β and γ are required in this more complex model. Figure is from Christopoulos and Kenakin 2002.

in conformation, driven by the efficacy of the agonist, to the active receptor complex AR_a which signals the cellular effect.

Simple ternary complex model (Figure 1.6b) The inclusion of G protein (G) in models adds at least one further step (or two according to Figure 1.5). Formation of the high affinity agonist–receptor–G protein (AR_aG) ternary complex is the active complex from which the response is effected. This model imposes a linear sequence of steps for the activation of G protein and does not permit the formation of receptor–G protein complexes in the absence of agonist. Formation of RG is however described by the ternary complex model in Figure 1.5A but no activity to the complex is formally implicit.

Extended ternary complex model (Figures 1.5B & 1.6c) The extended ternary complex model includes receptor activation in the absence of agonist by formation of the R_aG complex. Potentially this is a means of incorporating constitutive activity into the scheme where the receptor can activate G protein in the absence of agonist by formation of R_aG.

Cubic ternary complex model (Figure 1.6d) Thermodynamics require the potential existence of complexes consisting of G protein and inactive receptor (R_iG). Observations of ligand-specific coupling of G protein and GPCRs (such as for the β_2-adrenoceptor (Wenzel-Seifert and Seifert 2000) provide evidence of a sophisticated system for which more complete, but complex, models may be more appropriate.

Models derived from the ternary complex model have been adapted and developed in order to describe other aspects of GPCR function such as allosterism and multiple receptor conformations (Birdsall and Lazareno 2005, Christopoulos and Kenakin 2002, Kenakin 2003). Work within the receptor group here at NIMR has developed a quaternary complex model which is compatible with the actions of the allosteric enhancer PD 81,723 which enhances agonist binding at the human adenosine A_1 receptor (Browning 2003, Browning *et al.* 2000c).

1.2.3 Drug discovery for G protein-coupled receptors.

The importance of GPCRs as targets for therapeutic intervention was reinforced when the total number of GPCR genes in the human body was estimated by sequencing of the human genome (Lander *et al.* 2001). Of the several hundred GPCR genes identified, approximately half have been proposed as receptors for endogenous signals such as peptides, lipids, neurotransmitters and nucleotides (Vassilatis *et al.* 2003) providing potential targets for therapeutic intervention. Not only do GPCRs represent a huge family of drug targets, but it has been estimated that up to

Figure 1.6 Other models of G protein-coupled receptor activation.

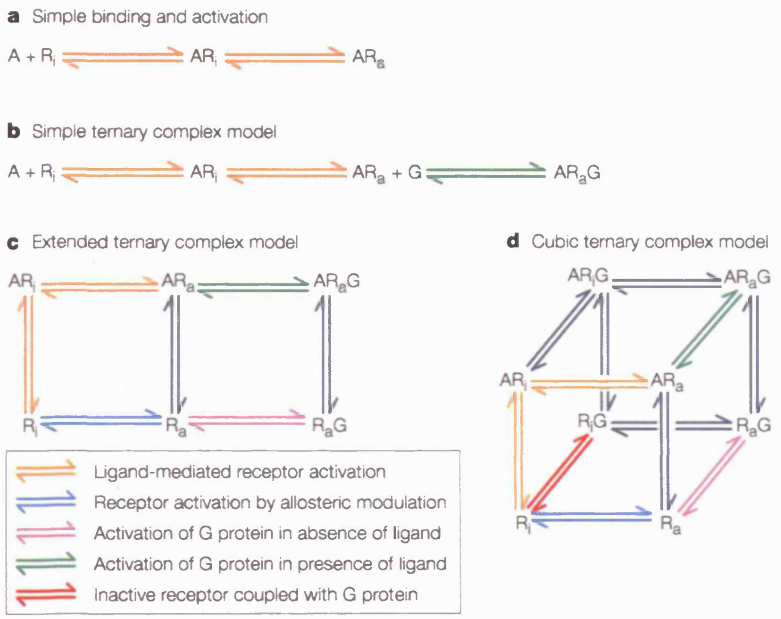

Figure 1.6: Many models have been developed in attempts to quantitatively model the activation of G protein-coupled receptors. Above are shown four of the more simple, but more commonly employed, models which are described in more detail starting on page 28. The Figure was taken from Ellis 2004, which was adapted from that in Kenakin 2002. Figure 1.5 on page 30 describes the ternary complex model where formation of receptor–G protein complexes is allowed in the absence of agonist.

half of all modern drugs may act by either enhancing (agonists) or inhibiting (antagonists) the activation of GPCRs (Chalmers and Behan 2002). Currently GPCRs exhibit a general suitability for therapeutic intervention, so-called "drugability," but there remains great untapped potential not only in the search for interesting compounds but also in the identification of novel mechanisms in the control of receptor activation.

A problem in the search for molecules specific for individual GPCRs is the existence of related receptor subtypes. For example there are five subtypes of muscarinic acetylcholine receptor in which the structure of the acetylcholine binding site (the orthosteric binding site) is highly conserved between subtypes (Hulme *et al.* 1990). Other sites on muscarinic receptors have been characterised at which the binding of other ligands can influence binding at the orthosteric binding site. Such allosteric ligands offer the potential to develop agents with "absolute subtype specificity" where the allosteric ligand can bind to one receptor subtype with positive or negative cooperativity and to the other receptor subtypes with neutral cooperativity. One example of this is the enhancement of acetylcholine binding (by means of positive cooperativity) at the muscarinic M_4 receptor by thiochrome which shows neutral cooperatively at the other receptor subtypes (Lazareno *et al.* 2004), and selectively low affinity at the muscarinic M_5 receptor (see Birdsall and Lazareno 2005 for review on allosterism at muscarinic receptors). Cinacalcet, which acts at the calcium-sensing G protein-coupled receptor, is the first allosteric ligand to successfully make it to market and is used to lower parathyroid hormone levels in patients with uncontrolled secondary hyperparathyroidism (Block *et al.* 2004).

Proteins which modulate GPCR activity, including other GPCRs, are also targets for therapeutic intervention. The regulator of G protein signalling (RGS)-family of proteins can have a direct influence on the behaviour of GPCRs and provide novel opportunities for drug discovery (Neubig and Siderovski 2002). The consideration of the composition of the receptor signalling complex in the development of models and assays presents tremendous complexities. Receptor homo- and hetero-oligomerisation along with other protein-protein interactions may in the future provide even more opportunities for drug discovery.

1.3 GPCR-mediated signal transduction across the cell membrane.

G protein-coupled receptors transduce physiological signals across the cell membrane. That is they convert an extracellular signal (such as the presence of a neurotransmitter) into an intracellular signal (such as a change in the activity of an enzyme like adenylate cyclase). While more simple (but

experimentally testable) models of receptor activation may incorporate only the ligand, receptor and G protein, it is clear there are many other factors which influence the behaviour of GPCRs. A vast number of proteins have been proposed to influence GPCR function, of which only a small proportion are described below. GPCRs may be selectively localised into or out of a heterogeneous network of domains on the cell surface where differences in protein composition may alter GPCR function.

The cell membrane is not a homogeneous bilayer assembly of lipids, but is composed of heterogeneous regions of varying lipid and protein composition. Traditionally different membrane domains have been defined by their method of isolation or visualisation rather than by functional characterisation. The most well described cell membrane domains are those that can be easily isolated by their low buoyant density. Typically isolation is achieved by disruption of cell membranes by treatment with detergents, such as Triton X-100, followed by ultracentrifugation and subsequent flotation in a sucrose gradient to separate membrane fractions by their buoyant density. These detergent-resistant membranes are generally characterised by enriched levels of more saturated lipids such as cholesterol, glycolipids and sphingolipids and are often termed "lipid rafts." Lipid rafts do not appear to have a consistent protein or lipid composition and the lipid profile isolated can depend on the detergent used and the method of isolation (for review see Pike 2004). The heterogeneity of isolation methodology and raft composition has led to a degree of confusion regarding the classification and terminology of rafts, caveolae, cholesterol-enriched membranes, glycosphingolipid-enriched membranes, detergent-insoluble glycosphingolipid-enriched membranes, low-density membranes, Triton X-100 insoluble floating fraction, liquid-ordered domains and detergent-resistant membranes. In this document the terms "raft" and "lipid raft" are used in a broad general manner to describe all membrane regions characterised by lighter buoyant density and enrichment for caveolin and more saturated lipids.

The functional roles of lipid rafts are manifest by their ability to include and exclude proteins from regions of the cell membrane. They appear to function as more structured membrane domains floating within more fluid, but less structured, regions of the cell membrane. Experiments investigating the diffusional behaviour of the μ opioid receptor observed two distinct modes of diffusion. A short-term rapid diffusion, postulated to be diffusion confined within lipid raft domains, and a long-term slow diffusion of the raft itself through the cell membrane (Daumas *et al.* 2003). GPCRs, including the adenosine A_1 receptor (Escriche *et al.* 2003, Gines *et al.* 2001), and Gα subunits, such as Gα_i (Elenko *et al.* 2003), have been shown to accumulate in lipid rafts following agonist treatment and receptor activation. The selective localisation in rafts of other proteins which influence the activity of the A_1 receptor and Gα_i may mediate mechanisms con-

trolling receptor signalling such as desensitisation and internalisation. In contrast, the thyrotropin receptor (a GPCR) when expressed in CHO cells is predominantly present in lipid rafts regardless of the presence of thyrotropin (Latif *et al.* 2003). In *Drosophila* the affinity of glutamate at the metabotropic glutamate receptor has been observed to depend on whether the receptor is associated within lipid raft domains (Eroglu *et al.* 2003). As appears to be the case for many aspects of GPCR behaviour, the nature of association in or out of lipid rafts and the interaction with additional proteins are dependent on the nature of the receptor and not consistent for all GPCRs.

An important element of the control of GPCR activation is the ability to reduce the level of signalling from activated receptors. The reduction in the level of receptor signalling, even in the continued presence of agonist stimulation, is generally termed "densensitisation." Desensitisation can operate directly at the level of the receptor and is usually accomplished by phosphorylation of the C terminus or third intracellular loop of the GPCR (Ferguson 2001). GPCRs can be phosphorylated by second-messenger kinases such as protein kinase A (PKA) and protein kinase C (PKC), or by G protein-coupled receptor kinases (GRKs; for review see Pitcher *et al.* 1998). Desensitisation may also occur at the level of G proteins where the large RGS family of GTPase activating proteins accelerate the rate of GTP hydrolysis (De Vries *et al.* 2000). Slower processes which result in receptor desensitisation include degradation of the receptor itself in lysosomes, and down-regulation of receptor transcription and translation.

Desensitisation by PKA- and PKC-mediated GPCR phosphorylation can be more "heterologous" than desensitisation mediated by GRKs which can be more agonist-specific. Phosphorylation of the β_2 adrenergic receptor by PKA has been shown to encourage coupling of the receptor to $G\alpha_i$ rather than $G\alpha_s$, changing the downstream response to β_2 adrenergic receptor activation (Zamah *et al.* 2002). Seven members of the GRK family have been identified, of which GRKs 1, 4 and 7 have more specific actions while the other GRKs regulate a larger number of receptors (Ferguson 2001). GRK2, also known as β-adrenergic receptor kinase, is believed to be distributed widely and phosphorylate a large number of GPCRs (Krupnick & Benovic 1998).

Signalling by activated GPCRs is further reduced by the internalisation of receptors following continued agonist stimulation. The β-arrestin family of proteins are involved in many GPCR signalling functions and have important effects on GPCR behaviour (for review see Pierce and Lefkowitz 2001). As well as serving other physiological roles, β-arrestins are important in the internalisation of the β_2 adrenergic receptor (Ferguson *et al.* 1995) and the muscarinic M_2 receptor (Krupnick & Benovic 1998). Arrestins bind to phosphorylated receptors and can form high affinity agonist–receptor–arrestin complexes (Gurevich *et al.* 1997) which may be responsible for a small proportion of high affinity agonist binding which can be insensitive to guanine nucleotides.

While some GPCRs exist as constitutive oligomers, such as the $GABA_B$ receptor, other GPCRs may not form constitutive oligomers but may at times form transient or ligand-dependent oligomeric complexes. Formation of temporary oligomeric complexes requires individual GPCRs to locate other available receptors before they can form an oligomer. Increasing the local concentration of the receptor, by clustering into or out of membrane domains such as rafts, may favour this. Selective localisation of membrane proteins may not only control the concentration and type of GPCR available, in the case of hetero-oligomerisation, but also the availability of other proteins important in GPCR function and signalling such as G proteins or RGS proteins.

1.4 Adenosine and adenosine receptors.

Extracellular nucleotides and nucleosides such as adenosine and ATP are involved in many different physiological functions. The actions of extracellular ATP and other nucleotides (such as ADP, UTP and UDP) are mediated through the the P2 class of purinoceptors which include the P2X family of ligand-gated ion channels, and the P2Y family of G protein-coupled receptors (for reviews see Vial *et al.* 2004 and von Kugelgen and Wetter 2000, for P2X and P2Y receptors respectively). The P1 class of purinoceptors consists of four G protein-coupled receptors for adenosine (A_1, A_{2A}, A_{2B}, and A_3) each encoded by distinct genes (Fredholm *et al.* 2000). Conservation of the four adenosine receptors in several different species is visualised in Figure 1.7 on page 44. In general, functional classification separates adenosine receptors into their ability to inhibit (in the case of A_1 and A_3) and stimulate ($A_{2A}$and A_{2B}) adenylate cyclase activity following receptor activation. Activation of A_1 and A_3 adenosine receptors can also increase levels of intracellular Ca^{2+} and alter the electrical potential across the cell membrane. Figure 1.8 on page 45 illustrates these immediate downstream consequences of adenosine receptor activation.

Adenosine receptors are expressed throughout the human body, and adenosine A_1 receptors are found in abundance in the cardiovascular system and the brain (for reviews see Fredholm *et al.* 1999, Fredholm *et al.* 2000). Levels of adenosine can increase as a result of oxidative stress and ischemia where inhibition of synaptic excitability is believed to be the consequence of adenosine A_1 receptor activation. Depression of rat hippocampal slice excitability induced by in vitro ischaemia can be reduced by the selective adenosine A_1 receptor antagonist DPCPX at concentrations of 50-500 nM (Latini *et al.* 1999). Adenosine is generally perceived as a molecule with inhibitory actions within the brain and heart, with roles including overall reduction in wakefulness and protective inhibition of metabolism following ischaemic injury.

Adenosine is produced within the cell and in extracellular regions and can be transported across

the cell membrane passively and actively. In both environments adenosine can be synthesised by dephosphorylation of AMP and metabolised by adenosine deaminase into inosine. Adenosine deaminase has been described in extracellular plasma, membrane-bound and in the cytosol (for review see Deussen 2000). The molecular structure of adenosine is illustrated in Figure 2.1 along with other adenosine A_1 receptor agonists and antagonists.

Reported values of the concentration of endogenous adenosine in rat brain range from 30 nM to 30 μM (Cohen *et al.* 1996a, Porkka-Heiskanen *et al.* 1997 and Latini *et al.* 1999). It is difficult to measure the concentration of endogenous adenosine in the immediate receptor environment, although electrophysiological studies observed a maximum local adenosine concentration of 30 μM during an ischaemic episode (Latini *et al.* 1999). Estimation of the affinity of adenosine for adenosine receptors is difficult due to the presence of endogenous adenosine in purified cell membranes. Typically adenosine deaminase is applied to remove endogenous adenosine, but adenosine deaminase itself has to be removed if adenosine is then used as a ligand. Reported affinities of adenosine are 7 x10^7 and 1.3 x10^5 M^{-1} for the high and low affinity states of the adenosine A_1 receptor (Cohen *et al.* 1996a). Local μM adenosine concentrations would therefore largely occupy and activate the high affinity adenosine A_1 receptor state.

Few adenosine receptor ligands have made it into clinical use, other than adenosine itself which can be used in the treatment of excessively rapid beating of the heart. However adenosine receptors are molecular targets of the most widely consumed recreational drug in the world, namely caffeine (for review see Fredholm *et al.* 1999). Adenosine receptors remain attractive targets for drug development due to their widespread distribution throughout the human body and roles in many important physiological and pathophysiological processes. Interest is only increased by the current lack of clinically effective ligands targeting adenosine receptors and the general interest in G protein-coupled receptors as therapeutic targets.

1.4.1 The adenosine A_1 receptor.

The adenosine A_1 receptor is expressed throughout the brain and is found both pre- and post-synaptically. Activation of the adenosine A_1 receptor inhibits neurons pre-synaptically by reducing the release of neurotransmitter and post-synaptically by modulating ionic currents. The inhibitory actions of adenosine A_1 receptor activation are transduced largely through activation of G_i and G_o G proteins mediating activation of phospholipases, inhibition of Ca^{2+} conductance and activation of K^+ conductance as illustrated in Figure 1.8 (for review see Haas and Selbach 2000). Immunoprecipitation of Gα subunits from stable CHO cell lines expressing the human adenosine A_1 receptor

showed the receptor to activate $G\alpha_i$, $G\alpha_{q/11}$ and $G\alpha_s$ G protein α subunits (Cordeaux *et al.* 2000). Also, differential activation of $G\alpha_i$, $G\alpha_q$ and $G\alpha_s$ may be dependent on the nature of the agonist bound at the receptor (Cordeaux *et al.* 2004).

The adenosine A_1 receptor is of use experimentally for a number of reasons. Agonists of varying efficacy and radiolabelled agonists and antagonists are readily available for the A_1 receptor. The A_1 receptor shows a large separation between high and low agonist affinity binding constants ("GTP shift") which provides a large window with which to investigate the effect of agonist efficacy or guanine nucleotides on the nature of agonist binding. The A_1 receptor also possesses an allosteric binding site, permitting its use as a model of allosterism at GPCRs. Finally, the A_1 receptor is a member of the large rhodopsin family of GPCRs and shares similarities with a large number of other GPCRs. All these features, along with physiological interest in the A_1 receptor itself, make the adenosine A_1 receptor an interesting and useful model GPCR.

The adenosine A_1 receptor was originally cloned using a canine thyroid library (Libert *et al.* 1992) and soon afterwards the receptor was cloned from other mammals including humans. Both the human and mouse adenosine A_1 receptors are translated from two exons separated by a single intron while transcription is controlled by two upstream promoters. The human adenosine A_1 receptor amino acid sequence is 326 residues long and shows a characteristic seven transmembrane domain composition with a very short N-terminus (10 residues) and an eighth helix in the plane of the membrane at the C-terminus (Figure 1.9 on page 46). The sequence contains a potentially palmitoylated cysteine residue in the C-terminus (residue 309), a potential N-linked glycosylation site in the second extracellular loop (residue 159) and a putative disulphide bond between cysteine residues in the first (residue 80) and second (residue 169) extracellular loops. The estimated molecular weight of the human adenosine A_1 receptor from its sequence is 36.5 kDa.

Targeted disruption of the adenosine A_1 receptor in mice removed the effect of adenosine on excitatory neurotransmission and altered the neuronal response to hypoxia (Johansson *et al.* 2001). In normal conditions mice with targeted disruption of the adenosine A_1 receptor showed normal viability (up to an age of 50 days) supporting a largely protective role for the receptor.

Adenosine A_1 receptor activation is modulated by both desensitisation and internalisation. Wetherington and Lambert (2002) showed desensitisation of the adenosine A_1 receptor following chronic agonist application in rat hippocampal neurons. Also, pre-synaptic A_1 receptors desensitised much more slowly than post-synaptic A_1 receptors, suggesting the mechanism of desensitisation differ in different membrane domains of the same cell. Although adenosine A_1 and A_3 receptors share generally inhibitory actions, the A_3 receptor is desensitised much more quickly (Palmer *et al.* 1996, Trincavelli *et al.* 2002). Different sensitivity of the A_1 and A_3 receptors

to phosphorylation may contribute to the differences observed in desensitisation (Ferguson *et al.* 2000). Other studies have shown ligand-induced internalisation of the A_1 receptor involving accumulation of the receptor into low-density gradient fractions characterised by increased levels of caveolin (Escriche *et al.* 2003, Gines *et al.* 2001). Recently, Briddon *et al.* (2004) observed the intracellular accumulation of the fluorescently labelled A_1 receptor antagonist XAC-BY630 following longer periods of incubation, which was blocked to an extent by the unlabelled antagonist DPCPX. This suggests that XAC-BY630 can accumulate within the cell by a receptor-dependent mechanism such as receptor internalisation. It is unclear whether relocation of the adenosine A_1 receptor into less-dense caveolin-enriched membrane domains is important in receptor function or whether it is primarily a mechanism of ligand-induced receptor internalisation.

There is little evidence of adenosine A_1 receptor homo-oligomerisation. A provisional immunoblotting and immunoprecipitation report described the isolation of adenosine A_1 receptor dimers from pig brain cortex, however these complexes were not stable in the presence of agonist or antagonist (Ciruela *et al.* 1995). The adenosine A_1 receptor has been reported to form hetero-oligomeric complexes with other GPCRs including the dopamine D_1 receptor (Gines *et al.* 2000), metabotropic glutamate type 1α receptor (Ciruela *et al.* 2001), and the $P2Y_1$ receptor (Yoshioka *et al.* 2001). Of the three reports listed, the report by Ciruela *et al.* is of the most interest because they characterised the interaction of mGlu1α and A_1 receptors in detail in transiently transfected cells and also provided evidence for co-localisation of the two receptors *in vivo*, in rat cerebellar neurons.

Adenosine A_1 receptor agonists.

Adenosine, the endogenous agonist for adenosine receptors is of limited use as an experimental tool because adenosine deaminase is routinely added in order to remove adenosine found in membrane preparations. Consequently estimation of the affinity of adenosine is difficult, as discussed above. Adenosine provides the structural core for other adenosine receptor agonists and partial agonists. Figure 1.10 on page 47 shows the three positions on adenosine which are modified in the creation of the agonists and partial agonists illustrated in Figure 2.1 on page 50. CHA and PIA are two adenosine receptor agonists which have been modified at the N^6-position of the adenosine purine. Both CHA and PIA are resistant to adenosine deaminase and exhibit affinities for the human adenosine A_1 receptor up to 10-fold greater than adenosine (Cohen *et al.* 1996a). Affinities of CHA and PIA for the human adenosine A_1 receptor are determined in Chapter 4. All adenosine receptors, but especially the adenosine A_1 receptor, show strong stereoselectivity for *R*-PIA rather than the *S*-isomer (Klotz *et al.* 1998). The human adenosine A_1 receptor shows almost 40-fold

higher affinity for *R*-PIA than *S*-PIA (the structure of *R*-PIA is shown in Figure 2.1 with the chiral centre illustrated at the top of the molecule). The lower efficacy adenosine A_1 receptor agonists GR162900 and GR161144 (Figure 2.1 and Sheehan *et al.* 2000) are modified at both the N^6-position of the purine ring and the 5'-position of the ribose. GR190178 is modified at all three positions described in Figure 1.10 and shows the highest efficacy out of the three GR compounds, although still considerably less than CHA or PIA. The affinity and measure of efficacy of the three GR compounds for the human adenosine A_1 receptor are characterised in Chapter 4.

Adenosine A_1 receptor antagonists and inverse agonists.

The adenosine receptor antagonist caffeine is arguably "the most widely consumed behaviourally active substance in the world" (Fredholm *et al.* 1999). Caffeine is a member of the methylxanthine class of compounds which includes other adenosine receptor antagonists such as theophylline and DPCPX (illustrated in Figure 2.1). In humans DPCPX is selective for the adenosine A_1 receptor over the other adenosine receptor subtypes by at least 30-fold, and in the rat by over 1000-fold (Klotz et al. 1998). Consequently [^{3}H]DPCPX has established itself as the ligand of choice for measuring the adenosine A_1 receptor B_{max}. DPCPX is actually an inverse agonist at the adenosine A_1 receptor, although it is generally referred to as an antagonist.

Allosterism at the adenosine A_1 receptor.

Increasing interest in GPCR pharmacology and drug discovery is being driven by the potential of allosteric compounds. The compound PD 81,723 is an allosteric enhancer of agonist binding at the adenosine A_1 receptor (Bhattacharya and Linden 1995, Bruns and Fergus 1990, Cohen 1995). Work in the group prior to this study investigated the mechanism of action of PD 81,723 on the binding of a series of ligands with a range of intrinsic activities to the coupled and uncoupled states of the human adenosine A_1 receptor. The results were explained by the ability of PD 81,723 to activate the adenosine A_1 receptor from the allosteric site on the receptor and by its ability to act as a co-agonist with agonist binding to the orthosteric site to increase affinity of the A_1 receptor for its G protein (Browning 2003, Browning *et al.* 2000c).

1.4.2 Adenosine A_1 receptor–G protein fusion proteins.

Proteins where a G protein α-subunit is covalently attached to the C-terminus of a GPCR have been developed for several different receptors including the β_2 adrenoceptor (Bertin *et al.* 1994), α_{2A} adrenoceptor (Wise *et al.* 1997), IP prostanoid receptor (Fong and Milligan 1999), 5-HT_{1A} receptor (Kellet *et al.* 1999) and adenosine A_1 receptor (Bevan *et al.* 1999, Wise *et al.* 1999).

Typically the attached G proteins are modified by mutation of the cysteine residue near the C-terminus of the G protein. This has the effect of rendering the mutated G protein insensitive to ADP-ribosylation by pertussis toxin, which functionally inactivates members of the G_i family of G proteins. However, mutation of the cysteine residue can interfere with the normal interactions between receptor and G protein and effects can vary depending on the amino acid to which the residue to mutated (Jackson *et al.* 1999). Often GPCR–G protein fusion proteins are constructed in order to constrain the system to a 1:1 stoichiometry. The fusion of pertussis toxin insensitive G proteins to the receptors enables the use of pertussis toxin to inactivate endogenous G protein with which the receptor might otherwise interact. Even when there is an available G protein in close proximity for each receptor both high and low affinity agonist binding is observed. Despite the 1:1 stoichiometry of receptor to G protein, the GPCR–G protein fusion constructs appear to behave in much the same manner as when not covalently attached to G protein.

Adenosine A_1 receptor–G protein fusion constructs have been used to investigate features of receptor-G protein interaction. Wise *et al.* 1999 reported little difference in the ability of the adenosine A_1 receptor to couple to the G proteins $G\alpha_{i1}$, $G\alpha_{i2}$, $G\alpha_{i3}$ and $G\alpha_{o1}$. They also showed for a range of agonists no selective activation of any adenosine A_1 receptor–$G_{i/o}$ protein combination studied. Waldhoer *et al.* 1999 used adenosine A_1 receptor–G protein constructs ($G\alpha_{i1}$ and $G\alpha_o$) to investigate the kinetics of the formation and dissociation of the ternary complex (agonist-receptor-G protein). Adenosine A_1 receptor–$G\alpha_{i1}$ fusion proteins were created where the pertussis toxin sensitive cysteine was replaced with glycine or isoleucine. The two fusion proteins show different affinities of the receptor for the G protein. Using both constructs they found receptor activation was the rate limiting step in ternary complex formation rather than the availability and recruitment of G protein.

Klaasse *et al.* 2004 observed similar allosteric modulation by PD 81,723 for the adenosine A_1 receptor alone and A_1 receptor–G protein fusion constructs, using $G\alpha_{i1}$ subunits where the cysteine residue conferring pertussis toxin sensitivity was replaced with one of eight different amino acids (Gly, Ile, Phe, His, Pro, Arg, Ser, Val). The affinity of agonist CPA increased by more than 8-fold for the fusion proteins than the receptor alone, whereas DPCPX showed no significant difference in affinity between the receptor alone and the fusion proteins. This provides further evidence of relatively "wild-type" behaviour for adenosine A_1 receptor–G protein fusion constructs. Functional analysis of receptor activation by means of [^{35}S]GTPγS binding showed increased basal levels of receptor activation (constitutive activity) for the fusion proteins relative to the adenosine A_1 receptor alone.

1.4.3 Adenosine A_1 receptor–GFP fusion proteins.

The labelling of proteins by covalent attachment of green fluorescent protein (GFP) is a phenomenally popular technology in the investigation of protein localisation, trafficking and expression (Tsien 1998). There have been only limited reports of the effects of labelling the adenosine A_1 receptor with GFP. The functional analysis of membranes prepared from stable CHO cell lines expressing either the human adenosine A_1 receptor–$G\alpha_i$ (A_1R-$G\alpha_i$) or adenosine A_1 receptor–GFP–$G\alpha_i$ (A_1R-GFP-$G\alpha_i$) fusion constructs found little difference in the response to agonist activation in the absence of pertussis toxin (Bevan *et al.* 1999). This provided evidence that GFP may be attached to the human adenosine A_1 receptor without disrupting receptor behaviour. The $G\alpha_i$ subunit used in both fusion constructs was resistant to inactivation by pertussis toxin. However, in the presence of pertussis toxin, only the A_1R-GFP-$G\alpha_i$ construct showed stimulation of [^{35}S]GTPγS accumulation by the adenosine A_1 receptor agonist NECA. Confocal microscopy of the A_1R-GFP-$G\alpha_i$ construct in live CHO cells observed GFP fluorescence in cytoplasmic membranes and the cell membrane.

1.4.4 Studies investigating the effect of adenosine A_1 receptor expression level.

Previous studies within the receptor group at NIMR have used two stable CHO cell lines expressing the human adenosine A_1 receptor at high (A_1HE) and low (A_1LE) levels (Cohen 1995, Browning 2003). Features of agonist binding to the adenosine A_1 receptor at equilibrium were dependent on the level of receptor expression, but not quantitatively compatible with all the predictions of the ternary complex model of agonism (Browning *et al.* 2000b). Differences in the functional response to agonist activation of the adenosine A_1 receptor, characterised by [^{35}S]GTPγS accumulation, were observed using the two cell lines (Browning *et al.* 2000a,c). Also, the effect of the allosteric enhancer PD 81,723 was investigated at both levels of receptor expression (Browning *et al.* 2000c).

The dissociation of radiolabelled agonist from A_1HE membranes was incomplete, and in preliminary experiments was enhanced by the presence of an excess concentration of unlabelled agonist (so-called "agonist-induced agonist dissociation;" Browning 2003). This behaviour was not observed at low levels of adenosine A_1 receptor expression using the A_1LE membranes. The kinetics of agonist dissociation and dependence on the level of receptor expression and the nature of competing unlabelled ligand were not characterised. These observations provided the basis from which a large proportion of the work presented in this study developed.

Using membranes prepared from stable CHO cell lines expressing different levels of the human

adenosine A_1 receptor differences have been identified in some agonist potencies and "agonist trafficking" at two levels of receptor expression (Cordeaux *et al.* 2000). The concept of "agonist trafficking," where the nature of the functional response to receptor activation can be influenced by a particular agonist, may be of help in improved understanding of the functional response to receptor activation (Kenakin 1995).

1.5 Project Aims.

The aim of this project was to investigate in detail the effect of the level of receptor expression on the binding of agonists and antagonists at the human adenosine A_1 receptor. Membranes prepared from a large number of stable CHO cell lines expressing the adenosine A_1 receptor or A_1R-GFP fusion proteins were used in order to investigate in detail the effect of receptor expression level on agonist binding at equilibrium and the kinetics of agonist binding directly at the adenosine A_1 receptor. The work presented in this thesis is described in five chapters of experimental results;

Chapter 3 describes the creation by flow cytometry of the series of stable CHO cell lines expressing the A_1R-GFP fusion proteins at a wide range of expression levels.

Chapter 4 examined in detail the effect of the level of A_1 receptor expression on the binding of agonists and antagonists at equilibrium.

Chapter 5 characterised in detail the kinetics of agonist and antagonist binding at the adenosine A_1 receptor and describes novel details of the promotion of [^{3}H]agonist dissociation by unlabelled agonist, so-called "agonist-induced agonist dissociation."

Chapter 6 describes the dependence of agonist-induced agonist dissociation on the level of adenosine A_1 receptor expression.

Chapter 7 investigated the distribution of the adenosine A_1 receptor and A_1R-GFP fusion proteins in cell membrane fractions separated by their buoyant density.

Figure 1.7 Adenosine receptor phylogenetic tree.

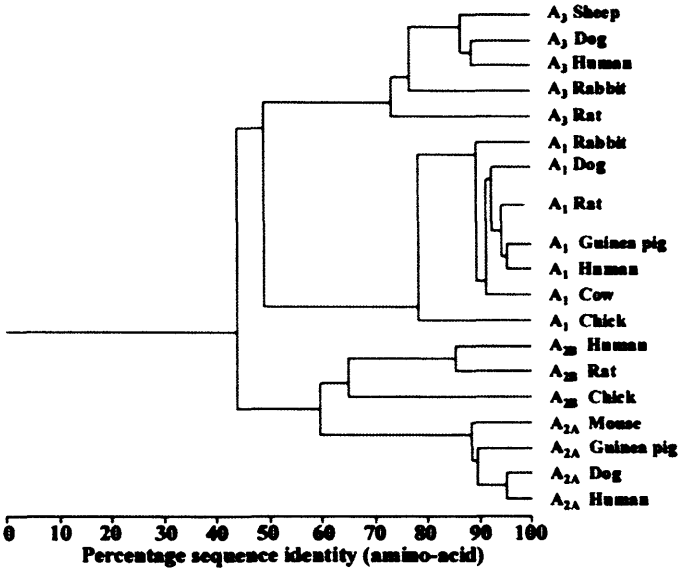

Figure 1.7: Phylogenetic tree of A_1, A_{2A}, A_{2B}, and A_3 adenosine receptor subtypes. Taken from Fredholm *et al.* 2001, which was redrawn from that available at http://www.gpcr.org/7tm/seq/001_007_001/001_007_001.TREE20.html (as of April 2005).

Figure 1.8 Adenosine receptor coupling.

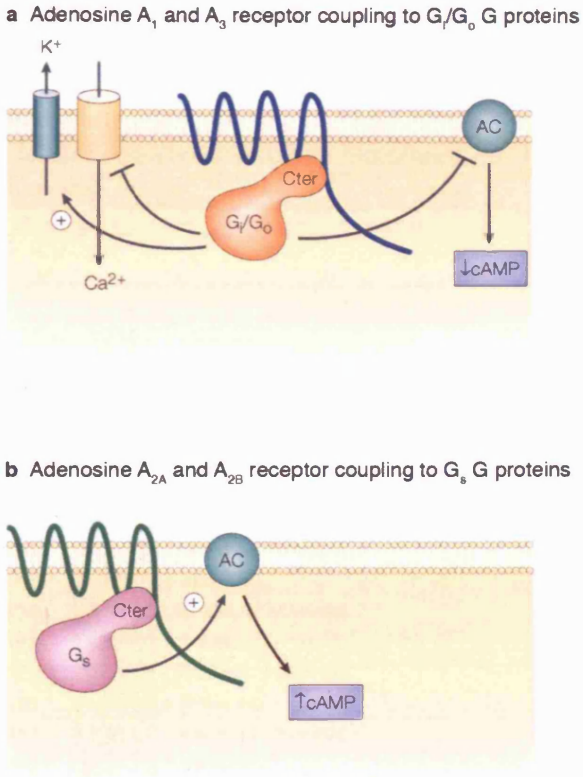

Figure 1.8: **(a)** The inhibitory actions of adenosine A_1 and A_3 receptor activation are associated with activation of $G\alpha_i$ and $G\alpha_o$ G proteins and the subsequent inhibition of adenylate cyclase (AC) activity, activation of K^+ channels and inhibition of Ca^{2+} channels. It appears the A_1 receptor can also activate $G\alpha_S$ and $G\alpha_q$ subunits to a lesser extent than $G\alpha_i$ and in an agonist-specific manner (Cordeaux *et al.* 2004) **(b)** Activation of adenosine A_{2A} and A_{2B} receptors stimulate the activity of adenylate cyclase. Figure adapted from Ellis 2004.

Figure 1.9 The human adenosine A_1 receptor amino acid sequence.

General information

Entry name	**AA1R_HUMAN**
Accession number	**P30542**, Q8TAM8
Created	Rel. 25, 1-APR-1993
Sequence update	Rel. 25, 1-APR-1993
Annotation update	Rel. 47, 1-MAY-2005

Description and origin of the Protein

Description	Adenosine A1 receptor.
Gene name(s)	ADORA1
Organism source	Homo sapiens (Human).

Features

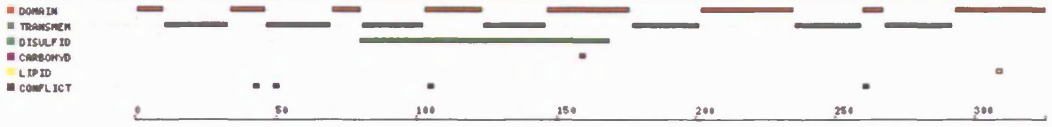

Key	Begin	End	Length	Description
DOMAIN	1	10	10	Extracellular (Potential).
TRANSMEM	11	33	23	1 (Potential).
DOMAIN	34	46	13	Cytoplasmic (Potential).
TRANSMEM	47	69	23	2 (Potential).
DOMAIN	70	80	11	Extracellular (Potential).
TRANSMEM	81	102	22	3 (Potential).
DOMAIN	103	123	21	Cytoplasmic (Potential).
TRANSMEM	124	146	23	4 (Potential).
DOMAIN	147	176	30	Extracellular (Potential).
TRANSMEM	177	201	25	5 (Potential).
DOMAIN	202	235	34	Cytoplasmic (Potential).
TRANSMEM	236	259	24	6 (Potential).
DOMAIN	260	267	8	Extracellular (Potential).
TRANSMEM	268	292	25	7 (Potential).
DOMAIN	293	326	34	Cytoplasmic (Potential).
DISULFID	80	169	90	By similarity.
CARBOHYD	159	159	1	N-linked (GlcNAc...) (Potential).
LIPID	309	309	1	S-palmitoyl cysteine (Potential).

Sequence information

Length: **326 aa**, molecular weight: **36512 Da**, CRC64 checksum: **1B555893BCDEC9A6**

```
SQ   Sequence   326 BP;
     MPPSISAFQA AYIGIEVLIA LVSVPGNVLV IWAVKVNQAL RDATFCFIVS LAVADVAVGA        60
     LVIPLAILIN IGPQTYFHTC LMVACPVLIL TQSSILALLA IAVDRYLRVK IPLRYKMVVT       120
     PRRAAVAIAG CWILSFVVGL TPMFGWNNLS AVERAWAANG SMGEPVIKCE FEKVISMEYM       180
     VYFNFFVWVL PPLLLMVLIY LEVFYLIRKQ LNKKVSASSG DPQKYYGKEL KIAKSLALIL       240
     FLFALSWLPL HILNCITLFC PSCHKPSILT YIAIFLTHGN SAMNPIVYAF RIQKFRVTFL       300
     KIWNDHFRCQ PAPPIDEDLP EERPDD                                            326
```

Figure 1.9: The amino acid sequence of the human adenosine A_1 receptor. Also shown are details including the entry name and accession number, and the proposed composition of features such as transmembrane domains and post-translational modifications. The image was taken from http://srs.ebi.ac.uk/.

Figure 1.10 The modification of adenosine to create other adenosine receptor agonists.

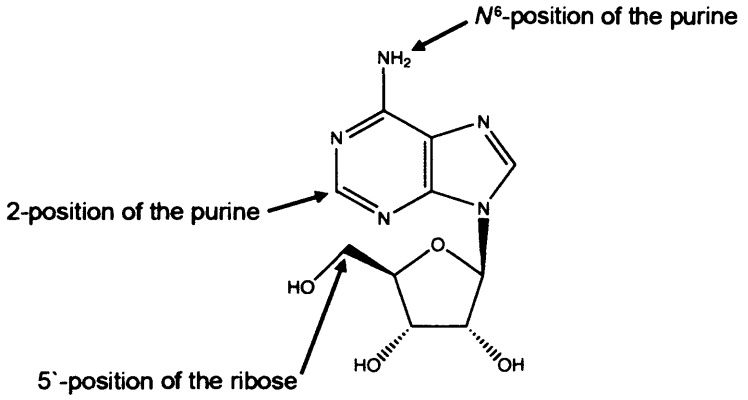

Figure 1.10: Adenosine is typically modified in three positions (indicated above) in order to alter affinity and specificity for adenosine receptors and sensitivity to degradation by adenosine deaminase. Figure 2.1 on page 50 illustrates the structures of adenosine receptor agonists CHA, PIA, GR190178, GR162900 and GR161144 which show modifications at one or more of the three positions and are all insensitive to adenosine deaminase. The above illustration was redrawn from that in Klotz 2000.

Chapter 2

Materials and methods.

2.1 Materials.

Cell Culture

Chinese hamster ovary (CHO) cells stably expressing the human adenosine A_1 receptor at two different densities were a kind gift from Prof. Stephen Hill, The University of Nottingham. Stable CHO cell lines expressing either HA-A_1R, A_1R-GFP or A_1R-GFP-$G\alpha_i$ fusion proteins were a kind gift from Dr. Chris Browning, GlaxoSmithKline, Stevenage. The A_1R-GFP-$G\alpha_i$ construct had Cys351 of the $G_i\alpha$ sequence mutated to glycine, thereby rendering the G protein insensitive to ADP ribosylation by pertussis toxin (Bevan *et al.* 1999). DMEM-F12 media, G418 and HBSS were from Sigma. Penicillin, streptomycin, glutamine and trypsin versene were from in-house media supplies. All plastic culture vessels were BD Falcon. BCA Protein Assay Reagent Kit (including 2 mg/ml BSA ampules) was from Pierce Biotechnology. Foetal calf serum was from Labtech International (batch no. F-2395).

Compounds

ADA (A-9876), CHA (C-9901), DMSO (D-8779), DPCPX (C-101), GTP (G-8877), Hepes (H-3375), N0840 (N-154), PIA (P-4532), polyethyleneimine (P-3143), Saponin (S-1252), Theophylline (T-1633) and Tris (T-1503) were from Sigma. EDTA was from Fisons. GR1690178, GR161144 and GR162900 (see Figure 2.1 on page 50) were a kind gift from Dr. Chris Browning, GlaxoSmithKline, Stevenage.

Radioligand binding

[^{3}H]CHA (29.5 and 32.3 Ci/mmol) and [^{3}H]DPCPX (108.3, 111.6 and 120.0 Ci/mmol) were from Perkin Elmer Life Sciences, Inc. [^{3}H]CHA (24 Ci/mmol) was from Moravek Biochemicals, California. Ready Safe scintillation fluid and 6 ml Pony vials were from Packard Bioscience. GF/B glass fibre filter paper was from Whatman. Printed Filtermat A, Meltilex A and Sample Bags were from Wallac, Finland.

Density gradient separation of membrane fractions

OptiPrep (60% w/v iodixanol in water) was from Axis-Shield PoC AS, Oslo. Triton X-100 (T 9284) and Protease Inhibitor Cocktail in DMSO (P 8340) was from Sigma. Open-top 5 ml polyallomer centrifuge tubes were from Beckman. OptiPrep is the trademark name for sterile 60% (w/v) solution of iodixanol in water.

SDS-PAGE and Western blotting

10% and 4–12% Bis-Tris NuPAGE Novex gels, NuPAGE MOPS SDS running buffer (20x), NuPAGE transfer buffer (20x), NuPAGE Sample Buffer (4x), PVDF Membrane Filter Paper Sandwich and SeeBlue Plus2 Pre-Stained Standard were from Invitrogen Ltd, Paisley. Dithiothreitol was from Sigma. Rabbit polyclonal primary antibodies for A_1R (ab3460 and ab13295), D_1R (ab12969), $G\alpha_{i1+2}$ (ab3522) Caveolin1 (ab2910) and Fyn (ab13955) were from Abcam Ltd, Cambridge. Rabbit polyclonal primary antibodies for $G\alpha_{12}$ (S-20), $G\alpha_{13}$ (A-20) and $G\alpha_{i1}$(I-20) were from Santa Cruz Biotechnology Inc, California. Goat polyclonal primary antibody for $G\alpha_{i/o/t/z}$(D-15) was from Santa Cruz Biotechnology Inc, California. Rabbit polyclonal IgG antibody for GFP (A-11122) was from Molecular Probes Europe BV, The Netherlands. Rabbit polyclonal HRP-linked secondary antibody to goat IgG (ab6741) was from Abcam Ltd, Cambridge. Donkey polyclonal HRP-linked secondary antibody to rabbit IgG (NA934) was from Amersham Biosciences UK Ltd. Tween-20 (polyoxyethylene sorbitan monolaurate) was from Bio-Rad Laboratories, California. Marvel Dried Skimmed Milk powder was from Premier International Foods (UK) Ltd. Enhanced chemiluminescence (ECL) detection system was from Amersham Biosciences UK Ltd. PBS was from in-house media supplies. Blue-light sensitive Kodak X-OMAT AR autoradiography film (8 x 10 inch) was from Kodak. Table 2.1 on page 57 lists all the primary antibodies used for Western blots presented in Chapters 2, 3 and 7.

Figure 2.1 The structures of adenosine A_1 receptor ligands used in this study.

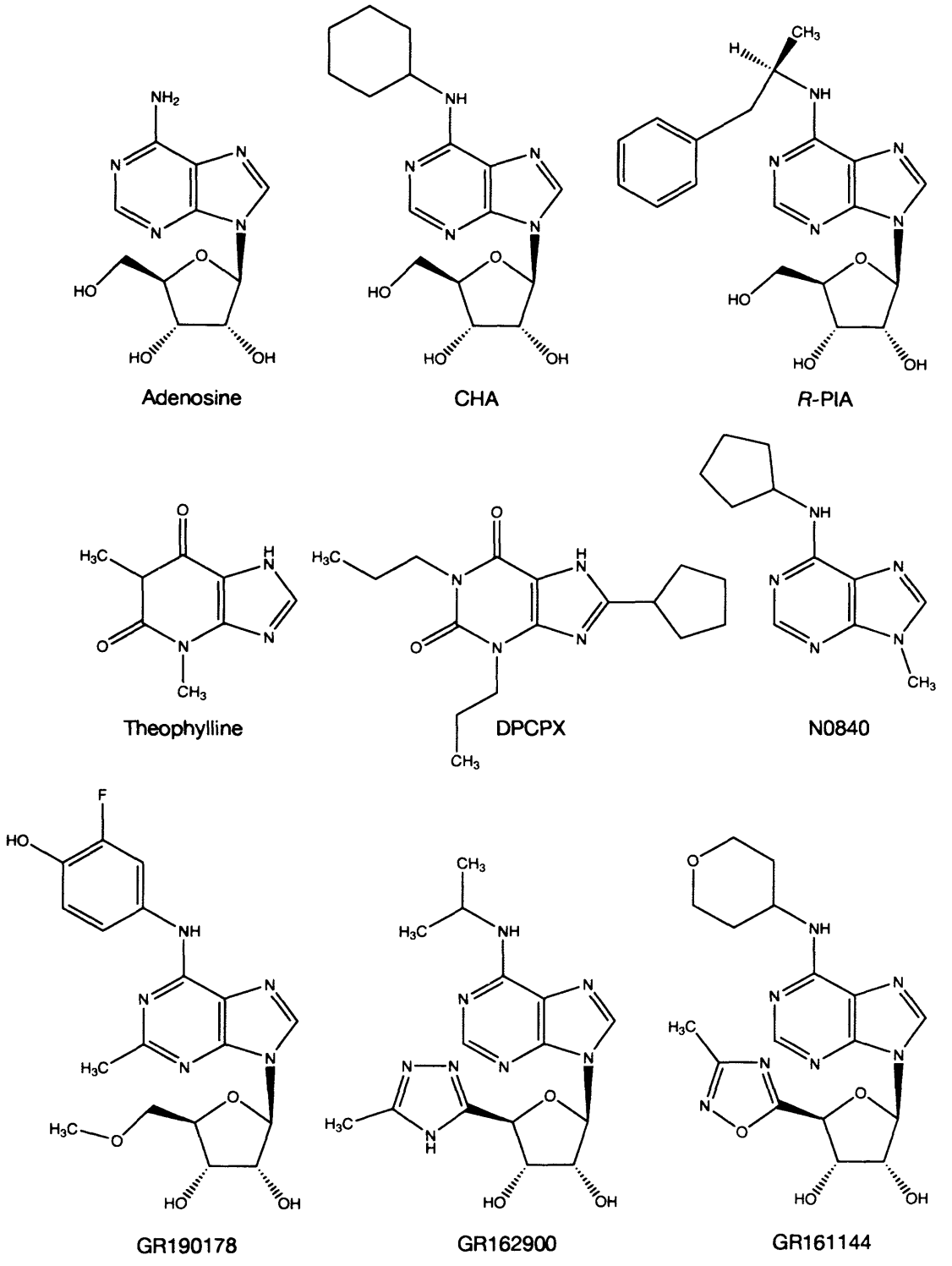

Figure 2.1: CHA and PIA are high efficacy agonists at the human adenosine A_1 receptor. GR190178, GR162900 and GR161144 are agonists of lower efficacy. DPCPX, N0840 and theophylline are antagonists / inverse agonists. Adenosine is shown for comparison.

2.2 Methods.

2.2.1 Cell culture

Stable CHO cell lines were maintained in a routine fashion in DMEM-F12 medium supplemented with penicillin, streptomycin, glutamine and 10% foetal calf serum (all foetal calf serum in this study was from the same batch) at 37°C in 5% CO_2. Typically cells were detached using trypsin versene and passaged 1:10 to 1:20 approximately every 3 days. For preparation of membranes, cells from a confluent 175 cm^2 flask were seeded into a 1750 cm^2 cell culture roller bottle with 300 ml media and incubated at 37°C in normal air (although roller bottle is airtight when closed) while rotating at approximately 0.5 rpm. Membranes were harvested after 4-7 days incubation. Media was exchanged for fresh media if the roller bottles were incubated for longer than 4 days.

2.2.2 Membrane preparation

All radioligand binding presented in this thesis was performed using membranes prepared from CHO cell lines stably expressing the human adenosine A_1 receptor or A_1R fusion constructs.

The preparation of cell membranes was based on previous protocols (Cohen *et al.* 1996a&b, Browning 2003). Briefly, membranes from cells grown in 1750 cm^2 roller bottles were harvested when the cells were between 80% and fully confluent. Cells were washed with HBSS at room temperature and incubated and lysed with a hypotonic homogenisation buffer (20 mM Hepes, 10 mM EDTA, pH 7.4, 4°C), detached by gentle agitation, and separated by slow centrifugation for 5 min at 3000 rpm at 4°C. The lysed cells were resuspended in homogenisation buffer, disrupted in a Polytron homogeniser (12,000 rpm for 15 sec or 3 intervals of 5 sec) and the membranes separated by centrifugation at 40,000 *g* for 20 min at 4°C. The membrane pellet was resuspended in membrane buffer (20 mM Hepes, 0.1 mM EDTA, pH 7.4, 4°C), disrupted in a Polytron homogeniser and centrifuged at 40,000 *g* as above. The membrane pellet was resuspended in membrane buffer, passed through a 27G needle and stored in 0.5 ml aliquots at -70°C. The protein concentration of thawed membranes was determined in triplicate using the Pierce BCA Protein Assay reagent kit in 96 well microplates (Smith *et al.* 1985). Absorbance at 550 nm was referenced against serial dilutions of BSA.

2.2.3 Equilibrium radioligand binding

All equilibrium binding assays were performed at RT in a final volume of 1 ml in binding assay buffer as described previously, 20 mM Hepes, 100 mM NaCl, 10 mM $MgCl_2$, pH 7.4, (Cohen *et*

al. 1996b). Saturation assays were performed in quadruplicate, competition assays in triplicate or quadruplicate. In order to remove endogenous adenosine which would interfere with the assays, membranes were pre-incubated with approximately 3 U/ml adenosine deaminase (ADA) for 30 min at RT, and stored on ice afterwards. No apparent difference was observed in association time courses of [^{3}H]CHA to A_1HE membranes following incubation with 1 or 10 U/ml adenosine deaminase (data not shown), suggesting the typical concentration of 3 U/ml ADA to be adequate at removing adenosine. All equilibrium binding assays contained 30 μg/ml of the membrane permeabilising agent saponin unless indicated. For radioligand equilibrium saturation binding studies, radioligand was incubated with 10 to 37 μg/ml of membrane protein in the presence of 30 μg/ml saponin for 60 min before rapid filtration onto glass fibre filters soaked in 0.1% polyethyleneimine using either a 48 well Brandell cell harvester or a 96 well Tomtec Mach III M Harvester 96. Following filtration, the glass fibre filters were rapidly washed three times with ice cold water. The 48 well filters were transferred to liquid scintillation vials and 4 ml of scintillation fluid added. Typically vials were left for 24 hours, but at least overnight, at RT to allow the filters to become universally translucent. Vials were shaken thoroughly before counting in a Beckman LS 5000CE liquid scintillation counter for 5 or 20 min. 96 well filters were dried overnight at RT or 1 hour at 50°C, then Meltilex scintillation sheets were melted onto the filters using a Wallac 1495-021 Microsealer, and bound radioligand counted in a Wallac 1450 Microbeta Liquid Scintillation and Luminescence Counter. In all experiments non-specific radioligand binding was determined in the presence of 3 mM theophylline.

A simplified [^{3}H]DPCPX saturation and [^{3}H]DPCPX / CHA competition assay was developed to estimate [^{3}H]DPCPX B_{max} and affinity from three concentrations of radioligand, and fr_H, pK_H and pK_L from the inhibition of [^{3}H]DPCPX binding by three concentrations of CHA (see Figure 4.7 on page 93). The [^{3}H]DPCPX saturation curve was measured in triplicate; the [^{3}H]DPCPX (1 nM) / CHA competition was in duplicate. Reactions were incubated for one hour at RT before harvesting on a 48 well Brandell harvester and counting as described above.

2.2.4 The Kinetics of radioligand binding

A reverse time course strategy to enable simultaneous filtration of samples was used to measure the kinetics of radioligand association and dissociation (Hulme & Birdsall 1992). Briefly, membranes were incubated with 3 U/ml ADA for 30 min at RT and the reaction quenched on ice. For association assays, membranes were incubated with radioligand in a final volume of 100 μl, and the reaction terminated by rapid filtration as described above (Chapter 2.2.3, page 51). For dissociation assays, membranes were incubated with radioligand in a final volume of 100 μl as above for the

period of association, and dissociation initiated by 20-fold dilution (2 ml) into binding assay buffer. Following the period of dissociation, the reaction was terminated by rapid filtration as described above (Chapter 2.2.3, page 51).

A simplified assay of the dissociation of [^{3}H]CHA was developed in order to allow fitting the equation for two-phase exponential dissociation to four time points (0, 10, 60 and 180 min) and a plateau of NSB (see Figure 4.7 on page 93).

2.2.5 FACS analysis and single cell selection

Polyclonal CHO cell lines expressing either the A_1R-GFP or A_1R-GFP-Gα_i fusion constructs were analysed and sorted by Chris Atkins (Laboratory of Immunoregulation, NIMR) on a DakoCytomation MoFlo High-Performance Cell Sorter using an excitation wavelength of 488 nm. Individual cells were directed into separate wells on 96 well plates containing media as detailed above (Chapter 2.2.1, page 51). Media was changed after 3 days. After 6 days, 12 colonies from each 96 well plate that were growing well were chosen and transferred to 12 well plates with 2 ml media in each well. Media was changed after 3 days, and after one week 24 A_1R-GFP and 23 A_1R-GFP-G$\alpha_i$colonies were selected and transferred into 25 cm^2 flasks with 4 ml media. A variety of fast and slower growing colonies were chosen for transfer to 25 cm^2 flasks. When confluent, cell lines in 25 cm^2 flasks were transferred to 175 cm^2 flasks. From confluent 175 cm^2 flasks, stocks were stored in liquid nitrogen and 1750 cm^2 roller bottles seeded and harvested as described above (Chapter 2.2.2, page 51). The entire process from individual cells through to confluency in 1750 cm^2 roller bottles took between 24 and 39 days, depending on the rate of growth. Cell lines expressing higher levels of either fusion construct grew more slowly than those of lower expression levels. It is possible that stimulation of the A_1R by endogenously produced adenosine has a negative influence on the rate of cell growth. Presence of the A_1R inverse agonist DPCPX (10^{-7} M) did not affect growth rate, receptor yield or equilibrium binding properties. This suggested that stimulation of the A_1R by endogenous adenosine was not contributing to slower growth.

2.2.6 Fluorescence microscopy

Stable CHO cell lines expressing either the A_1R-GFP or A_1R-GFP-Gα_i fusion constructs were visualised on a Deltavision cooled CCD imaging system incorporating an Olympus IX70 inverted microscope and a Photometrics CH350L liquid cooled CCD camera with a Kodak KAF1400 sensor. The objective lens used was 40x Olympus UPL APO. Images were captured on an SGI O_2 workstation running Softworx image acquisition and deconvolution software under SGI IRIX. Further

analysis and manipulation of images was performed using ImageJ 1.28 for Mac and Linux, Wayne Rasband, National Institutes of Health, USA, http://rsb.info.nih.gov/ij.

2.2.7 Density gradient membrane fractionation

All density gradient materials, procedures and incubations were performed on ice or at 4°C. Using the same membrane preparations as used for radioligand binding (Chapter 2.2.2, page 51), 1 mg of membrane protein was isolated by centrifugation at 5,000 *g* for 5 min, and resuspended in 500 μl TNET buffer (50 mM Tris, 150 mM NaCl, 5mM EDTA, 0.5% Triton X-100, pH 7.4), and incubated on ice for 20 min. The sample was vortexed, and adjusted to 35% iodixanol (500 μl sample + 700 μl 60% iodixanol) in a 5 ml Beckman polyallomer centrifuge tube. 3 ml of 30% iodixanol (in TNET buffer) was placed carefully and slowly above the sample, and 5% iodixanol added until the centrifuge tube was full (approximately 900 μl). Samples were spun at 170,000 *g* (37,402 rpm in a Beckman SW55Ti rotor) for 4 hours. Fractions of 730 μl were removed carefully from the top of the centrifuge tube, and any pellet resuspended in 730 μl of TNET buffer. Fractions were stored at -70°C. The density of individual fractions was determined by measurement in duplicate of the absorbance at 340 nm after repeated 1:1 dilution in 0.85% NaCl, referenced against 0.85% NaCl alone.

2.2.8 SDS-PAGE and Western blotting

Samples were prepared, electrophoresed and transferred to PVDF according to Invitrogen's instructions. Briefly, NuPAGE Sample Buffer containing membrane protein or density gradient fractions was heated to 90°C for 1–2 min, followed by the addition of reducing agent dithiothreitol (final 50 mM) and a thorough vortex. Samples were added to NuPAGE Bis-Tris PAGE gels submerged in NuPAGE SDS Running Buffer containing NuPAGE Antioxidant to maintain reducing conditions. Gels were run at 200 V for typically 50 min. Gels were removed and protein transferred onto PVDF at 25 V for 1.5 hours in NuPAGE Transfer Buffer (with 10% methanol). Different heating temperatures (65, 80 and 90°C) and times (1 and 2 min) did not make any visible difference to the appearance of A_1HE or A_1R-GFP-Gα_i samples when electrophoresed, transferred and blotted for A_1R (ab3460), (Figure 2.2 on the next page). The band of greatest molecular weight in the A_1R-GFP-Gα_i samples of Figure 2.2 may show an increase in intensity with temperature, however this band is extremely faint in comparison to the main A_1R-GFP-Gα_i band.

All PVDF membrane incubations and washes were performed with gentle agitation. PVDF membranes were rinsed in water, and NSB blocked by incubation for 2 hours at RT or overnight at

Figure 2.2 Optimisation of sample heating before gel electrophoresis.

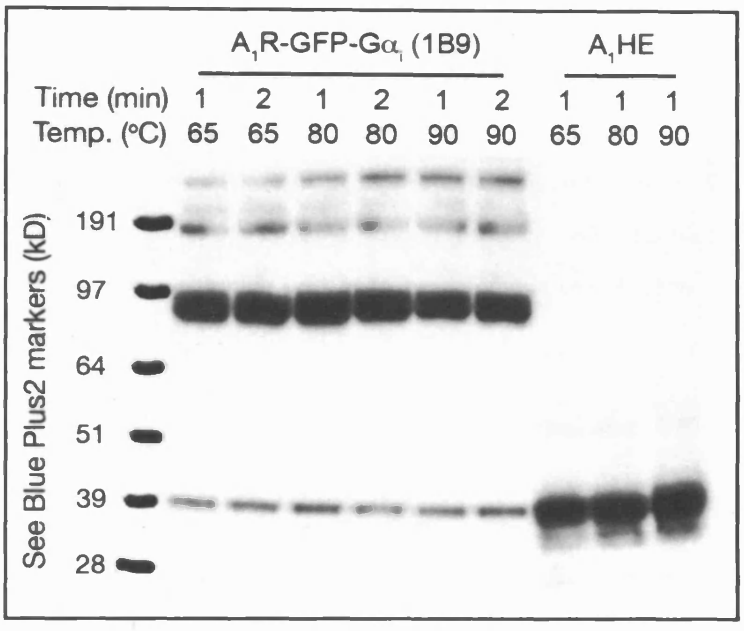

Figure 2.2: The effect of the period and temperature of heating prior to SDS-PAGE and Western blot analysis was investigated using membranes from A_1HE and A_1R-GFP-Gα_i cell lines (see Table 4.3 on page 95 for equilibrium binding properties of A_1R-GFP-Gα_i cell line 1B9) and adenosine A_1 receptor antibody ab3460. No obvious difference can be observed between the different A_1HE or A_1R-GFP-Gα_i heating conditions, therefore conditions of 90°C and 1 min were used for subsequent sample preparation. The human adenosine A_1 receptor should be approximately 37 kDa in size which generally agrees with the See Blue Plus2 Pre-stained markers shown above. The A_1R-GFP-Gα_i construct should be approximately 104 kDa (37, 27 and 40 kDa for A_1R, GFP and Gα_i respectively), although the exact size coded by the construct is unknown. The See Blue Plus2 markers appear to underestimate the size of the A_1R-GFP-Gα_i construct, which is typically identified as two bands in close proximity in other Westerns, for example Figure 3.5 on page 71.

4°C in blocking buffer (PBS, 0.1% Tween-20, 5% milk powder). PVDF membranes were incubated for 1 hour at RT with primary antibody diluted in blocking buffer. Table 2.1 on the following page lists the primary antibodies used for Western blotting throughout this study. PVDF membranes were washed in PBS-T (PBS, 0.1% Tween-20) for 15 and 5 min, followed by incubation for 1 hour at RT with secondary antibody diluted in blocking buffer. PVDF membranes were washed in PBS-T for 15 min followed by 4 washes of 5 min each.

Enhanced chemiluminescence (ECL) detection of bound secondary antibody was performed entirely according to supplied instructions (Amersham), followed by short exposure to blue-light sensitive autoradiography film and developed in a Fujifilm FPM-3800A film processor.

All blots shown in this document are from separate gels and subsequent Western blots, apart from Caveolin. No membranes were stripped and re-probed. Western blots for caveolin were performed on PVDF membranes which had been used for one of the other primary antibodies, washed thoroughly in PBS-T, and re-probed for caveolin.

2.3 Data analysis.

All radioligand binding experiments were performed in either duplicate, triplicate, quadruplicate or sextuplicate. Results are expressed as mean ± standard error of mean, of n independent experiments.

All linear regression and non-linear least-squares analysis was performed using GraphPad Prism versions 3 and 4 for Macintosh, GraphPad Software, San Diego California USA, http://www.graphpad.com. The equations used by Prism are described below.

2.3.1 Analysis of binding at equilibrium

Saturation binding; Specific binding (SB) was estimated by subtraction of non-specific binding (NSB) from total binding (TB) and was analysed by non-linear regression using the equation,

$$SB = \frac{B_{max} \cdot [L]}{K_D + [L]}$$

where B_{max} is the maximum binding capacity of the membrane preparation for ligand L of dissociation constant K_D.

One-site competition binding; Competition of radioligand binding to a single binding site was

Table 2.1 Primary antibodies used for Western blot analysis presented in this study.

Antibody	Description	Figures
A_1R (ab3460)	Immunogen peptide CQPKPPIDEDLPEEKAED corresponding to the extreme C-terminus of the rat adenosine A_1 receptor	2.1 3.5 3.6 7.3 7.6
A_1R (ab13295)	Immunogen peptide attached to keyhole limpet haemocyanin (KLH) corresponding to the third cytoplasmic loop of the A_1R (peptide sequence not supplied by the manufacturer)	3.5
GFP (A-11122)	Manufacturer's information; "Raised against GFP isolated directly from *Aequorea victoria*"	3.6 7.6
$G\alpha_i$ (ab3522)	Immunising peptide KNNLKDCGLF corresponding to the C-terminus of human $G\alpha_i$	7.3 7.6 7.7
$G\alpha_{i1}$ (I-20)	Manufacturer's information; "Raised against a peptide mapping within a highly divergent domain of rat $G\alpha_{i1}$"	3.5
$G\alpha_{13}$ (A-20)	"Raised against a peptide mapping at the amino terminus of mouse $G\alpha_{13}$"	7.3
Caveolin (ab2910)	"Immunising peptide (MSGGKYVDSEGHLYTVP) corresponds to amino acid residues 1-17 from human caveolin-1"	7.3 7.6
Fyn (ab13955)	"Immunogen; Recombinant protein expressed in E. coli (Human)"	7.4

Table 2.1: Above are listed the primary antibodies used in the Western blots presented in Chapters 2, 3 and 7 of this document.

analysed using the equation,

$$Bound\,radioligand = NSB + \frac{TB - NSB}{1 + 10^{(x - \log IC_{50})}}$$

where x is log(concentration of competing unlabelled ligand), and IC_{50} is the mid-point of inhibition dose response curve. LogIC_{50} values were converted to pK_i values using the Cheng Prusoff correction (Cheng & Prusoff 1973), where $[L^*]$ is concentration of radioligand with dissociation constant K_D^*,

$$pK_i = -logIC_{50} + log(1 + \frac{[L^*]}{K_D^*})$$

Two-site competition binding; Competition of radioligand binding to two binding sites of different affinity for the unlabelled competing ligand was analysed using the equation,

$$Bound\,radioligand = NSB + ONE + TWO$$

$$ONE = \frac{SPAN.fr_H}{1 + 10^{(x - \log IC_{50H})}}$$

$$TWO = \frac{SPAN.(1 - fr_H)}{1 + 10^{(x - \log IC_{50L})}}$$

$$SPAN = TB - NSB$$

where fr_H is fraction of binding of high affinity, $logIC_{50H}$ and $logIC_{50L}$ are mid-points of high and low affinity components of inhibition of radioligand binding. $logIC_{50H}$ and $logIC_{50L}$ were converted to pK_H and pK_L, the negative log dissociation constants, respectively using the Cheng Prusoff correction.

2.3.2 Analysis of the kinetics of binding

One phase exponential association; Simple mono-exponential association of a radioligand was analysed using the equation,

$$Y = Y_{max}.(1 - \exp(-kx))$$

which starts at zero and ascends to Y_{max} with a rate constant x.

Two phase exponential association; The association of radioligand with two components was analysed using the equation,

$$Y = Y_{max1}(1 - \exp(-k_1 x)) + Y_{max2}(1 - \exp(-k_2 x))$$

which starts at zero and ascends to $Y_{max1} + Y_{max2}$ with rate constants k_1 and k_2.

One phase exponential decay; Mono-exponential dissociation of radioligand was analysed using the equation,

$$Y = SPAN.\exp(-kx) + PLATEAU$$

which starts at $SPAN + PLATEAU$ and decays to $PLATEAU$ with a rate constant k.

Two phase exponential decay; The dissociation of radioligand with two components was analysed using the equation,

$$Y = SPAN_1.\exp(-k_1 x) + SPAN_2.\exp(-k_2 x) + PLATEAU$$

which starts at $SPAN_1 + SPAN_2 + PLATEAU$ and decays to $PLATEAU$ with rate constant k_1 and k_2.

2.3.3 Statistical analysis

Unpaired t tests were used to estimate whether there was a statistically significant difference between mean log affinities. It was assumed that the data followed a generally Gaussian distribution and that both data sets had the same variances (same standard deviations). F tests to compare variances were performed at the same time as t tests, and most variances were not significantly different. The threshold P value for statistical analysis was 0.05. P values greater than 0.05 were regarded as not significant. Such analysis was used as an indication of statistical significance, but as Harvey Motulsky writes (Motulsky 2003);

> "Statistically significant" is not the same as "scientifically important."

Statistical significance should be interpreted in the context of the experimental procedure, the data gathered, other related observations and whether in general it makes sense. All statistical analysis was performed using GraphPad Prism 4 for Macintosh, GraphPad Software, San Diego California USA, http://www.graphpad.com.

Chapter 3

The creation and molecular characterisation of multiple stable cell lines expressing different levels of adenosine A_1 receptor-GFP fusion proteins.

3.1 Introduction.

Receptor function and radioligand binding studies have identified differences in the behaviour of the human adenosine A_1 receptor in membranes prepared from two stable CHO cell lines expressing the receptor at high (A_1HE) and low (A_1LE) levels (Cohen 1995, Browning 2003). These studies have provided evidence that features of adenosine A_1 receptor behaviour are dependent on the level of receptor expression. The aim of the work presented in this chapter was to create a series of stable CHO cell lines expressing either A_1R-GFP or A_1R-GFP-Gα_i fusion proteins at many different levels. Membranes prepared from these cell lines were then used to characterise the dependence of aspects of A_1R behaviour on the level of receptor expression. These observations were compared to those using the two cell lines expressing the adenosine A_1 receptor alone (A_1HE and A_1LE). These further investigations are described in Chapters 4, 5, 6 and 7. The use of GFP brightness as an indication of the level of receptor expression allowed rapid and specific isolation,

by means of flow cytometry, of individual cells expressing either the A_1R-GFP or A_1R-GFP-Gα_i fusion proteins from polyclonal stable CHO cell lines.

3.2 Flow cytometric analysis of stable CHO cell lines expressing human adenosine A_1 receptor-GFP fusion proteins.

A stable polyclonal CHO cell line expressing the adenosine A_1 receptor with Green Fluorescent Protein (GFP (Tsien, 1998)) and the G protein subunit Gα_i covalently fused in series to the A_1R C terminal (A_1R-GFP-Gα_i) was a kind gift from Dr Chris Browning, GlaxoSmithKline, Stevenage. Membranes prepared from this unsorted polyclonal cell line exhibited a [^{3}H]DPCPX B_{max} of 2.79 ± 0.33 pmol/mg protein and log affinity of 8.78 ± 0.12 (mean ± s.e.m., n = 3, see Table 4.3 on page 95 for more details).

In order to create a series of clonal cell lines expressing the adenosine A_1 receptor over a range of densities, individual A_1R-GFP-Gα_i cells of different GFP brightness were isolated by fluorescence activated cell sorting (FACS) into separate wells of four 96 well plates. 96 individual cells were isolated from four different gates of increasing GFP fluorescence (see Figure 3.1 on page 63). Six cell lines from each of the four gates were grown successfully to confluency and stocks stored in liquid nitrogen, except for sort 4 where only five selected cell lines grew sufficiently well. A total of 23 cell lines expressing the A_1R-GFP-Gα_i construct were created. Figure 3.2 on page 64 shows examples of flow cytometric analysis for cell lines from each of the four gates. Three of the lines appeared monodisperse but the cell line in analysis 3 has split into two populations of different GFP brightness. The [^{3}H]DPCPX B_{max} of membranes prepared from cell lines 1C1, 2A3, 3A3 and 4F2 shown in Figure 3.2 are 2.80 ± 0.23, 3.45 ± 0.13, 3.30 ± 0.37 and 2.85 ± 0.57 pmol/mg protein respectively (n = 2, see Table 4.3 on page 95 for more details). Despite selection by gate 4, cell line 4F2 does not show a high level of A_1R-GFP-Gα_i expression by either flow cytometry (this figure) or radioligand binding analysis (Table 4.3). However, other cells selected by gate 4 did mature into cell lines expressing a high level of the A_1R-GFP-Gα_i construct. It should be noted that selection of individual cells of high GFP brightness does not discriminate between normal sized cells expressing a high density of A_1R-GFP-Gα_i and larger cells expressing a lower density of A_1R-GFP-Gα_i.

A stable polyclonal CHO cell line expressing the adenosine A_1 receptor with GFP covalently fused in series (A_1R-GFP) to the A_1R C terminal was also a kind gift from Dr. Chris Browning, GlaxoSmithKline, Stevenage. Figure 3.3 on page 65 shows a FACS plot of GFP brightness (x-axis) against a measurement of cell size (y-axis) for the polyclonal A_1R-GFP cell line before selection of

individual cells. It is referenced against a polyclonal cell line expressing the adenosine A_1 receptor covalently labelled with the influenza A virus haemagglutinin (HA) epitope tag (HA-A_1R). The cells naturally exhibit a level of fluorescence during the analysis ("auto-fluorescence") for which the strength of signal is dependent on the size of the cell. The FACS plot of the HA-A_1R cell line in Figure 3.3 shows this characteristic linear dependence of cell auto-fluorescence with cell size. Specific GFP fluorescence is distinguished by its independence from cell size where increased GFP brightness is observed without an increase in cell size. This has been described in some instances as a "GFP-shift." Both FACS plots in Figure 3.3 contain a region marked "R7" where cells expressing a significant level of GFP would be expected. The cell line expressing HA-A_1R did not contain any cells with GFP fluorescence, however the A_1R-GFP cell line did show a small number (0.34% of 17429 cells were within region R7) with the characteristic FACS GFP-shift. Two 96 well plates of individual A_1R-GFP cells were selected from region R7 by flow cytometry. From these two 96 well plates, 24 cells were grown into mature stable cell lines. Membranes prepared from the unsorted A_1R-GFP cell line did not show any specific [^{3}H]DPCPX binding in contrast to membranes prepared from the A_1R-GFP-Gα_i cell line described above. Table 4.3 on page 95 describes the equilibrium binding properties of all 23 A_1R-GFP-Gα_i and 24 A_1R-GFP cell lines created by this process.

3.3 Localisation by fluorescence microscopy of the A_1R-GFP-Gα_i construct in live cells.

The cellular distribution of GFP, and therefore the adenosine A_1 receptor, was visualised in live A_1R-GFP-Gα_i cells on a Deltavision cooled CCD imaging system (Figure 3.4 on page 67), as described in Materials and Methods (Chapter 2.2.6 on page 53). Three cell lines were studied thoroughly, one of lower A_1R-GFP-Gα_i expression from gate 1 of the single cell sort and two of higher expression from gate 4. The cells were transferred to chambered microscope coverslips containing media 24 hours before visualisation. Typically the cells of higher expression grew more slowly, were larger and showed greater variation in cell morphology and A_1R-GFP-Gα_i localisation. In general the cells appeared to show accumulation of the A_1R-GFP-Gα_i construct in perinuclear regions of the cell and in the cell membrane. A small number of cells from high expression cell lines were too large to fit in the camera's field of vision shown in Figure 3.4 on page 67. Growth in the presence of 10^{-7} M of the A_1R antagonist DPCPX did not obviously alter the distribution of A_1R-GFP-Gα_i fluorescence or the general appearance of the cells, suggesting increased stimulation of expressed A_1R by endogenously produced adenosine at greater levels of receptor expression was

Figure 3.1 Flow cytometry profile of the polyclonal A_1R-GFP-Gα_i cell line.

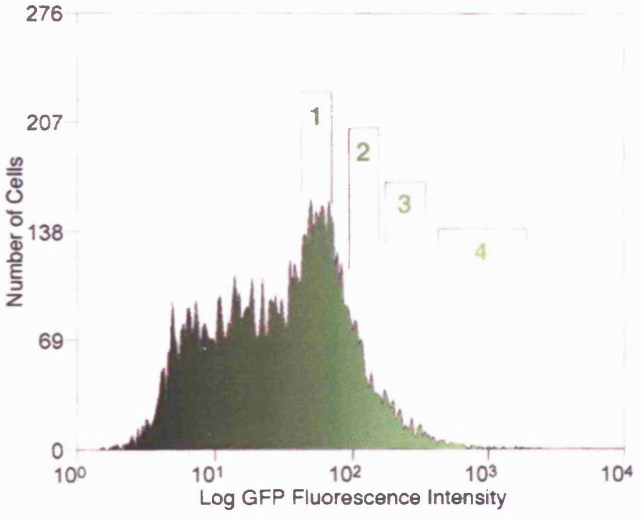

Figure 3.1: Flow cytometry profile of the stable polyclonal A_1R-GFP-Gα_i cell line prior to sorting 96 individual cells within each of the four gates shown (1 to 4). Six isolated cells from each gate were grown successfully to confluency (only five from gate 4) and stocks stored in liquid nitrogen. GFP fluorescence (x-axis) is in arbitrary units of fluorescence.

Figure 3.2 Flow cytometric analysis of cell lines expressing the A_1R-GFP-Gα_i fusion construct.

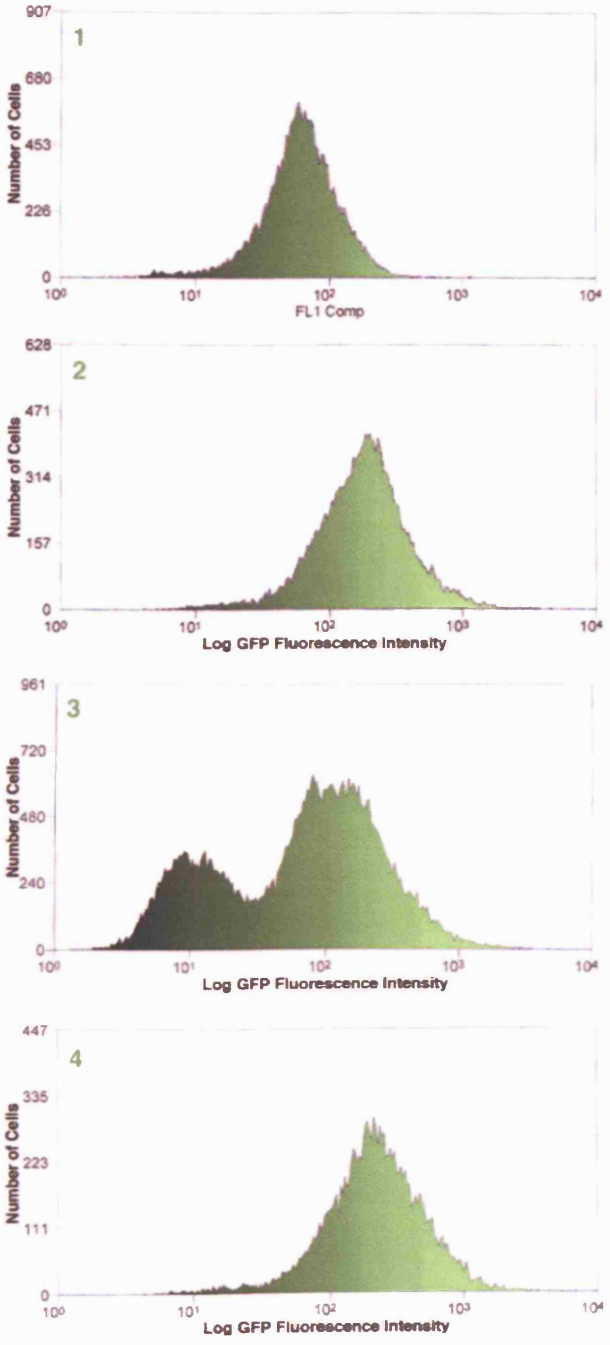

Figure 3.2: Flow cytometric analysis of cell lines originating from single cells selected within each of the four gates (1 to 4) described in Figure 3.1 on the previous page. Cell line 3 shows two populations of different GFP brightness. See Table 4.3 on page 95 for equilibrium binding properties of membranes prepared from the cell lines shown here (1=1C1, 2=2A3, 3=3A3, 4=4F2). GFP fluorescence (x-axis) is in arbitrary units of fluorescence.

Figure 3.3 The selection of individual cells expressing the A_1R-GFP fusion construct.

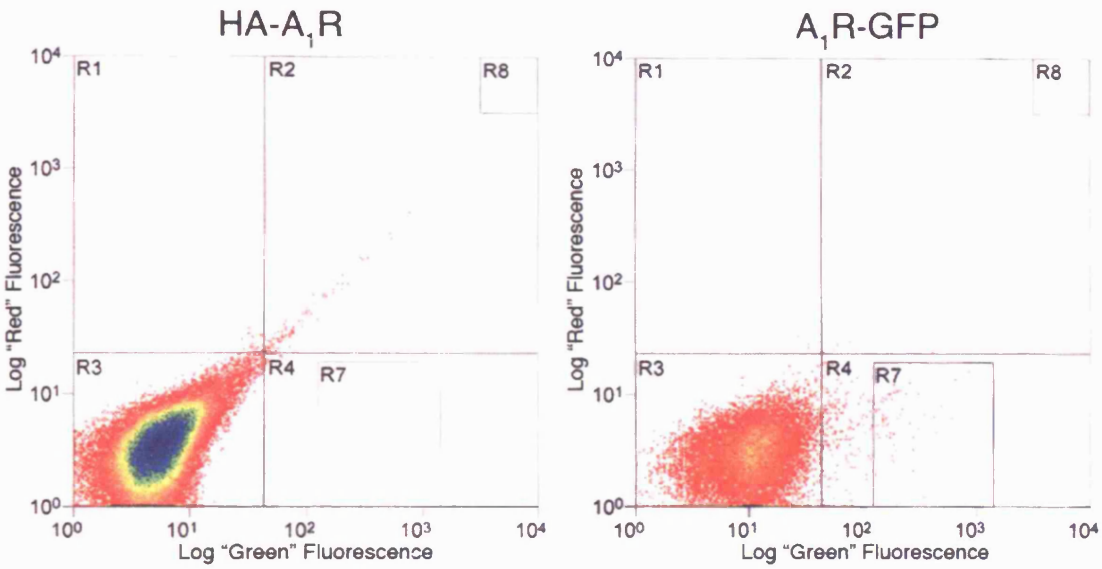

Figure 3.3: FACS plots of GFP brightness (x-axis; fluorescence intensity using 530±20 nm "green" emission filter) against a measurement of cell autofluorescence and therefore cell size (y-axis; fluorescence intensity using 570±20 nm "red" emission filter). Fluorescence intensity is expressed in log arbitrary units of fluorescence as in Figures 3.1 and 3.2.

A stable polyclonal CHO cell line expressing the A_1R-GFP construct was referenced against a stable CHO cell line expressing HA-tagged A_1R (HA-A_1R). In general, the A_1R-GFP cell line showed a low level of A_1R-GFP expression. Two 96-well plates of individual cells were selected from region R7 of the A_1R-GFP plot. A variety of slow and fast growing colonies were grown from individual cells into mature cell lines, and 24 chosen for use in this study. 17429 cells are shown on the A_1R-GFP plot, of which 60 (0.34%) fall within region R7. 75006 cells are shown on the HA-A_1R plot, of which none are found in region R7.

not responsible for slower growth and variations in cellular morphology.

Cell lines expressing the A_1R-GFP construct showed a cellular morphology and GFP localisation that could not be distinguished from that shown for A_1R-GFP-Gα_i in Figure 3.4 (data not shown).

3.4 Western blot analysis of cell membranes expressing the human adenosine A_1 receptor and GFP fusion constructs.

Antibodies against the adenosine A_1 receptor, GFP and Gα_i were used to identify the presence and molecular constitution of the A_1R-GFP and A_1R-GFP-Gα_i fusion constructs in membrane preparations used for radioligand binding analysis. Details of the antibodies used in the Western blots shown in this Chapter, and throughout the rest of this study are described in Table 2.1 on page 57. Figures 3.5 and 3.6 (pages 71 and 72 respectively) show representative Western blots of solubilised membrane preparations expressing the adenosine A_1 receptor and the A_1R fusion constructs. Along with membranes prepared from the the A_1HE and A_1LE cell lines, a selection of A_1R-GFP and A_1R-GFP-Gα_i membranes were chosen expressing the fusion constructs over a range of densities. Membranes from A_1R-GFP cell lines 5H6, 5C6, 6E10 and 5E10 covered a 6-fold range of receptor expression from 1.3 to 8.2 pmol/mg protein (see Table 4.3 on page 95 for further equilibrium binding details). A_1R-GFP-Gα_i membranes 2H7, 3D4, 4E8 and 4H1 showed a 7-fold range of receptor expression from 1.8 to 13.4 pmol/mg protein (Table 4.3). Membranes prepared from A_1HE and A_1LE cell lines showed a 13-fold range in adenosine A_1 receptor density with mean levels of receptor expression ([^{3}H]DPCPX B_{max}) of 8.19 $\pm$ 0.35 and 0.60 $\pm$ 0.12 pmol/mg protein respectively (n = 5).

Membranes prepared from a stable CHO cell line expressing the human M_1 muscarinic receptor (M_1R) were a kind gift from Dr Sebastian Lazareno (MRC Technology) and were chosen as a negative control for the Western blots. However, A_1R antibody ab3460 identified a band of the same size as the human adenosine A_1 receptor (approximately 37 kDa) within the M_1R membranes (lane 3 on Figure 3.5a). 3 nM [^{3}H]DPCPX showed no significant specific binding at these M_1R membranes (data not shown). In view of this nonspecific band at 37 kDa in the M_1R membranes, another adenosine A_1 receptor antibody (ab13295) was utilised (Figure 3.5b). This antibody is directed at the third intracellular loop of the receptor compared to the extreme C terminus for ab3460 (Table 2.1). A_1R antibody ab13295 also identified a band running at similar speed to the 39 kDa pre-stained marker in all samples, although there was greater contrast in intensity between the A_1HE and A_1LE bands (lanes 1 and 2, Figure 3.5b). With longer periods of exposure to

Figure 3.4 Fluorescence microscopy of live cells expressing the A_1R-GFP-Gα_i fusion construct.

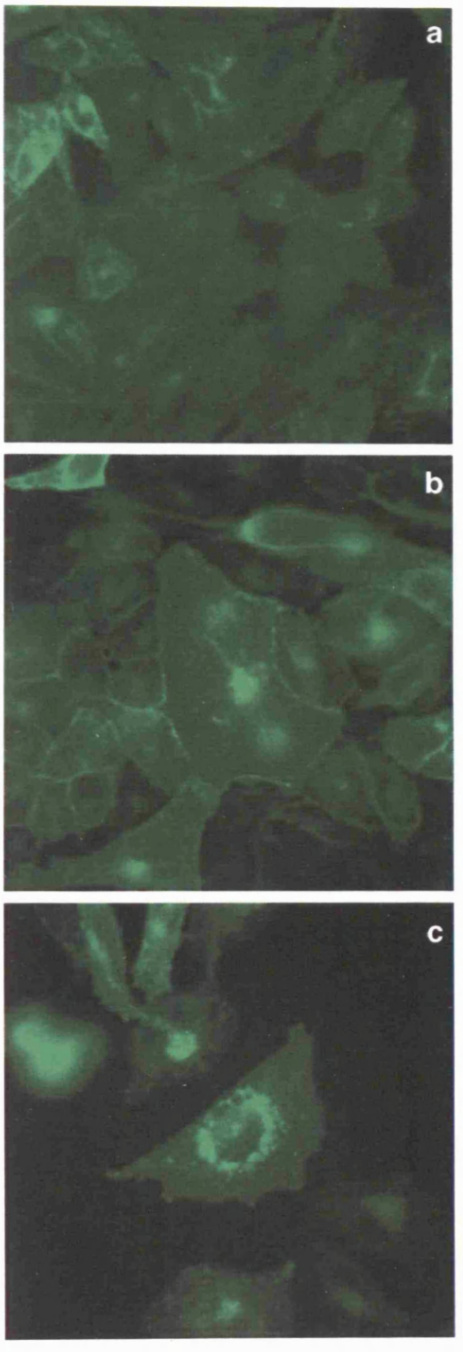

Figure 3.4: Typical cellular localisation of the A_1R-GFP-Gα_i fusion protein expressed in cells selected in gate 1 (a) and 4 (b and c) of single cell sort described in Figure 3.1 on page 63.

autoradiography film, ab13295 identifies weak bands in lanes 1 and 3 corresponding to the size of the A_1R which are not visible on the blot shown in Figure 3.5b. Therefore the specificity of the ab13295 primary antibody for the adenosine A_1 receptor alone is not absolute and it only detects high levels of adenosine A_1 receptor expression. Primary antibody ab13295 also identified several other "non-specific" bands of which only one is visible in Figure 3.5b, of greater mobility than the 39 kDa band. It was not investigated whether this band indicates proteolysis or "nicking" of the adenosine A_1 receptor or whether it is one of the several non-specific bands identified by antibody ab13295. The intensity of these other non-specific bands was entirely independent of [^{3}H]DPCPX B_{max} and they appear unlikely to be the adenosine A_1 receptor.

Western blot analysis of A_1HE and A_1LE membranes.

The human adenosine A_1 receptor has an estimated molecular size of 37 kDa in the absence of any glycosylation (Figure 1.9 on page 46). As described above, a sharp band close to the 39 kDa pre-stained marker was observed in all samples using the adenosine A_1 receptor antibody ab3460 (Figure 3.5a). This band is within the expected range of molecular weight for the adenosine A_1 receptor but as it was observed in all samples, even in membranes expressing the human M_1 muscarinic receptor (M_1R) it is assumed to reflect a non A_1 receptor protein. The slight increase in intensity and "fuzziness" of the A_1HE sample (lane 2) in Figure 3.5a is in agreement with the A_1R antibody ab3460 labelling a broad 39 kDa band with low sensitivity. Western blot analysis using A_1R antibody ab13295, such as that shown in Figure 3.5b, showed a greater degree of contrast between A_1LE and A_1HE membrane samples (lanes 1 and 2 respectively). Both A_1R antibodies identified a stronger broad band at 39 kDa in A_1HE samples than A_1LE, which is consistent with this band being, or at least containing, the adenosine A_1 receptor.

Western blot analysis of A_1R-GFP and A_1R-GFP-Gα_i membranes.

The A_1R-GFP construct has a theoretical molecular size of 64 kDa (37 and 27 kDa for A_1R and GFP respectively). Lanes 4 to 7 of both Figures 3.5a and 3.5b show a band likely to be A_1R-GFP but which runs faster than the 64 kDa pre-stained marker. A lower intensity band at the same mobility in the blots was more clearly observed in lane 4 following longer exposure (not shown). The A_1R-GFP band is routinely characterised as a "fuzzy" band rather than a crisp distinct band even following short exposures (not shown). As described above, both A_1R antibodies identified a band of approximately 39 kDa in all samples including the A_1R-GFP and A_1R-GFP-Gα_i membranes. These bands may represent non-specific labelling by the antibodies rather than the presence of non-fusion adenosine A_1 receptor in the membrane preparations. The small band in lane 8 in

Figure 3.5a was an artifact of that particular gel rather than the sample, and was not observed in other Western blots of the same sample (such as Figure 3.5b).

In all samples the A_1R-GFP-Gα_i construct was identified as two closely spaced bands, or "doublet," illustrated in lanes 8 to 11 in Figures 3.5a and 3.5b. The A_1R-GFP-Gα_i band in lane 8 in Figure 3.5a was visualised more clearly following longer exposures (not shown). The molecular explanation of the doublet is not clear although the slower moving band could represent glycosylated receptor. The A_1R-GFP-Gα_i doublet was observed when using antibodies for A_1R (Figures 3.5a and 3.5b), GFP (Figure 3.6) and Gα_i (Figure 3.5c).

In A_1R-GFP-Gα_i membranes the A_1R antibodies routinely identified two weak bands of greater molecular size than the strong A_1R-GFP-Gα_i doublet. These two higher molecular size bands can be seen in Figure 3.5 using A_1R antibody ab13295 (A_1R-GFP-Gα_i lanes 9–11) and Figure 3.6 using A_1R antibody ab3460. These bands of greater molecular size were very faint relative to the main A_1R-GFP-Gα_i bands.

The A_1R-GFP-Gα_i doublet ran slightly faster than the 97 kDa pre-stained marker, however the A_1R-GFP-Gα_i construct is expected to show a molecular size of 104 kDa. The Invitrogen See Blue Plus2 pre-stained markers utilised in Figures 3.5 and 3.6 may not accurately identify the expected molecular size of the A_1R-GFP and A_1R-GFP-Gα_i fusion constructs. Figure 3.7 on page 73 compares estimates of different pre-stained protein markers with un-stained protein standards, generally considered to be more accurate. The un-stained markers (lane c of Figure 3.7) are in better agreement with the expected molecular sizes of the fusion constructs. The Invitrogen See Blue Plus2 Pre-stained markers may be underestimating the molecular size of the bands of greater size.

Two of the A_1R-GFP-Gα_i membranes in Figures 3.5a and 3.5b (lanes 10 & 11) contain a truncated construct identified by antibodies for A_1R and GFP, but not Gα_i (Figure 3.5c). This is suggestive of proteolysis of the full-length construct and may be due to cleavage or degradation of part of the fused Gα_i possibly during cell growth as membrane preparations were performed on ice at all times in order to reduce protein degradation. The presence of EDTA in membrane preparation buffers will also have helped to further inhibit the action of proteases dependent on divalent cations.

The expected molecular weight of endogenous human G$\alpha_{i\text{-}1}$ is approximately 40 kDa (Bray *et al.* 1987) and the Gα_i antibody used in Figure 3.5 identifies, as expected, a band of this size in all of the membranes used, including the larger A_1R-GFP-Gα_i construct when present. The G$\alpha_{i\text{-}1}$ band however appears more intense in the membranes expressing higher levels of the A_1R-GFP-Gα_i construct, suggesting either limited proteolysis of the construct or up-regulation of native

$G\alpha_{i-1}$ expression.

3.5 Discussion.

The work presented in this chapter describes the creation of 23 stable CHO cell lines expressing the A_1R-GFP-$G\alpha_i$ fusion construct, and 24 stable CHO cell lines expressing the A_1R-GFP construct at different levels. Membranes prepared from these cell lines were used in the investigations described in the following chapters along with membranes prepared from CHO cell lines expressing the human adenosine A_1 receptor at two different levels (A_1LE and A_1HE). Figure 3.8 on page 77 shows the four gate approach versus one gate used for FACS isolation of individual cells resulted in similar ranges of expression of both GFP fusion constructs. Little difference was observed in the mean level of A_1R-GFP-$G\alpha_i$ expression from cell lines selected in gates 1 and 2. Cell lines grown from cells selected within gates 3 and 4 showed higher levels of A_1R-GFP-$G\alpha_i$ expression. All but two of the A_1R-GFP-$G\alpha_i$ cell lines fell within the range of receptor expression of the A_1R-GFP cell lines selected using just one gate. Both approaches appear to successfully create a series of cell lines expressing their GFP fusion protein at a similar range of densities. Membranes prepared from the polyclonal A_1R-GFP cell line before FACS showed no specific [^{3}H]DPCPX binding. The growth of mature cell lines from individual cells showing GFP fluorescence provides a means of rescuing the expression of the A_1R-GFP construct.

Typically cell lines expressing greater levels of either fusion construct grew more slowly. This relationship is visualised in Figure 3.9 on page 78 where cell lines with a higher [^{3}H]DPCPX B_{max} took significantly longer ($P = 0.005$) to progress from single cells to harvested membrane preparations. A similar significant relationship ($P = 0.02$) was observed when the period of incubation in 1750 cm^2 roller bottles before membrane preparation was plotted against [^{3}H]DPCPX B_{max} (data not shown). To investigate whether stimulation of the adenosine A_1 receptor by endogenously produced adenosine or by the constitutive activity of the receptor slowed the growth of cell lines expressing greater levels of the fusion constructs, membranes were prepared from both high and low expressing cell lines grown in the presence of the inverse agonist DPCPX (10^{-7} M). No differences in cellular morphology or equilibrium radioligand binding properties were observed (data not shown), suggesting that stimulation of the A_1R by endogenous adenosine was not contributing to the slower growth of highly expressing cell lines.

There was a degree of heterogeneity between different cell lines expressing the same construct. As well as differences in the level of expression of the construct ([^{3}H]DPCPX B_{max}), differences were observed in the molecular composition of the expressed construct and the FACS GFP profiles.

Figure 3.5 Western blots of membranes containing A_1R and GFP fusion constructs.

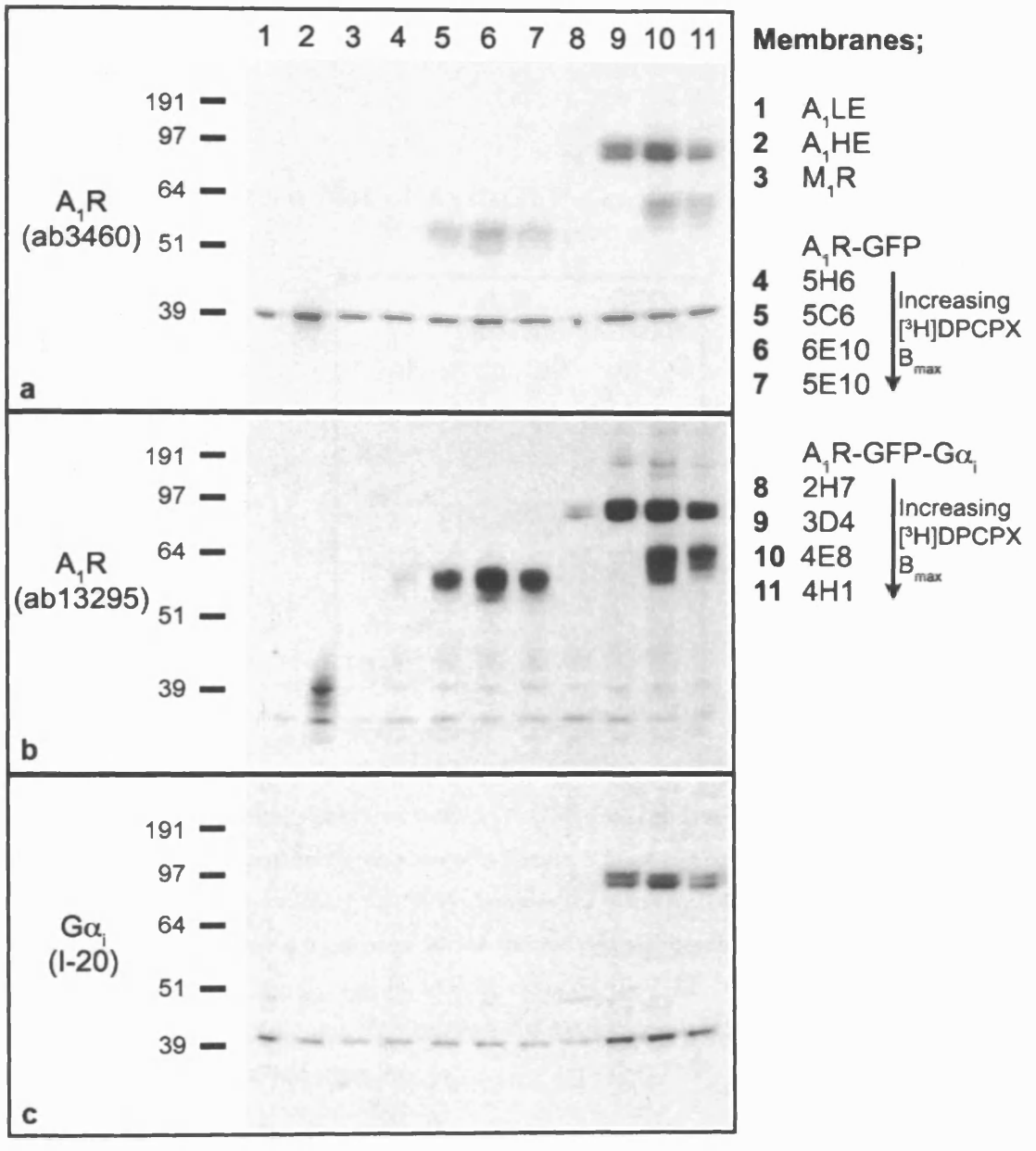

Figure 3.5: Membranes from cell lines expressing different levels of A_1R and both fusion constructs were probed by Western blot using two A_1R antibodies (**a** and **b**) and an antibody for $G\alpha_i$ (**c**). 20 μg of total membrane protein was loaded in each well. Invitrogen See Blue Plus2 Pre-stained markers are shown with molecular weights indicated in kDa.

Figure 3.6 Western blot of A_1R-GFP-Gα_i fusion constructs for A_1R and GFP.

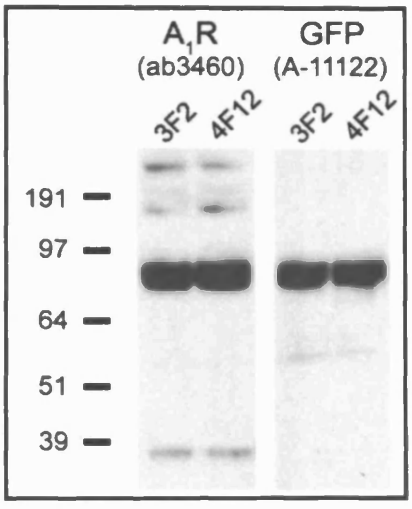

Figure 3.6: Using membranes prepared from A_1R-GFP-Gα_i cell lines 3F2 and 4F12, A_1R antibody ab3460 identifies the same bands as shown in Figure 3.5 on the previous page. Western blot of the membranes using an antibody for GFP identifies the same A_1R-GFP-Gα_i doublet band as the A_1R antibody. See Table 4.3 on page 95 for the radioligand binding properties. The very faint band observed between the 51 and 64 kDa markers on the GFP blot is also observed in A_1HE and A_1LE membranes. See Figure 7.6 on page 193 for a Western blot using the GFP antibody on fractionated A_1R-GFP membranes.

Figure 3.7 Comparison of the pre-stained markers used for Western blot analysis with unstained protein standards.

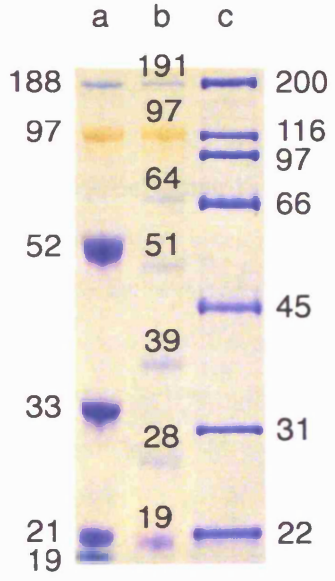

Figure 3.7: The Invitrogen SeeBlue Plus2 Pre-Stained Standard used throughout the Western blots presented in this study (**lane b**) were compared to Invitrogen MultiMark Multi-Colored Standard (**lane a**) and Bio-Rad un-stained Broad Range SDS-PAGE Standards (**lane c**; visualised by Coomassie Blue stain). All molecular sizes indicated are in kilodaltons. Electrophoresis conditions and buffers used were the same as for all gels prior to Western blot.

Figures 3.5a and 3.5b show two of the A_1R-GFP-Gα_i membrane preparations contain a truncated construct missing a large fraction of the Gα_i component (lanes 10 and 11) while two other A_1R-GFP-Gα_i membrane preparations showed no evidence of truncation even after prolonged exposure of the X-ray film (not shown). Proteolysis, or incomplete translation, of the A_1R-GFP-Gα_i construct may still result in functional receptor without large effects on binding or function being observed.

Figure 3.2 shows that despite originating from a single selected cell, some of the fusion cell lines may not be monoclonal and may have at some point in their growth split into two populations expressing different levels of the receptor. Also of interest is the FACS profile of cell line 4F2 in Figure 3.2. 4F2 was grown from a single cell which showed a large GFP signal (gate 4 in Figure 3.1). Despite this selection, the mature cell line showed a relatively low level of A_1R-GFP-Gα_i expression with a [^{3}H]DPCPX B_{max} of less than 3 pmol/mg protein (Table 4.3 and is also clearly distinguished in Figure 3.8). However, Chapter 4 shows that features of agonist binding to membranes prepared from cell line 4F2, including the fraction of total agonist binding which is of high affinity (fr_H), show more similarity with cell lines expressing the construct at a much higher density. Again, there appears to be heterogeneity between the cell lines characterised even at similar levels of receptor expression.

Striking visual differences were observed between cell lines expressing different levels of the fusion constructs. Although hard to present quantitatively, cell lines expressing lower levels of the fusion constructs were more homogeneous in appearance. The cell lines characterised by greater [^{3}H]DPCPX B_{max} were more varied in their morphology and showed great differences in their size with some cells many times larger than the normal size observed at low levels of expression. Although analysis was very qualitative, there appear to be cell morphological consequences to increased expression of either the A_1R-GFP or A_1R-GFP-Gα_i fusion construct.

Other studies have characterised the cellular localisation and molecular composition of membranes prepared from CHO cell lines expressing adenosine A_1 receptor fusion constructs. By means of Western blot analysis, Bevan *et al.* 1999 reported successful identification of the human adenosine A_1 receptor alone, and A_1R-Gα_i and A_1R-GFP-Gα_i fusion constructs. Similar to the results presented in Figures 3.5a and 3.5b, a faint band of the same size as the A_1R alone was observed in the membranes expressing the fusion constructs. The A_1R alone can be discerned, but was not described by the paper, as a "doublet" within a generally fuzzy band. However it is not possible to detect in their published Western blot whether the A_1R-Gα_i and A_1R-GFP-Gα_i fusion constructs are present as doublets or not. The paper did not include information on whether they observed high molecular sized A_1R-GFP-Gα_i bands as described here Figures 2.2, 3.5b, and 3.6.

GPCRs show different extents of glycosylation and different sensitivities to disruption of glycosylation, for example by treatment with tunicamycin (an inhibitor of glycosylation) or site-directed mutagenesis. Different GPCRs expressed in the same type of cell line can show different responses to the inhibition of glycosylation. For example, the treatment with tunicamycin of S49 cells (a mouse lymphoma cell line) which express the prostaglandin E_1 receptor (a GPCR) decreases E_1 receptor function whereas tunicamycin has no effect on the expression, binding and function of β-adrenergic receptors expressed by S49 cells (George *et al.* 1986). Glycosylation may also contribute to heterogeneous Western blot observations and can show effects including "fuzzy" bands, two bands in close proximity ("doublets"), or bands of greatly different molecular size (as for muscarinic receptors; see van Koppen and Nathanson, 1990). The human prostacyclin receptor (also a G protein-coupled receptor) shares a number of similar characteristics with the adenosine A_1 receptor. The human prostacyclin receptor activates adenylate cyclase by means of G_s proteins, and has a molecular weight of approximately 41 kDa with an N-linked glycosylation site on its short N-terminus (16 residues compared to 10 residues for the A_1R N-terminus). Glycosylation of the human prostacyclin receptor has been observed by Western blot as two bands in close proximity with the band of greater mass removed after the treatment of cells with tunicamycin (Zhang *et al.* 2001). The "fuzziness" of lane 2 in Figures 3.5a and 3.5b and the fusion protein "doublets" may be indications of glycosylation of the adenosine A_1 receptor. Both the A_1 and A_{2A} adenosine receptors contain a potential N-linked glycosylation site in the second extracellular loop. Figure 1.9 on page 46 shows this asparagine residue at position 159 for the human adenosine A_1 receptor. The adenosine A_1 receptor has been reported to exist in a glycosylated form in rat cerebral cortex and adipose tissue, migrating to approximately 38 kDa (Stiles 1986). Following treatment with endoglycosidase F in order to remove any N-linked or complex carbohydrate chains, the A_1 receptor was estimated at 32 kDa in both cerebral and adipose tissue. The A_1 receptor was relatively insensitive to α-mannosidase providing evidence for glycosylation of largely complex-type carbohydrate chains. The implications and functional significance of A_1 receptor glycosylation are unknown. The adenosine A_{2A} receptor from bovine brain contains one glycosylation site containing either complex or high mannose-type carbohydrate chains (Barrington *et al.* 1990). It would have been possible to investigate the importance of glycosylation for adenosine A_1 receptor activation by treating the cells with tunicamycin prior to membrane preparation, or the membranes with α-mannosidase and endoglycosidase F to investigate the type of any glycosylation present. This was not investigated.

In summary, the results presented in this Chapter describe the isolation of individual cells, expressing either the A_1R-GFP or A_1R-GFP-Gα_i fusion constructs, from which mature cell lines

were grown. The characterisation of selected mature cell lines by microscopy, FACS and Western blot analysis showed a level of heterogeneity of both the cellular morphology and molecular composition between cell lines expressing the same A_1R fusion construct.

Membranes prepared from the cell lines created and characterised in this chapter were then studied in detail, the results of which are presented in the Chapters that follow. Chapter 4 investigates the effect of receptor expression level on equilibrium binding properties of the A_1R using the A_1R-GFP and A_1R-GFP-$G\alpha_i$ membranes. Chapter 6 uses the fusion membranes to investigate the dependence of the kinetics of binding on the level of A_1R expression. Chapter 7 investigates the localisation of the A_1R-GFP and A_1R-GFP-$G\alpha_i$ fusion proteins in domains of the cell membrane isolated by means of density gradient fractionation.

Figure 3.8 The level of receptor expression related to flow cytometry selection.

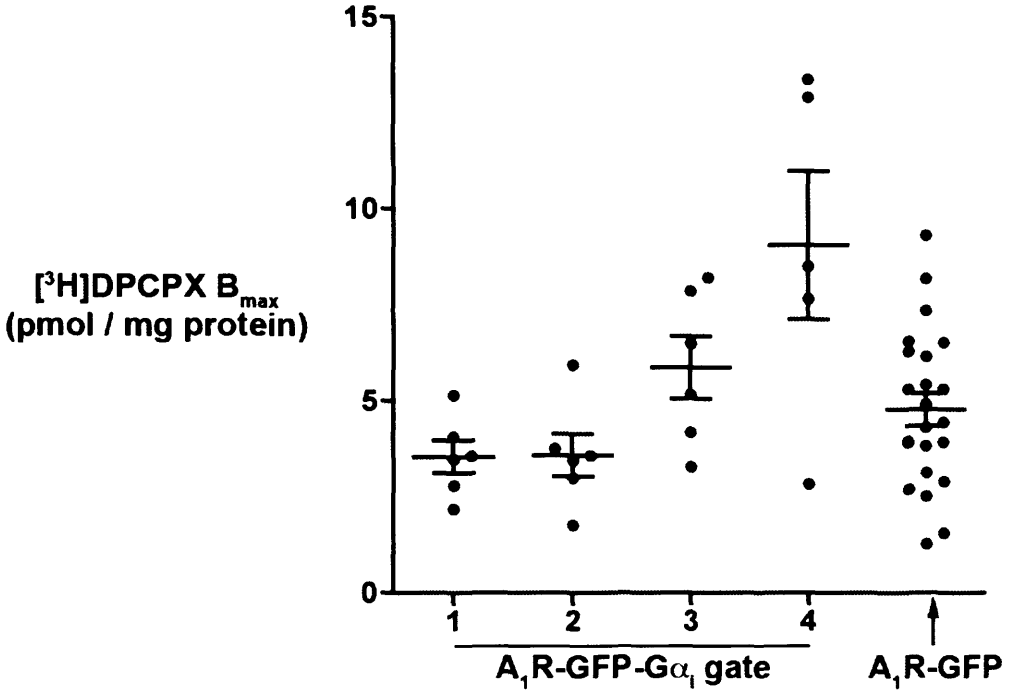

Figure 3.8: The [^{3}H]DPCPX B_{max} of A_1R-GFP-Gα_i membranes prepared from cell lines grown from individual cells selected by gates 1 to 4, as described in Figure 3.1 on page 63. The mean [^{3}H]DPCPX B_{max} ($\pm$ s.e.m.) for membranes from cell lines selected by each flow cytometry gate is indicated by the black bar. For comparison, the [^{3}H]DPCPX B_{max} of A_1R-GFP membranes are shown. Individual A_1R-GFP cells were selected using only one gate, as described in Figure 3.3 on page 65. The [^{3}H]DPCPX B_{max} data illustrated above is listed in Table 4.3 on page 95.

Figure 3.9 Cell lines expressing greater levels of A_1R-GFP-Gα_i and A_1R-GFP fusion proteins typically grow more slowly.

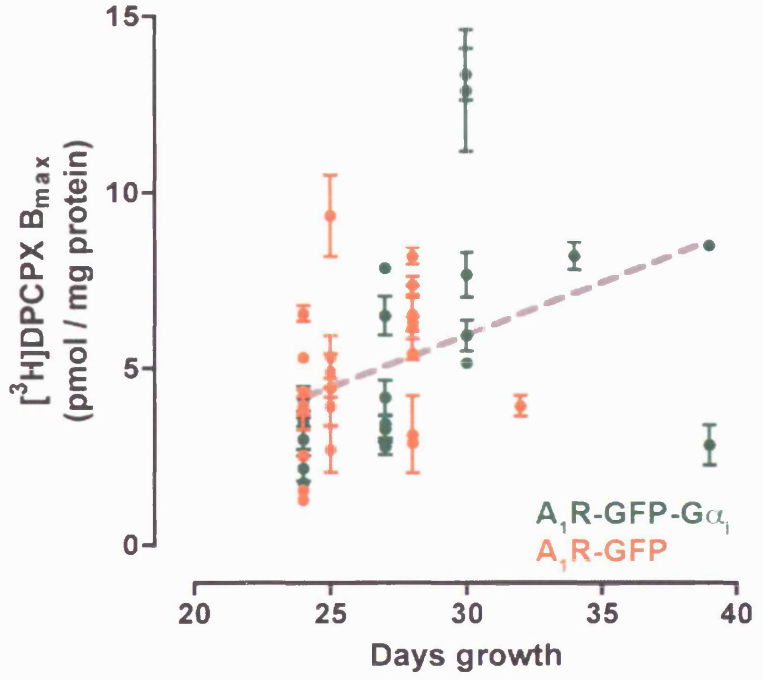

Figure 3.9: The graph describes the dependence of the level of receptor expression (y-axis) on the period of growth (x-axis) from a single cell to the harvesting of membrane preparations. Non-linear regression of combined A_1R-GFP-Gα_i and A_1R-GFP data generated a line with a significantly non-zero slope, indicated by broken line (slope = 0.3, P = 0.005). A similar significant relationship (P = 0.02) was observed using the period of growth in 1750 cm^2 roller bottles prior to membrane preparation rather than total days growth shown above (data not shown).

Chapter 4

The effect of receptor expression level on equilibrium binding properties of the human adenosine A_1 receptor.

4.1 Introduction.

Previous studies within the receptor group at NIMR have investigated aspects of the binding and functional properties of the human adenosine A_1 receptor (Cohen, 1995; Cohen *et al.*, 1996a,b). Two stable CHO cell lines recombinantly expressing the adenosine A_1 receptor at low (A_1LE) and high (A_1HE) densities have also been useful for comparing predictions of mathematical models of drug receptor interactions with binding properties of the A_1R (Browning, 2003; Browning *et al.*, 2000a,b,c). Subtle differences observed in the equilibrium radioligand binding properties and the kinetics of radioligand association of the two cell lines were associated with more profound differences in the dissociation of radioligands at the two levels of A_1R expression.

Chapter 3 describes the creation and molecular characterisation of a series of cell lines expressing the GFP fusion proteins A_1R-GFP and A_1R-GFP-Gα_i at different densities. The aim of the work presented in this Chapter was to examine whether the equilibrium binding properties of the A_1R-GFP and A_1R-GFP-Gα_i fusion proteins;

- differ from each other and the A_1R alone, and
- whether these properties are sensitive to the level of receptor expression.

4.2 Radiolabelled agonist and antagonist saturation equilibrium binding to the human adenosine A_1 receptor expressed at two different densities.

The equilibrium agonist and antagonist binding properties of membranes prepared from A_1LE and A_1HE cell lines were characterised in order to provide core A_1R binding data against which the GFP fusion proteins could be compared. If the A_1R-GFP and A_1R-GFP-Gα_i fusion proteins showed similar agonist and antagonist binding affinities as the A_1R alone, then the series of cell lines described in the previous Chapter would be useful as a model of the effect of receptor expression level on adenosine A_1 receptor behaviour.

Specific binding of the A_1R antagonist [^{3}H]DPCPX and agonist [^{3}H]CHA to both A_1LE and A_1HE membranes was saturable (Figure 4.1 on the next page). [^{3}H]DPCPX bound to A_1LE membranes with B_{max} 0.60 $\pm$ 0.12 pmol/mg protein and log affinity constant (log K_A) 8.62 $\pm$ 0.06 (n = 5), and to A_1HE membranes with B_{max} 8.19 $\pm$ 0.35 pmol/mg protein and log K_A 8.72 $\pm$ 0.03 (n = 5) (see Table 4.1 on page 88). [^{3}H]CHA bound to A_1LE membranes with B_{max} 0.38 $\pm$ 0.05 pmol/mg protein and log K_A 8.48 $\pm$ 0.08 (n = 7), and to A_1HE membranes with B_{max} 3.20 $\pm$ 0.27 pmol/mg protein and log K_A 8.60 $\pm$ 0.05 (n = 7). In general, A_1HE membranes exhibited a 14 fold greater total number of A_1R binding sites ([^{3}H]DPCPX B_{max}) than A_1LE membranes. [^{3}H]CHA bound with high affinity to a smaller population of binding sites than [^{3}H]DPCPX in both A_1LE and A_1HE (Table 4.1), consistent with well established observations of agonist binding heterogeneity at the adenosine A_1 receptor (Cohen *et al.*, 1996b) and GPCRs in general (for example Birdsall *et al.*, 1978). The fraction of high affinity agonist binding sites was greater for A_1LE relative to A_1HE (0.63 versus 0.39). Unpaired t tests showed no significant difference between the A_1HE and A_1LE mean log affinity constants, for both [^{3}H]DPCPX and [^{3}H]CHA. Also, the affinities of [^{3}H]DPCPX and [^{3}H]CHA for the adenosine A_1 receptor were indistinguishable, showing no significant difference in unpaired t tests. Therefore both [^{3}H]DPCPX and [^{3}H]CHA showed no difference in affinity between A_1HE and A_1LE membranes, and the affinities of [^{3}H]DPCPX and [^{3}H]CHA themselves were indistinguishable although independent. Unpaired t tests showed a significant difference between A_1HE and A_1LE B_{max} in the case of both [^{3}H]DPCPX and [^{3}H]CHA ($P < 0.0001$). Difference in means was considered significant only if $P < 0.05$ (as described in Chapter 2.3.3 on page 59).

All radioligand binding experiments described in this Chapter were incubated for one hour, unless otherwise stated, before filtration onto glass fibre filters. Experiments investigating the

Figure 4.1 [^{3}H]Antagonist and [^{3}H]agonist saturation curves at the A_1R expressed at two densities.

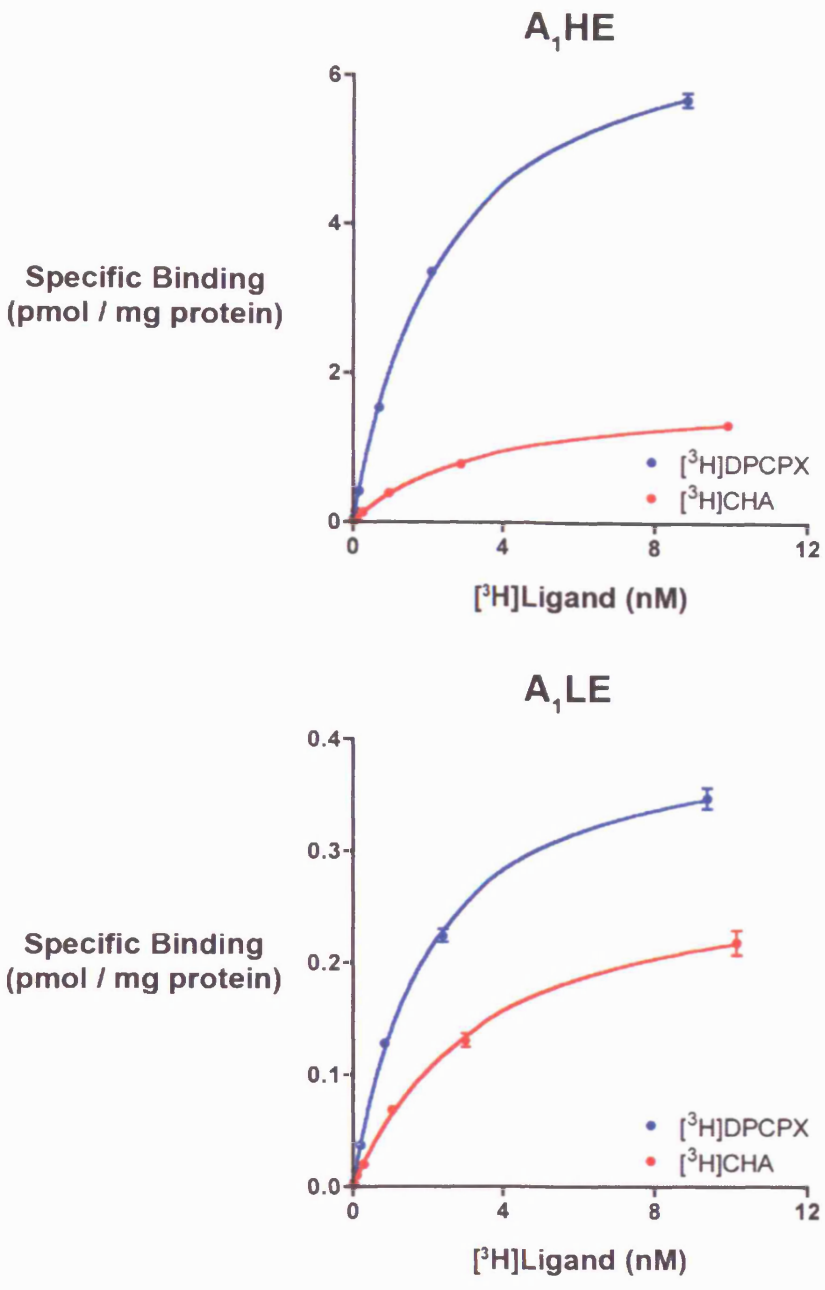

Figure 4.1: Representative saturation curves for the binding of [^{3}H]DPCPX (antagonist) and [^{3}H]CHA (agonist) to A_1HE and A_1LE membranes. The best fit parameters estimated by non-linear regression of the above curves were; [^{3}H]DPCPX log affinity 8.63 & 8.73 and B_{max} 7.23 & 0.42 pmol/mg protein (A_1HE and A_1LE respectively), [^{3}H]CHA log affinity 8.48 & 8.47 and B_{max} 1.76 & 0.29 pmol/mg protein (A_1HE and A_1LE respectively). The means of estimated parameters are described in Table 4.1 on page 88. Data plotted above are mean ± s.e.m. of a single experiment performed in quadruplicate.

effect of incubation time on the saturation of A_1HE membranes by [^{3}H]CHA observed an increase in B_{max} between association times of 5 min and 4 hours when incubated at RT. Figure 4.2 on the following page shows [^{3}H]CHA saturation experiments performed using A_1HE membranes after six association times ranging from 5 min to 4 hours (240 min). The saturation data were transformed to a Scatchard plot which is also illustrated in Figure 4.2. The Scatchard plot provides an alternative means to visualise the B_{max} and K_D (x-axis intercept and $\frac{-1}{slope}$ respectively) of [^{3}H]CHA for A_1HE membranes at the six association times. However for quantitative analysis of saturation data the Scatchard plot is less reliable than direct non-linear regression.

Figure 4.3 on page 84 examines the dependence of [^{3}H]CHA B_{max} and K_D on the incubation time using non-linear regression data from two experiments, one of which is illustrated in Figure 4.2. The B_{max} of [^{3}H]CHA for A_1HE membranes increased exponentially with time extrapolating to a maximum of 4.1 pmol/ mg protein and to 2.2 pmol/ mg protein at zero time. While [^{3}H]CHA B_{max} increases from 5 min to 4 hours, the estimate of [^{3}H]CHA K_D appeared constant from 30 min to 4 hours (Figure 4.3). Periods of incubation of less than 30 min may unreliably estimate the affinity of [^{3}H]CHA. Unfortunately the errors are large, performing the experiment more than twice would likely reduce the errors however the interpretation would not be expected to change significantly.

Figure 4.3a may provide an insight into the availability of G protein to the adenosine A_1 receptor. The increase in [^{3}H]CHA binding after 30 minutes appears to be due to an increase in high affinity agonist binding capacity rather than a change in K_D. The rate of this increase in [^{3}H]CHA binding from the data shown in Figure 4.3a was 0.016 min^{-1}. Using the estimates of B_{max} which showed a constant K_D (30, 60, 120 and 240 min) the same estimates of the rate of increase and maximum B_{max} were obtained (0.0016 min^{-1} and 4.1 pmol / mg protein respectively). This rate of increase in available high affinity agonist binding sites may be a representation of the rate at which the adenosine A_1 receptor can recruit extra G protein from other regions of the cell membrane.

4.3 The effect of unlabelled ligands on binding of the radiolabelled antagonist [^{3}H]DPCPX to the human adenosine A_1 receptor expressed at two different densities.

The ability of unlabelled ligands to inhibit the binding of [^{3}H]DPCPX at the adenosine A_1 receptor was investigated. Three unlabelled antagonists (DPCPX, N0840 and theophylline) inhibited spe-

Figure 4.2 [^{3}H]CHA saturation curves of A_1HE membranes at different association times.

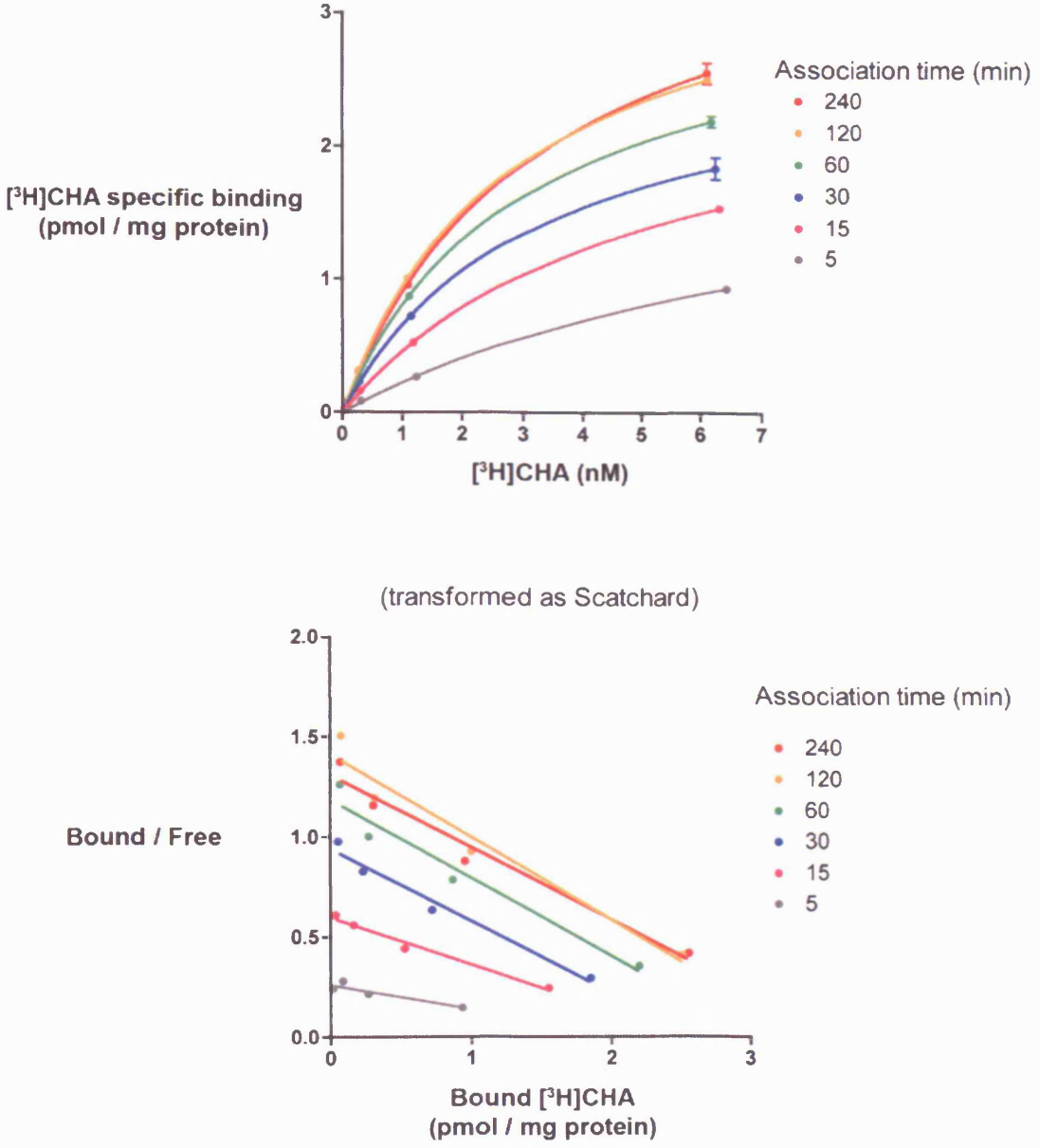

Figure 4.2: Representative [^{3}H]CHA saturation curves from a single experiment investigating the effect of the length of incubation (association time) on the saturation of A_1HE membranes by [^{3}H]CHA. [^{3}H]CHA B_{max} and affinity were estimated from non-linear regression of the saturation curves, and the curves were transformed to a Scatchard plot for visual inspection. The final assay volume was 100 μl and was performed at RT. Data were corrected for depletion of the concentration of [^{3}H]CHA.

Figure 4.3 The dependence of [^{3}H]CHA B_{max} and K_D with incubation time.

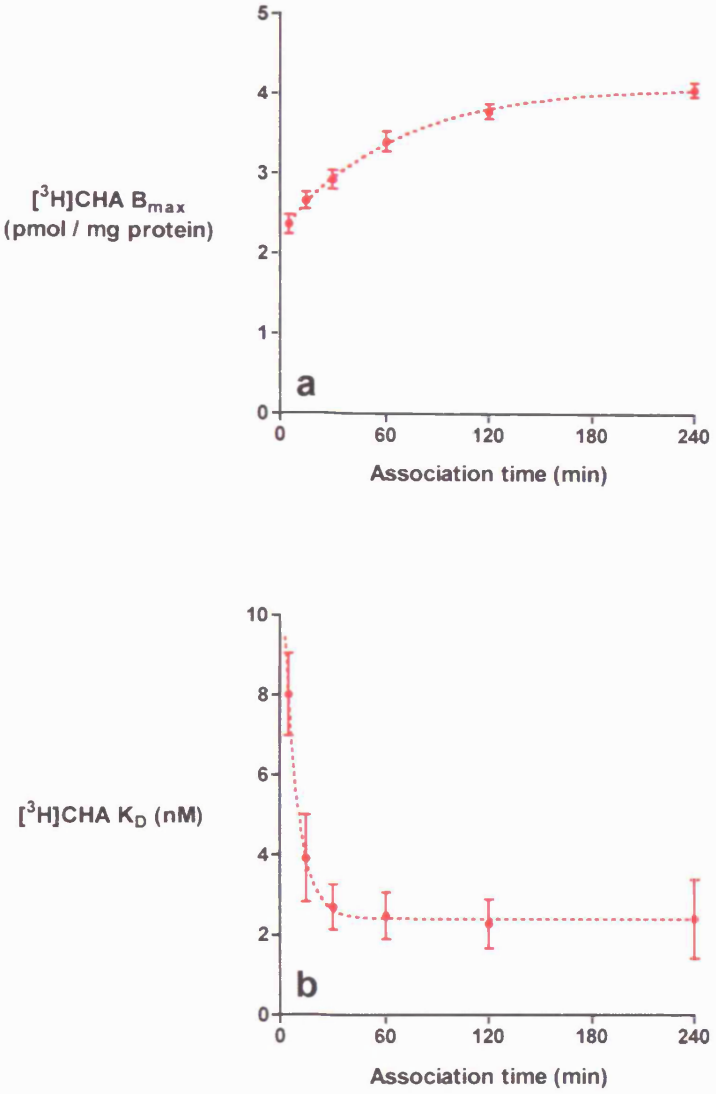

Figure 4.3: **(a)** [^{3}H]CHA B_{max} at A_1HE membranes increases exponentially with association time asymptoting to a maximum of 4.1 pmol / mg protein. **(b)** The estimate of [^{3}H]CHA K_D appears to be reliable from 30 min onwards. All data shown in the above Figures are the mean of two independent experiments (± s.e.m.) performed in a final volume of 100 μl at RT, one of which is illustrated in Figure 4.2 on the previous page. The estimates of [^{3}H]CHA B_{max} and K_D were obtained from nonlinear regression of saturation curves, and not from linear regression of Scatchard transformations (although the estimates obtained from the Scatchard plots were in general agreement with those from nonlinear regression).

cific [^{3}H]DPCPX binding over a 1000-fold range in affinity. As well as enabling the characterisation of ligands which are not radiolabelled, competition assays allow investigation of low affinity agonist binding which may occur at high concentrations that would make direct saturation prohibitive. The effect of two unlabelled agonists of high efficacy (CHA and PIA) on the binding of [^{3}H]DPCPX to A_1HE and A_1LE membranes was investigated. In addition, [^{3}H]DPCPX competition assays were used to examine the binding of three agonists of lower efficacy.

[^{3}H]DPCPX / antagonist competition experiments.

DPCPX, N0840 and theophylline inhibited 100% of the specific [^{3}H]DPCPX binding to A_1HE membranes (Figure 4.4 on the following page). N0840 bound with log affinity 6.23 ± 0.07 (n = 3) and theophylline with log affinity 5.40 ± 0.15 (n = 3). The log affinity of N0840 reported here is similar to a K_i of 0.54 μM reported in [^{3}H]PIA / N0840 competition experiments at rat cerebral cortex membranes (Ukena *et al.* 1987). The binding of DPCPX was of approximately 100-fold higher affinity than N0840. The Cheng Prusoff correction is not appropriate when the labelled and unlabelled ligands are the same. In this situation it is more appropriate to analyse the results as a saturation curve resulting from increasing degrees of isotopic dilution of [^{3}H]DPCPX by cold DPCPX. Possibly as a consequence of adsorption issues during the serial dilution of cold DPCPX the data in Figure 4.4 underestimates the affinity of DPCPX relative to that shown in direct [^{3}H]DPCPX saturation experiments (Table 4.1). The most accurate estimate of DPCPX affinity was obtained from the direct saturation curves (Table 4.1).

[^{3}H]DPCPX / agonist competition experiments.

The highly efficacious A_1R agonist CHA inhibited 100% of the specific [^{3}H]DPCPX binding to both A_1LE and A_1HE membranes in a biphasic manner (Figure 4.5 on page 89). The inhibition curves were analysed by a two-site model for which mean parameters are described in Table 4.2 on page 88. The observed high affinity CHA binding constant (log K_H A_1LE 8.75 ± 0.16 (n = 4), A_1HE 8.57 ± 0.06 (n = 7)) was similar to that observed in the saturation experiments (Table 4.1). Additionally, a low affinity CHA binding component was observed (log K_L A_1LE 5.68 ± 0.17 (n = 4), A_1HE 5.79 ± 0.05 (n = 7)), approximately 1000-fold lower in affinity. Unpaired t tests found no significant difference between the membranes from the two cell lines for both high and low CHA affinities. The observation of low affinity specific CHA binding agrees with the inability of [^{3}H]CHA to identify as many high affinity binding sites as [^{3}H]DPCPX when [^{3}H]CHA is used at nM concentrations (Table 4.1). The fraction of total CHA binding of high affinity (fr_H) observed in competition equilibrium binding assays was higher in A_1LE membranes (0.71 ± 0.02, n = 4) than

Figure 4.4 The displacement of [^{3}H]DPCPX binding by unlabelled antagonists.

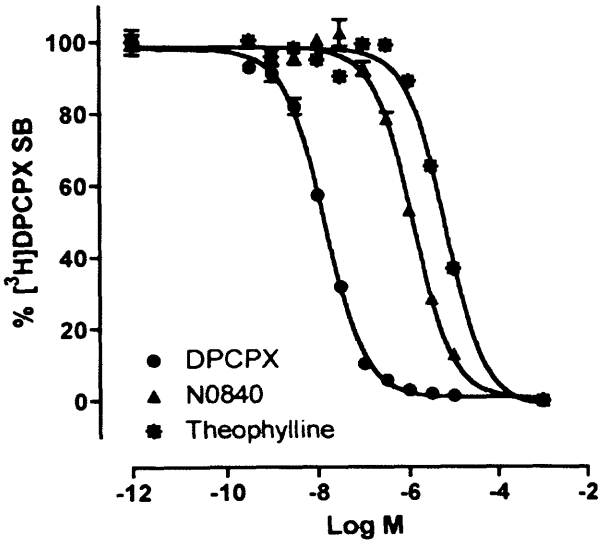

Mean parameters from the analysis of competition curves.

unlabelled ligand	log affinity (n = 3)
N0840	6.23 ± 0.07
Theophylline	5.40 ± 0.15
DPCPX*	8.12 ± 0.11*

Figure 4.4: Representative individual [^{3}H]DPCPX competition curves on A_1HE membranes using the antagonists N0840 and theophylline, and DPCPX for comparison. The mean [^{3}H]DPCPX concentration was 0.66 ± 0.08 nM (n = 3). Mean log affinity estimates of three independent experiments are shown in the table. * DPCPX competition curve and the estimate of mean log affinity is shown only for comparison, as Cheng Prusoff correction of [^{3}H]DPCPX / DPCPX competition curves is not appropriate. The estimate of DPCPX affinity here is an underestimate compared to direct [^{3}H]DPCPX saturation (Table 4.1 on page 88).

in A_1HE (0.52 ± 0.02, n = 7) as found in the direct saturation experiments. The mean estimates of fr_H for each cell line were significantly different (P = 0.0005). Similar to CHA, the A_1R agonist PIA inhibited all specific [^{3}H]DPCPX binding in a biphasic manner with log affinities 8.72 ± 0.03 and 6.17 ± 0.04 (n = 2). 54% of PIA binding was of high affinity (Table 4.2). The two estimates of fr_H using CHA and PIA for A_1HE membranes were in reasonable agreement with each other, although with only two observations using PIA this was not tested statistically. Therefore the difference in agonist binding between A_1LE and A_1HE membranes is due to a difference in fr_H and not a difference in either affinity.

[^{3}H]DPCPX / CHA competition assays on A_1HE membranes in the presence of 100 μM GTP exhibited only low affinity CHA binding (fr_H = 0). The mean log affinity of CHA for A_1HE membranes in the presence of 100 μM GTP was 5.68 ± 0.03 (n = 3), similar to the low affinity CHA binding component observed in the absence of GTP (Table 4.2).

For a number of reasons the [^{3}H]DPCPX / CHA competition assays were performed using concentrations of [^{3}H]DPCPX below its K_D . Although lower concentrations of [^{3}H]DPCPX showed lower levels of total binding than for higher concentrations, non-specific binding was reduced to a greater extent, and increased the signal to noise ratio. Higher concentrations of [^{3}H]DPCPX would increase the difference between the observed IC_{50}^{-1} values and the affinities calculated by application of the Cheng Prusoff correction, potentially leading to increased uncertainty from increased reliance on the precision of the correction factor. For [^{3}H]DPCPX / CHA competition assays at A_1HE and A_1LE membranes the mean correction factors were 0.313 ± 0.001 (n = 7) and 0.312 ± 0.001 (n = 4) log units respectively.

Compounds GR190178, GR161144 and GR162900 (shown in Figure 2.1 on page 50) are A_1R agonists of lower efficacy than CHA or PIA. A limited number of studies (n = 2) investigating the ability of these lower efficacy agonists to inhibit [^{3}H]DPCPX binding were performed and are described in Figure 4.6 on page 91. Direct two-site analysis of [^{3}H]DPCPX competition assays using CHA and GR190178 are relatively straightforward as they show a clear separation of affinities ($\frac{K_H}{K_L}$). The two-site nature of the inhibition curves is apparent from visual inspection of the curves. However, competition curves using ligands of low efficacy such as GR161144 and GR 162900 are more difficult to analyse directly by non-linear regression due to decreased separation of their high and low binding affinity constants. To compensate for this, the competition assay was performed in the presence and absence of 100 μM GTP. Both curves (± GTP) are performed in the same rack of tubes at the same time in order to reduce variability and to increase the reliability of analysis using shared parameters from both curves. The curve in the presence of GTP was best fit to a one-site model and the low affinity binding constant was obtained. Two-site analysis of the curve

Table 4.1 Parameters describing antagonist ([^{3}H]DPCPX) and agonist ([^{3}H]CHA) saturation binding curves of the human adenosine A_1 receptor.

[^{3}H]DPCPX saturation	Bmax (pmol / mg protein)	log affinity
A_1HE (n = 5)	8.19 ± 0.35	8.72 ± 0.03
A_1LE (n = 5)	0.60 ± 0.12	8.62 ± 0.06
[^{3}H]CHA saturation	**Bmax (pmol / mg protein)**	**log affinity**
A_1HE (n = 7)	3.20 ± 0.38 (39% of [^{3}H]DPCPX Bmax)	8.60 ± 0.05
A_1LE (n = 7)	0.38 ± 0.05 (63% of [^{3}H]DPCPX Bmax)	8.48 ± 0.08

Table 4.1: Summary of [^{3}H]DPCPX (antagonist) and [^{3}H]CHA (agonist) saturation experiments using A_1HE and A_1LE membranes. Representative curves are shown in Figure 4.1 on page 81. Unpaired t tests showed no significant difference between the affinities of [^{3}H]DPCPX or [^{3}H]CHA for membranes prepared from either cell line. In addition, although independent, the affinities of [^{3}H]DPCPX and [^{3}H]CHA for the adenosine A_1 receptor were indistinguishable. These saturation assays were performed in quadruplicate, and values shown represent the mean ± s.e.m. of n independent experiments.

Table 4.2 Two-site analysis of [^{3}H]DPCPX / agonist competition curves.

CHA	fr_H	log K_H	log K_L
A_1HE (n = 7)	0.52 ± 0.02	8.57 ± 0.06	5.79 ± 0.05
A_1LE (n = 4)	0.71 ± 0.02	8.75 ± 0.16	5.68 ± 0.17
PIA	fr_H	log K_H	log K_L
A_1HE (n = 2)	0.54 ± 0.01	8.72 ± 0.03	6.17 ± 0.04

Table 4.2: Data shown represents the mean ± s.e.m. of n independent experiments performed in triplicate on each membrane type. The effect of PIA, another high efficacy A_1R agonist, on the binding of [^{3}H]DPCPX at A_1HE membranes was investigated. Mean [^{3}H]DPCPX concentrations were 0.76 ± 0.06 and 0.84 ± 0.06 nM for A_1HE and A_1LE membranes respectively in the CHA competition assays, and 0.58 ± 0.07 nM in the PIA assays. Unpaired t tests found no significant difference between the two membranes for both high and low CHA affinities. The difference between CHA fr_H means was significant (P = 0.0005).

Figure 4.5 The biphasic displacement of [^{3}H]DPCPX binding by CHA.

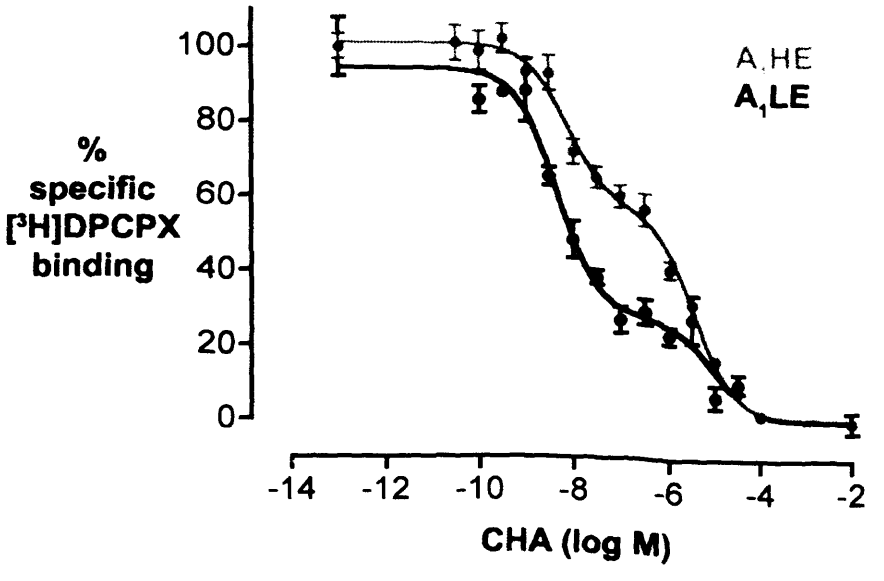

Figure 4.5: Representative [^{3}H]DPCPX / CHA competition curves of the effect of CHA on the binding of 0.7 nM [^{3}H]DPCPX to A_1HE (grey) and A_1LE (black) membranes. The A_1LE curve shows a higher fraction of CHA binding which is of high affinity (fr_H) than A_1HE. Data shown are mean ± s.e.m. of a single experiment performed in triplicate. Competition assays were analysed by an equation describing two-site competition binding, with mean estimates described in Table 4.2 on the preceding page.

in the absence of GTP was constrained to 0% and 100% (bottom and top respectively) and the low affinity binding constant obtained in the presence of GTP. This left only fr_H and the high affinity binding constant to be estimated from the two-site curve. Figure 4.6 illustrates this approach using GR190178, GR161144, GR162900 and, for comparison, CHA. The estimates of CHA affinities in Figure 4.6 are similar to those observed in Table 4.2. GR161144 and GR162900 exhibit a small, 5 to 10-fold difference in affinities, GR190178 shows almost a 100-fold difference and CHA a 700-fold GTP shift. No difference was observed between the fraction of binding which is of high affinity (fr_H) for CHA, GR190178 and GR161144. GR162900 does appear to exhibit a lower fr_H which is consistent with other reports (Browning 2003).

4.4 Radioligand equilibrium binding to A_1R-GFP and A_1R-GFP-Gα_i fusion constructs expressed at different densities.

Stable polyclonal CHO cell lines stably expressing either the A_1R-GFP or A_1R-GFP-Gα_i fusion constructs were a kind gift from Dr Chris Browning, GlaxoSmithKline, Stevenage. In order to create monoclonal cell lines expressing different levels of these constructs, individual cells were isolated and grown into mature cell lines as described in Chapter 3 above. In order to facilitate characterisation of the equilibrium binding properties of membranes from such a large number of cell lines (24 for A_1R-GFP and 23 for A_1R-GFP-Gα_i), simplified [^{3}H]DPCPX saturation and [^{3}H]DPCPX / CHA competition assays were required. These are described in Figures 4.7 and 4.8 (on pages 93 and 94 respectively). The simplified assays were designed in order to estimate the following equilibrium binding parameters;

- total number of [^{3}H]DPCPX binding sites (B_{max}),
- [^{3}H]DPCPX affinity,
- CHA binding affinities K_H and K_L, and
- fraction of CHA binding which is of high affinity (fr_H).

[^{3}H]DPCPX saturation curves using three radioligand concentrations (0.1, 1 and 10 nM) were measured in triplicate with both total and non-specific binding being determined at each concentration. Two concentrations (0.1 and 1 nM) lower than the affinity of [^{3}H]DPCPX for the A_1R were chosen to accurately estimate K_D, and a further concentration 10-fold greater (10 nM) in order

Figure 4.6 Inhibition of [^{3}H]DPCPX binding at A_1HE membranes by A_1R agonists of differing efficacy.

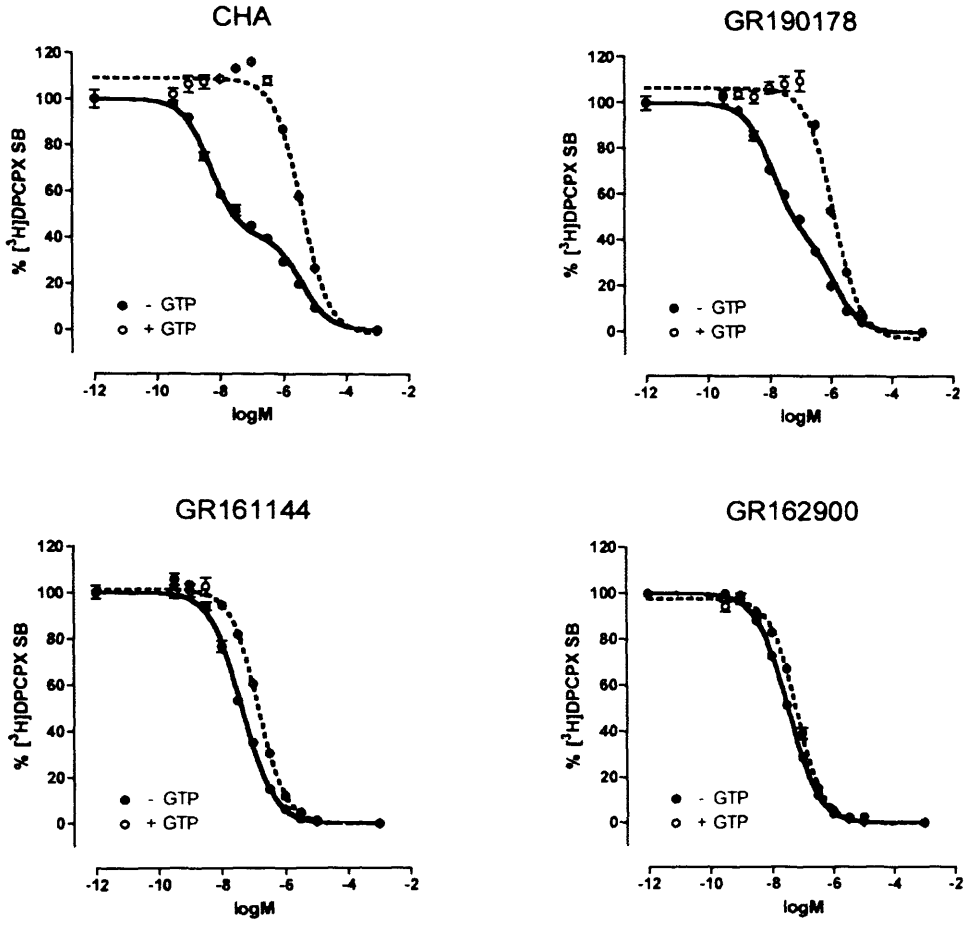

Mean parameters from the analysis of competition curves.

Unlabelled ligand	100 μM GTP	fr_H	log K_H	log K_L	$\frac{K_H}{K_L}$
CHA	+	[0]	-	5.70 ± 0.02	
(n = 2)	-	0.60 ± 0.003	8.56 ± 0.05	-	728 ± 49
GR190178	+	[0]	-	6.21 ± 0.003	
(n = 2)	-	0.58 ± 0.01	8.13 ± 0.11	-	85 ± 20
GR161144	+	[0]	-	7.14 ± 0.03	
(n = 2)	-	0.60 ± 0.05	8.03 ± 0.08	-	8.2 ± 2.0
GR162900	+	[0]	-	7.47 ± 0.03	
(n = 2)	-	0.43 ± 0.05	8.30 ± 0.002	-	6.7 ± 0.4

Figure 4.6: Representative curves and mean non-linear regression estimates of equilibrium agonist binding parameters for CHA and agonists of lower efficacy using A_1HE membranes. Log K_L was estimated in the presence of 100 μM GTP (broken curves) and used to constrain the two-site curve (solid curves) so that fr_H and log K_H were the only variables estimated by two-site non-linear regression. Top and bottom of the two-site curves were fixed to 100% and 0% respectively. Non-linear regression analysis of the data in the presence of GTP was not constrained. The ratio of agonist affinities ($\frac{K_H}{K_L}$, alternatively termed "GTP shift") is generally considered an indication of agonist efficacy.

to estimate B_{max} by sufficiently saturating the receptor whilst still maintaining a good ration of total to non-specific binding. 10 nM [^{3}H]DPCPX would be expected saturate approximately 80% of available [^{3}H]DPCPX binding sites, according to the Langmuir isotherm ($bound\,L = \frac{B_{max}.[L]}{K_D+[L]}$, where $[L]$ is concentration of ligand L with dissociation constant K_D at a receptor preparation with maximum binding capacity B_{max}).

The 1 nM [^{3}H]DPCPX / CHA competition assay using three concentrations of CHA was measured in duplicate, and used the 1 nM [^{3}H]DPCPX values from the saturation curve for total and non-specific binding. The concentrations of CHA were chosen to be approximately at the midpoints of the high and low affinity components of the two-phase inhibition curve, along with a concentration of CHA at the expected point of inflection between the two components in order to estimate fr_H. Figure 4.8 on page 94 illustrates in greater detail the analysis of the simplified competition assay. The combined saturation and competition assay occupied 24 binding assay tubes, allowing two membranes to be characterised in one 48-tube rack. In retrospect the assay could have been simplified further as the results obtained were precise and reproducible as shown by the size of the error bars in Figures 4.7 and 4.8.

Table 4.3 on page 95 lists the mean equilibrium binding properties of membranes prepared from all the A_1R-GFP and A_1R-GFP-Gα_i cell lines using the simplified assay. Also shown are the equilibrium binding properties of membranes made from the polyclonal A_1R-GFP-Gα_i cell line before cytometric selection of the cell line series. Membranes prepared from the A_1R-GFP-Gα_i series of cell lines ranged in [^{3}H]DPCPX B_{max} from approximately 1.8 to 13 pmol/mg protein. Membranes from the A_1R-GFP series of cell lines showed a comparable range of [^{3}H]DPCPX B_{max} (1.3 to 9.3 pmol/mg protein).

The mean [^{3}H]DPCPX log affinities of the A_1R-GFP and A_1R-GFP-Gα_i membranes were similar (8.88 $\pm$ 0.01 (n = 46) and 8.72 $\pm$ 0.02 (n = 65) respectively; see Table 4.4 on page 99), as illustrated in Figure 4.9 on page 96. The [^{3}H]DPCPX affinity of membranes from most A_1R-GFP and A_1R-GFP-Gα_i cell lines fell within a two-fold range (0.3 log units). Comparison by unpaired t test observed a significant ($P < 0.0001$) but small (0.16 log unit) difference between the mean affinity of [^{3}H]DPCPX for A_1R-GFP and A_1R-GFP-Gα_i membranes. When the A_1R-GFP and A_1R-GFP-Gα_i [^{3}H]DPCPX log affinities were analysed together, [^{3}H]DPCPX affinity was not dependent on the level of receptor expression (no significant non-zero slope). When analysed separately by linear regression no significant non-zero slope was observed for A_1R-GFP-Gα_i membranes but A_1R-GFP did show a significant slope ($P = 0.006$). The affinity of [^{3}H]DPCPX for the A_1R-GFP and A_1R-GFP-Gα_i membranes was similar to that observed for A_1HE and A_1LE (Table 4.4).

Figure 4.7 Simplified [^{3}H]DPCPX saturation and [^{3}H]DPCPX / CHA competition binding assays.

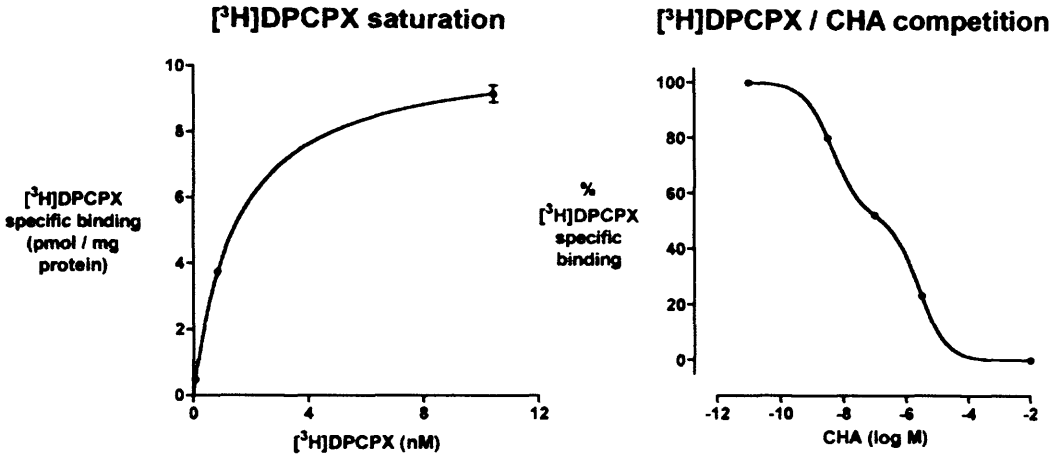

Figure 4.7: The equilibrium binding properties of membranes prepared from all the A_1R-GFP and A_1R-GFP-Gα_i cell lines were estimated by a combined three-point saturation and five-point competition assay. Figure 4.8 on the following page describes in greater detail the analysis of the simplified competition assay. The graphs shown on this figure are from a single experiment using membranes prepared from A_1R-GFP cell line 6D2 (the error bars on the competition curve are present but too small to be visible).

Figure 4.8 The estimation of CHA affinities and fr_H using a simplified [^{3}H]DPCPX / CHA competition assay.

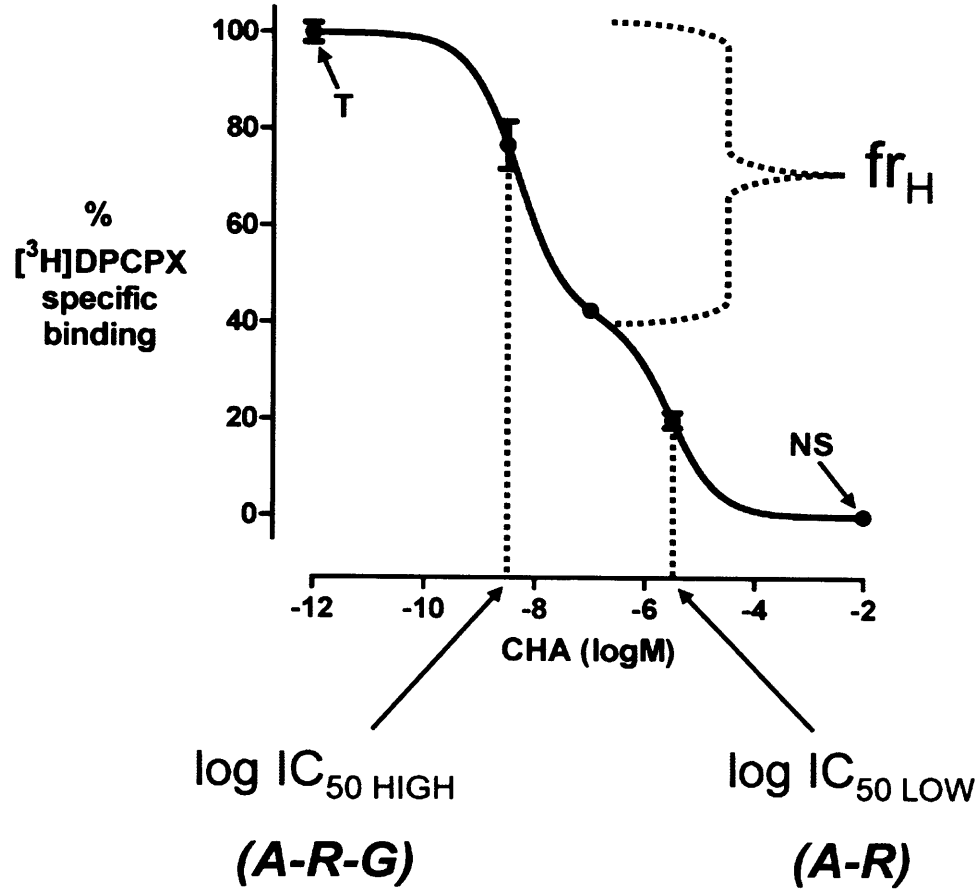

Figure 4.8: The affinities of agonist binding to the adenosine A_1 receptor (IC_{50} HIGH and IC_{50} LOW) and the fraction of binding which is of high affinity (fr_H) can be reliably estimated using three concentrations of unlabelled CHA along with total (T) and non-specific (NS) levels of [^{3}H]DPCPX binding in the absence of CHA. All competition curves were normalised as a percent of maximum specific binding and best fit by an equation describing two-site competition binding. The top and bottom of the curves were fixed to 100% and 0% respectively leaving only three variables to be estimated (fr_H, IC_{50} HIGH and IC_{50} LOW). The use of mean IC_{50} HIGH and IC_{50} LOW values to constrain the fit even more so that fr_H was the only variable, did not noticeably improve the reliability of fr_H estimation and was not pursued further. Shown above is a single experiment using membranes prepared from A_1R-GFP cell line 5F4 (see Table 4.3 for details). Log IC_{50} values were corrected to log affinity values using the Cheng Prusoff correction. In order to increase the reliability between different estimates of CHA affinity the mean log affinity of [^{3}H]DPCPX for all the cell lines from each fusion construct was used for the Cheng Prusoff correction, rather than the individual estimates for that particular cell line.

Table 4.3 The equilibrium binding properties of membranes prepared from all the A_1R-GFP and A_1R-GFP-Gα_i cell lines.

		[^{3}H]DPCPX saturation		[^{3}H]DPCPX / CHA competition		
		B_{max} (pmol / mg protein)	log affinity	fr_H	log K_H	log K_L
A_1R-GFP-Gα_i	2H7	1.77 ± 0.08	8.70 ± 0.13	0.64 ± 0.04	8.69 ± 0.10	6.42 ± 0.05
	1B9	2.18 ± 0.36	8.90 ± 0.18	0.66 ± 0.07	8.51 ± 0.39	6.26 ± 0.07
	1C1	2.80 ± 0.23	8.50 ± 0.08	0.66 ± 0.06	8.63 ± 0.06	6.02 ± 0.19
	4F2	2.85 ± 0.57	8.78 ± 0.12	0.39 ± 0.08	8.61 ± 0.35	5.75 ± 0.04
	2H6	3.00 ± 0.29	8.52 ± 0.12	0.62 ± 0.04	8.61 ± 0.15	6.13 ± 0.13
	3A3	3.30 ± 0.37	8.76 ± 0.14	0.58 ± 0.04	8.55 ± 0.27	6.07 ± 0.10
	2A3	3.45 ± 0.13	8.79 ± 0.11	0.64 ± 0.06	8.53 ± 0.15	6.34 ± 0.11
	1C9	3.48 ± 0.13	8.48 ± 0.09	0.58 ± 0.06	8.53 ± 0.06	5.81 ± 0.01
	1G3	3.57 ± 0.24	8.71 ± 0.03	0.57 ± 0.02	8.54 ± 0.21	6.39 ± 0.14
	2C3	3.59 ± 0.03	8.66 ± 0.09	0.67 ± 0.03	8.51 ± 0.10	5.88 ± 0.02
	2G3	3.77 ± 0.41	8.73 ± 0.02	0.57 ± 0.03	8.63 ± 0.21	6.36 ± 0.15
	1H9	4.06 ± 0.44	8.72 ± 0.03	0.60 ± 0.04	8.58 ± 0.16	6.21 ± 0.12
	3F5	4.19 ± 0.49	8.69 ± 0.05	0.62 ± 0.02	8.52 ± 0.08	6.05 ± 0.15
	1A5*	(5.15)	(8.54)	(0.68)	(8.61)	(5.95)
	3C4	5.18 ± 0.00	8.63 ± 0.11	0.57 ± 0.02	8.51 ± 0.13	6.02 ± 0.04
	2H8	5.96 ± 0.44	8.72 ± 0.05	0.56 ± 0.02	8.42 ± 0.14	5.75 ± 0.00
	3D4	6.52 ± 0.55	8.73 ± 0.06	0.55 ± 0.02	8.59 ± 0.01	5.94 ± 0.02
	4F12	7.69 ± 0.64	8.75 ± 0.07	0.50 ± 0.02	8.34 ± 0.06	5.85 ± 0.10
	3F2	7.88 ± 0.05	8.72 ± 0.09	0.57 ± 0.04	8.40 ± 0.02	5.92 ± 0.07
	3C2	8.23 ± 0.39	8.74 ± 0.07	0.60 ± 0.00	8.37 ± 0.34	5.90 ± 0.07
	4E8	8.53 ± 0.02	8.78 ± 0.01	0.43 ± 0.01	8.29 ± 0.18	5.78 ± 0.09
	4B8**	12.95 ± 1.73	8.82 ± 0.05	0.52 ± 0.05	8.27 ± 0.32	5.88 ± 0.10
	4H1	13.41 ± 0.73	8.73 ± 0.06	0.46 ± 0.02	8.15 ± 0.43	5.64 ± 0.12
	mean	-	*8.71 ± 0.02*	-	*8.49 ± 0.03*	*6.01 ± 0.05*
A_1R-GFP	5H6	1.28 ± 0.05	8.95 ± 0.00	0.70 ± 0.01	8.63 ± 0.22	6.45 ± 0.06
	5E4	1.56 ± 0.05	8.97 ± 0.03	0.72 ± 0.03	8.56 ± 0.17	6.57 ± 0.09
	6B7	2.53 ± 0.09	9.09 ± 0.07	0.67 ± 0.02	8.45 ± 0.05	6.16 ± 0.19
	6E3	2.72 ± 0.65	9.02 ± 0.14	0.62 ± 0.01	8.39 ± 0.53	5.92 ± 0.24
	5C4	2.91 ± 0.11	8.99 ± 0.04	0.61 ± 0.01	8.50 ± 0.18	5.93 ± 0.21
	6G6	3.15 ± 1.10	8.98 ± 0.03	0.67 ± 0.03	8.48 ± 0.02	6.03 ± 0.03
	6H3	3.85 ± 0.58	8.80 ± 0.03	0.69 ± 0.03	8.62 ± 0.08	5.90 ± 0.14
	5E3	3.94 ± 0.55	8.92 ± 0.05	0.64 ± 0.03	8.27 ± 0.47	5.93 ± 0.20
	5H9	3.94 ± 0.27	8.79 ± 0.04	0.67 ± 0.03	8.56 ± 0.16	5.59 ± 0.19
	5F4	3.97 ± 0.30	8.89 ± 0.02	0.60 ± 0.02	8.39 ± 0.23	5.85 ± 0.01
	6G5	4.34 ± 0.15	8.93 ± 0.00	0.67 ± 0.04	8.63 ± 0.14	6.13 ± 0.00
	5B8	4.47 ± 0.27	8.73 ± 0.06	0.66 ± 0.05	8.46 ± 0.22	5.73 ± 0.01
	6H11	4.93 ± 0.49	8.87 ± 0.03	0.64 ± 0.01	8.51 ± 0.25	5.94 ± 0.12
	5D7	5.33 ± 0.10	8.92 ± 0.01	0.69 ± 0.02	8.62 ± 0.15	5.91 ± 0.05
	6F12	5.34 ± 0.60	8.80 ± 0.06	0.63 ± 0.00	8.64 ± 0.16	5.81 ± 0.13
	5F5	5.45 ± 0.09	8.89 ± 0.00	0.63 ± 0.02	8.47 ± 0.16	5.97 ± 0.07
	5C6	6.18 ± 0.31	8.86 ± 0.03	0.62 ± 0.03	8.38 ± 0.15	5.84 ± 0.03
	6E5	6.32 ± 1.06	8.82 ± 0.09	0.64 ± 0.02	8.52 ± 0.06	5.86 ± 0.02
	5H4	6.55 ± 0.48	8.78 ± 0.06	0.69 ± 0.02	8.48 ± 0.12	5.79 ± 0.03
	6E10	6.58 ± 0.22	8.84 ± 0.00	0.71 ± 0.04	8.60 ± 0.13	5.63 ± 0.15
	6E4	7.39 ± 0.26	8.91 ± 0.01	0.58 ± 0.00	8.54 ± 0.11	5.99 ± 0.05
	5E10	8.22 ± 0.24	8.80 ± 0.00	0.59 ± 0.02	8.41 ± 0.12	5.82 ± 0.04
	6D2	9.35 ± 1.16	8.86 ± 0.03	0.51 ± 0.03	8.42 ± 0.23	5.85 ± 0.05
	6C9	-	-	-	-	-
	mean	-	*8.89 ± 0.02*	-	*8.50 ± 0.02*	*5.94 ± 0.05*
	overall mean	-	*8.80 ±0.02*	-	*8.50 ± 0.02*	*5.98 ± 0.03*
unsorted A_1R-GFP-Gα_i**		2.79 ± 0.33	8.78 ± 0.12	0.61 ± 0.02	8.52 ± 0.23	5.88 ± 0.13

Table 4.3: Equilibrium binding properties of all A_1R-GFP and A_1R-GFP-Gα_i membranes, estimated using the simplified binding assay described in Figure 4.7 on page 93. All estimates are n=2, except * (n=1) and ** (n=3). Results from membranes 1A5 were not included in calculation of the mean values shown because they were only n=1. Membranes from cell line 6C9 did not show any specific [^{3}H]DPCPX binding. Values shown are expressed as mean ± $\frac{range}{2}$ (where n=2) or mean ± s.e.m. (n=3), and where shown as ± 0.00 are ± < 0.005.

Figure 4.9 [^{3}H]DPCPX affinity is similar for A_1R-GFP and A_1R-GFP-Gα_i, and is essentially independent of B_{max}.

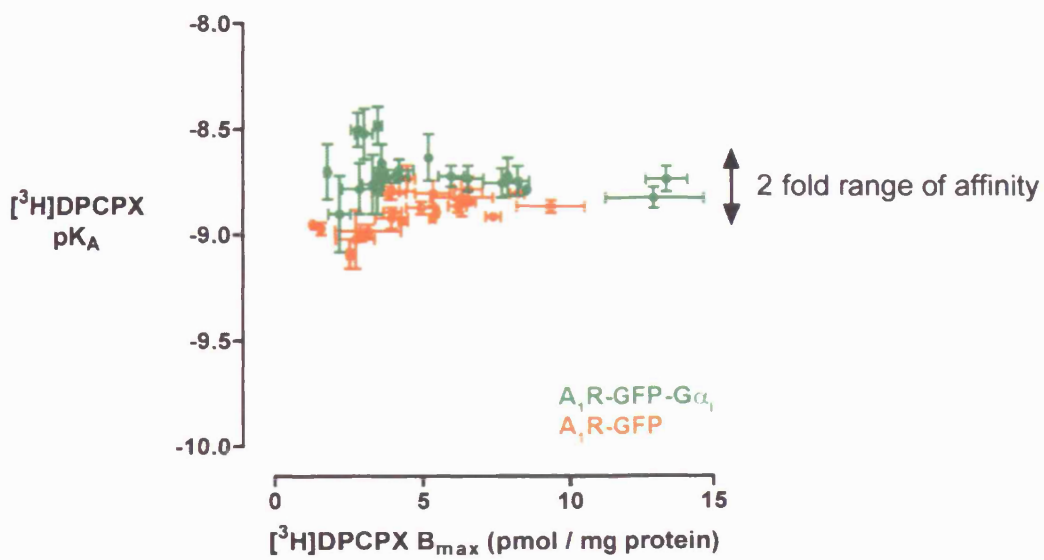

Figure 4.9: Graph of [^{3}H]DPCPX B_{max} against [^{3}H]DPCPX affinity from Table 4.3 on the previous page. Although there is a statistically significant difference between mean [^{3}H]DPCPX affinities for A_1R-GFP and A_1R-GFP-Gα_i membranes ($P < 0.0001$, see Table 4.4 on page 99), the difference is small (0.16 log affinity units) and most values fall within a 2-fold range of affinity (0.3 log units) as indicated on the graph.

Both affinities of CHA were not significantly different between A_1R-GFP and A_1R-GFP-Gα_i membranes, and agreed with direct [^{3}H]CHA saturation of A_1R-GFP-Gα_i membranes (Table 4.5 on page 99). Table 4.5 also shows the CHA affinities for A_1HE and A_1LE membranes for comparison. Comparison by unpaired t test of the mean estimates of high affinity CHA binding to the A_1R-GFP-Gα_i construct by competition and saturation experiments showed no significant difference (Table 4.5).

Linear regression of the dependence of CHA affinity on the level of receptor expression (Figure 4.10 on page 100) showed both log K_H and log K_L to have significantly non-zero slopes ($P = 0.004$ & $P < 0.0001$ for log K_H and log K_L respectively). However, these slopes were very shallow (-0.03 and -0.05 for log K_H and log K_L respectively) and statistical significance may have been encouraged by the large number of x values ($n = 102$). Estimation of log K_L is more difficult at low levels of expression when using the five-point competition assay due to increased fr_H, as can be seen in Figure 4.10 where the estimate of log K_L at the lowest levels of expression appears to be higher than most others. Weighting of errors was not employed in any of the analysis in this study, however the effect of weighting on the estimation of log K_L using the simplified competition assay was investigated. Weighting by $\frac{1}{Y}$ and $\frac{1}{SD^2}$ did not alter the estimates of CHA affinities and fr_H at low, medium and high levels of expression. This may be due to the generally small size of the errors observed in the assay, as can be seen in the competition curves used as examples in Figures 4.7 and 4.8 (pages 93 and 94 respectively). Accurate estimation of CHA log K_L at the lowest levels of receptor expression would require detailed competition assays, such as those shown in Figure 4.6 on page 91. A real dependence of log K_L on the level of receptor expression is probably unlikely as no difference is observed in log K_L and log K_H values for A_1HE and A_1LE membranes, and most of the data for A_1R-GFP and A_1R-GFP-Gα_i is consistent with these values.

While the affinities of both [^{3}H]DPCPX and CHA are essentially independent of the level of receptor expression, the fraction of CHA binding which is of high affinity (fr_H) is dependent on the level of expression. Figure 4.11 on page 101 illustrates the dependence of fr_H (estimated by the simplified five-point competition assay) on the level of A_1R-GFP and A_1R-GFP-Gα_i expression. Linear regression of each construct individually shows significant non-zero slopes (both slopes are -0.01 with $P < 0.0001$ & $P = 0.004$ for A_1R-GFP-Gα_i and A_1R-GFP respectively). The dependence of fr_H on the level of receptor expression is similar to the behaviour reported above using A_1HE and A_1LE membranes. Figure 4.12 on page 102 combines the fr_H values as a function of expression level from A_1LE, A_1HE with all the A_1R-GFP and A_1R-GFP-Gα_i cell line membranes. Linear regression of A_1R-GFP and A_1R-GFP-Gα_i fr_H combined again shows a significantly non-zero slope ($P < 0.0001$) which agrees with the A_1HE and A_1LE membranes shown for comparison.

There is one outlier to the correlation of fr_H with A_1R-GFP-Gα_i expression (cell line 4F2) which is discussed later.

The incubation of low and high expression A_1R-GFP-Gα_i cell lines with pertussis toxin for 24 hours before membrane preparation inhibited all detectable high affinity agonist binding, indistinguishable from the effect of 100 μM GTP (data not shown). The Gα_i subunit in the A_1R-GFP-Gα_i fusion construct may have been mutated in order to be insensitive to pertussis toxin, although this was not confirmed. If the Gα_i subunit on the A_1R-GFP-Gα_i fusion construct is insensitive to pertussis toxin, the complete sensitivity of high affinity agonist binding at the A_1R-GFP-Gα_i fusion protein to pertussis toxin suggests that the fused Gα_i subunit does not couple well to the attached A_1R. The equilibrium binding properties presented here are very similar at A_1R-GFP, A_1R-GFP-Gα_i and A_1HE membranes showing the fused Gα_i has little influence on binding at the A_1R-GFP-Gα_i construct. This validates the series of A_1R-GFP-Gα_i cell lines differentially expressing A_1R as a model for investigating the effect of receptor expression alone on receptor behaviour.

4.5 Discussion.

The work presented in this chapter describes the binding of the inverse agonist DPCPX and a selection of agonists of varying efficacy at the human adenosine A_1 receptor. Membranes were prepared from stable cell lines expressing the adenosine A_1 receptor and A_1 receptor-GFP fusion proteins at a range of densities, and were used to investigate the effect of receptor expression density on features of binding at equilibrium. The affinity of DPCPX for the adenosine A_1 receptor was essentially independent of the level of receptor expression. The affinities of the high efficacy agonist CHA for the A_1 receptor were also largely independent of the level of receptor expression. However, the fraction of specific CHA binding of high affinity (fr_H) was clearly dependent on the level of receptor expression for the adenosine A_1 receptor alone and the A_1R-GFP and A_1R-GFP-Gα_i fusion constructs.

Heterogeneous agonist binding at the adenosine A_1 receptor measured using A_1LE and A_1HE membranes.

Previous studies here have investigated the properties of two stable CHO cell lines expressing the adenosine A_1 receptor at different densities, A_1LE and A_1HE (Browning 2003, Browning et al. 2001a,b,c). Here, characterisation of those cell lines has been continued in detail. A_1HE membranes exhibited a 14-fold greater mean [^{3}H]DPCPX B_{max} than A_1LE membranes and 8-

Table 4.4 Mean log affinities of [^{3}H]DPCPX for A_1HE, A_1LE, A_1R-GFP and A_1R-GFP-Gα_i membranes.

	[^{3}H]DPCPX log K_A
A_1HE (n = 5)	8.72 ± 0.03
A_1LE (n = 5)	8.62 ± 0.06
A_1R-GFP-Gα_i (n = 65)	8.72 ± 0.02
A_1R-GFP (n = 46)	8.88 ± 0.01

Table 4.4: The mean affinities shown for both fusion constructs are the mean of all individual observations rather than the mean of means shown on Table 4.3. The mean affinities of [^{3}H]DPCPX for A_1R-GFP and A_1R-GFP-Gα_i membranes were significantly different ($P < 0.0001$). The estimates of [^{3}H]DPCPX affinity for the fusion constructs were generated by the the three-point [^{3}H]DPCPX saturation assay (in triplicate), whereas the A_1HE and A_1LE membranes were characterised by means of six-point [^{3}H]DPCPX saturation assays (in quadruplicate) and are reproduced from Table 4.1 on page 88.

Table 4.5 Mean log affinities of CHA for A_1HE, A_1LE, A_1R-GFP and A_1R-GFP-Gα_i membranes.

	log K_L	log K_H	[^{3}H]CHA satn. log K_A
A_1R-GFP (n = 41)	**6.02 ± 0.14**	**8.42 ± 0.06**	(no data)
A_1R-GFP-Gα_i (n = 61)	**6.05 ± 0.05**	**8.47 ± 0.04**	8.55 ± 0.04 (n = 3)
A_1HE (n = 7)	5.79 ± 0.05	8.57 ± 0.06	8.60 ± 0.05 (n = 7)
A_1LE (n = 4)	5.68 ± 0.17	8.75 ± 0.16	8.48 ± 0.08 (n = 7)

Table 4.5: Shown are the means of all the individual estimates of CHA affinity on A_1R-GFP and A_1R-GFP-Gα_i membranes using the simplified binding assay (highlighted in **pink**). For comparison, results from [^{3}H]CHA saturation experiments and experiments using A_1HE and A_1LE membranes are shown (these were not generated using the simplified assay and are reported in Tables 4.1 and 4.2 on page 88). The mean values at the bottom of each section shown in Table 4.3 are the means of the mean of each cell line, whereas the table here describes the mean of all the individual estimates. Also, the A_1R-GFP-Gα_i means above include data not presented in Table 4.3. t tests showed no significant difference in the log K_L and log K_H means, for both A_1R-GFP and A_1R-GFP-Gα_i membranes.

Figure 4.10 The affinities of CHA for A_1R-GFP and A_1R-GFP-Gα_i are essentially independent of B_{max}.

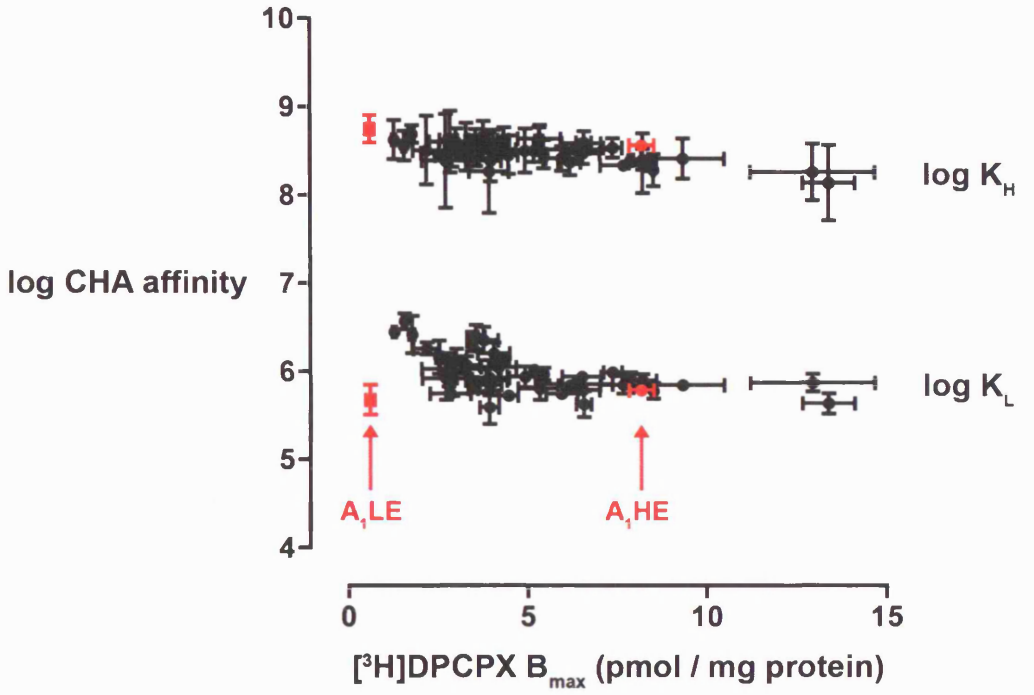

Figure 4.10: Shown above are the affinities of CHA for A_1R-GFP and A_1R-GFP-Gα_i fusion constructs, as detailed in Table 4.3, plotted against [^{3}H]DPCPX B_{max}. These estimates were all measured using the simple three-point saturation and five-point competition assays. Linear regression observed significantly non-zero slopes for both log K_H and log K_L (slopes -0.03 & -0.05 and $P = 0.004$ & $P < 0.0001$ for log K_H and log K_L respectively). The number of data points for each affinity was 102. Also shown, for visual comparison, are mean estimates of CHA log affinities for A_1LE and A_1HE membranes (from Tables 4.1 and 4.2). The A_1LE and A_1HE data (●) were measured using more detailed competition and saturation assays rather than the smaller simple assays used for the A_1R-GFP and A_1R-GFP-Gα_i membranes.

Figure 4.11 CHA fr_H is dependent on $[^3H]$DPCPX B_{max}.

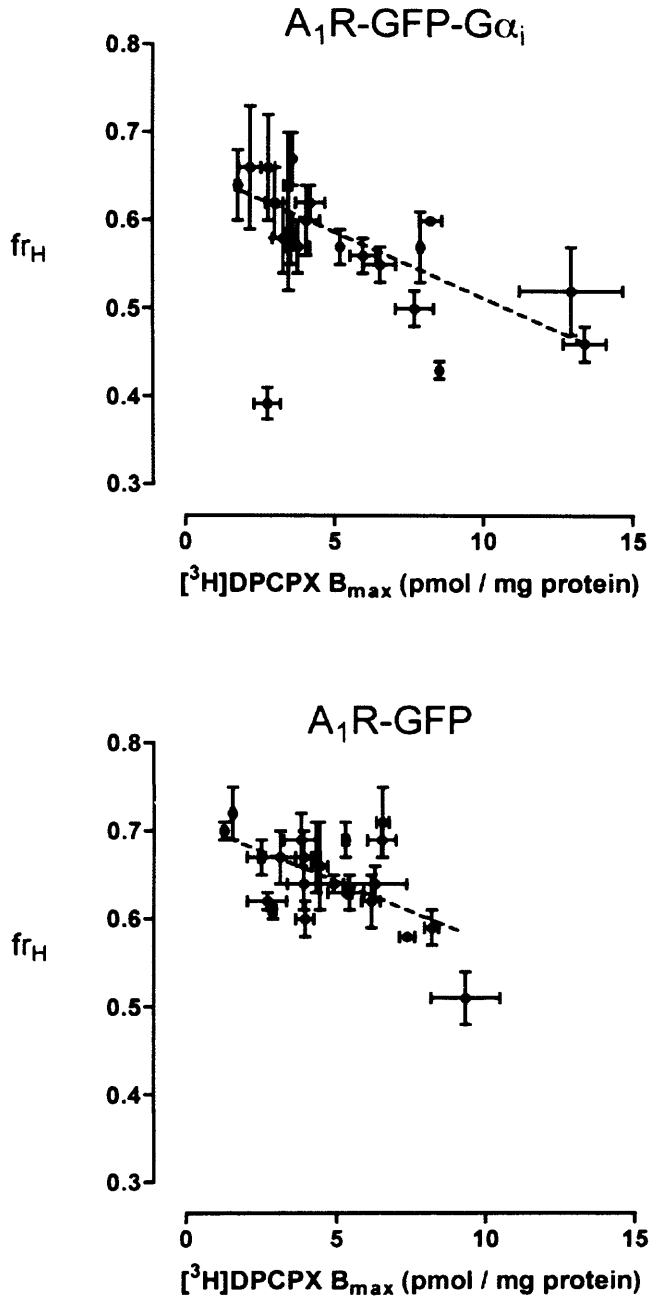

Figure 4.11: The fraction of CHA binding which is of high affinity (fr_H) is dependent on the level of A_1R-GFP and A_1R-GFP-Gα_i expression. Linear regression of the data in both graphs showed significantly non-zero slopes (both slopes -0.01; $P < 0.0001$ & $P = 0.004$ for A_1R-GFP-Gα_i and A_1R-GFP respectively, illustrated by the broken straight lines). Table 4.3 on page 95 lists the parameters illustrated in the graphs above.

Figure 4.12 The fraction of high affinity agonist binding (fr_H) is dependent on the level of A_1R, A_1R-GFP and A_1R-GFP-$G\alpha_i$ expression.

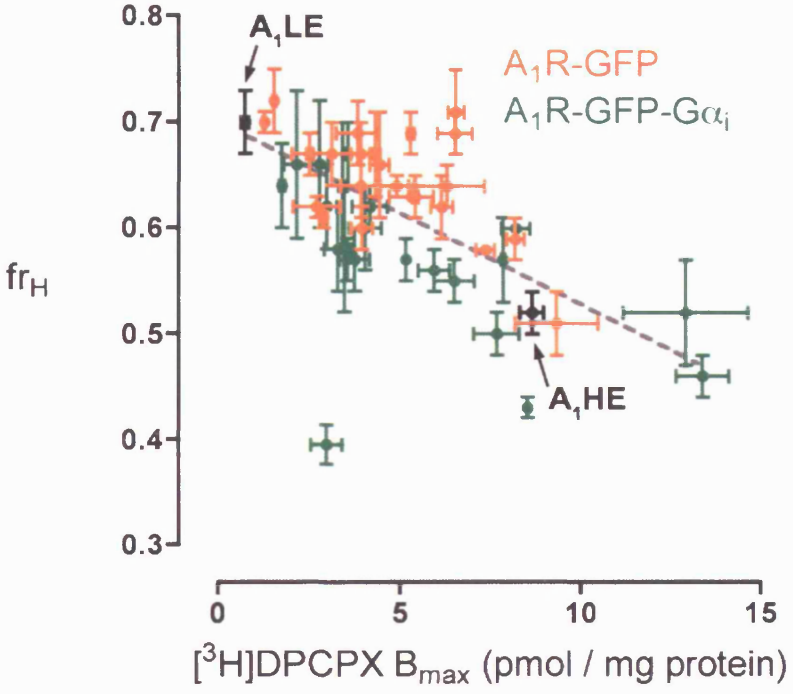

Figure 4.12: Shown above are the data from the two graphs in Figure 4.11 on the preceding page along with A_1HE and A_1LE for comparison, showing the dependency of fr_H on the level of receptor expression. As observed for both constructs individually, linear regression of A_1R-GFP and A_1R-GFP-$G\alpha_i$ data combined showed a significantly non-zero slope (slope -0.02, $P < 0.0001$, illustrated by the straight line shown).

fold greater levels of high affinity [^{3}H]CHA binding (Table 4.1). The mean log affinity constants for both [^{3}H]DPCPX and [^{3}H]CHA were independent of the type of membranes used. Previous characterisation of [^{3}H]DPCPX binding at A_1LE and A_1HE membranes showed no significant ($P > 0.05$) difference in pK_D values (Browning 2003). Cordeaux *et al.* 2000 reported over 3-fold higher affinity of [^{3}H]DPCPX at membranes from stable CHO cell lines expressing a lower (0.2 pmol/mg protein) rather than at higher (3.4 pmol/mg protein) level of the human adenosine A_1 receptor. They also reported 2-fold higher affinity of the A_1 receptor antagonist XAC at the higher level of receptor expression although this may not be a significant difference. However these experiments were performed in a different buffer system (Tris-EDTA), in a smaller volume (200 μl) and incubated for an increased period of time (90 min) compared to the results presented here.

Although A_1LE membranes showed lower levels of both [^{3}H]DPCPX and [^{3}H]CHA high affinity binding than A_1HE, the fraction of total high affinity binding (fr_H) which was available for [^{3}H]CHA was much greater (63% compared to 39% for A_1HE; Table 4.1). CHA binding at A_1HE and A_1LE membranes measured by [^{3}H]DPCPX / CHA competition experiments was of two components, approximately 1000-fold different in affinity (Table 4.2). As shown by direct radioligand saturation the estimates of fr_H by competition experiments were greater at A_1LE (71%) than A_1HE (52%) membranes. Despite being similar, the estimates of fr_H from saturation and competition experiments were not in absolute agreement although this was not determined statistically. A number of factors may contribute to differences in estimates of fr_H observed by competition and saturation experiments. Differences in the number of ligands present, the nature of binding of each ligand, the association kinetics of each ligand and methods of data analysis are different for saturation and competition experiments.

Estimates of [^{3}H]CHA B_{max} increased with longer periods of incubation up to four hours (Figure 4.3a). The K_D of [^{3}H]CHA appeared constant from incubation times of approximately 30 min onwards (Figure 4.3b). The non-linear regression shown in Figure 4.3a extrapolates to a level of [^{3}H]CHA specific binding of 2.2 pmol/mg protein at zero association time, which is approximately half of the maximum of 4.1 pmol/mg protein. Half of the maximum number of high affinity [^{3}H]CHA binding sites are available immediately and half are the result of a slow increase. Such 1:1 stoichiometries of binding site populations raises the intriguing thought of whether this is a reflection of receptor dimerisation. This is discussed later in this document. Chapter 5 investigates the kinetics of the binding of [^{3}H]DPCPX and [^{3}H]CHA to A_1HE and A_1LE membranes in detail. In contrast to the binding of [^{3}H]CHA, [^{3}H]DPCPX rapidly reached its maximum within a matter of minutes. There appear to be subtle differences in the binding of [^{3}H]CHA and [^{3}H]DPCPX which may be responsible for the different estimates of fr_H by means of

competition and saturation experiments. Possible mechanisms behind the changes in [^{3}H]DPCPX and [^{3}H]CHA binding with time are discussed later in Chapter 5.

Heterogeneous agonist binding at G protein-coupled receptors has been widely reported for a considerable period of time (Birdsall *et al.* 1978). Heterogeneous agonist binding at the adenosine A_1 receptor has been observed for both recombinantly expressed and native receptor. The work presented here along with previous work within the group has characterised in detail heterogeneous agonist binding at the adenosine A_1 receptor recombinantly expressed in stable CHO cell lines (Browning 2003, Cohen *et al.* 1996b). The adenosine A_1 receptor agonist PIA has been observed to inhibit 38% of antagonist binding with high affinity in guinea pig forebrain (Kollias-Baker *et al.* 1994). [^{3}H]DPCPX / PIA competition experiments in the presence of 10 mM $MgCl_2$ at rat cortical membranes have observed a fr_H of 0.75 (Finlayson *et al.* 2003). These observations are in contrast to the estimate of fr_H observed here at A_1HE membranes which was 0.54 $\pm$ 0.01 (n = 2, Table 4.2). However these are quite different preparations, two from endogenously expressed rat A_1 receptor and the other from recombinantly expressed human A_1 receptor which show quite different levels of receptor expression.

In summary, the affinities of [^{3}H]DPCPX, [^{3}H]CHA and CHA were not different between membranes from A_1HE and A_1LE cell lines. However the fraction of CHA binding which was of high affinity (fr_H) was clearly reduced at A_1HE membranes compared to A_1LE. The fr_H observed in A_1HE membranes was only reduced by one third, compared to A_1LE membranes, despite the large increase in B_{max} (Tables 4.1 and 4.2). Assuming [^{3}H]CHA binds with high affinity to the A_1R as part of the agonist-receptor-G protein ternary complex, such an increase in receptor number alone would be expected to result in a fr_H of approximately 0.05 for A_1HE membranes. The observed fr_H in A_1HE membranes of 0.52 implies there is a change in the system between A_1LE and A_1HE membranes, such as an increase in G protein availability. The dependence of fr_H on the level of receptor expression was investigated in greater detail using membranes prepared from stable cell lines expressing either the A_1R-GFP or A_1R-GFP-Gα_i fusion constructs, and is discussed further below.

The binding of low efficacy agonists at the adenosine A_1 receptor.

The ratio of agonist affinities for the "high affinity" G protein-coupled (K_H) and "low affinity" G protein-uncoupled (K_L) receptor states has long been linked with agonist efficacy (Birdsall *et al.* 1978 and Kent *et al.* 1980). Previous work here used adenosine A_1 receptor low efficacy agonists GR190178, GR161144 and GR162900 in order to investigate the ability of the ternary complex model to describe the relationship of this ratio to relative agonist efficacy (Browning

2003, Sheehan *et al.* 2000). The work presented in this study attempted to measure with greater accuracy the equilibrium binding properties of these ligands before their use in kinetic experiments presented in Chapter 5.

[^{3}H]DPCPX competition curves using low efficacy agonists such as GR161144 and GR162900 are difficult to analyse directly by non-linear regression due to the reduced separation of their high and low affinity constants. [^{3}H]antagonist / agonist competition experiments are often analysed by one-site models with a variable Hill slope of the inhibition curve (for example see Finlayson *et al.* 2003). Shallow Hill slopes indicate heterogeneous agonist inhibition of [^{3}H]antagonist binding. However one-site competition curves with variable Hill slopes do not provide estimates of the two agonist affinity constants or the fraction of agonist binding which is of high affinity. Therefore in order to more accurately describe biphasic binding of partial agonists the competition assay was modified and performed in the presence and absence of 100 μM GTP. Both curves ($\pm$ GTP) were performed in the same rack of tubes at the same time in order to reduce variability and to increase the reliability of analysis using shared parameters from both curves. The curve in the presence of GTP was best fit to a one-site model and the low affinity binding constant was obtained. Two-site analysis of the curve in the absence of GTP was constrained to 0% and 100% (bottom and top respectively) and the low affinity binding constant obtained in the presence of GTP. This left only fr_H and the high affinity binding constant to be estimated from the two-site curve.

The work presented here shows the adenosine A_1 receptor agonists GR190178, GR161144 and GR162900 all exhibit reduced "GTP shift" than the high efficacy agonist CHA when examined in competition binding experiments with [^{3}H]DPCPX (Figure 4.6 on page 91). That is, they show a reduced difference between the high (K_H) and low (K_L) affinity constants of agonist binding at equilibrium. This can be expressed as the ratio of agonist affinities ($\frac{K_H}{K_L}$), alternatively termed "GTP shift." If this is related to agonist efficacy, then the competition curves presented in Figure 4.6 suggest a rank order of efficacy at the human adenosine A_1 receptor of CHA $\gg$ GR190178 $\gg$ GR161144 $>$ GR162900. This is in agreement with previous work on these compounds (Browning 2003, Sheehan *et al.* 2000).

The best fit curves and estimates of fr_H in Figure 4.6 are possibly not visually reliable. Other studies have observed decreased fr_H with reduced ligand efficacy at the adenosine A_1 receptor (Lorenzen *et al.* 1996), and visual inspection of the data in Figure 4.6 appears to indicate this too, but non-linear regression does not resolve a difference in fr_H between CHA, GR190178 and GR161144. The experiments described in Figure 4.6 using the partial agonists were performed using A_1HE membranes which exhibited an unusually high fr_H compared to other batches of A_1HE membranes. However, of interest is the estimate of fr_H relative to the other agonists in

the experiment, rather than comparison of absolute fr_H values between different experiments. Non-linear regression of the [^{3}H]DPCPX / GR162900 competition curves does identify a reduced fr_H compared to CHA, GR190178 and GR161144. Previous [^{3}H]DPCPX competition binding experiments here by Chris Browning using a slightly different approach indicated that GR190178 and GR161144 both exhibited reduced fr_H compared to CHA (Browning 2003). An estimate of fr_H for GR162900 was not resolved as the [^{3}H]DPCPX competition data could not be adequately described by a two-site competition curve.

The [^{3}H]DPCPX competition assay performed in the same rack of tubes both in the presence and absence of GTP enabled estimation of the GTP shift for partial agonists of very low efficacy such as GR162900. The results provide evidence that agonists of very low efficacy may also exhibit reduced fr_H. This implies that fr_H may be dependent on the nature of the bound agonist as well as the molecular composition of the receptor signalling complex.

Equilibrium antagonist and agonist binding at membranes expressing the A_1R-GFP or A_1R-GFP-Gα_i fusion constructs.

A simplified combined [^{3}H]DPCPX saturation and [^{3}H]DPCPX / CHA competition assay was designed in order to characterise the equilibrium binding properties of membranes prepared from all 24 A_1R-GFP and 23 A_1R-GFP-Gα_i cell lines. Details of this assay are described on page 90, and in Figures 4.7 and 4.8 on pages 93 and 94 respectively. The simplified assay enabled rapid and efficient characterisation of a large number of membrane preparations in a single experiment and the results obtained were precise and reproducible. Table 4.3 on page 95 lists mean parameters estimated using the simplified assay for all membranes expressing the A_1R-GFP or A_1R-GFP-Gα_i fusion constructs. Tables 4.4 and 4.5 compare mean [^{3}H]DPCPX and [^{3}H]CHA affinities estimated using the simplified assay (A_1R-GFP and A_1R-GFP-Gα_i membranes) and more detailed experiments (A_1LE and A_1HE membranes). In general the mean log affinities obtained were similar for each membrane type (A_1LE, A_1HE, A_1R-GFP and A_1R-GFP-Gα_i) although a thorough experimental and statistical comparison of the reliability of the simplified assay compared to more thorough experiments was not performed. Of more interest was not the absolute accuracy of the estimates obtained by the simplified assay, but instead whether there was a dependence of any of the parameters on the level of receptor expression.

When [^{3}H]DPCPX log affinity results for both the A_1R-GFP or A_1R-GFP-Gα_i fusion constructs were combined, [^{3}H]DPCPX affinity was not dependent on the level of receptor expression. Also, the A_1R-GFP-Gα_i [^{3}H]DPCPX log affinity data alone was not dependent on the level of receptor expression. However the A_1R-GFP membranes did show a significant reduction in

[^{3}H]DPCPX log affinity with increased receptor expression. Estimation of [^{3}H]DPCPX affinity at very low levels of expression was at times more difficult due to the much reduced level of specific [^{3}H]DPCPX binding. Visual inspection of the data presented in Figure 4.9 on page 96 shows a greater spread of log affinity estimates at low levels of expression for the A_1R-GFP-Gα_i construct. This may be a reflection of the reduced accuracy of affinity estimates at low levels of expression with low levels of specific binding. Why the A_1R-GFP membranes appear to exhibit increased [^{3}H]DPCPX affinity at low levels of receptor expression is unclear. However as the A_1R-GFP-Gα_i membranes, along with A_1LE and A_1HE membranes, show no evidence of any dependence of [^{3}H]DPCPX affinity on receptor expression it would be difficult to propose a mechanism by which the level of A_1R-GFP expression appreciably determines [^{3}H]DPCPX affinity.

No significant difference was observed between the two fusion constructs for both the high and low CHA affinity constants estimated by means of the simplified 5-point [^{3}H]DPCPX / CHA competition assay. Table 4.5 on page 99 shows mean CHA log affinities for A_1LE, A_1HE, A_1R-GFP and A_1R-GFP-Gα_i membranes and compares them to direct [^{3}H]CHA saturation data. In general the CHA log affinity estimates of membranes expressing the fusion constructs are similar to that of the A_1LE and A_1HE membranes, although the fusion constructs show a reduced "GTP shift" compared to A_1LE and A_1HE. From Table 4.5 GTP shifts of 251, 263, 602 and 1174 (for A_1R-GFP, A_1R-GFP-Gα_i, A_1HE and A_1LE respectively) can be calculated. It should be noted that the A_1LE and A_1HE CHA affinity constants were estimated by means of detailed competition assays, whereas the A_1R-GFP and A_1R-GFP-Gα_i membranes were characterised by the 5-point competition assay. However, the simplified assay was not designed for absolute accuracy in order to compare estimates outwith the assay, but was designed in order to investigate the effect of receptor expression on features of equilibrium binding.

No significant difference was observed between the two fusion constructs for either the low (K_L) or high (K_H) mean log affinity constants of CHA binding. The two fusion constructs have indistinguishable mean affinities for CHA. Therefore the data from both constructs were pooled in order to investigate the effect of receptor expression level on the estimate of each CHA affinity constant. In addition to the CHA affinity constants for both fusion constructs Figure 4.10 on page 100 also shows the affinities of CHA for A_1LE and A_1HE membranes for comparison. Although again it should be noted that the A_1LE and A_1HE data was generated from detailed competition binding experiments and the A_1R-GFP and A_1R-GFP-Gα_i data was from the simplified 5-point competition assay. Both log K_L and log K_H appear to be essentially independent of [^{3}H]DPCPX B_{max}. Both affinity constants show a significant, but shallow, dependence on receptor expression (Figure 4.10). Repeat analysis of individual observations (rather than the means shown in Table 4.3)

showed the same shallow dependence of the CHA affinity constants on [^{3}H]DPCPX B_{max}.

In general it appears the affinities of [^{3}H]DPCPX and CHA are essentially independent of the level of expression of either the A_1R-GFP or A_1R-GFP-Gα_i fusion construct. Where a significant dependence on [^{3}H]DPCPX B_{max} was observed the slopes were shallow. In agreement with observations at A_1LE and A_1HE membranes, the affinities of both a high efficacy agonist and an inverse agonist are constant over a large range of levels of expression of the human adenosine A_1 receptor.

Detailed characterisation of the effect of receptor density on fr_H.

As discussed above, membranes prepared from cell lines expressing A_1R, A_1R-GFP or A_1R-GFP-Gα_i all showed similar affinities for [^{3}H]DPCPX and CHA which were essentially independent of the level of receptor expression. However the fraction of CHA binding which was of high affinity (fr_H) was clearly dependent on the level of receptor expression. The relationship between [^{3}H]DPCPX B_{max} and CHA fr_H observed at A_1LE and A_1HE membranes was confirmed in detail using membranes from all of the A_1R-GFP and A_1R-GFP-Gα_i cell lines. Figure 4.11 on page 101 illustrates the significant dependence of fr_H on the level of receptor expression for both the A_1R-GFP and A_1R-GFP-Gα_i series of membranes. Figure 4.12 on page 102 shows that the dependence of fr_H on [^{3}H]DPCPX B_{max} was similar for the adenosine A_1 receptor alone (A_1LE and A_1HE membranes) and the A_1R-GFP and A_1R-GFP-Gα_i fusion constructs. Although linear regression was used to determine a significant relationship or not, it is not known whether the nature of the relationship is indeed linear or whether fr_H plateaus at the extreme low and/or high levels of receptor expression.

Membranes from A_1R-GFP-Gα_i cell line 4F2 show a [^{3}H]DPCPX B_{max} and CHA fr_H that do not follow the relationship observed at all the other membranes (Table 4.3). 4F2 is clearly distinguished in the lower left region of Figures 4.11 and 4.12. Cell line 4F2 was selected as an individual cell of high fluorescence by means of gate 4 (Figure 3.1 on page 63), and cells from the mature 4F2 cell line were analysed by flow cytometry (Figure 3.2 on page 64) and observed to exhibit a low mean GFP brightness similar to cell lines created from cells selected by gates 2 and 3. While 4F2 exhibits reduced GFP fluorescence and [^{3}H]DPCPX B_{max}, it exhibits a low fr_H of 0.39 more similar to cell lines expressing much greater levels of the A_1R-GFP-Gα_i construct. Careful re-examination of the competition binding assay results clearly showed that this unusually low fr_H was indeed a property of the membranes and not an experimental artifact. In general membranes from most A_1R-GFP-Gα_i and all A_1R-GFP cell lines show a similar dependence of fr_H on the level of receptor expression. However membranes from cell line 4F2 show that it is possible in rare

situations to observe low fr_H at low levels of receptor expression.

Previous work here investigated the ability of the ternary complex model to predict the change in fr_H with level of receptor expression at A_1LE and A_1HE membranes (Browning 2003). While the ternary complex model was able to predict a reduction in fr_H at increased levels of receptor expression with no change in agonist or antagonist affinity, the predictions were not quantitatively compatible with observations at A_1LE and A_1HE membranes. As for A_1LE and A_1HE membranes discussed above, membranes prepared from cell lines expressing greater levels of the A_1R fusion constructs show lower fr_H but appear to be able to recruit greater amounts of G protein. The change in fr_H with receptor expression implies that the stoichiometry of adenosine A_1 receptor and G protein may change as the concentration of receptor increases. Also, studies have provided evidence that at increased level of adenosine A_1 receptor expression the receptor can stimulate functional responses through pertussis toxin-insensitive G proteins as well as pertussis toxin sensitive G proteins (Cordeaux *et al.* 2000). It is possible the increase in available G protein at higher levels of receptor expression may be the consequence of increased availability of pertussis toxin-sensitive G protein and also an increased ability to couple to pertussis toxin sensitive G protein.

The equilibrium binding properties of A_1R-GFP and A_1R-GFP-Gα_i are not sensitive to the presence of the tethered GFP or Gα_i. These constructs appear to interact with free G protein as effectively as the A_1R alone. This validates their use as models of the behaviour of the adenosine A_1 receptor alone. As the fused Gα_i does not appear to contribute to the radioligand binding properties of the A_1R-GFP-Gα_i construct, the presence of the truncated construct in some membranes (Figure 3.5 on page 71) may not be of pharmacological significance. Bevan *et al.* 1999 reported no coupling of tethered Gα_i at the A_1R-Gα_i construct, and much reduced potency for NECA stimulation of [^{35}S]GTPγS binding at the A_1R-GFP-Gα_i construct expressed in CHO cell membranes when endogenous Gα_i was inactivated by pertussis toxin. At best the tethered Gα_i of the A_1R-GFP-Gα_i fusion appears to couple to the receptor much more weakly than does endogenous Gα_i. It is possible this reduced level of coupling is not measurable by the [^{3}H]DPCPX / CHA competition assay used in the present study.

In summary, the equilibrium binding properties of membranes prepared from 49 cell lines (A_1LE, A_1HE, 23 for A_1R-GFP-Gα_i and 24 for A_1R-GFP) were characterised in detail. The affinities of DPCPX and CHA at these membranes were essentially independent of the level of receptor expression. While the affinities of CHA were independent of receptor density, the fraction of CHA binding of high affinity (fr_H) was clearly observed to decrease with greater levels of receptor expression. These observations provide evidence that the composition of the receptor signaling

complex is dependent on the level of receptor expression. The receptor signalling complex may be composed of several different proteins, and changes in its composition has the potential to alter many aspects of receptor behaviour and signalling. The A_1R-GFP and A_1R-GFP-Gα_i constructs appear to be valid models of the adenosine A_1 receptor alone.

Chapter 5

The kinetics of agonist and antagonist binding at the human adenosine A_1 receptor.

5.1 Introduction.

The kinetics of binding at GPCRs provides insights into both the binding of ligand and the response of the receptor to ligand. In common with the nature of equilibrium agonist binding, the kinetics of agonist binding at the adenosine A_1 receptor are complex. Previous work within the receptor group at NIMR described novel observations of agonist and antagonist binding at the human adenosine A_1 receptor expressed in stable CHO cell lines. These observations included two-phase exponential association of the antagonist [^{3}H]DPCPX and incomplete dissociation of the agonist [^{3}H]CHA (Cohen *et al.* 1996b, Browning 2003). In this Chapter the nature of association and dissociation of [^{3}H]DPCPX and [^{3}H]CHA at A_1HE membranes has been characterised in detail and compared briefly to other adenosine A_1 receptor membrane preparations.

5.2 Description of methodology.

To study the kinetics of radioligand dissociation a reverse time course strategy to enable simultaneous filtration was developed based on previous studies (Cohen *et al.*, 1996b; Hulme and Birdsall, 1992). A reverse time course strategy offers significant benefits in assay throughput by allowing many time points to be filtered simultaneously at the end of their incubation. A rack of 48 tubes,

or a 96-well plate, containing many different incubation times and, on occasion, both association and dissociation time courses can be processed rapidly and uniformly at the same time.

Prior to the initiation of dissociation, radioligand and membrane were incubated in a volume of 100 μl for between 5 min and 3 hours. Following the period of association, dissociation was initiated by means of a 20 fold dilution into buffer in order to reduce the concentration of radioligand significantly below its K_D. In order to reduce interference arising from the rebinding of radioligand even at these reduced concentrations, the 20 fold dilution contained in many experiments an excess concentration of unlabelled competing ligand, generally termed a "chase". The presence of GTP in the chase solution was employed in some experiments to investigate the effect of disruption of receptor-G protein coupling on radioligand dissociation. A dissociation incubation of between 5 min and 3 hours followed before simultaneous filtration onto glass fibre filters. Briefly outlined, the methodology employed to characterise the kinetics presented in this Chapter (and Chapter 6) was as follows;

1. Membranes were prepared from stable CHO cell lines expressing the adenosine A_1 receptor alone (A_1HE and A_1LE), or either of the A_1R-GFP and A_1R-GFP-Gα_i fusion constructs (Chapter 2.2.2 on page 51).

2. The membrane preparations were incubated with adenosine deaminase for 30 min at RT (22^{o}C) in order to remove endogenous adenosine which, if not removed, would inhibit the binding of radiolabelled and unlabelled ligands. Membranes were diluted and placed on ice after adenosine deaminase incubation.

3. Radioligand and membranes were incubated in a small volume (100 μl) at RT for 1 hour. [For association assays the incubation was terminated at the appropriate time here by rapid filtration onto glass fibre filters.]

4. The dissociation experiments were initiated by means of a 20-fold dilution of the 100 μl aliquots from step 3 above (addition of 2 ml buffer in the presence or absence of chase ligand) reducing the concentration of radioligand to well below its K_D.

5. Dissociation of the radioligand was terminated at given times by rapid filtration onto glass fibre filters.

Figure 5.1 on page 115 illustrates differences between measuring the dissociation of bound radioligand by dilution with buffer and dissociation by dilution in the presence of a competing unlabelled ligand (or "chase"). Each of the points are explained in more detail below;

Initial association. Prior to dissociation radioligand (**L**) is incubated with the receptor (**R**) for a period of time, which on occasion is sufficient for the system to reach a state of equilibrium (**L** + **R** $\rightleftharpoons$ **L.R**) (Figure 5.1a). In the case of high affinity agonist binding to the adenosine A_1 receptor, **L.R** is the high affinity agonist-receptor-G protein ternary complex.

Dissociation by dilution alone. Dissociation of **L** from **L.R** can be performed by dilution of the radioligand well below its K_D. The radioligand **L** will then dissociate from the receptor until it reaches an equilibrium corresponding to the new lower concentration of radioligand (Figure 5.1b). Even at low concentrations the radioligand binds to the receptor to an extent and the observed rate of dissociation will be a consequence of both the "on" and "off" rates of the radioligand for the receptor. This re-association should be negligible if the radioligand is diluted to $< 0.1\ K_D$.

Prevention of rebinding of a radioligand by a "chase" ligand. When dissociation is performed by dilution in the presence of a high concentration of a competing unlabelled ligand (**X**), the binding site is rapidly occupied by unlabelled ligand as radioligand dissociates from the receptor (Figure 5.1c). Due to the very much higher concentration of unlabelled ligand than radioligand the receptor effectively remains occupied by unlabelled ligand and re-association of radioligand to the receptor is blocked. The rate of dissociation of radioligand observed in the presence of a high concentration of unlabelled ligand is predominantly determined by the radioligand off-rate and is not influenced by the on-rate. The addition of chase ligand combined with dilution of the association incubation offers a number of experimental benefits when studying the adenosine A_1 receptor over the addition of a small volume of very concentrated chase ligand with minimal dilution. As non-specific binding can depend on the amount of radioactivity present rather than the concentration of radioligand, an assay volume of 100 μl requires less radioactivity than the same concentration of radioligand in a greater volume of 2 ml. Therefore the incubation of membranes and radioligand in a small volume (100 μl) followed by dilution into a large volume (2 ml) may reduce non-specific binding of radioligand compared to incubation in a greater volume (such as 1 or 2 ml) followed by addition of a small volume of very concentrated chase ligand. Also, it may be difficult to make sufficiently concentrated solutions of chase ligand if the chase solution itself will be significantly diluted by addition to the association incubation.

Effect of the chase ligand and its nature on the dissociation rates. In simple monomeric systems the kinetics of dissociation should be independent of the method of dissociation and the pharmacology of chase ligand (Figure 5.1d). The kinetics of dissociation by means of

dilution only should be compatible with dissociation by dilution containing a high concentration of unlabelled chase ligand. Although chase ligand prevents re-association of radioligand to the receptor, the extent and kinetics of dissociation by the two methods may not be absolutely identical. If the receptors are clustered together the dilution protocol allows the possibility that the radioligand, after dissociation from one receptor molecule, can have a high probability of rebinding to a nearby unoccupied receptor because of the locally high concentration of receptors. This option is not available to the chase protocol because all neighbouring receptors are occupied by the chase ligand.

5.3 The kinetics of the association of [^{3}H]DPCPX to the adenosine A_1 receptor.

[^{3}H]DPCPX associated rapidly to membranes prepared from the A_1HE cell line, with observed rate constants of association (k_{obs}) of 0.26 ± 0.01 and 0.30 ± 0.01 min^{-1} at 0.2 and 1.0 nM [^{3}H]DPCPX respectively (both n = 2). Levels of bound [^{3}H]DPCPX reached a maximum after approximately 20 minutes, before decaying to a plateau. Association of 0.3 nM [^{3}H]DPCPX appeared to exhibit a larger difference between maximum and final equilibrium specific binding than 1 nM [^{3}H]DPCPX (data not shown). 100 μM GTP increased specific [^{3}H]DPCPX binding consistent with its ability to disrupt receptor-G protein complexes and increase the binding of inverse agonists and the decrease in [^{3}H]DPCPX binding at long incubation times appeared to be attenuated in the presence of GTP (not shown).

All membranes used for the radioligand binding experiments presented in this study were incubated with 3 U/ml of the adenosine catabolising agent, adenosine deaminase, for 30 min before incubation with radioligand. The [^{3}H]DPCPX association kinetics described in the above paragraph were treated in this manner as well. The pretreatment of A_1HE membranes with adenosine deaminase and the membrane permeabilising agent saponin before incubation with [^{3}H]DPCPX was investigated further. The association of 0.3 nM [^{3}H]DPCPX to A_1HE membranes following different 30 min pre-incubation conditions is shown in Figure 5.2 on page 117. Adenosine deaminase and saponin pre-treatment both increased [^{3}H]DPCPX binding at all time points. The greatest difference between maximum and plateau [^{3}H]DPCPX SB was observed in the absence of adenosine deaminase. Complex antagonist-GPCR association curves of this form are unusual, but have been described in GPCR systems such as the muscarinic M_2 receptor for the split receptor (Novi *et al.*, 2003). However, a straightforward mechanism may be responsible for the decay of

Figure 5.1 Different conditions used to investigate the dissociation of ligand from a receptor.

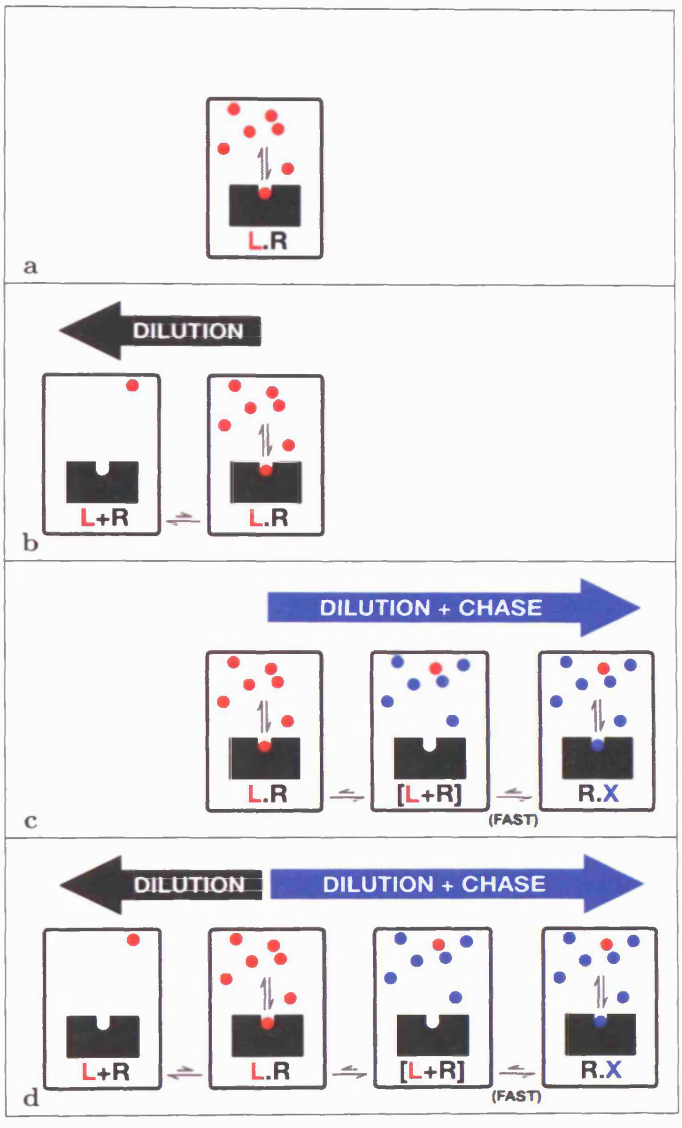

Figure 5.1: **(a)** Prior to dissociation, radioligand (**L**) is incubated with receptor (**R**), often until the system reaches equilibrium (**L** + **R** $\rightleftharpoons$ **L.R**). **(b)** Following dissociation by dilution alone the level of bound radioligand is reduced according to the new lower concentration of **L**. **(c)** In the presence of a high concentration of competing unlabelled "chase" ligand (**X**), **L** will not re-associate to the receptor once it has dissociated. **(d)** In simple monomeric systems the kinetics of dissociation should be independent of the method of dissociation and the pharmacology of chase ligand. See page 113 for more detailed description.

bound [^{3}H]DPCPX with time; slow release of endogenous adenosine from the membrane preparation may progressively compete with the binding of [^{3}H]DPCPX. Pre-incubation of membranes with both adenosine deaminase and saponin almost entirely removes the slower inhibitory component observed in the binding of [^{3}H]DPCPX. It is possible that the reason saponin is required in the membrane pre-incubation is that it enables adenosine deaminase access to all the adenosine present in the membrane preparation. In all binding assays presented here (other than Figure 5.2) membranes were incubated with adenosine deaminase, but not saponin, for 30 min prior to incubation with radioligand (Chapter 2.2.3 on page 51). 30 μg/ml saponin was present in all binding assays during incubation of radioligand with membranes.

5.4 The kinetics of the dissociation of [^{3}H]DPCPX from the adenosine A_1 receptor.

[^{3}H]DPCPX dissociated rapidly from A_1HE, A_1LE and A_1R-GFP-Gα_i membranes and the data could be described reasonably well by a simple mono-exponential function (Figure 5.3 on page 118). Following dissociation by dilution, [^{3}H]DPCPX binding decays to levels expected from the diluted concentration of [^{3}H]DPCPX. Dilution in the presence of a high concentration of competing unlabelled ligand (10^{-6} M DPCPX or 10^{-4} M CHA) results in dissociation of [^{3}H]DPCPX to non-specific levels. The mean rate constants of dissociation (k_{off}) for A_1HE, A_1LE and A_1R-GFP-Gα_i membranes in all conditions were 0.22 $\pm$ 0.01 (n = 5), 0.24 $\pm$ 0.02 (n = 3) and 0.23 $\pm$ 0.02 (n = 14) min^{-1}respectively ($t\frac{1}{2}$ 3.2, 2.9 and 3.0 min respectively). The low number of replicate estimates deters conclusive analysis of variance, and the s.e.m.s of each mean overlap, showing a lack of any significant difference with the data above. Addition in the 2 ml chase of saponin, which permeabilises vesicular structures in the membrane preparation (Cohen *et al.*, 1996b), did not noticeably alter the rate of dissociation of [^{3}H]DPCPX. The rate constant of dissociation was similar when 10^{-6} M DPCPX, 10^{-4} M CHA, 10^{-4} M GTP or 10 μg/ml saponin was present in the chase solution (or indeed when 10^{-4} M CHA, 10^{-4} M GTP and 10 μg/ml saponin were all present). The rate of dissociation of [^{3}H]DPCPX from the adenosine A_1 receptor appears to be independent of the agonist or antagonist pharmacology of the competing chase ligand used to prevent [^{3}H]DPCPX rebinding. Non-linear regression suggests the dissociation of [^{3}H]DPCPX might not be absolutely monoexponential, possibly possessing more than one component, although this was only an indication as the deviations from monoexponential curves were small and were not investigated further.

Figure 5.2 The association of [^{3}H]DPCPX to A_1HE membranes.

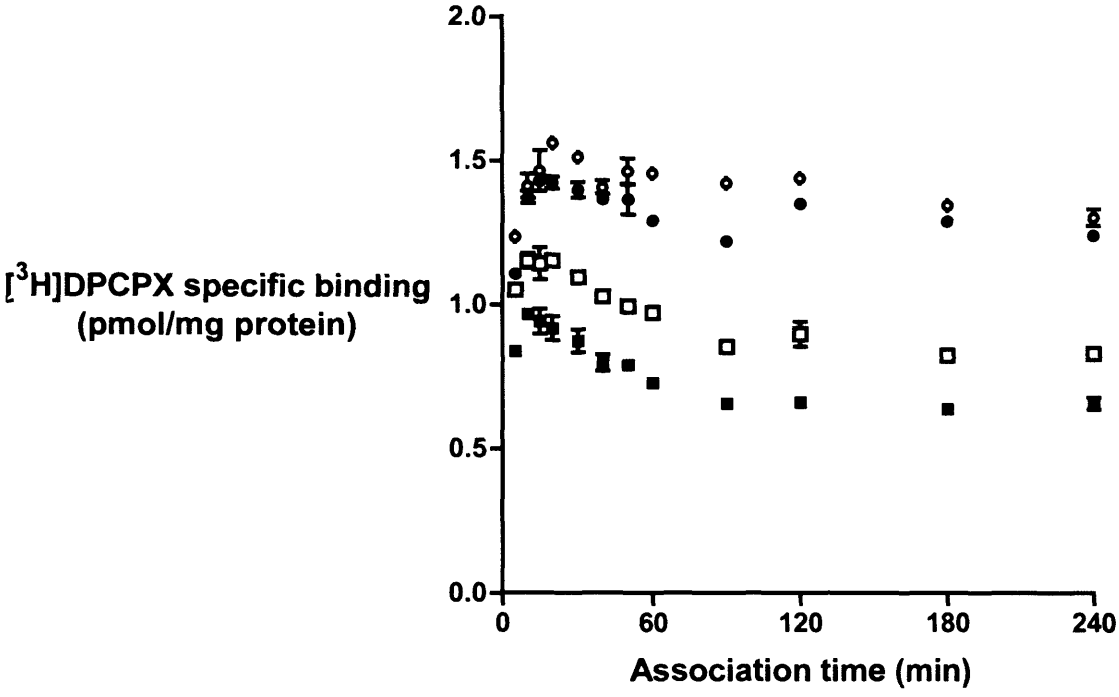

30 min 22^{o}C membrane pre-incubation conditions		
	Adenosine deaminase (1.2 U/ml)	Saponin (30 μg/ml)
○	+	+
●	+	-
□	-	+
■	-	-

Figure 5.2: Representative experiment investigating the association of 0.3 nM [^{3}H]DPCPX to A_1HE membranes, performed in duplicate. The effect of 1.2 Units/ml adenosine deaminase and 0.2 mg/ml saponin in the 30 min membrane pre-incubation prior to association is shown. 30 μg/ml saponin was present in all association time points, as for all radioligand binding experiments.

Figure 5.3 The dissociation of [^{3}H]DPCPX from the adenosine A_1 receptor.

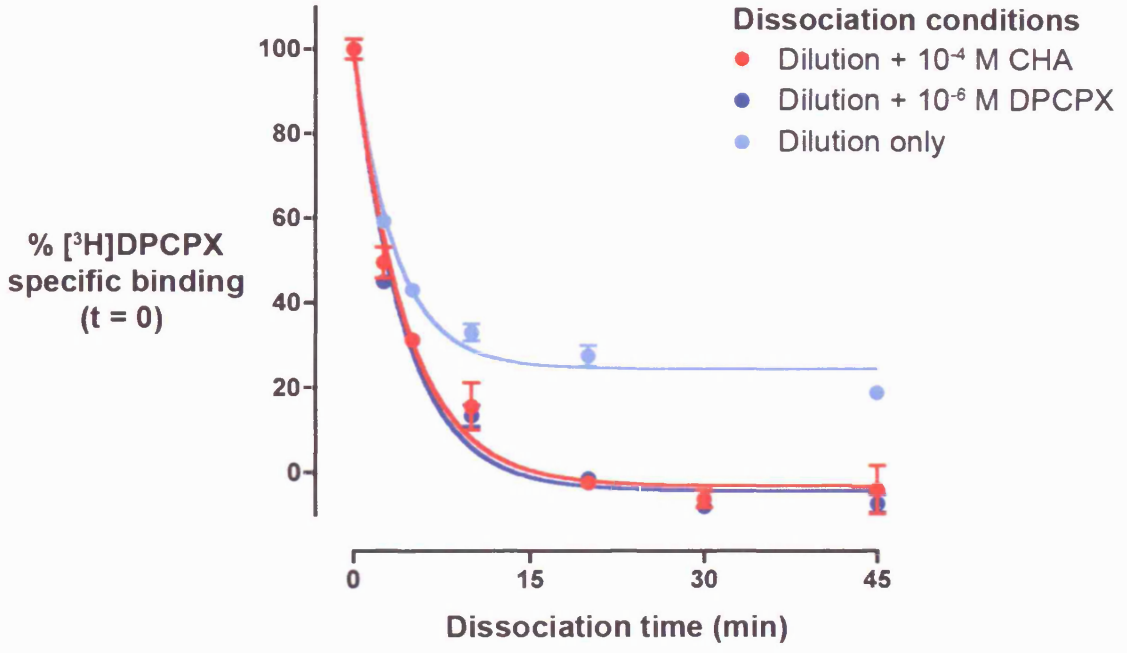

Figure 5.3: Representative [^{3}H]DPCPX dissociation curves, showing the dissociation of [^{3}H]DPCPX from A_1LE membranes by 20-fold dilution in the presence or absence of CHA or DPCPX chase. The concentration of [^{3}H]DPCPX before 20-fold dilution was 10 nM. The rate constant of dissociation was similar when 10^{-6} M DPCPX or 10^{-4} M CHA was present in the 2 ml chase solution (k_{off} 0.23 and 0.22 min^{-1} respectively for the curves above). All [^{3}H]DPCPX dissociation experiments were performed at RT (22^{o}C).

5.5 The kinetics of the association of [^{3}H]CHA to A_1HE and A_1R-GFP-Gα_i membranes.

The association of [^{3}H]CHA to A_1HE membranes was best described by a two-phase model of exponential association. The two-phase exponential association of [^{3}H]CHA was observed in the usual association assay volume of 100 μl and also in volumes of 2 ml. Data from a single experiment investigating the dependence of the association of [^{3}H]CHA on the concentration of [^{3}H]CHA in a volume of 100 μl is shown in Figure 5.4 on the following page. Higher concentrations of [^{3}H]CHA showed a greater extent of binding and also a faster initial rate of association, as would be expected. Figure 5.5 on page 122 plots mean parameters describing the two components of the association of [^{3}H]CHA to A_1HE membranes. The observed rate of the fast component of [^{3}H]CHA association was dependent on the concentration of [^{3}H]CHA (Figure 5.5a). Linear regression of all the individual observations (rather than mean values) showed a significantly non-zero slope (P = 0.007) with a y-axis intercept of 0.1 min^{-1} and a slope of 0.02. For a simple binding process the equation, $k_{obs} = k_{+1}.[L^*] + k_{-1}$, describes the observed association with the y-axis intercept (0.1 min^{-1}) representing the off rate (k_{-1}) of [^{3}H]CHA[1]. This estimate agrees with the mean fast rate constant for the dissociation of [^{3}H]CHA from A_1HE membranes in the presence of a high concentration of CHA (in order to measure dissociation of [^{3}H]CHA without rebinding) which was 0.12 $\pm$ 0.01 (n = 28). [The kinetics of the dissociation of [^{3}H]CHA from the A_1R are described later, in Chapter 5.6 beginning on page 124.]

The product of the observed rate (k_{obs}) and amplitude of the association of [^{3}H]CHA is the initial rate. This parameter is the gradient of the association curves at $t \rightarrow 0$, and is useful as it combines two estimates from experimental observations. Figure 5.5c shows the clear dependence of the initial rate on the concentration of [^{3}H]CHA for the fast component of the association of [^{3}H]CHA. Linear regression observed a significantly non-zero slope (P < 0.0001) as indicated on the graph by the broken line. Figures 5.5a and 5.5c show the fast component of the association of [^{3}H]CHA is entirely dependent on the concentration of [^{3}H]CHA. This is consistent with this component being a simple bimolecular interaction obeying the law of mass action.

The slow component of the association of [^{3}H]CHA to A_1HE membranes is illustrated in the same manner in Figures 5.5b and 5.5d. The dependence of the slow component of [^{3}H]CHA association on the concentration of [^{3}H]CHA is less distinct than for the fast component. Linear regression of k_{obs} against [^{3}H]CHA concentration for the slow component did not show a sig-

[1] $k_{obs} = k_{+1}.[L^*] + k_{-1}$; k_{obs} is the observed rate, k_{+1} and k_{-1} are the on and off rates respectively and $[L^*]$ is the concentration of [^{3}H]CHA.

Figure 5.4 Two-phase exponential association of [^{3}H]CHA to A_1HE membranes.

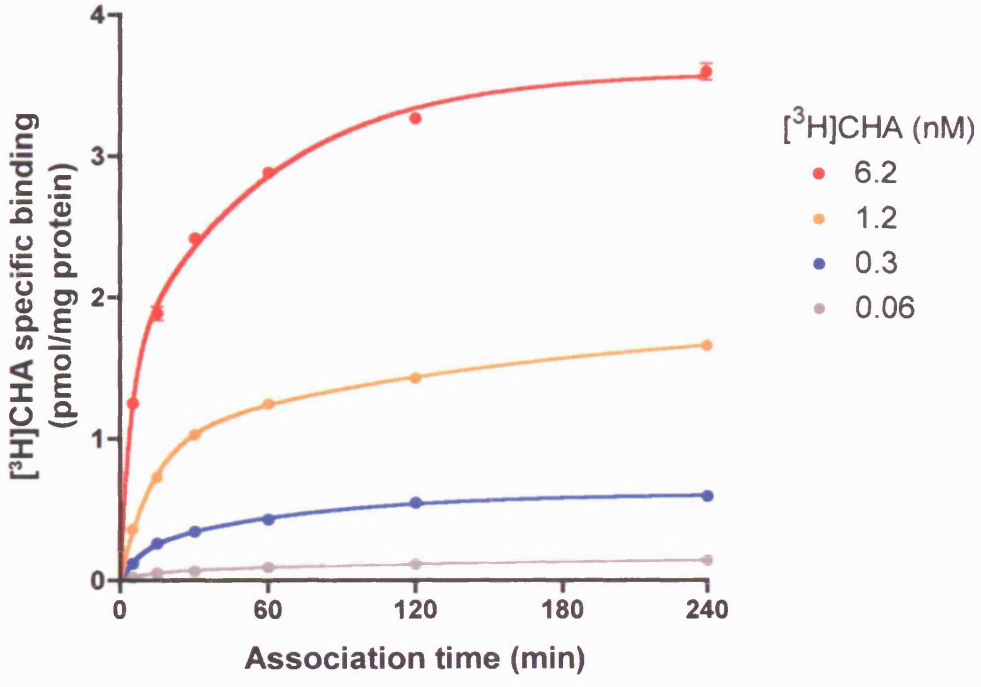

Figure 5.4: Representative [^{3}H]CHA association curves from a single experiment indicating the extent and initial rate of association to A_1HE membranes are dependent on the concentration of [^{3}H]CHA. The association of [^{3}H]CHA at the four concentrations shown was best fit in all cases to a two phase model of exponential association. The [^{3}H]CHA association curves shown were performed in a total volume of 100 μl. The association curves above are the same data as shown in Figure 4.2 on page 83, but expressed as association time courses rather than [^{3}H]CHA saturations.

nificantly non-zero slope (Figure 5.5b), however linear regression of the initial rate did show a significantly non-zero slope (P = 0.04, line not shown on Figure 5.5d). It is possible that the slow component of the association of [^{3}H]CHA to A_1HE membranes is not entirely dependent on the concentration of [^{3}H]CHA, although with the limited data presented here it is difficult to establish an absolute relationship either way. The initial fast association of [^{3}H]CHA appears to be the result of binding to readily available high affinity agonist binding sites, forming the high affinity agonist-receptor-G protein complex. The slow rate of [^{3}H]CHA association may be influenced by a factor other than [^{3}H]CHA concentration, which may include the recruitment of extra G protein into the receptor environment.

The data described in Figure 5.5 also provides an insight into the relative amplitudes of the fast and slow components of [^{3}H]CHA association. There is not enough information at higher concentrations of [^{3}H]CHA to directly estimate the maximum of each amplitude, but the data from Figure 5.4 when expressed as a saturation curve (Figure 4.3 on page 84) extrapolates to a maximum [^{3}H]CHA B_{max} of 4.1 pmol/mg protein. Fitting the data shown in Figures 5.5e and 5.5f to a sigmoidal dose-response curve constrained to a top of 2.05 (50% of 4.1) and bottom of 0 generates a curve which is compatible with the observed results. Little difference was observed between best fit sigmoidal dose response curves with fixed or variable slopes. Best fit sigmoidal dose response curves for both components showed similar log EC_{50}'s of 8.5 and 8.8 (fast and slow respectively). The data appears to be consistent with a model where there is a 1:1 stoichiometry between the amplitudes of the two components of [^{3}H]CHA association. However there is not enough data to establish this definitively. 1:1 stoichiometries of kinetic processes and equilibrium binding properties becomes of interest when considering receptor dimerisation, and is discussed later.

Preliminary investigations characterised the association of [^{3}H]CHA (11 $\pm$ 3 nM, n = 2) to membranes prepared from A_1R-GFP-Gα_i cell lines 2H7 and 3D4 ([^{3}H]DPCPX B_{max} 1.8 and 6.5 pmol/mg protein respectively, see Table 4.3 on page 95). Table 5.1 on page 123 lists mean estimates of k_{obs} and the initial rate obtained in the same manner as for A_1HE described above and illustrated in Figure 5.5. For both membranes the association of [^{3}H]CHA was best described by a two phase model of exponential association. There is insufficient data to determine with certainty whether there is a real difference in the rates of [^{3}H]CHA association between membranes prepared from A_1R-GFP-Gα_i cell lines 2H7 and 3D4, although there is the suggestion of faster association with membranes from cell line 3D4 which expresses a higher concentration of the A_1R-GFP-Gα_i construct. All rate constants of association shown in Table 5.1 were faster for membranes 3D4 than 2H7.

Figure 5.5 The dependence of the rate of association of [^{3}H]CHA to A_1HE membranes on the concentration of [^{3}H]CHA.

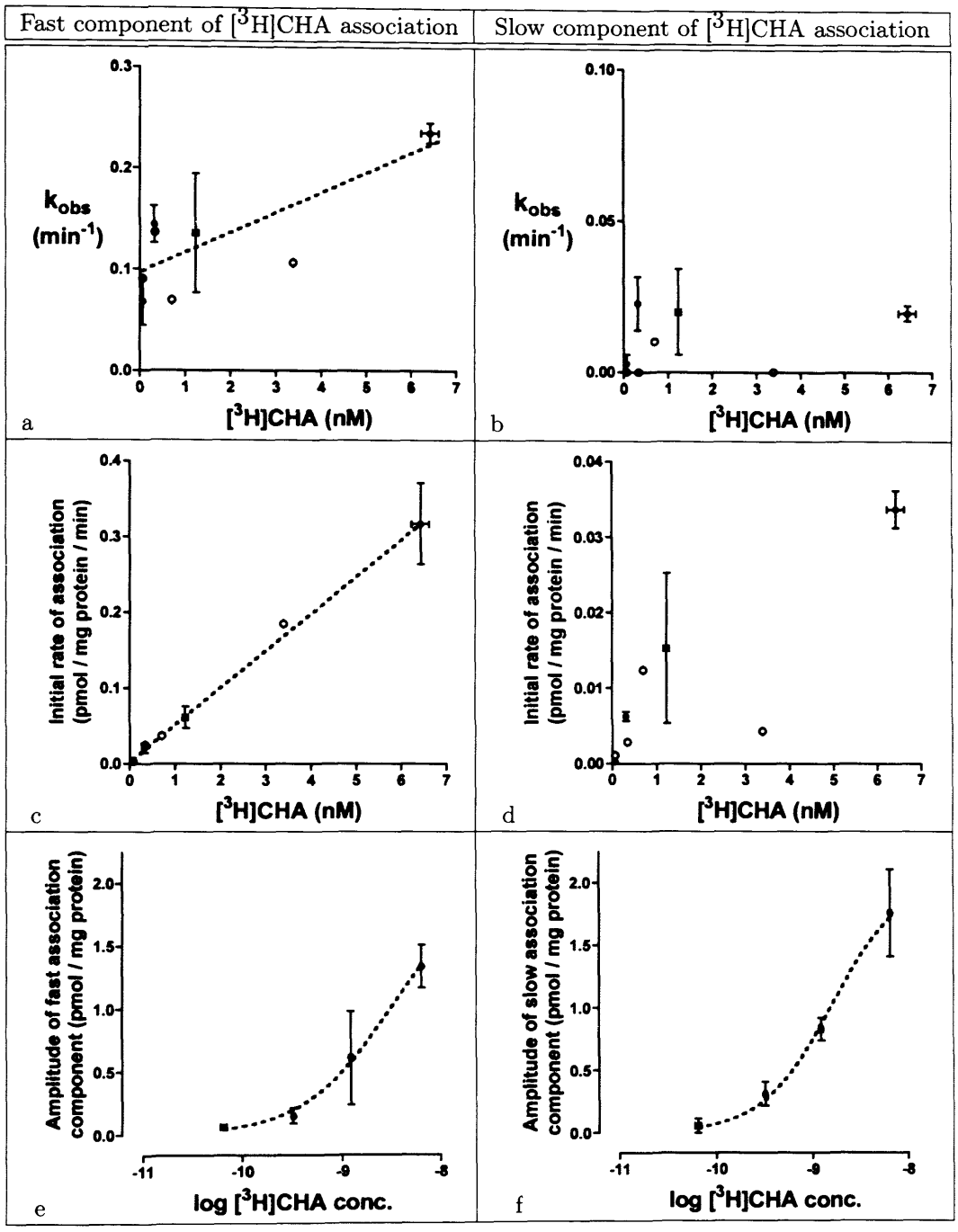

Figure 5.5: **(a & b)** The effect of the concentration of [^{3}H]CHA on the observed rates of the two components of association to A_1HE membranes in volumes of 100 μl (•) and 2 ml (o). **(c & d)** The kinetics of [^{3}H]CHA association are also represented as initial rates, the product of the observed rate constant and the amplitude of each component. **(e & f)** The amplitude of each component of [^{3}H]CHA association plotted against log [^{3}H]CHA concentration. Data are shown for 100 μl and are the mean (± s.e.m.) of two independent experiments, one of which is shown in Figure 5.4. The 2 ml data are from a single experiment.

Table 5.1 Preliminary data on the kinetics of the association of [^{3}H]CHA to A_1R-GFP-Gα_i membranes.

A_1R-GFP-Gα_i membranes	2H7	3D4
$k_{obs,\ fast}$ (min^{-1}, n = 2)	0.22 ± 0.10	0.30 ± 0.03
$k_{obs,slow}$ (min^{-1}, n = 2)	0.013 ± 0.004	0.023 ± 0.009
fast initial rate of association (pmol/mg protein/min, n = 2)	0.11 ± 0.04	0.39 ± 0.08
slow initial rate of association (pmol/mg protein/min, n = 2)	0.005 ± 0.002	0.013 ± 0.005
[^{3}H]DPCPX B_{max} from Table 4.3 (pmol/mg protein)	1.77 ± 0.08	6.52 ± 0.55
High affinity [^{3}H]CHA binding capacity (pmol/mg protein)	1.13	3.57

Table 5.1: Association time courses for the association of [^{3}H]CHA to membranes prepared from A_1R-GFP-Gα_i cell lines 2H7 and 3D4 were performed as for A_1HE membranes (six total and non-specific points each in duplicate; as shown in Figure 5.4). Data was fit to a two-phase model of exponential association. Data shown are mean non-linear regression parameters for the rate constant of association of [^{3}H]CHA (k_{obs}) from two independent experiments. The initial rate of association, the product of the observed rate of association (k_{obs}) and the amplitude of the component, is the gradient of the association curves at $t \rightarrow 0$ as plotted for A_1HE membranes on Figure 5.5 on the previous page. The mean concentration of [^{3}H]CHA was 11 ± 3 nM (n = 2). The high affinity [^{3}H]CHA binding capacity is the population of total agonist binding which is of high affinity and was obtained by multiplying [^{3}H]DPCPX B_{max} and fr_H from Table 4.3 on page 95.

5.6 The kinetics of agonist dissociation from A_1HE membranes.

The dissociation of radiolabelled agonist from A_1LE and A_1HE membranes was investigated in the same manner as for [^{3}H]DPCPX. In contrast to the dissociation of [^{3}H]DPCPX, the dissociation of radiolabelled agonist was complex, heterogeneous and sensitive to the pharmacology of chase ligand. As for the association of agonist to the adenosine A_1receptor, dissociation typically exhibited two components of different rate constants. The slower component observed has traditionally been termed "agonist locking," postulated to be the result of the formation of pseudo-irreversible agonist-receptor complexes (Cohen *et al.*, 1996b; Waldhoer *et al.*, 1999). Agonist dissociation with "agonist locking" is typically described by a mono-exponential dissociation of agonist, to a plateau greater than non-specific binding. The results presented here instead favour two phase exponential dissociation to non-specific levels over a period of several hours in the presence of a high concentration of competing unlabelled ligand. In this section the dissociation of [^{3}H]CHA from the adenosine A_1receptor is investigated in detail.

5.6.1 Dissociation of [^{3}H]CHA from A_1HE membranes by 20-fold dilution.

Following 1 hour association at 22^{o}C in a volume of 100 μl, the dissociation of [^{3}H]CHA from A_1HE membranes by means of 20-fold dilution (2 ml) in assay buffer was mono-exponential and incomplete (Figure 5.6 on page 126). Mean levels of bound [^{3}H]CHA remaining after dissociation by 20-fold dilution are shown in Table 5.2 on page 126. The level of [^{3}H]CHA specific binding remaining following dilution was far greater than that expected from the remaining concentration of [^{3}H]CHA. Figure 5.6 illustrates that the dissociation of [^{3}H]CHA by 20-fold dilution does not decay to expected levels and was best described by a one-phase model of exponential dissociation to a plateau. The extent of dissociation of [^{3}H]CHA after 10 and 60 min was not dependent on the concentration of [^{3}H]CHA. After 180 min dissociation the level of bound [^{3}H]CHA showed a significant (P = 0.02), but shallow, dependence on the concentration of [^{3}H]CHA (Figure 5.7a on page 127. However, at all three dissociation time points and at all concentrations of [^{3}H]CHA the level of bound [^{3}H]CHA remaining was far in excess of the levels expected from the concentration of free [^{3}H]CHA following 20-fold dilution. Preliminary data on the dependence of the rate of dissociation of [^{3}H]CHA on the concentration of [^{3}H]CHA is shown in Figure 5.7b. The dissociation of [^{3}H]CHA from A1HE membranes by 20-fold dilution appears to be a simple mono-exponential

process (for which the rate constant of dissociation is dependent on the concentration of [^{3}H]CHA) which decays to a plateau of pseudo-irreversibly bound [^{3}H]CHA which is not reversed by 20-fold dilution alone.

Dissociation of [^{3}H]CHA initiated by 20-fold dilution containing 10^{-4} M GTP resulted in rapid loss of most bound [^{3}H]CHA (Figure 5.6). This indicates that the majority of bound [^{3}H]CHA which is not dissociated by 20-fold dilution is associated with high affinity agonist-receptor-G protein complexes. Dissociation of [^{3}H]CHA in the presence of 10^{-4} M GTP was best described by a two-phase exponential decay to non-specific levels. Most bound [^{3}H]CHA is rapidly removed by GTP although a fraction (approximately 15%) dissociates slowly. The dissociation of [^{3}H]CHA in the presence of GTP is described in more detail in Section 5.6.4 on page 143.

5.6.2 The dissociation of [^{3}H]CHA in the presence of a high concentration of unlabelled ligand.

When the dissociation of radioligand is performed by dilution into buffer, the level of binding at equilibrium should be dependent on the final concentration of radioligand. The observed rate of dissociation should not be dependent on the concentration of radioligand. Dissociation can also be measured by dilution in a high concentration of an unlabelled competing ligand, generally termed a "chase." This prevents rebinding of radioligand once it has dissociated, and results in an observed rate of dissociation which should be close to the off-rate (k_{off}) of that ligand. Figure 5.1 on page 115 illustrates the differences between the two approaches. Having investigated the dissociation of [^{3}H]CHA from A_1HE membranes by 20-fold dilution (described above), the dissociation of [^{3}H]CHA in the presence of high concentrations of unlabelled agonist or antagonist is described here.

Following 1 hour association at 22^{o}C, the dissociation of [^{3}H]CHA from A_1HE membranes was sensitive to the presence and agonist or antagonist pharmacology of the chase ligand (Figure 5.8 on page 129). The dissociation curves performed in the presence of chase ligand were complex and were not well described by a simple mono-exponential model of dissociation, as used for the dissociation of [^{3}H]CHA by 20-fold dilution alone. Instead, the dissociation of [^{3}H]CHA when performed in high concentration of chase ligand was best fit in by far the majority of cases by a two-phase model of exponential dissociation to a plateau of non-specific levels. As can be seen in Figure 5.8, dissociation in the presence of 10^{-4} M CHA (CHA chase) resulted in greater dissociation of [^{3}H]CHA than either 10^{-6} M DPCPX (DPCPX chase) or dilution alone. Table 5.3 on page 130 shows mean levels of bound [^{3}H]CHA remaining (as a percent of $t = 0$) at three time points when

Figure 5.6 Dissociation of [^{3}H]CHA from the A_1R-G protein complex by 20-fold dilution.

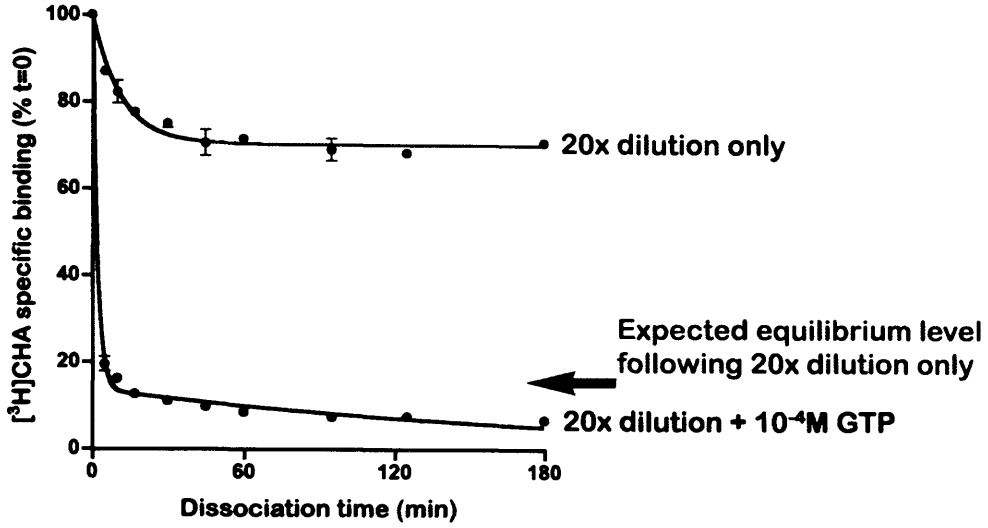

Figure 5.6: Representative curves of the dissociation of [^{3}H]CHA from A_1HE membranes. In the experiment shown above, 5.5 nM [^{3}H]CHA was incubated with 20 μg of A_1HE membrane protein for one hour at 22^{o}C in a total volume of 100 μl. Dissociation was initiated by a 20-fold dilution into 2 ml of buffer at RT. Dissociation of [^{3}H]CHA was performed in the absence (blue curve) and presence (black curve) of 10^{-4} M GTP. The expected level of specific binding following 20-fold dilution of 5.5 nM [^{3}H]CHA is indicated by the blue arrow. Dissociation of [^{3}H]CHA by dilution only was best fit by a model of mono-exponential decay to a plateau (dissociation rate constant estimates are illustrated in Figure 5.7b on page 127). In the presence of 10^{-4} M GTP the dissociation of [^{3}H]CHA was best described by a two-phase model of exponential decay to non-specific levels.

Table 5.2 Bound [^{3}H]CHA remaining after dissociation by 20-fold dilution.

Dissociation time (min)	10	60	180
[^{3}H]CHA % specific binding remaining (n = 22)	87.4 ± 1.2	70.9 ± 1.3	65.4 ± 1.6

Table 5.2: Mean levels of bound [^{3}H]CHA remaining after 10, 60 and 180 min dissociation by 20-fold dilution. The level of bound [^{3}H]CHA remaining after 10 and 60 min was not dependent on the concentration of [^{3}H]CHA (data not shown). A significant (P = 0.02), but shallow, dependence of the level of bound [^{3}H]CHA remaining after 180 min on the concentration of [^{3}H]CHA was observed and is illustrated in Figure 5.7a on page 127.

Figure 5.7 The dependence of the rate and extent of dissociation of [^{3}H]CHA from A_1HE membranes on the concentration of [^{3}H]CHA.

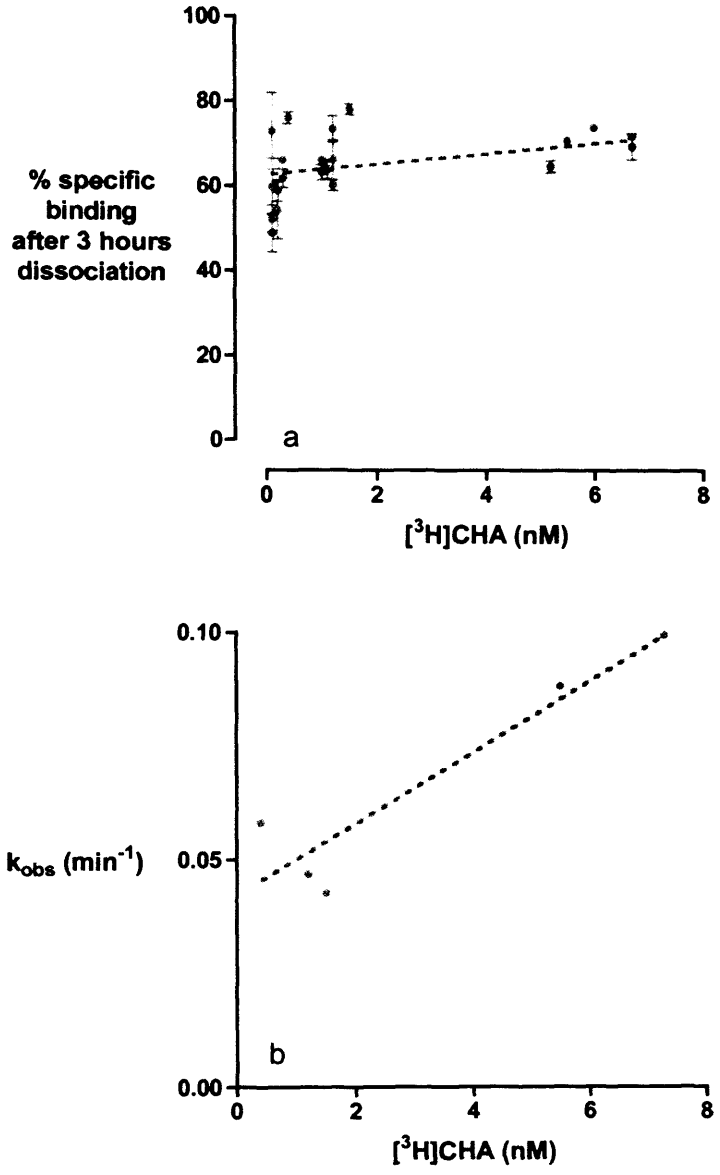

Figure 5.7: **(a)** The level of bound [^{3}H]CHA remaining after 3 hours (180 min) of dissociation following 20-fold dilution in buffer (as a percentage of bound [^{3}H]CHA at $t = 0$) is to an extent dependent on the concentration of [^{3}H]CHA during association (and hence also during dissociation). Linear regression showed a slope with a shallow but significantly non-zero slope ($P = 0.02$), indicated by the broken line. Results shown are the mean ($\pm$ s.e.m.) of observations performed in duplicate. **(b)** Preliminary data indicates the observed rate of [^{3}H]CHA dissociation (k_{obs}) following 20-fold dilution alone may be dependent ($P = 0.02$) on the concentration of [^{3}H]CHA during the association phase of the experiment. Results shown are individual estimates of the rate of dissociation obtained by non-linear regression using a model of one-phase exponential decay. In both graphs the x-axis is the concentration of [^{3}H]CHA during the 60 min association prior to initiation of dissociation by 20-fold dilution.

dissociation is performed by dilution alone or dilution in the presence of either CHA or DPCPX chase. At all time points CHA chase enhanced the dissociation of [^{3}H]CHA to a greater extent than DPCPX chase or dilution alone. The enhancement of the dissociation of [^{3}H]CHA by dilution containing DPCPX (relative to dilution alone) was negligible after 10 min but more pronounced after 60 and 180 min (Table 5.3). Enhanced dissociation of [^{3}H]CHA by CHA relative to DPCPX is a novel finding, consistent with the presence of a cooperative system. Table 5.4 on page 130 describes mean parameters of the two-phase exponential dissociation of [^{3}H]CHA by dilution in the presence of DPCPX or CHA. Unpaired t tests showed no significant difference for both the fast and slow rate constants of dissociation between the two chases. However, the amplitude of each component was significantly different for each chase ($P < 0.0001$ and $P = 0.0001$ for the fast and slow component respectively). The two rate constants of dissociation were approximately 100 fold different. When the data are analysed by a 2-exponential model, enhancement of [^{3}H]CHA dissociation by CHA appears to be manifest as a change in the relative amplitudes of the two components of dissociation rather than a difference in the rate constants of dissociation. None of the four parameters of dissociation ($k_{-1,FAST}$, $span_{FAST}$, $k_{-1,SLOW}$, & $span_{SLOW}$) for both CHA and DPCPX chase were dependent on the concentration of [^{3}H]CHA during the 60 min association prior to dissociation (Figure 5.9 on page 131). This is in contrast to the apparent dependence of the rate of dissociation of [^{3}H]CHA by 20-fold dilution alone on the concentration of [^{3}H]CHA. The mean concentration of [^{3}H]CHA during the 100 μl 60 min association was 4.6 $\pm$ 0.8 nM ($n = 11$) covering a range of 0.4 to 8.4 nM.

The ability of CHA to enhance the dissociation of [^{3}H]CHA relative to dilution alone and dilution containing DPCPX is a phenomenon that can be described as "agonist-induced agonist dissociation." Agonist-induced agonist dissociation was also observed using membranes from A_1LE, A_1R-GFP and A_1R-GFP-Gα_i cell lines. The dependence of features of the kinetics of agonist dissociation is described in Chapter 6 on page 165.

Identical experiments using the high efficacy adenosine A_1 receptor agonist [^{3}H]NECA at A_1HE membranes were very similar to the experiments described above using [^{3}H]CHA. The dissociation of [^{3}H]NECA in the presence of 10^{-6} M DPCPX or 10^{-4} M CHA was best described by a two-phase exponential decay to non-specific levels and CHA showed a greater ability than DPCPX to enhance the dissociation of [^{3}H]NECA (data not shown).

Figure 5.8 The dissociation of [^{3}H]CHA from A_1HE membranes by dilution in the presence of a high concentration of CHA or DPCPX.

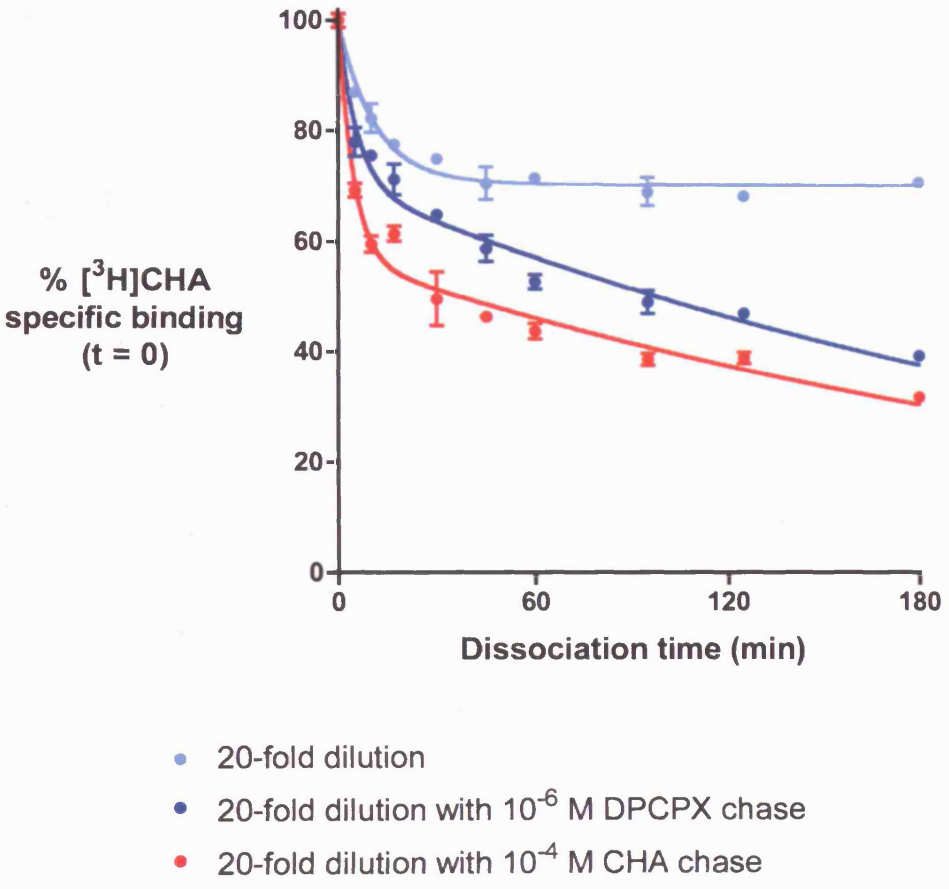

Figure 5.8: Representative [^{3}H]CHA dissociation curves by dilution in the presence or absence of CHA or DPCPX. Dissociation by 20-fold dilution alone (●) was best fit by a model of mono-exponential dissociation decaying to a plateau, as described in Section 5.6.1. Dissociation of [^{3}H]CHA in the presence of 10^{-4} M CHA (●) or 10^{-6} M DPCPX (●) were best fit by a model of two-phase exponential dissociation decaying to non-specific levels. Data shown is a single experiment performed in duplicate, except for the t=0 time point which was measured in sextuplicate.

Table 5.3 Mean levels of bound [^{3}H]CHA remaining after dissociation in the presence of a high concentration of competing unlabelled ligand.

Dissociation time (min)	10	60	180
Dissociation by 20-fold dilution, % specific binding remaining (± s.e.m.) (from Table 5.2, n = 22)	87.4 ± 1.2	70.9 ± 1.3	65.4 ± 1.6
20-fold dilution in the presence of 10^{-6} M DPCPX (n = 28)	86.1 ± 1.6	64.0 ± 1.7	46.6 ± 1.6
20-fold dilution in the presence of 10^{-4} M CHA (n = 29)	67.6 ± 1.4	44.2 ± 1.2	35.3 ± 1.2

Table 5.3: Mean levels of bound [^{3}H]CHA remaining at A_1HE membranes after 10, 60 and 180 min of dissociation by 20-fold dilution, or dilution in the presence of a high concentration of CHA or DPCPX. Three time points from the full dissociation curves were chosen for tabulation.

Table 5.4 Mean best fit parameters describing the two-phase exponential dissociation of [^{3}H]CHA from A_1HE membranes.

Two-phase exponential dissociation	Fast		Slow	
Rate (k_{-1}) and amplitude (span)	k_{-1} (min^{-1})	span (%SB)	k_{-1} (min^{-1})	span (%SB)
10^{-6} M DPCPX chase (n = 9)	0.12 ± 0.05	34.3 ± 1.8	1.4 ± 0.5 x10^{-3}	65.4 ± 2.0
10^{-4} M CHA chase (n = 10)	0.17 ± 0.03	48.3 ± 1.8	1.6 ± 0.4 x10^{-3}	51.0 ± 2.1

Table 5.4: Mean parameters (± s.e.m.) from two-phase exponential dissociation of [^{3}H]CHA from A_1HE membranes in the presence of CHA or DPCPX. Unpaired t tests showed no significant difference for both the fast and slow rate constants of dissociation between the two chases. The amplitudes of both the fast and slow components were significantly different between the two chases ($P < 0.0001$ and $P = 0.0001$ for fast and slow respectively). The mean concentration of [^{3}H]CHA during the 60 min association prior to initiation of dissociation was 4.1 ± 0.8 and 4.5 ± 0.8 nM for DPCPX and CHA chases respectively. Figure 5.9 on the next page shows the range of [^{3}H]CHA concentrations used and investigates the dependence of all four parameters for both chases on the concentration of [^{3}H]CHA.

Figure 5.9 The four kinetic parameters describing the dissociation of [^{3}H]CHA in the presence of CHA or DPCPX chase.

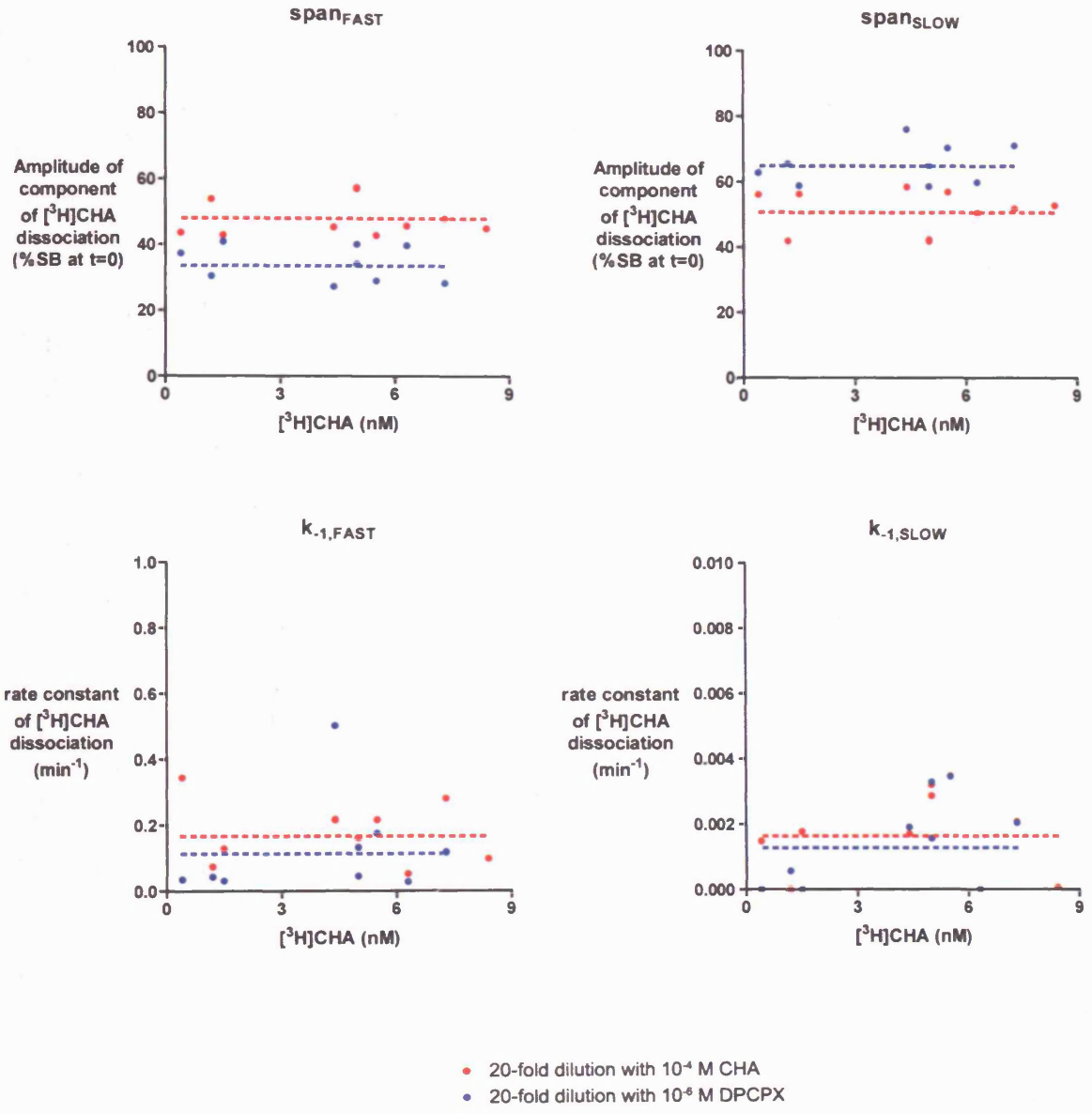

Figure 5.9: The four kinetic parameters ($k_{-1,FAST}$, $span_{FAST}$, $k_{-1,SLOW}$, $span_{SLOW}$) describing [^{3}H]CHA dissociation in the presence of CHA or DPCPX chase are independent of the concentration of [^{3}H]CHA prior to dilution. Linear regression found no significant dependence of any of the four parameters for either chase on the concentration of [^{3}H]CHA prior to 20-fold dilution. Mean values reported in Table 5.4 on the previous page are indicated as straight lines above.

5.6.3 The effect of ligand efficacy and the potency of unlabelled ligands on the dissociation of [^{3}H]CHA.

In the experiments described above, concentrations of CHA and DPCPX well above their K_D values for the adenosine A_1 receptor were used above to prevent rebinding of [^{3}H]CHA following dissociation from the receptor. Both ligands enhanced the dissociation of [^{3}H]CHA to a greater extent that 20-fold dilution alone, and 10^{-4} M CHA showed a greater ability to enhance [^{3}H]CHA dissociation than 10^{-6} M DPCPX. These high concentrations may cause non-specific effects on dissociation therefore the potency of chase ligands to enhance the dissociation of [^{3}H]CHA was investigated. In order to do so, the dissociation assay above was modified to reduce the number of time points but increase the number of variables.

5.6.3.1 The simplified "5-point" dissociation assay.

A simplified "5-point" dissociation assay was designed which enabled up to six concentrations of chase ligand at three dissociation time points to be measured in duplicate along with the t=0 point in sextuplicate; all on one 48-tube rack. The 5-point dissociation assay could also be adapted to use several different chase ligands, concentrations of [^{3}H]CHA, or different membrane preparations. As shown above, dissociation curves using an equation for two-phase exponential decay could be fitted to the reduced number of points (see Figure 5.10 on page 134 for an example of curves fitted to 5-point dissociation results). In detail, the 5-point dissociation assay was composed as described below.

1. $t = 0$ was performed in sextuplicate (as for the detailed dissociation time course experiments) in order to accurately characterise the level of bound [^{3}H]CHA immediately prior to dilution (all other points were in duplicate). Non-linear regression was not fixed at 100% for $t = 0$.

2. The 10 min dissociation time point was chosen in order to estimate the fast component of dissociation.

3. The 60 min time point was chosen because the fast component of dissociation appeared to be largely complete by then.

4. The 180 min time point; the dissociation of [^{3}H]CHA between 60 and 180 min should be largely the result of the slow component of [^{3}H]CHA dissociation.

5. Non-specific binding; as for the detailed dissociation time course experiments the two-phase exponential decay curves were constrained to a plateau of non-specific binding.

The 5-point dissociation assay was also used to characterise the kinetics of dissociation of [^{3}H]CHA from membranes prepared from the A_1R-GFP and A_1R-GFP-Gα_i cell lines. The 5-point dissociation assay enabled rapid characterisation of membranes from all 23 A_1R-GFP-Gα_i cell lines and a selection of A_1R-GFP cell lines in order to investigate the dependence of the kinetics of [^{3}H]agonist dissociation on the level of receptor expression, for which the results are presented in Chapter 6.

Table 5.5 on page 135 details mean estimates of all four parameters of [^{3}H]CHA dissociation in the presence of CHA or DPCPX ($k_{-1,FAST}$, $span_{FAST}$, $k_{-1,SLOW}$, and $span_{SLOW}$) using the 5-point dissociation assay. The effect of the concentration of [^{3}H]CHA during the 60 min association on the kinetics of dissociation was investigated and is shown in Figure 5.11 on page 136. Over a 100-fold range of [^{3}H]CHA concentration (0.1 to 11 nM) all four parameters of dissociation were not observed to be dependent on the concentration of [^{3}H]CHA, except for the fast rate constant of dissociation ($k_{-1,FAST}$) in the presence of DPCPX which did show a significant dependence on the concentration of [^{3}H]CHA ($P = 0.02$). As all the other parameters were not dependent on the concentration of [^{3}H]CHA the estimates were pooled-together in order to generate a larger sample size ($n = 18$) for which the means are listed in Table 5.5. Table 5.5 generated using the 5-point dissociation assay can be directly compared to the same parameters estimated by the detailed dissociation assay (Table 5.4 on page 130). Both tables show that the amplitudes of both the fast and slow components are significantly different depending on whether CHA or DPCPX is used as the chase ligand. In both tables the ability of CHA to enhance the dissociation of [^{3}H]CHA to a greater extent than DPCPX appears to be manifest as an increase in the amplitude of the fast component rather than a change in the rate constants of dissociation. The mean estimate of $k_{-1,FAST}$ in the presence of DPCPX chase for the 5-point dissociation assay is shown within square brackets in Table 5.5, because of the failure to prove independence from the concentration of [^{3}H]CHA. Although not proved statistically, Tables 5.5 and 5.4 essentially appear to be in good agreement. It appears that the simplified "5-point" dissociation assay is a reliable alternative to the full length "11-point" dissociation assay and enabled experiments which would have been prohibitive (in time and consumption of materials) using the more detailed assay.

5.6.3.2 The enhancement of [^{3}H]CHA dissociation by partial agonists.

So far the ability of unlabelled ligands to enhance the dissociation of [^{3}H]CHA from the adenosine A_1 receptor has been investigated using only two ligands, an agonist of high efficacy (CHA) and an inverse agonist (DPCPX). Here experiments investigating the ability of partial agonists GR190178, GR161144 and GR162900 and the antagonist N0840 to enhance the dissociation of [^{3}H]CHA are

Figure 5.10 Examples of 5-point [^{3}H]CHA dissociation curves.

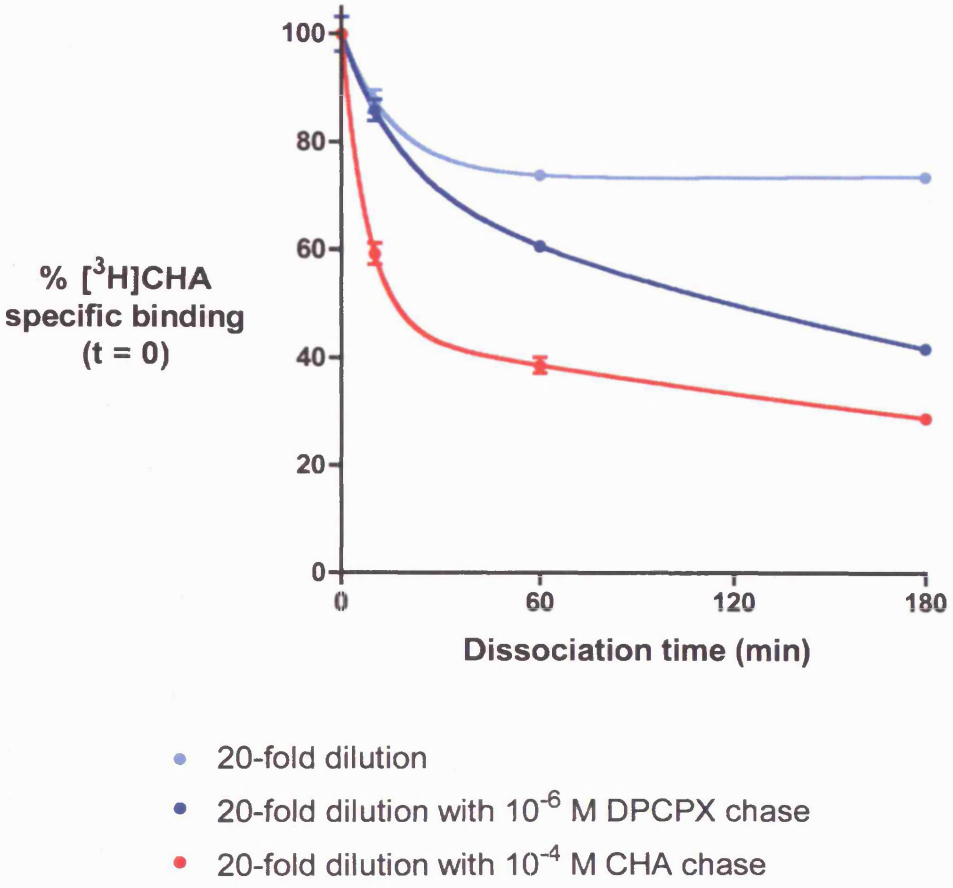

Figure 5.10: Representative A_1HE [^{3}H]CHA dissociation curves using three dissociation time points (10, 60 and 180 min in duplicate) and one time point immediately prior to initiation of dissociation ($t = 0$, in sextuplicate). The 100 μl association volume was incubated for 60 min, as usual, prior to initiation of dissociation by addition of 2 ml buffer. Dissociation by 20-fold dilution alone (•) was fitted to a model of mono-exponential dissociation to a plateau. Dissociation of [^{3}H]CHA in the presence of CHA (•) or DPCPX (•) were analysed using a model of two-phase exponential decay constrained to a plateau of non-specific binding. The above curves are similar in nature to the more detailed dissociation assay shown in Figure 5.8 on page 129.

Table 5.5 Mean parameters describing two-phase exponential dissociation of [^{3}H]CHA from A_1HE membranes using the 5-point dissociation assay.

Two-phase exponential dissociation	Fast		Slow	
Rate (k_{-1}) and amplitude (span)	k_{-1} (min^{-1})	span (%SB)	k_{-1} (min^{-1})	span (%SB)
10^{-6} M DPCPX chase (n = 18)	*[0.05 ± 0.01]*	37.7 ± 4.3	2.0 ± 0.4 x10^{-3}	62.5 ± 4.2
10^{-4} M CHA chase (n = 18)	0.09 ± 0.01	50.0 ± 1.6	2.0 ± 0.1 x10^{-3}	50.0 ± 1.6

Table 5.5: Mean parameters (± s.e.m.) from two-phase exponential dissociation of [^{3}H]CHA from A_1HE membranes using the simplified 5-point dissociation assay illustrated in Figure 5.10 on the preceding page. Both the fast and slow amplitudes showed a significant difference between each chase (P = 0.01 and P = 0.009 for fast and slow spans respectively). There was no significant difference between the mean values for the slow rate constant of dissociation. The fast rate constant of dissociation was significantly different between the two chases (P = 0.009) however the fast rate constant of [^{3}H]CHA dissociation with DPCPX chase was dependent on the concentration of [^{3}H]CHA (P = 0.02) and is shown within square brackets. Figure 5.11 on the next page illustrates this dependence along with all the other kinetic parameters for both chases in the same manner as Figure 5.9. The mean concentrations of [^{3}H]CHA during the 60 min association prior to dissociation were 2.4 ± 0.6 nM and 3.0 ± 0.8 (for CHA and DPCPX chases respectively, both n = 18) and the ranges of concentrations are shown in Figure 5.11.

Figure 5.11 The four kinetic parameters describing [^{3}H]CHA dissociation in the presence of CHA or DPCPX chase; estimated using the "5-point" dissociation assay.

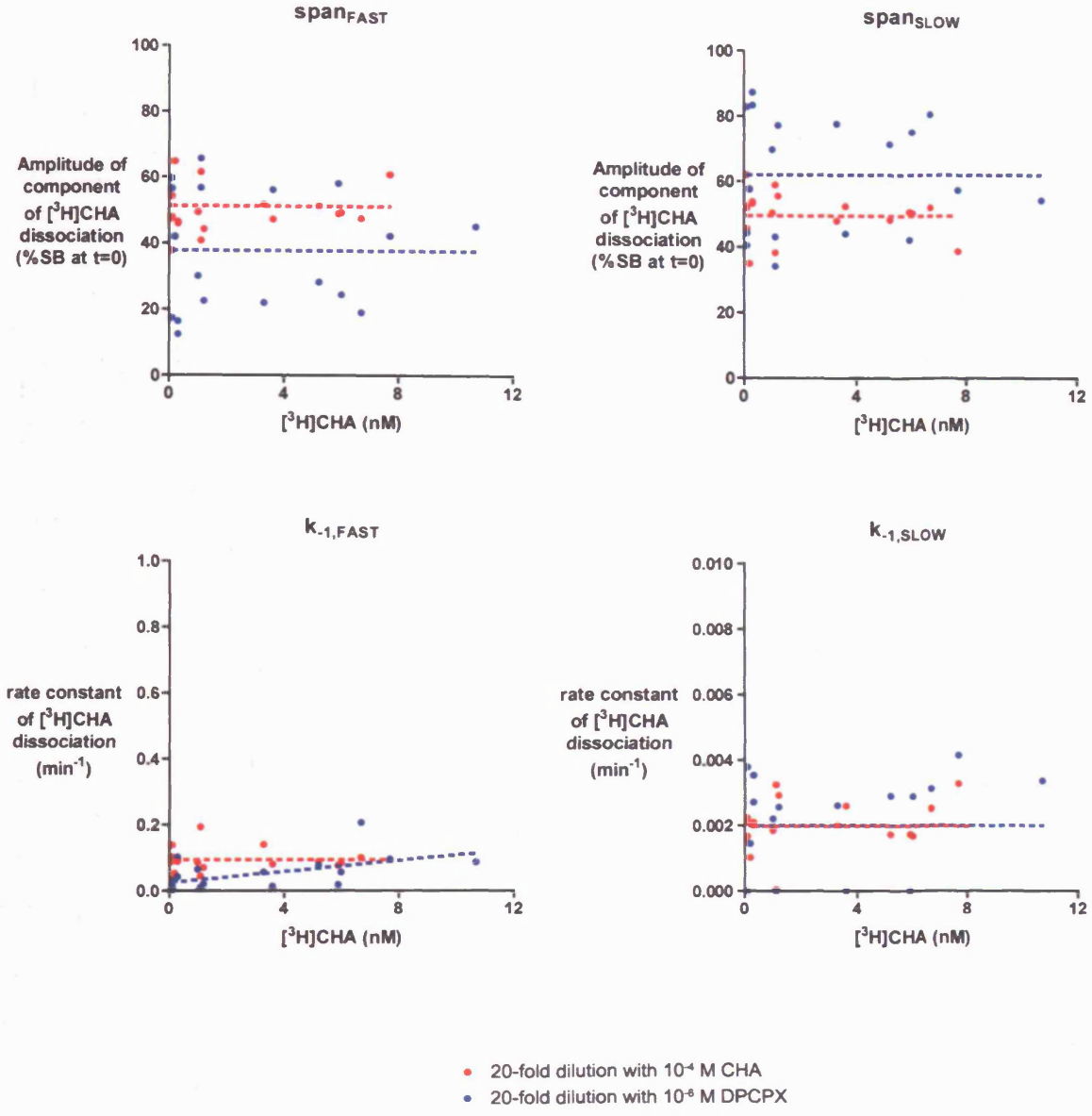

Figure 5.11: Using results from the 5-point dissociation assay, the dependence on the concentration of [^{3}H]CHA prior to dissociation (x-axis) of the four kinetic parameters ($k_{-1,FAST}$, $span_{FAST}$, $k_{-1,SLOW}$, $span_{SLOW}$) describing [^{3}H]CHA dissociation in the presence of CHA (●) or DPCPX (●) chase was investigated. Linear regression found no significant dependence of any of the four parameters for either chase on the concentration of [^{3}H]CHA prior to dilution, except for the rate constant of dissociation for the fast component in the presence of DPCPX chase ($P = 0.02$). Where the parameter was not dependent on the concentration of [^{3}H]CHA the mean value reported in Table 5.5 is indicated as a straight line. Linear regression of the fast rate constant of dissociation in the presence of DPCPX is indicated by the broken line shown. For comparison, y-axis are drawn with the same scale as in Figure 5.9 on page 131.

described. The equilibrium binding properties of the partial agonists GR190178, GR161144 and GR162900 are described in Figure 4.6 on page 91 where the ratio of affinities ($\frac{K_H}{K_L}$) may agree with their observed efficacy at the adenosine A_1 receptor. The 5-point dissociation assay was used to investigate the ability of these ligands to enhance the dissociation of [^{3}H]CHA from A_1HE and A_1R-GFP membranes. Table 5.6 on the next page lists the levels of bound [^{3}H]CHA remaining following 10, 60 and 180 min dissociation in the presence of 10^{-6} M GR190178, GR161144, GR162900 and N0840. All four unlabelled chase ligands shown in Table 5.6 were used at a concentration of 10^{-6} M. In all four membrane preparations shown in Table 5.6, GR190178 appears more effective at enhancing the dissociation of [^{3}H]CHA than GR161144 and GR162900 especially at the shorter dissociation time points. N0840 is least effective at enhancing the dissociation of [^{3}H]CHA, although it is also the ligand with the lowest affinity for the adenosine A_1 receptor. N0840 was shown in Chapter 4 to have a log affinity of 6.23 ± 0.07 (n = 3) for the adenosine A_1 receptor (Figure 4.4 on page 86). It is likely that 10^{-6} M N0840 is not sufficient to maximally enhance the dissociation of [^{3}H]CHA.

Mean values describing the kinetics of [^{3}H]CHA dissociation from the data reported in Table 5.6 are not reported because of the limited number of experiments performed along with uncertainty of the effective concentration for maximum enhancement of dissociation (investigated below). Also, the kinetics of dissociation of [^{3}H]CHA from membranes prepared from the A_1R-GFP and A_1R-GFP-Gα_i cell lines is described in much more detail in Chapter 6.

5.6.3.3 The potency of chase ligands to enhance the dissociation of [^{3}H]CHA.

The 5-point dissociation assay was also used to estimate the potency of chase ligands to enhance [^{3}H]CHA dissociation, using five concentration of chase ligand at three dissociation time points. Figure 5.12 on page 140 shows typical dose-response curves of the ability of CHA and DPCPX to enhance the dissociation of [^{3}H]CHA relative to 20-fold dilution with no chase ligand. The y-axis in each of the graphs in Figure 5.12 on page 140 is the difference between the level of bound [^{3}H]CHA remaining following 20-fold dilution alone, and the level of bound [^{3}H]CHA remaining in the presence of the chase ligand. The units of the y-axis are the same as for the dissociation curves, such as Figure 5.10. Where possible, the data were fit by a sigmoidal dose response curve with the bottom constrained to zero. The maxima of curves shown in Figure 5.12 agree quantitatively with the mean levels of bound [^{3}H]CHA remaining shown in Table 5.3 on page 130. After 10 min DPCPX chase does not enhance the dissociation of [^{3}H]CHA relative to 20-fold dilution alone, however enhancement of dissociation is observed after 60 min and to a greater extent after 180 min. The CHA chase enhances the dissociation of [^{3}H]CHA at all time points measured, and with

Table 5.6 Enhancement of the dissociation of [^{3}H]CHA from A_1HE and A_1R-GFP membranes in the presence of ligands of intermediate efficacy.

	Dissociation time (min)		
10^{-6} M chase ligand	10	60	180
A_1HE membranes			
GR190178	65.1 ± 6.8	37.6 ± 3.5	28.1 ± 3.4
GR161144	68.9 ± 4.6	40.2 ± 3.9	30.1 ± 3.7
GR162900	69.8 ± 3.8	42.5 ± 2.0	29.8 ± 2.8
N0840	64.5 ± 3.8	47.7 ± 8.6	37.8 ± 8.8
A_1R-GFP membranes 5H6 ([^{3}H]DPCPX B_{max} 1.28 ± 0.05 pmol/mg protein)			
GR190178	59.0 ± 4.0	37.5 ± 0.7	28.0 ± 0.8
GR161144	62.2 ± 4.6	39.6 ± 2.4	27.5 ± 0.1
GR162900	68.5 ± 2.1	41.4 ± 2.4	30.2 ± 1.2
N0840	74.9 ± 3.5	54.8 ± 1.7	45.2 ± 1.5
A_1R-GFP membranes 5H9 ([^{3}H]DPCPX B_{max} 3.94 ± 0.27 pmol/mg protein)			
GR190178	63.9 ± 4.3	37.4 ± 1.1	26.8 ± 0.9
GR161144	67.6 ± 1.8	37.7 ± 3.2	27.3 ± 1.8
GR162900	74.3 ± 4.6	42.0 ± 2.0	27.9 ± 0.7
N0840	74.2 ± 3.5	52.5 ± 1.6	42.8 ± 0.8
A_1R-GFP membranes 6D2 ([^{3}H]DPCPX B_{max} 9.35 ± 1.16 pmol/mg protein)			
GR190178	61.3 ± 3.2	34.3 ± 0.6	20.2 ± 3.8
GR161144	61.4 ± 1.0	34.3 ± 0.8	25.2 ± 0.3
GR162900	71.1 ± 2.0	39.6 ± 0.8	28.0 ± 0.6
N0840	71.4 ± 2.3	55.1 ± 0.6	47.0 ± 3.1

Table 5.6: The extent of [^{3}H]CHA dissociation from A_1HE and A_1R-GFP membranes at three time points was investigated using four unlabelled ligands of intermediate efficacy (all four used at 10^{-6} M). Data shown is the level of bound [^{3}H]CHA remaining expressed as percent of specific binding at t=0 (as in Table 5.3 on page 130), and are mean (± s.e.m.) of three experiments (n = 3) each performed in duplicate (as for all previous dissociation assays reported). Equilibrium binding properties of the A_1R-GFP membranes are listed in Table 4.3 on page 95. The equilibrium binding properties of ligands GR190178, GR161144 and GR162900 are investigated in Figure 4.6 on page 91, and N0840 in Figure 4.4 on page 86.

low nM potency providing evidence of a specific high affinity interaction driving the mechanism of agonist-induced agonist dissociation (Figure 5.12). The enhancement of [^{3}H]CHA dissociation by DPCPX after 180 min was also of low nM potency. The limited enhancement of [^{3}H]CHA dissociation by DPCPX after 60 min made fitting of dose response curves unreliable. Routinely no enhancement of [^{3}H]CHA dissociation by DPCPX after 10 min was observed, and so is indicated by a straight line in Figure 5.12. The high concentrations of CHA (10^{-4} M) and DPCPX (10^{-6} M) chases used for Table 5.3 and other Figures are clearly far in excess of those required to effect a maximum enhancement of dissociation. However there appear to be no additional non-specific interactions and no apparent negative consequences to the use of such high concentrations. The nM potency of the enhancement of [^{3}H]CHA dissociation and the differences between DPCPX and CHA chases point to the kinetic phenomenon being related to specific binding at the adenosine A_1 receptor.

As with the kinetics of the dissociation of [^{3}H]CHA in the presence of an unlabelled chase ligand, the potency of chase ligand to enhance [^{3}H]CHA dissociation (log EC_{50}) was also not dependent on the concentration of [^{3}H]CHA added during the 60 min association. Figure 5.13 on page 141 shows the lack of any effect of [^{3}H]CHA concentration on the log EC_{50} of CHA chase after 180 min dissociation time. As neither the extent (after 10, 60 & 180 min), kinetics ($k_{-1,FAST}$, $span_{FAST}$, $k_{-1,SLOW}$, & $span_{SLOW}$) and chase potency (log EC_{50}) of [^{3}H]CHA dissociation in the presence of CHA or DPCPX chase were dependent on the concentration of [^{3}H]CHA, estimates from the four concentrations of [^{3}H]CHA shown in Figure 5.13 were pooled in order to increase the sample size (n = 8).

The experiments reported in Table 5.6 investigated the ability of the partial agonists GR190178, GR161144 and GR162900 and the antagonist N0840 to enhance the dissociation of [^{3}H]CHA. These were all performed at a concentration of chase ligand of 10^{-6} M. However the log affinity of N0840 for A_1HE membranes was approximately 10^{-6} M (Figure 4.4 on page 86). It is likely that the reduced ability of N0840 to enhance the dissociation of [^{3}H]CHA compared to the agonist chases (Table 5.6) is due to an insufficient concentration of N0840. Figure 5.14 on page 142 shows examples of chase ligand dose response curves using GR190178, GR161144, GR162900 and N0840 performed in the same manner as for CHA and DPCPX. After 180 min GR190178, GR161144 and GR162900 appear to have a lower log EC_{50}s than CHA or DPCPX. The enhancement of [^{3}H]CHA dissociation by N0840 has not reached a maximum by 10^{-6} M, which suggests that affinity at equilibrium may be related to the potency of the enhancement of [^{3}H]CHA dissociation.

Mean log EC_{50}s of the enhancement of [^{3}H]CHA dissociation by all the chase ligands examined are reported in Table 5.7 on page 144. As suggested by the individual dose response curves

Figure 5.12 CHA and DPCPX dose-response curves of the enhancement of [^{3}H]CHA dissociation from A_1HE membranes.

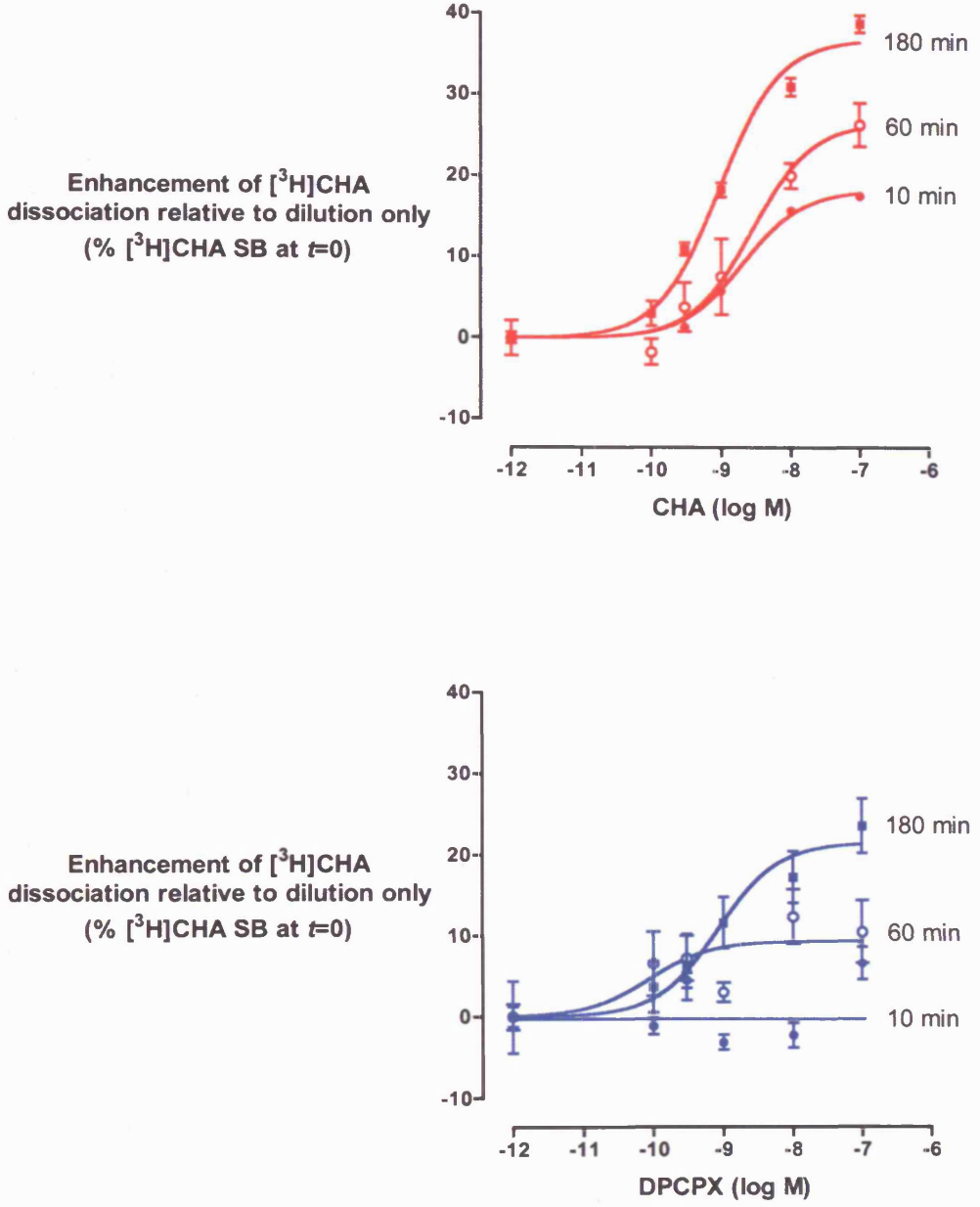

Figure 5.12: Representative CHA and DPCPX dose response curves of their ability to enhance the dissociation of [^{3}H]CHA relative to dilution only. Three dissociation time points are shown (10, 60 and 180 min). The 10 min DPCPX data was not well fitted by a sigmoidal dose response curve, so is indicated as a straight line. Data shown is from an individual experiment performed in duplicate. Sigmoidal dose response curves were constrained to a bottom of 0. Mean parameters from non-linear regression of dissociation dose response curves are shown in Table 5.7 on page 144.

Figure 5.13 The potency of the enhancement of the dissociation of [^{3}H]CHA from A_1HE membranes by CHA or DPCPX is not dependent on the concentration of [^{3}H]CHA.

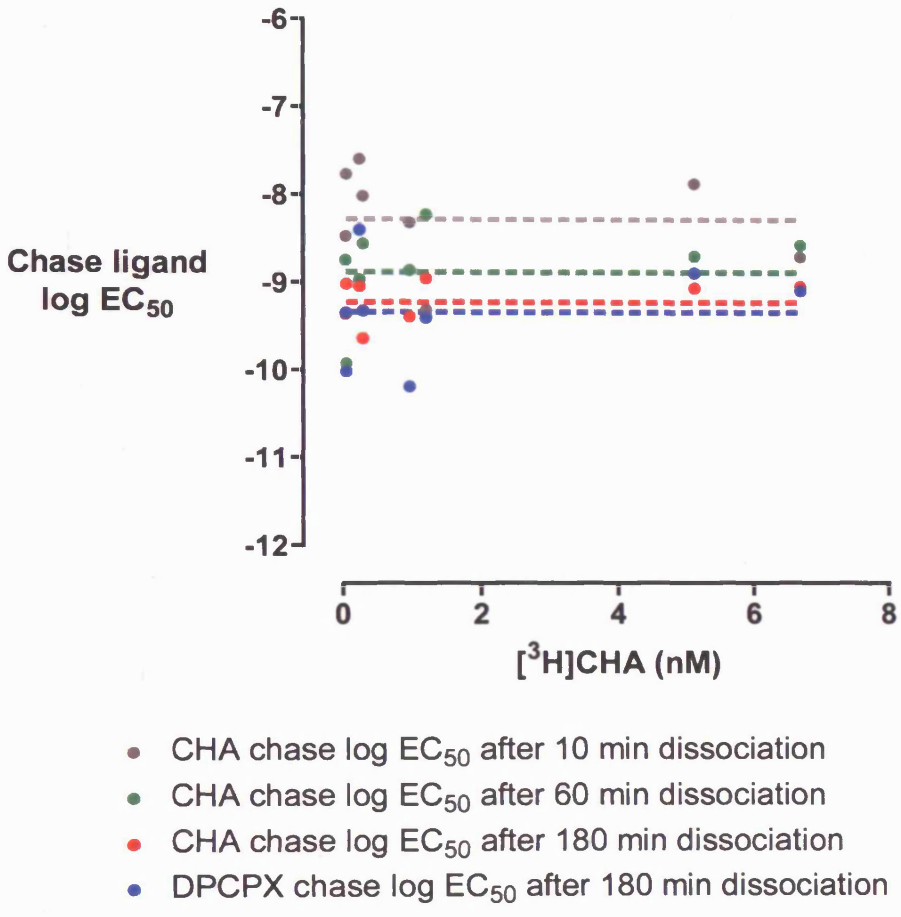

Figure 5.13: In the presence of 10^{-4} M CHA or 10^{-6} M DPCPX chase the chase potency (log EC_{50}) of the enhancement of [^{3}H]CHA dissociation was independent of the concentration of [^{3}H]CHA prior to dilution. Shown are individual estimates of potency (log EC_{50}) for the enhancement of [^{3}H]CHA dissociation. The fitting of sigmoidal dose response curves to data obtained for DPCPX chase after 10 and 60 min dissociation was unreliable and is not reported. The mean values of each condition are indicated as the straight lines shown. As none of the parameters were dependent on the concentration of [^{3}H]CHA, the estimates were pooled for each chase ligand for a larger sample size (n = 8 for CHA and DPCPX chases) and are shown in Table 5.7 on page 144.

Figure 5.14 Dose response curves of enhanced [^{3}H]CHA dissociation from A_1HE membranes using chase ligands of intermediate efficacy.

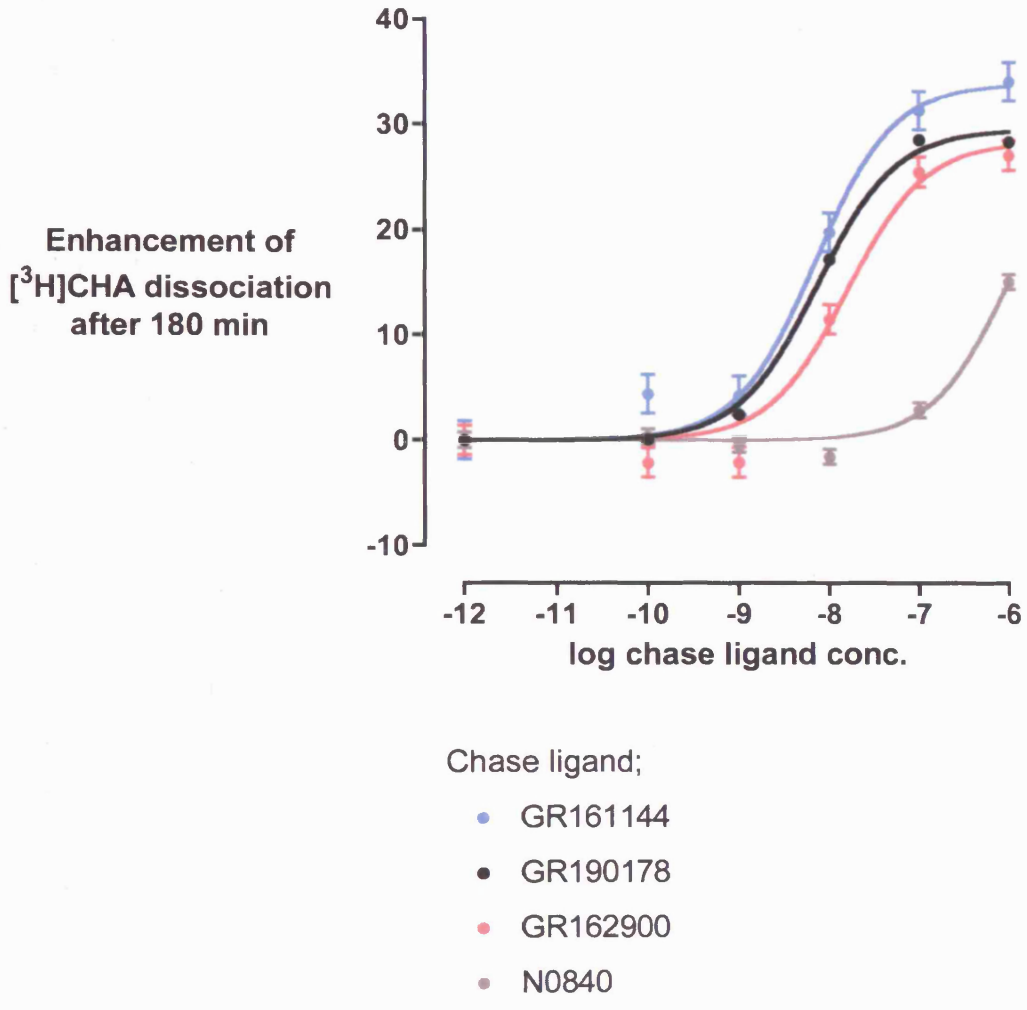

Figure 5.14: Representative individual dose response curves of the enhancement of the dissociation of [^{3}H]CHA from A_1HE membranes after 180 min by agonists GR190178, GR161144, GR162900 and the antagonist N0840. Data shown are mean values (± s.e.m.) from a single experiment measured in duplicate. The GR190178 points have an error which is too small to be visible on the graph above. Sigmoidal dose response curves were constrained to a bottom of 0. Mean parameters from non-linear regression of dissociation dose response curves are shown in Table 5.7 on page 144.

(Figures 5.12 and 5.14), the estimates of log EC_{50} appear to increase in potency with time and CHA and DPCPX chases appear to be more potent than the partial agonists and N0840. Just as CHA and DPCPX show similar high affinity binding to the adenosine A_1 receptor at equilibrium (Chapter 4.2 on page 80), their ability to enhance the dissociation of [^{3}H]CHA is also of similar low nM potency. However the maximum enhancement estimated by the sigmoidal dose response curves ($Enhancement_{max}$) after 180 min dissociation time was significantly different ($P = 0.0001$) between the CHA and DPCPX chases. Both rate constants for the dissociation of [^{3}H]CHA were not significantly different between CHA and DPCPX chases (Tables 5.4 and 5.6), showing agonist-induced agonist dissociation to be manifest as an increase in the amplitude of the fast component of the dissociation of [^{3}H]CHA. Table 5.7 supports this by showing equal potency of both CHA and DPCPX to enhance the dissociation of [^{3}H]CHA, with agonist-induced agonist dissociation the result of a greater extent of dissociation. Casual inspection of the log EC_{50} values reported in Table 5.7 indicates an increase in the potency of CHA with increasing dissociation time. This is also illustrated in Figure 5.13. This trend appears to decrease with agonists of progressively lower efficacy, to the extent where GR162900 shows similar potency at all three time points.

No results are presented for DPCPX chase after 10 and 60 min dissociation time in Table 5.7 as sigmoidal dose response curves could not be reliably fit to the small, if any, enhancement of [^{3}H]CHA dissociation. The maximum projected level of the enhancement of [^{3}H]CHA dissociation ($Enhancement_{max}$) by N0840 is not reported because N0840 was not used at sufficiently high concentrations to determine the limit of its ability to enhance dissociation of [^{3}H]CHA (as illustrated in Figure 5.14).

5.6.4 Enhanced [^{3}H]CHA dissociation by unlabelled ligands in the presence of GTP.

At nM concentrations most bound [^{3}H]CHA is removed rapidly from the adenosine A_1 receptor by 10^{-4} M GTP (Figure 5.6 on page 126). The ability of unlabelled ligands to enhance the dissociation of [^{3}H]CHA from A_1HE membranes in the presence of 10^{-4} M GTP was investigated. Figure 5.15 on page 146 shows typical [^{3}H]CHA dissociation curves illustrating agonist-induced agonist dissociation in the presence of GTP relative to 20-fold dilution with GTP alone. In the presence of GTP, DPCPX showed enhancement of [^{3}H]CHA dissociation intermediate between CHA and GTP, and GTP alone. The dissociation of [^{3}H]CHA in all three conditions containing GTP was best described by a two-phase model of exponential decay to non-specific levels. Table 5.8 on page 147 lists mean levels of bound [^{3}H]CHA remaining after dissociation for 10, 60 and 180

Table 5.7 The potency of the ability of unlabelled ligands to enhance the dissociation of [^{3}H]CHA from A_1HE membranes.

Dissociation time (min)	Chase ligand log EC_{50}	Enhancement$_{max}$ (%SB)
CHA chase (n = 8)		
10	-8.25 ± 0.20	17.1 ± 2.9
60	-8.81 ± 0.18	24.3 ± 1.4
180	-9.18 ± 0.09	27.8 ± 1.8
DPCPX chase (n = 8)		
180	-9.33 ± 0.20	14.6 ± 1.7
GR190178 chase (n = 2)		
10	-7.37 ± 0.35	11.7 ± 0.1
60	-7.87 ± 0.02	26.3 ± 1.0
180	-8.19 ± 0.10	31.7 ± 1.7
GR161144 chase (n = 2)		
10	-7.65 ± 0.20	12.5 ± 1.1
60	-7.80 ± 0.10	27.1 ± 0.9
180	-8.03 ± 0.10	34.7 ± 0.4
GR162900 chase (n = 2)		
10	-7.83 ± 0.14	4.8 ± 0.7
60	-7.64 ± 0.01	19.1 ± 0.6
180	-7.66 ± 0.12	30.8 ± 2.2
N0840 chase (n = 2)		
60	-6.37 ± 0.27	-
180	-5.52 ± 0.46	-

Table 5.7: Average (± s.e.m.) log EC_{50} and maximum enhancement values from nonlinear regression of sigmoidal dose response curves of the ability of unlabelled ligands to enhance the dissociation of [^{3}H]CHA relative to dilution only. Examples of individual chase ligand dose response curves are shown in Figures 5.12 (CHA & DPCPX) and 5.14 (GR190178, GR161144, GR162900 and N0840).

min in all three dissociation conditions in the presence of GTP (in the same manner as Tables 5.2, 5.3 and 5.6). As observed in the absence of GTP, CHA enhanced the dissociation of [^{3}H]CHA to the greatest extent at all time points. Estimation of the rate constant of the fast component of [^{3}H]CHA dissociation was ill-defined as the fast component was largely complete before the first dissociation time point (5 min; Figure 5.15). The smaller sample size (n = 4) compared to Tables 5.4 (n = 9 and 10) and 5.6 (n = 18) discourages meaningful statistical comparison, but again it appears that the ability of CHA to enhance the dissociation of [^{3}H]CHA is largely manifest as an increase in the amplitude of the fast component rather than a change in the rate constants of dissociation.

10^{-6} M DPCPX was equally effective at enhancing the dissociation of [^{3}H]CHA from A_1HE membranes in the presence or absence of 10^{-4} M GTP (Figure 5.16 on page 148). The relative ability of 10^{-4} M CHA to enhance the dissociation of [^{3}H]CHA was even more pronounced in the presence of GTP. Agonist-induced agonist dissociation is observed in the presence of GTP, and is very effective at enhancing the dissociation of [^{3}H]CHA from GTP-insensitive high affinity binding sites. GTP is present within cells in physiological conditions, so the observation of agonist-induced agonist dissociation in both the presence and absence of GTP supports the proposition that it may have a physiological function.

5.6.5 The effect of [^{3}H]CHA concentration on the dissociation of [^{3}H]CHA.

The association of [^{3}H]CHA to the adenosine A_1 receptor was best described by a two-phase exponential model of association. As described above, the fast rate constant of the association of [^{3}H]CHA to A_1HE membranes was dependent on the concentration of [^{3}H]CHA (Figure 5.5 on page 122). The fast component of association is consistent with a simple bi-molecular interaction of [^{3}H]CHA binding to readily available high affinity sites on the receptor. Whether the slow component of [^{3}H]CHA association is dependent on the concentration of [^{3}H]CHA was less clear. It is possible the slow component of association is largely driven by processes such as the recruitment of G protein into the receptor environment. The evidence from Figure 4.3, on page 84, is that at longer incubation times the increase in [^{3}H]CHA binding seems to be the result of an increase in [^{3}H]CHA B_{max} (recruitment of G protein) rather than an isomerisation which would result in an increase in affinity. Extrapolation to the y-axis intercept of the plot shown in Figure 5.5a agrees almost precisely with the observed fast rate constant of [^{3}H]CHA dissociation in the presence of CHA (0.12 ± 0.01 min^{-1}, n = 28). The y-axis intercept is the predicted off-rate if binding is simple. The presence of unlabelled CHA during dissociation prevents rebinding of dissociated [^{3}H]CHA, and provides a means of measuring the off-rate directly. Preliminary data indicated that the ob-

Figure 5.15 CHA and DPCPX enhance the dissociation of [^{3}H]CHA from A_1HE membranes even in the presence of GTP.

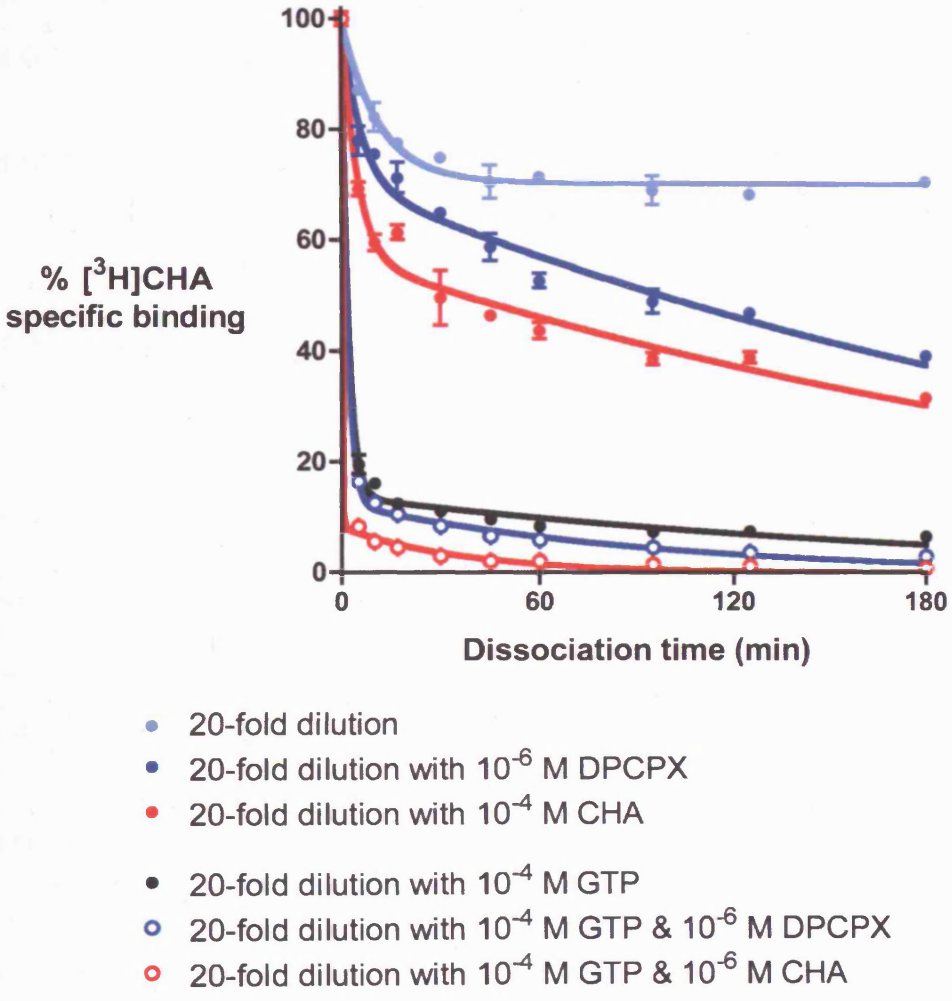

Figure 5.15: Representative [^{3}H]CHA dissociation curves by 20-fold dilution in the presence or absence of CHA, DPCPX and GTP. Data shown is a single experiment (also shown in Figure 5.8 on page 129) with measurements in duplicate, except for the t=0 time point which was measured in sextuplicate.

Table 5.8a Extent of bound [^{3}H]CHA remaining after dissociation from A_1HE membranes in the presence of GTP.

Dissociation time (min)	10	60	180
10^{-4} M GTP chase	22.1 ± 1.7 (n = 6)	11.6 ± 1.3 (n = 6)	9.3 ± 1.4 (n = 4)
10^{-4} M GTP + 10^{-6} M DPCPX	20.0 ± 2.1 (n = 5)	9.2 ± 1.6 (n = 5)	6.4 ± 1.7 (n = 4)
10^{-4} M GTP + 10^{-4} M CHA	9.1 ± 1.3 (n = 5)	3.5 ± 0.8 (n = 5)	3.1 ± 1.5 (n = 4)

Table 5.8b Two-phase exponential dissociation of [^{3}H]CHA from A_1HE membranes in the presence of GTP.

Two-phase exponential dissociation	Fast		Slow	
Rate (k_{-1}) and amplitude (span)	k_{-1} (min^{-1})	span(%SB)	k_{-1} (min^{-1})	span(%SB)
10^{-4} M GTP chase (n = 5)	0.58 ± 0.06	77.9 ± 2.3	8.9 ± 1.7 x10^{-3}	22.1 ± 2.3
10^{-4} M GTP + 10^{-6} M DPCPX (n = 4)	0.61 ± 0.09	79.8 ± 2.7	12 ± 3.5 x10^{-3}	20.2 ± 2.7
10^{-4} M GTP + 10^{-6} M CHA (n = 4)	2.3 ± 1.3	89.8 ± 1.3	20 ± 9.0 x10^{-3}	10.2 ± 1.3

Table 5.8: **(a)** Levels of bound [^{3}H]CHA remaining in the presence of 10^{-4} M GTP are expressed as percent of bound [^{3}H]CHA before dissociation (at t=0), as for Tables 5.2, 5.3 and 5.6 (pages 126, 130 and 138 respectively).

(b) As for the dissociation of [^{3}H]CHA in the absence of GTP, dissociation was fit to a model of two-phase exponential decay to a plateau of non-specific binding. [^{3}H]CHA and A_1HE membranes were incubated for 60 min at RT before initiation of dissociation by 20-fold dilution in the presence of 10^{-4} M GTP.

The mean concentrations of [^{3}H]CHA during the 60 min association were 3.9 ± 1.5, 3.2 ± 1.3 and 3.5 ± 1.1 nM where indicated in the above tables as n = 4, 5 and 6 respectively.

Figure 5.16 The relative enhancement of [^{3}H]CHA dissociation by CHA and DPCPX in the presence or absence of GTP.

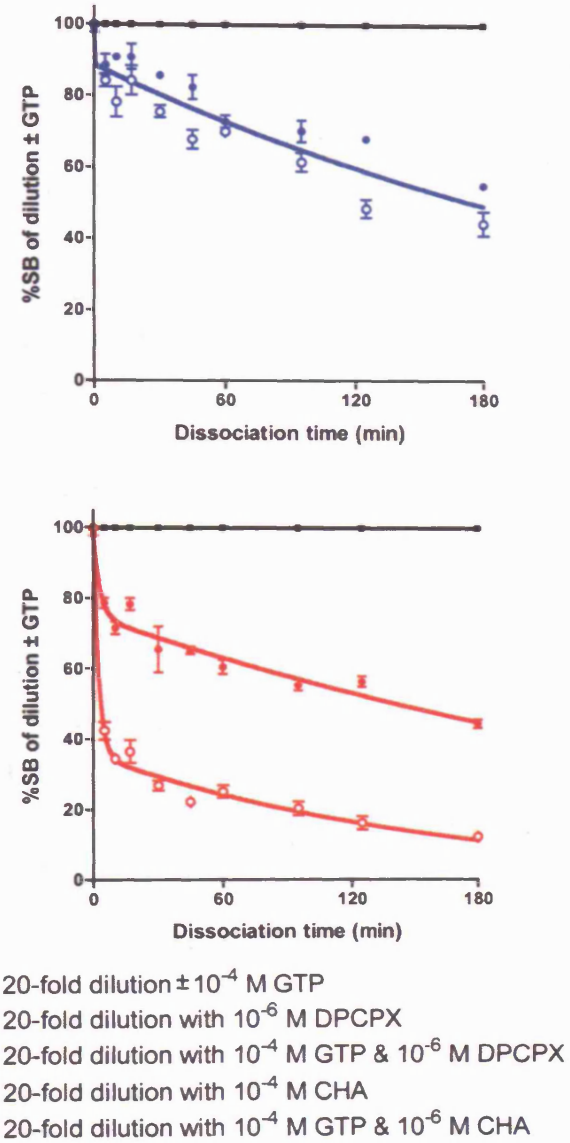

Figure 5.16: The data presented in Figure 5.15 on page 146 were transformed by normalising the level of bound [^{3}H]CHA remaining after 20-fold dilution to 100%. The level of bound [^{3}H]CHA remaining in the presence of CHA and DPCPX was then expressed as a percent of "dilution only" levels at each time point. Biphasic curves were fit to the data for illustrative purposes only. There was little apparent difference between the DPCPX chase response in the presence or absence of GTP, so the curve shown was generated using mean data of the two.

served rate of the dissociation of [^{3}H]CHA by 20-fold dilution alone may be dependent on the concentration of [^{3}H]CHA (Figure 5.7 on page 127). The 5-point dissociation assay was used to investigate the effect of concentration of [^{3}H]CHA on the kinetics of dissociation in the presence of CHA or DPCPX. The only parameter which showed a significant dependence on [^{3}H]CHA concentration was the fast rate constant of dissociation in the presence of DPCPX ($P = 0.02$; Figure 5.11 on page 136). DPCPX chase appears to show little enhancement of [^{3}H]CHA dissociation during the fast component of dissociation relative to 20-fold dilution alone (Table 5.3 on page 130). The slow component of [^{3}H]CHA dissociation may be largely responsible for the observed ability of DPCPX to enhance dissociation of [^{3}H]CHA relative to dilution alone. This is supported by the dependence on the concentration of [^{3}H]CHA of both the observed rate of dissociation by dilution alone (Figure 5.7) and the rate constant of the fast component of dissociation in the presence of DPCPX (Figure 5.13).

5.6.6 The effect of association time and temperature on [^{3}H]CHA dissociation.

Detailed time course experiments were designed in order to investigate how the rate and extent of the dissociation of [^{3}H]CHA from A_1HE membranes, and the differences in these values when DPCPX or CHA are used as chase ligand, vary with the period of [^{3}H]CHA association and the temperature of incubation. As part of this protocol, [^{3}H]CHA association time courses at the different temperatures were measured.

These associations of [^{3}H]CHA to A_1HE membranes were fit to a model of one phase exponential association although there was an indication that the association might be biphasic (described in more detail in Chapter 5.5 on page 119). The observed rate constant of association (k_{obs}) for 5.1 nM [^{3}H]CHA increased with incubation temperature, with k_{obs} of 0.024, 0.038 $\pm$ 0.003, 0.086 $\pm$ 0.004 and 0.174 $\pm$ 0.001 min^{-1} when measured at 15, 22, 30 and 37°C respectively ($n = 2$, except 15°C where $n = 1$). Figure 5.17 on the following page shows the association time courses at all four temperatures from one experiment. Receptor binding at 30 and 37°C was unstable after 90 and 30 min respectively and these later times were excluded from estimation of the association k_{obs} at these temperatures. The association curves presented in Figure 5.17 were fit to a two-phase model of exponential association for visualisation only. Quantitative interpretation of the two-phase association curves was unreliable and the mean rate constants of association (k_{obs}) presented above were estimated from one-phase exponential curves fit to the same data.

At each point in the [^{3}H]CHA association time course, dissociation was initiated as described

Figure 5.17 The effect of temperature on the association of [^{3}H]CHA at A_1HE membranes.

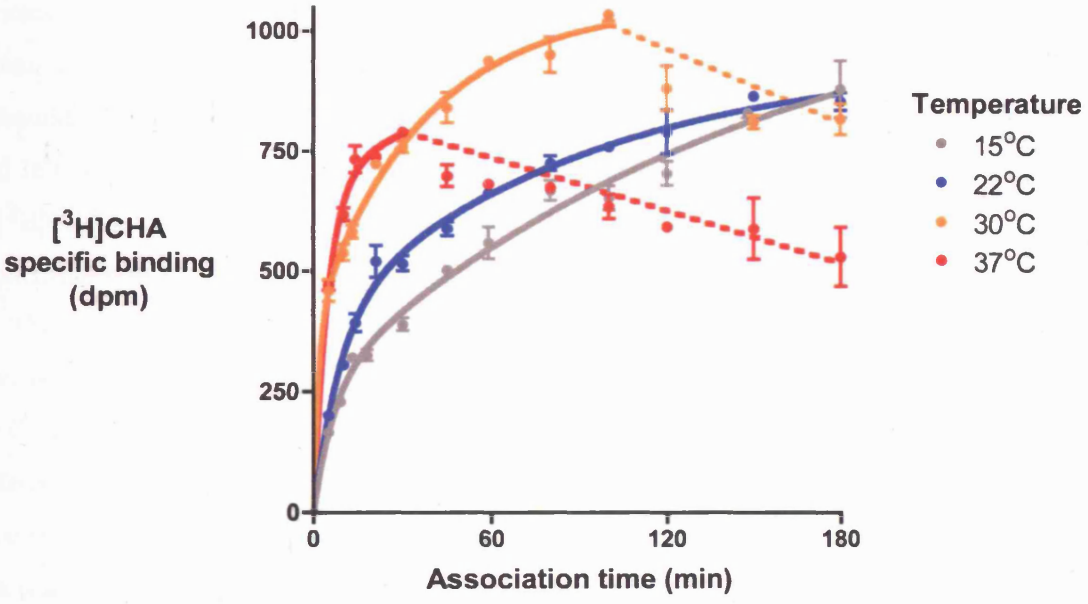

Figure 5.17: [^{3}H]CHA association time courses were performed at four different temperatures; 15°C, 22°C (room temperature), 30°C and 37°C. The data shown above are from a single experiment measured in duplicate. The initial rate of association increased with temperature up to 30°C. At 30°C binding was unstable and decayed after approximately 90 min. At 37°C levels of bound [^{3}H]CHA decreased from 30 min onwards. Where binding was largely stable, data were fit to a model of two-phase exponential association as for Figure 5.4 on page 120. The decay of [^{3}H]CHA binding at higher temperatures and longer times is indicated for visual clarity only as the straight broken lines shown.

above by means of a 20 fold dilution in the presence of either 10^{-4} M CHA (CHA chase) or 10^{-6} M DPCPX (DPCPX chase), and bound [^{3}H]CHA measured after 10 and 60 minutes. Three dissociation time points (0, 10 and 60 min) were chosen in order to obtain an estimate of the rate constant of the fast component of [^{3}H]CHA dissociation. Specific [^{3}H]CHA binding was normalised to observed levels immediately prior to initiation of dissociation (%SB at $t = 0$, as frequently used above for example in Figures 5.6, 5.8 and 5.10). The data from the dissociation time course experiments following different periods of association were combined in order to visualise the effect of association time. Figure 5.18 on the next page illustrates how data from dissociation time courses was combined to look at the effect of association time on the level of bound [^{3}H]CHA remaining after identical periods of dissociation. In this manner, Figure 5.18 describes the level of bound [^{3}H]CHA remaining after 60 min dissociation, following lengths of association between 5 and 180 min. Both the DPCPX and CHA chases were more effective at enhancing the dissociation of [^{3}H]CHA following shorter periods of association, i.e. "agonist-locking" increases with the period of incubation of membranes and [^{3}H]CHA prior to dilution and initiation of dissociation.

The dissociation time courses presented in Figure 5.18 were performed at 15°C. The effect of association time on the levels of bound [^{3}H]CHA remaining at all four temperatures (15, 22, 30 & 37°C) and two dissociation time points (10 and 60 min) is shown in Figure 5.19 on page 154. The difference between dissociation by CHA or DPCPX chase is greatest at lower temperatures and shorter association times (Figure 5.19). This difference is still present after 3 hours at 15 and 22°C, but is abolished after 60 min at 30°C and after 10-15 min at 37°C. CHA and DPCPX chases were both less effective at enhancing [^{3}H]CHA dissociation following longer periods of association. In all conditions, less agonist-locking is observed after shorter periods of association prior to dissociation.

Interestingly the dissociation of [^{3}H]CHA after 60 min by CHA chase appears to extrapolate to a non-zero y-axis intercept at zero association time independent of temperature (Figure 5.19). However, the y-axis intercept of dissociation in the presence of DPCPX appears to increase progressively with decrease in temperature. This raises the question of whether the dissociation of [^{3}H]CHA by agonist or antagonist chase ligand is differentially sensitive to temperature. This provides further evidence of mechanistic differences between the enhancement of [^{3}H]CHA dissociation by CHA and DPCPX. The y-axis intercept at zero association time may represent the initial, or preset, dissociation characteristics of the system that are modified as [^{3}H]CHA binds. It is unknown whether the fast and slow components of [^{3}H]CHA association represent two separate receptor complexes, or whether there is a degree of isomerisation or equilibrium between the two.

Figure 5.20 on page 155 illustrates in more detail the extrapolation of one of the curves in Figure 5.19 to its x-axis intercept. The x-axis intercept of approximately 30 min would relate to

Figure 5.18 The use of dissociation time course data to investigate the effect of association time on [^{3}H]CHA dissociation.

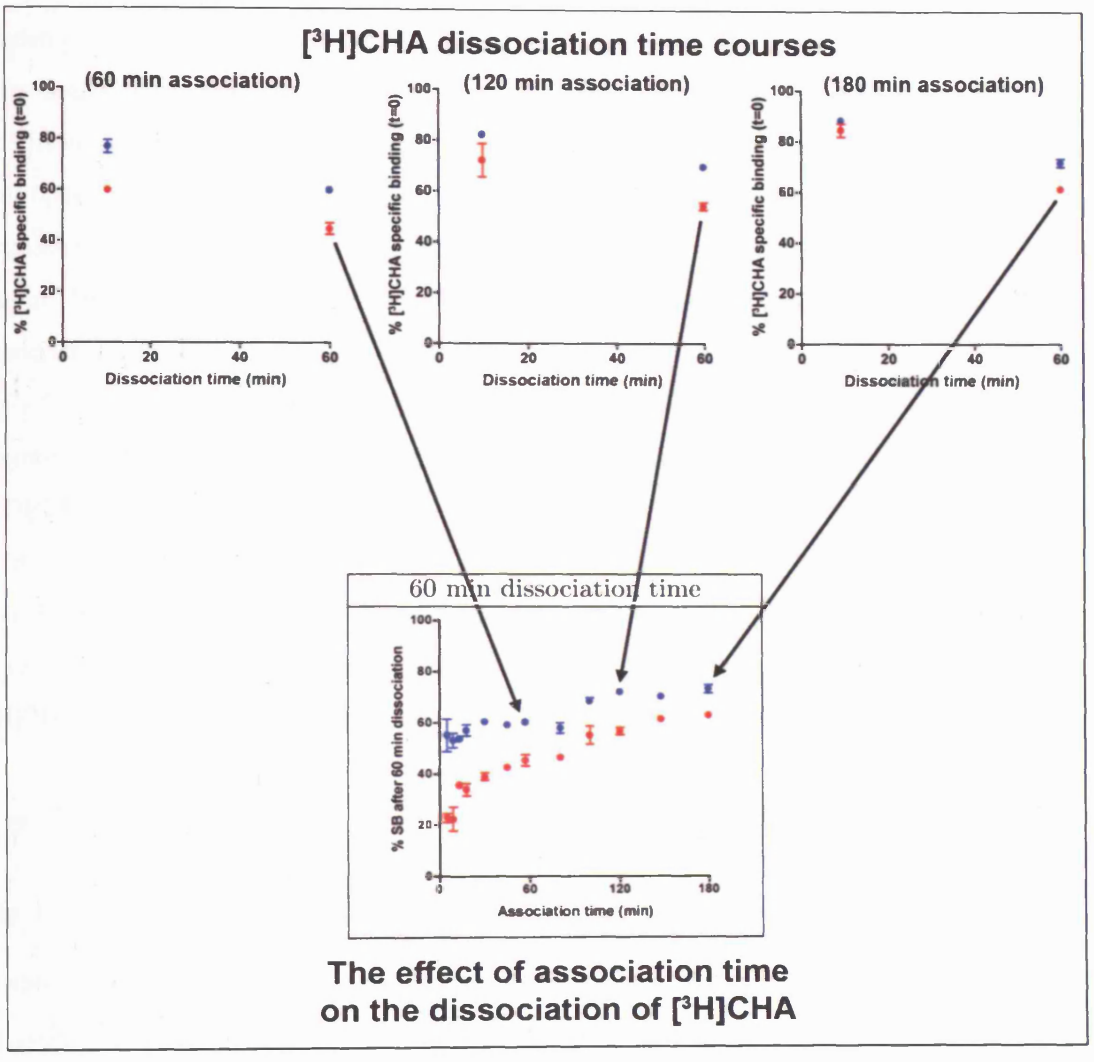

Figure 5.18: The dissociation of [^{3}H]CHA from A_1HE membranes was measured at two dissociation time points (10 and 60 min) following association for 5 to 180 min. Data from dissociation time course experiments was combined to investigate the effect of incubation time prior to dilution ("association time") on the level of bound [^{3}H]CHA remaining after 60 min dissociation by 20-fold dilution in the presence of 10^{-6} M DPCPX (●) or 10^{-4} M CHA (●) chase. The dissociation time courses above were performed at 15°C and are from a single experiment measured in duplicate. The concentration of [^{3}H]CHA during the 100 μl association incubation with A_1HE membranes was 5.8 nM.

the start of the 30 min membrane incubation with adenosine deaminase, prior to incubation with radioligand. It is possible that once the membranes are warmed to RT a mechanism involved in agonist-locked pseudo-irreversible binding is begun. It may be possible to investigate this further by altering the conditions of membrane preparation, such as preparing membranes in the presence of adenosine deaminase. Then pre-incubation with adenosine deaminase immediately prior to the assay would be unnecessary.

The initial rate constant of [^{3}H]CHA dissociation was estimated from specific binding measured after 0, 10 and 60 minutes of dissociation following each association time, essentially obtaining an estimate of the fast component of dissociation (see legend to Figure 5.21 on page 156). Unlike the rate of [^{3}H]CHA association, there was no evidence of a temperature dependence to the rate of dissociation over 60 minutes. In the absence of any obvious temperature dependence, the estimated k_{off}'s for all temperatures were pooled in order to investigate the effect of association time on k_{off} (Figure 5.21). CHA chase appeared to stimulate the initial rate of [^{3}H]CHA dissociation relative to DPCPX chase association times up to approximately 60 minutes.

Similar experiments investigating the effect of association time on the dissociation of [^{3}H]NECA from A_1HE membranes in the presence of 10^{-4} M CHA or 10^{-6} M DPCPX chase observed greater "agonist locking" following longer periods of association in the same manner as described above for [^{3}H]CHA (data not shown).

5.7 Discussion.

The kinetics of the binding of [^{3}H]DPCPX at the adenosine A_1 receptor.

Chapter 4 described the binding of antagonists DPCPX, theophylline and N0840 at the adenosine A_1 receptor at equilibrium as simple and monophasic. Work presented in this Chapter showed that the kinetics of antagonist binding at the adenosine A_1 receptor is simple, rapid and mono-exponential. The kinetics of the association of [^{3}H]DPCPX to the adenosine A_1 receptor was rapid and mono-exponential when endogenous adenosine was removed from the membrane preparation (Figure 5.2 on page 117). Previous studies have described the association of [^{3}H]DPCPX to the adenosine A_1 receptor as biphasic, composed of a rapid (0.17 min^{-1} for 0.2 nM [^{3}H]DPCPX) and much slower component (Cohen *et al.* 1996b). The reported slow component of the association of [^{3}H]DPCPX was removed in the presence of GTP and it was proposed that the decay of long-lasting adenosine-receptor-G protein complexes present in the membrane preparations was responsible for the slow association of [^{3}H]DPCPX. The nature of the association of [^{3}H]DPCPX presented in this study also provides evidence for the presence of endogenous adenosine within the membrane

Figure 5.19 The effect of association time and temperature on the dissociation of [^{3}H]CHA in the presence of DPCPX or CHA.

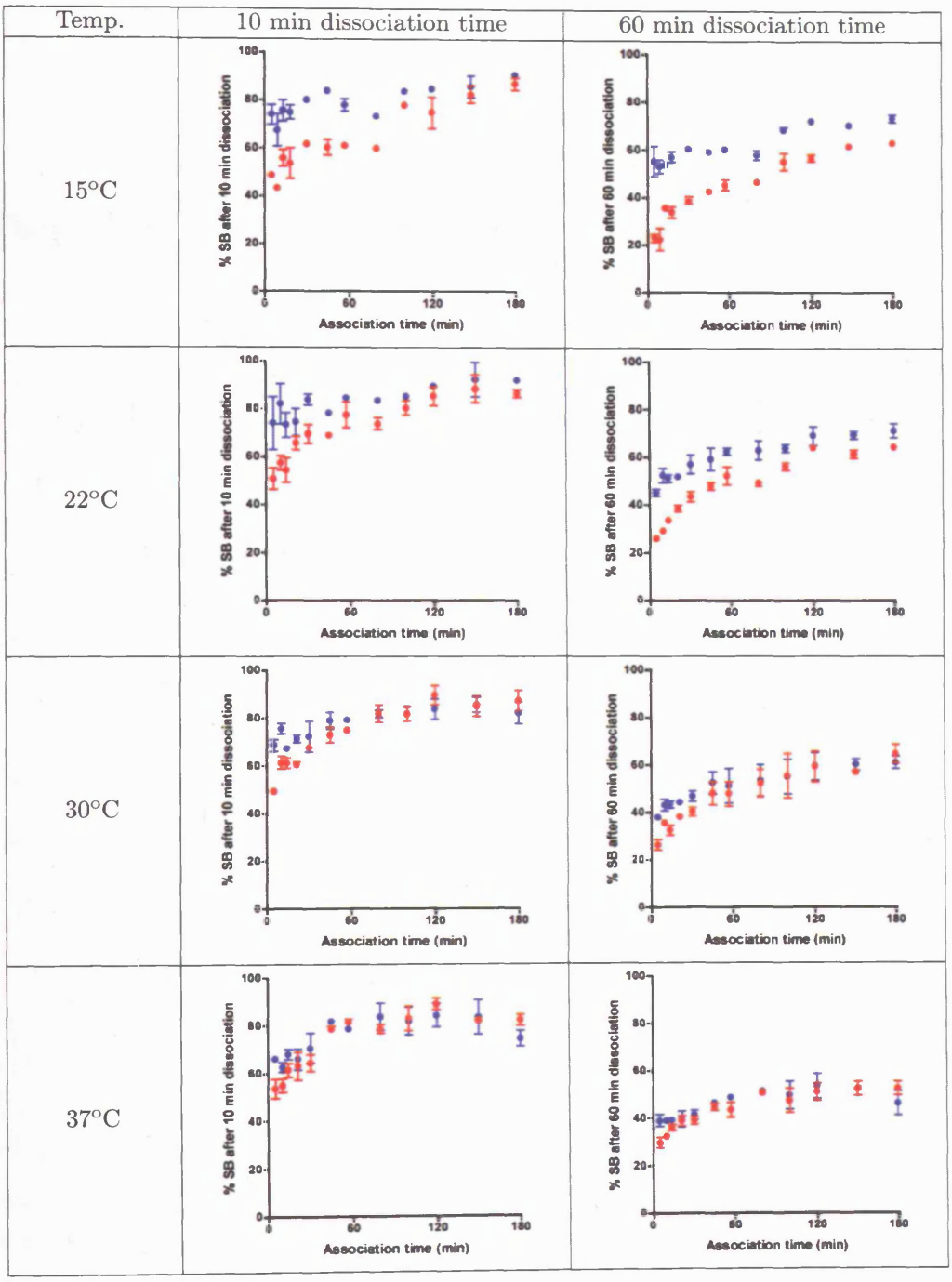

Figure 5.19: The association of [^{3}H]CHA with A_1HE membranes was performed in 100 μl volumes for 5 to 180 min, after which dissociation was initiated by 20-fold dilution (2 ml) in the presence of either 10^{-4} M CHA (●) or 10^{-6} M DPCPX (●) and bound [^{3}H]CHA measured after 10 and 60 minutes. Points are expressed as percent of [^{3}H]CHA specific binding observed at the same association time and no dissociation (%SB at dissociation $t = 0$). Results shown are the mean of two separate experiments measured in duplicate, except 15°C which is one experiment with points in duplicate. For 22, 30 and 37°C the mean concentration of [^{3}H]CHA in the 100 μl association was 5.5 ± 0.4 nM (n = 2). At 15°C the concentration of [^{3}H]CHA was 5.8 nM.

Figure 5.20 "Agonist locking" may be absent prior to membrane pre-incubation.

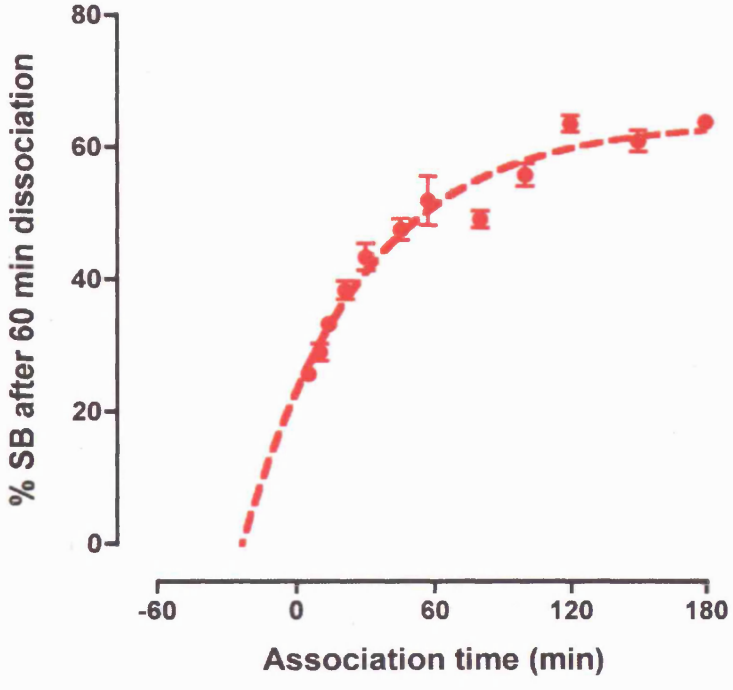

Figure 5.20: Non-linear regression of the data presented in Figure 5.19 to a simple exponential curve often extrapolated to an x-axis intercept between 0 and -60 min. Shown above is the effect of association time on the extent of [^{3}H]CHA binding following 60 min dissociation in the presence of 10^{-4} M CHA (as shown on Figure 5.19 on the preceding page). Non-linear regression of the individual data-sets used to generate the above graph best fit to curves with mean x-axis intercept of -24 $\pm$ 9 min and y-max of 65 $\pm$ 3 % with rate 0.020 $\pm$ 0.007 min^{-1} (n = 2).

Figure 5.21 The effect of association time on the fast rate constant of [^{3}H]CHA dissociation.

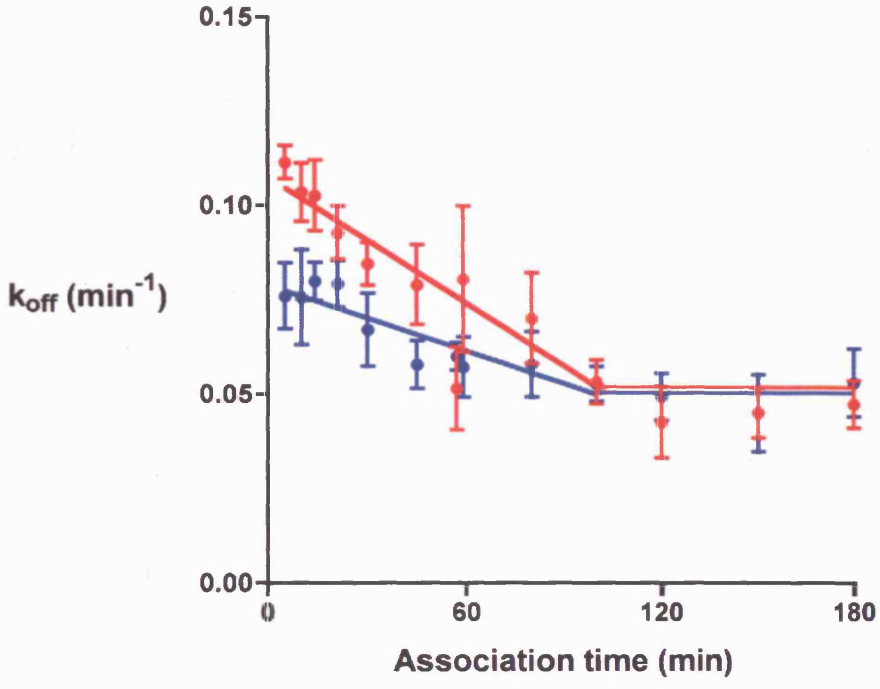

Figure 5.21: Effect of association time on the estimate of initial fast rate constant of [^{3}H]CHA dissociation (k_{off}) by 10^{-4} M CHA (red) or 10^{-6} M DPCPX (blue) chase. As described above, k_{off} was estimated from specific binding measured after 0, 10 and 60 minutes of dissociation following each association time. k_{off} was estimated using the equation, $y = span.e^{-kt} + plateau$, where y is [^{3}H]CHA SB following dissociation time t of 10 min, span is amplitude of dissociation to *plateau*, *plateau* is [^{3}H]CHA SB following 60 min dissociation, and k is estimate of dissociation rate constant (k_{off}). Lines are shown for illustrative purposes only.

preparations although not exclusively as pre-bound adenosine-receptor-G protein complexes. It appears that incubation of membrane preparations with adenosine deaminase for 30 min at RT is not sufficient to remove all endogenous adenosine present. Figure 5.2 provides evidence for the presence of adenosine in the membrane preparations which is not pre-coupled to receptor-G protein complexes and which progressively inhibits the association of [^{3}H]DPCPX.

The differences in the association of [^{3}H]DPCPX at the adenosine A_1 receptor described by Cohen *et al.* (1996b) and the data presented here appear to be the result of differences in the conditions during membrane preparation. Cohen *et al.* (1996b) prepared membranes in the presence of saponin unlike the membranes used in this study. The presence of saponin may trigger the release of adenosine stored in vesicular structures and expose adenosine to the adenosine A_1 receptor potentially resulting in the formation of "locked" adenosine–A_1 receptor–G protein complexes. The slow release of adenosine from these complexes may give rise to the slow increase in [^{3}H]DPCPX binding at longer incubation times observed by Cohen *et al.* (1996b). For the membranes used in the present study, in the absence of adenosine deaminase during the 30 min membrane preincubation (Figure 5.2; closed squares) it is likely that adenosine is being slowly released from the membranes and is the reason for the peaking of the [^{3}H]DPCPX association curve and subsequent decay caused by binding of adenosine. It should be noted that formation of a plateau at longer times does not necessarily indicate that adenosine release has stopped or slowed down because the plateau is approximately 50% of maximum levels of bound [^{3}H]DPCPX observed in the presence of both adenosine deaminase and saponin. This 50% level corresponds to the expected fraction of high affinity agonist binding sites and much higher levels of endogenous adenosine would be required to begin to occupy the low affinity binding sites. In the presence of adenosine deaminase (Figure 5.2; circles) the [^{3}H]DPCPX association curves show a slight decrease in binding at long times. An explanation may be that in the presence of adenosine deaminase, endogenous adenosine being released will be catabolised effectively but not instantly. A small amount of adenosine may therefore be capable of binding to the receptors to slowly form very long-lived adenosine–A_1 receptor–G protein complexes. It would be predicted that in the presence of GTP (or similar guanine nucleotide) this decrease in [^{3}H]DPCPX binding with time would not be observed. This was not tested experimentally here, although Cohen *et al.* (1996b) reports clearly monophasic [^{3}H]DPCPX association to the A_1 receptor in the presence of guanine nucleotide.

The dissociation of [^{3}H]DPCPX from the adenosine A_1 receptor was rapid and can be described by a simple mono-exponential function decaying to predicted levels of binding (Figure 5.3 on page 118). The rate constant of dissociation was not sensitive to the presence of GTP or a competing unlabelled ligand such as DPCPX or CHA. Dissociation of [^{3}H]DPCPX was not sen-

sitive to the agonist or antagonist pharmacology of the competing ligand. The rate constant of [^{3}H]DPCPX dissociation was similar for A_1HE, A_1LE and A_1R-GFP-Gα_i membranes. Simple mono-exponential dissociation of [^{3}H]DPCPX from the adenosine A_1 receptor is characteristic of a simple reversible bimolecular interaction between receptor and ligand. The dissociation of [^{3}H]DPCPX from recombinantly expressed adenosine A_1 receptor described here is similar to that observed at endogenous (Gerwins *et al.* 1990, Klotz *et al.* 1990) and recombinant (Cohen *et al.* 1996b) expressed A_1 receptor .

The biphasic association of [^{3}H]CHA at the human adenosine A_1 receptor.

The association of [^{3}H]CHA at A_1HE membranes was best described by a two-phase model of exponential association and the extent and initial rate of association were clearly dependent on the concentration of [^{3}H]CHA (Figure 5.4 on page 120). Both the observed rate (Figure 5.5a) and the estimated initial rate (Figure 5.5c) of the fast component of [^{3}H]CHA association were clearly dependent on the concentration of [^{3}H]CHA. This is consistent with fast rate of association being driven by the binding of [^{3}H]CHA at readily available high affinity binding sites. Generally these available high affinity binding sites are thought to be pre-coupled receptor-G protein complexes to which agonist binds to form the high affinity agonist-receptor-G protein ternary complex. The dependence of the slow component of [^{3}H]CHA association on the concentration of [^{3}H]CHA was much less distinct. With the limited data here it is difficult to establish an absolute relationship, although the observed rate constant of association for the slow component was not dependent on the concentration of [^{3}H]CHA (Figure 5.5b). It appears the slow component of [^{3}H]CHA association is significantly influenced by a process other than binding at immediately available high affinity binding sites. The slow increase in [^{3}H]CHA binding may be the result of formation of new high affinity binding sites by the recruitment of extra G protein into the receptor environment or promiscuous coupling to another G protein. The observed rate constants of [^{3}H]CHA association are consistent with reported bi-exponential association of 2 nM [^{3}H]CHA to CHO membranes recombinantly expressing the human adenosine A_1 receptor with observed rate constants of association of 0.08 $\pm$ 0.01 and 7 $\pm$ 6 x10^{-4} min^{-1} (Cohen *et al.* 1996b).

Although the results presented here are limited, the relative amplitudes of each component of high affinity [^{3}H]CHA association are consistent with a 1:1 stoichiometry at all concentrations of [^{3}H]CHA (Figure 5.5e & 5.5f). This was also observed in Chapter 4, where the slow increase in [^{3}H]CHA B_{max} with time had an amplitude of approximately 50% of maximum [^{3}H]CHA B_{max} (Figure 4.3 on page 84). When a GPCR such as the adenosine A_1 receptor exhibits a 1:1 stoichiometry of binding components or receptor states it raises the consideration of the presence of

receptor dimers: the receptor may exist in a dimeric form pre-coupled to a single G protein forming one high affinity agonist binding site for every dimeric complex. The slow component of binding may reflect the formation of a high affinity binding site resulting from structural rearrangement of the receptor signalling complex and the recruitment of extra G protein. The observation that the apparent log affinities of [^{3}H]CHA for the fast and slow components are similar (approximately 8.5 and 8.8 respectively) provides a rationalisation of why no heterogeneous high affinity agonist binding is detected.

Preliminary data showed both components of the association of [^{3}H]CHA to membranes expressing the A_1R-GFP-Gα_i fusion construct were comparable at high and low levels of receptor expression (Table 5.1 on page 123). The effect of the level of receptor expression on the association kinetics of [^{3}H]CHA was not investigated further.

The dissociation of [^{3}H]CHA from the human adenosine A_1 receptor.

In contrast to the rapid and complete dissociation of [^{3}H]DPCPX from the adenosine A_1 receptor, the dissociation of [^{3}H]CHA by 20-fold dilution was incomplete with levels of bound [^{3}H]CHA decaying to a plateau much greater than that expected for the remaining concentration of [^{3}H]CHA (Figure 5.6 on page 126). Such pseudo-irreversible agonist binding has often been termed "agonist locking." The mechanism of agonist locking is unknown. The majority, but not all, of bound [^{3}H]CHA was rapidly dissociated by dilution in the presence of 100 μM GTP showing agonist, receptor and G protein all influence formation of the "locked" complex. The observed rate of dissociation of [^{3}H]CHA (but not the relative amplitude) appeared to be dependent on the concentration of [^{3}H]CHA during the 60 min incubation prior to initiation of dissociation by 20-fold dilution (Figure 5.7 on page 127b). This dependence of dissociation on concentration is a strong indicator that a simple bi-molecular interaction behaving according to the law of mass action is not operating. Approximately one third of [^{3}H]CHA specific binding was capable of dissociating from A_1HE membranes following 20-fold dilution alone.

In the presence of a high concentration of unlabelled antagonist (DPCPX) or agonist (CHA), the dissociation of [^{3}H]CHA was enhanced relative to dilution alone and was best described by a model of two-phase exponential dissociation decaying to non-specific levels over a period of several hours. In addition, unlabelled CHA was able to enhance the dissociation of [^{3}H]CHA to a greater extent than DPCPX (Figure 5.8 and Table 5.3 on pages 129 and 130 respectively). The ability of CHA to enhance the extent of [^{3}H]CHA dissociation relative to DPCPX was manifest as a change in the amplitude of the fast component of dissociation, with both chase ligands showing indistinguishable effects on the rate constants of dissociation for each component (Table 5.4 on

page 130).

Studies have reported varying degrees of pseudo-irreversible "agonist locking" at the adenosine A_1 receptor. Following dilution alone, Stiles (1988) showed no dissociation of agonist from the solubilised adenosine A_1 receptor. Using membranes prepared from CHO cells recombinantly expressing the human adenosine A_1 receptor approximately 50% of total bound [^{3}H]CHA remained after 10-fold dilution in the presence of a chase of 3 mM theophylline (an adenosine A_1 receptor antagonist) (Cohen *et al.* 1996b). In the presence of an excess of unlabelled agonist, dissociation of 50-80% of specific bound radiolabelled agonist has been reported for the rat (Schwabe & Trost 1980), pig (Leid *et al.* 1988) and human (Waldhoer *et al.* 1999) adenosine A_1 receptor. The differences observed between these reports appear to be largely due to differences in methodology but may also be influenced in the use of adenosine A_1 receptor preparations of different receptor densities from different species. Reports of "agonist locking" in the literature are commonly reported as levels of bound ligand remaining or as mono-exponential decay to a plateau. The results presented here provide a novel detailed description of the dissociation of [^{3}H]CHA in the presence of an unlabelled ligand which was best described as a two-phase exponential decay with a 100-fold ratio in the rate constants of dissociation for the two components. Furthermore, the agonist CHA enhanced the dissociation of [^{3}H]CHA to a greater extent than DPCPX. This ability of an unlabelled agonist to enhance the dissociation of a radiolabelled agonist is termed "agonist-induced agonist dissociation."

In order to increase the throughput of the [^{3}H]CHA dissociation assay the number of data points was reduced to three dissociation time points along with total and non-specific binding (Figure 5.10 on page 134). The 5-point dissociation assay was reliable and generated results similar to those of the full-length dissociation assay (compare Tables 5.4 and 5.5, pages 130 and 135 respectively, for mean parameters from the full-length and 5-point dissociation assays respectively). The 5-point dissociation assay enabled the investigation of properties such as the potency of the enhancement of dissociation by chase ligand, which would have not been feasible with the full-length dissociation assay.

The potency of chase ligands to enhance the dissociation of [^{3}H]CHA from the human adenosine A_1 receptor.

The abilities of both CHA and DPCPX chase ligands to enhance the dissociation of [^{3}H]CHA were highly potent and specific (Table 5.7 on page 144) and independent of the concentration of [^{3}H]CHA (Figure 5.13 on page 141). The high potency of CHA (and the other agonists examined) suggest that the effects are mediated at receptor–G protein complexes and not at uncoupled receptors.

DPCPX chase showed no enhancement of [^{3}H]CHA dissociation after 10 min and only a little after 60 min. The differences between CHA and DPCPX chases shown in Figure 5.12 support the observations of the kinetics of [^{3}H]CHA dissociation where agonist-induced agonist dissociation is largely due to an increase in the amplitude of the fast component of dissociation. This is what appears to be reflected in Figure 5.12. In Table 5.7 (page 144) the potency of CHA chase increases with dissociation time which may be a reflection of being referenced against dilution alone which has generally reached a plateau after approximately 60 min. Of interest is to also estimate the potency of CHA chase relative to DPCPX chase rather than dilution alone. This may provide a reflection of the potency of the specific mechanism by which agonist-induced agonist dissociation is manifest.

It was not clear whether the difference in the ability of CHA and DPCPX to enhance the dissociation of [^{3}H]CHA was the result of their different efficacy or some other difference in the molecular properties of the two ligands. Unlabelled chase ligands of intermediate efficacy to CHA (a high efficacy agonist) and DPCPX (an inverse agonist) were employed in order to investigate the effect of chase ligand efficacy on agonist-induced agonist dissociation. The data presented in Table 5.6 on page 138 describes trend for GR190178 to be most effective at enhancing the dissociation of [^{3}H]CHA relative to GR161144 and GR162900. The rank order for enhancing dissociation of [^{3}H]CHA is GR190178 > GR161144 > GR162900 in essentially all of the data presented in Table 5.6. In Chapter 4, GR161144 and GR162900 were shown to have considerably reduced GTP shift at the adenosine A_1 receptor compared to GR190178 and CHA (Figure 4.6 on page 91).

In addition to the correlation between agonist efficacy and the extent to which an agonist can enhance the dissociation of [^{3}H]CHA, the potency of the these agonists to enhance dissociation is described in Table 5.7 on page 144. The observed increase in log potency from 10 to 180 min was 0.93 $\pm$ 0.22, 0.82 $\pm$ 0.37, 0.38 $\pm$ 0.22 and -0.17 $\pm$ 0.20, for CHA, GR190178, GR161144 and GR162900 respectively. The increase in agonist potency between 10 and 180 min follows the same rank order as for the extent of dissociation (Table 5.6) and GTP shift observed at equilibrium (Figure 4.6). The same rank order of increase in potency was observed between 10 and 60 min, and between 60 and 180 min. These observations provide strong evidence that estimates of agonist efficacy observed in equilibrium binding experiments can be related to other responses of the receptor to agonist binding, such as agonist-induced agonist dissociation observed here.

Only one limited report has been published describing the binding of GR190178, GR161144 and GR162900 at the human adenosine A_1 receptor. Equilibrium binding (including GTP shift) and functional assays ([^{35}S]GTPγS binding and elevation of intracellular Ca^{2+}) all showed a rank

order of efficacy of GR190178 > GR161144 > GR162900 (Sheehan *et al.* 2000). No significant difference in the stimulation of a cAMP-linked reported gene was observed for the three agonists, illustrating the added complexity in the interpretation of results from downstream amplification of the response to agonist binding at the receptor. In other responses the rank order of efficacy was GR190178 > GR161144 > GR162900 which was the same as that observed in the equilibrium and kinetic experiments presented here. The study reported another agonist, GR79236, which showed efficacy greater than GR190178 but less than NECA.

Further evidence of the specific and potent nature of the enhancement of agonist dissociation by an unlabelled chase is provided by the estimate of chase ligand log EC_{50} in Table 5.7. High efficacy ligands CHA and DPCPX show a high potency (sub-nanomolar) after 180 min, and partial agonists GR190178, GR161144 and GR162900 show decreasing potency. While the potency of a chase ligand to enhance the dissociation of [^{3}H]CHA from the adenosine A_1 receptor is dependent on ligand affinity, there appears to be little difference in the extent of that enhancement between agonists of very different efficacy. All the chase agonists studied here appear to show a similar ability to promote the extent of dissociation of [^{3}H]CHA after 180 min. The antagonists DPCPX and N0840 show a considerably reduced ability to enhance [^{3}H]CHA dissociation (although it should be noted N0840 chase was used at a concentration (10^{-6} M) which would not appear to be sufficient to produce a maximal response).

GTP-insensitive agonist-induced agonist dissociation.

The dissociation of [^{3}H]CHA by 20-fold dilution in the presence of 10^{-4} M GTP consisted of a very rapid initial dissociation followed by a slow decay of bound [^{3}H]CHA over several hours (Figure 5.6 on page 126). This is similar to previous characterisation of [^{3}H]CHA dissociation from the adenosine A_1 receptor in 10^{-3} M GTP which shows a slow decay of bound [^{3}H]CHA after a very rapid initial dissociation (Cohen *et al.* 1996b). Figure 5.15 on page 146 shows that even in the presence of GTP both CHA and DPCPX can further enhance the dissociation of [^{3}H]CHA from the adenosine A_1 receptor. The observation of agonist-induced agonist dissociation in the presence of GTP suggests that the phenomenon may be of physiological significance in live cells where GTP is present. Indeed, while the extent of the enhancement of [^{3}H]CHA dissociation by DPCPX was similar in the presence or absence of GTP, agonist-induced agonist dissociation was even more pronounced in the presence of GTP (Figure 5.16 on page 148). After 3 hours dissociation in the presence of both GTP and CHA only 3% of specific [^{3}H]CHA binding remained (Table 5.8a). The very rapid initial dissociation of [^{3}H]CHA in the presence of GTP made accurate estimation of the rate constant of dissociation for the fast component difficult, however Table 5.8b provides further

evidence that agonist-induced agonist dissociation is largely manifest as a change in the relative amplitude of each component.

Possible mechanisms of agonist-induced agonist dissociation.

In general the ability of CHA chase to enhance the dissociation of [^{3}H]CHA, relative to DPCPX chase, from A_1HE membranes was independent of the concentration of [^{3}H]CHA and was manifest as an increase in the amplitude, but not the rate, of the fast component of dissociation. Also, the dissociation of [^{3}H]CHA by CHA or DPCPX appears to be differentially sensitive to temperature (Figure 5.19). There appear to be differences between the mechanisms by which CHA and DPCPX enhance the dissociation of [^{3}H]CHA. The independence of the two rate constants of dissociation on the concentration of [^{3}H]CHA and the pharmacology of chase ligand (Figure 5.9) implies that the process of the dissociation of [^{3}H]CHA in the presence of an unlabelled ligand is not a simple bimolecular reaction following the law of mass action. There appears to be two dissociation processes, or two states of bound [^{3}H]CHA, that operate through a mechanism independent of concentration alone. DPCPX chase may enhance the dissociation of [^{3}H]CHA by preventing the rebinding of [^{3}H]CHA following dissociation. "Agonist-locking" by dilution alone may be a combination of; (i) the slowing of the already slow dissociation rate constant found in the presence of DPCPX or CHA, and (ii) the possibility of additional slow recruitment of additional G proteins to form by [^{3}H]CHA rebinding more high affinity complexes that was manifest in the association studies.

CHA is able to enhance the dissociation of [^{3}H]CHA to an even greater extent than DPCPX which suggests a more "active" mechanism than simple inhibition of rebinding. Agonist-induced agonist dissociation provides evidence for communication between bound unlabelled chase agonist and bound [^{3}H]CHA. This interaction was of high affinity and high potency. It is not known how this interaction may be communicated between agonist binding sites, although it could conceivably be transmitted directly through receptor-receptor contacts or through other protein components of the receptor signalling complex. Direct receptor-receptor interaction may be the consequence of receptor oligomerisation. The dependence of this receptor-receptor communication on the level of receptor expression favours the dynamic reversible formation of receptor oligomers rather than constitutive receptor oligomerisation.

In summary, the work presented in this Chapter describes the kinetics of [^{3}H]DPCPX binding at the human adenosine A_1 receptor as a simple and reversible bimolecular interaction between ligand and receptor. The association of [^{3}H]CHA to the adenosine A_1 receptor was biphasic and the rate constant of association of the fast component was dependent on the concentration

of [^{3}H]CHA. The slower component of [^{3}H]CHA association encompasses a process which is not dependent on the concentration of [^{3}H]CHA and may be a process such as the reorganisation of the receptor signalling complex and the recruitment of additional G protein to form further high affinity agonist binding sites. The ability of unlabelled chase ligands to enhance the dissociation of [^{3}H]CHA relative to 20-fold dilution alone was investigated in detail. Agonists of varying efficacy were able to considerably enhance the dissociation of [^{3}H]CHA relative to the antagonists DPCPX and N0840, and the magnitude of this enhancement was dependent on the efficacy of the agonist. Agonist-induced agonist dissociation provides evidence of highly specific and potent communication between high affinity agonist binding sites on adenosine A_1 receptors. Such receptor-receptor communication may be the consequence of receptor oligomerisation. Chapter 6 continues the investigation of the dissociation of [^{3}H]CHA from the adenosine A_1 receptor by investigating in detail the effect of the level of receptor expression on agonist-induced agonist dissociation.

Chapter 6

The dependence of agonist-induced agonist dissociation on the level of adenosine A_1 receptor expression.

6.1 Introduction.

Chapter 5 described the ability of unlabelled agonist to enhance the dissociation of [^{3}H]agonist from the adenosine A_1 receptor to a greater extent than unlabelled antagonist. This ability is termed "agonist-induced agonist dissociation" and is manifest as an increase in the amplitude of the fast rate constant of dissociation rather than an increase in the rate of either component. In this chapter agonist-induced agonist dissociation was investigated in more detail using membranes prepared from the series of cell lines expressing either the A_1R-GFP or A_1R-GFP-Gα_i fusion constructs at a range of levels of expression.

The aim of the work presented is to determine whether agonist-induced agonist dissociation is dependent on the level of receptor expression. This is of significance if agonist-induced agonist dissociation is mediated by receptor-receptor interaction and may provide an insight into whether the adenosine A_1 receptor exists as an oligomeric complex and whether the nature of this complex is dependent on the level of receptor expression.

6.2 The effect of the level of expression of the A_1R-GFP-Gα_i fusion construct on the extent and kinetics of dissociation of [^{3}H]CHA.

The series of cell lines expressing the A_1R-GFP-Gα_i fusion construct showed equilibrium binding indistinguishable from that of the adenosine A_1 receptor expressed alone (Chapter 4). The dependence of features of equilibrium binding on the level of A_1R-GFP-Gα_i expression agreed with observations of the adenosine A_1 receptor expressed at two different densities (A_1HE and A_1LE). Membranes prepared from the A_1R-GFP-Gα_i cell lines were chosen in order to investigate the effect of the level of receptor expression on agonist-induced agonist dissociation because they provided a large range of expression level and were considered to be a valid model of the adenosine A_1 receptor expressed alone.

6.2.1 The effect of the level of A_1R-GFP-Gα_i expression on the enhancement of [^{3}H]CHA dissociation by DPCPX.

Detailed [^{3}H]CHA dissociation time courses were performed using membranes prepared from 22 of the A_1R-GFP-Gα_i cell lines. The dissociation time courses were performed in the same manner as most of those presented in Chapter 5. Prior to incubation with [^{3}H]CHA the A_1R-GFP-Gα_i membranes were incubated at RT for 30 min with adenosine deaminase to remove endogenous adenosine. Membranes were incubated with [^{3}H]CHA for 60 min in a small volume (100 μl) before dissociation was initiated by 20-fold dilution containing either 10^{-6} M DPCPX or 10^{-4} M CHA. Dissociation was performed for periods between 5 min to 180 min.

Figure 6.1 on the next page shows the level of bound [^{3}H]CHA remaining after 60 min dissociation in the presence of DPCPX for all of the A_1R-GFP-Gα_i membranes. Linear regression of the mean level for each cell line (n = 22) and all the individual observations (n = 88) both showed no significant dependence of the level of bound [^{3}H]CHA on the level of expression of the A_1R-GFP-Gα_i construct after 60 min. Where the mean level of bound [^{3}H]CHA is shown for each cell line the error shown is the s.e.m. of at least two independent experiments. No dependence on the level of receptor expression was also observed for the majority of other dissociation time points (Figure 6.2 on page 168 and Table 6.1 on page 169). The decrease in bound [^{3}H]CHA with time in the presence of DPCPX is clearly illustrated on Figure 6.2. Table 6.1 provides strong evidence that the ability of DPCPX to enhance the dissociation of [^{3}H]CHA from the adenosine A_1 receptor is not dependent on the level of receptor expression.

Figure 6.1 The effect of the level of A_1R-GFP-Gα_i expression on the enhancement of [^{3}H]CHA dissociation by DPCPX after 60 min.

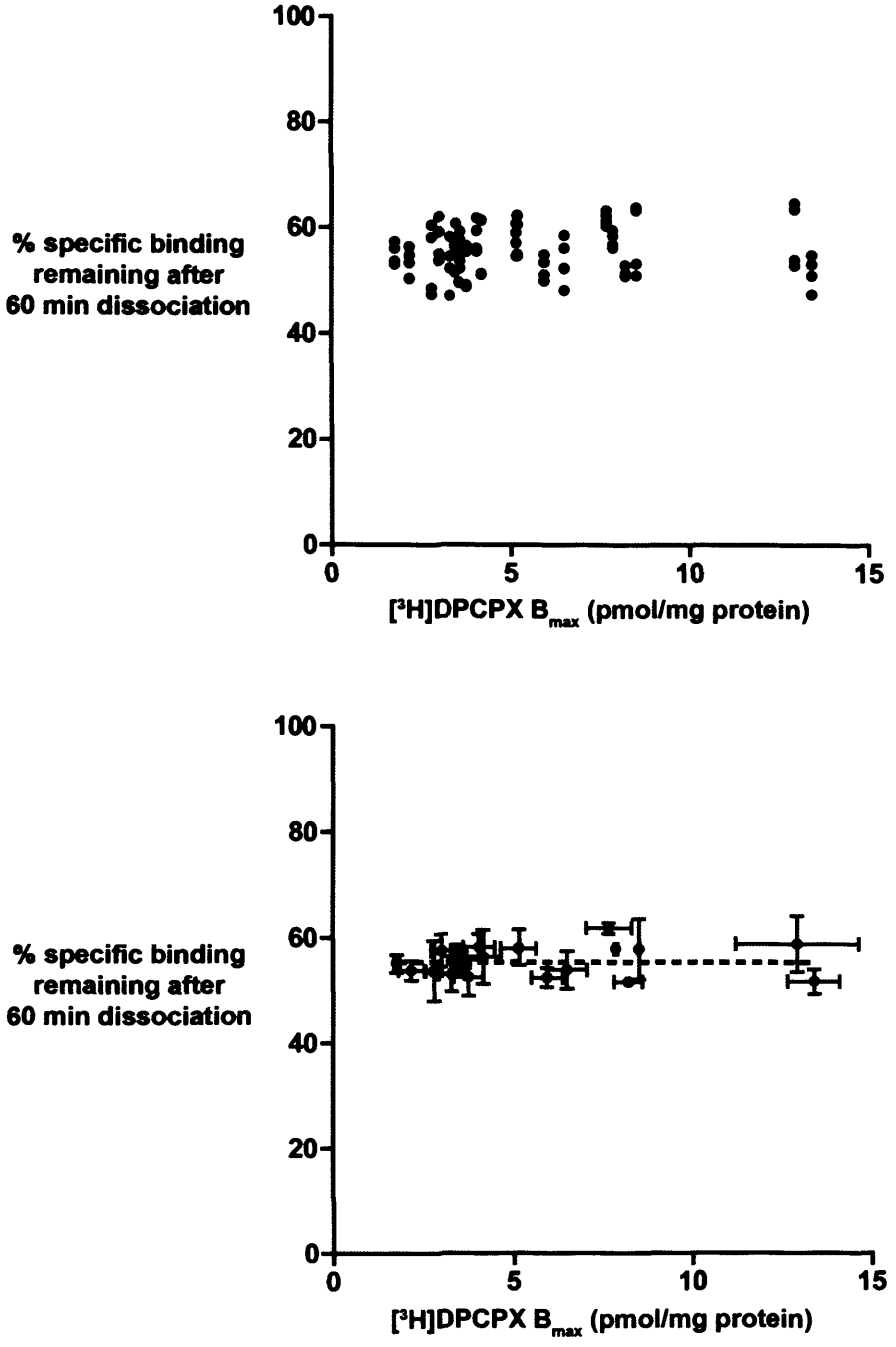

Figure 6.1: Comparison of all individual observations (top) and mean values (bottom) for each A_1R-GFP-Gα_i cell line in order to investigate if the enhancement of dissociation by DPCPX is dependent on the level of expression alone or whether the different cell lines influence the response. In both cases the level of bound [^{3}H]CHA remaining after dissociation for 60 min following 20-fold dilution in the presence of 10^{-6} M DPCPX was not dependent of the level of expression of the A_1R-GFP-Gα_i construct. A straight line is shown in order to indicate the mean, which is listed in Table 6.3 on page 174.

Figure 6.2 The effect of the level of A_1R-GFP-Gα_i expression on the enhancement of [^{3}H]CHA dissociation by DPCPX at four dissociation time points.

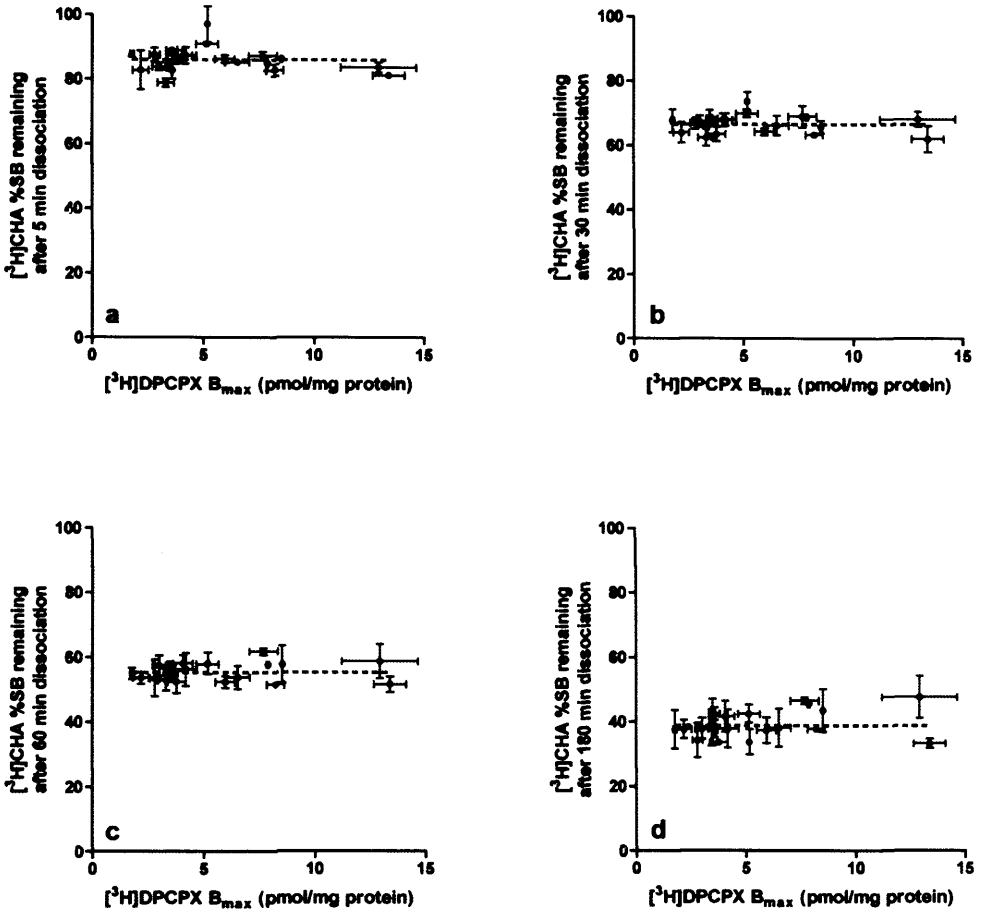

Figure 6.2: At the majority of dissociation time points measured, the ability of DPCPX to enhance the dissociation of [^{3}H]CHA was not dependent on the level of expression of the A_1R-GFP-Gα_i construct. Shown above are four dissociation time points where there was no observed dependence on the level of expression. The four dissociation times shown are 5, 30, 60 and 180 min (a, b, c and d respectively). The mean level of bound [^{3}H]CHA remaining at each dissociation time is indicated by the broken line.

Table 6.1 Statistical analysis of the dependence of DPCPX-enhanced [^{3}H]CHA dissociation on the level of A_1R-GFP-Gα_i expression.

Dissociation time (min)	Significantly non-zero slope?	P value	Slope	y-intercept
Linear regression of all individual observations (n = 88)				
5	Not Significant	-	-	-
10	Significant	0.0002	-0.60	83.4
17	Not Significant	-	-	-
30	Not Significant	-	-	-
45	Not Significant	-	-	-
60	Not Significant	-	-	-
95	Not Significant	-	-	-
125	Significant	0.03	0.41	41.8
180	Significant	0.04	0.43	37.0
Linear regression of mean values from each A_1R-GFP-Gα_i cell line (n = 22)				
5	Not Significant	-	-	-
10	Significant	0.02	-0.57	83.1
17	Not Significant	-	-	-
30	Not Significant	-	-	-
45	Not Significant	-	-	-
60	Not Significant	-	-	-
95	Not Significant	-	-	-
125	Not Significant	-	-	-
180	Not Significant	-	-	-

Table 6.1: The dependence of the enhancement of the dissociation of [^{3}H]CHA by 10^{-6} M DPCPX on the level of A_1R-GFP-Gα_i expression was determined for each dissociation time point. As illustrated in Figure 6.1 on page 167, the relationship was investigated using the mean for each cell line and all the individual observations. As for all statistical significance presented in this study, the dependence was considered significant if $P < 0.05$ (see Chapter 2.3.3 on page 59).

6.2.2 The effect of the level of A_1R-GFP-Gα_i expression on the enhancement of [^{3}H]CHA dissociation by CHA.

The effect of the level of expression of the A_1R-GFP-Gα_i construct on the ability of 10^{-4} M CHA to enhance the dissociation of [^{3}H]CHA after 60 min is shown in Figure 6.3 on the following page, with DPCPX data from Figure 6.1 shown for comparison. Linear regression showed a significant dependence of the level of bound [^{3}H]CHA on the level of expression of the A_1R-GFP-Gα_i construct (see Table 6.2 on page 173 for P values). At higher levels of receptor expression, CHA showed a greater ability to enhance the dissociation of [^{3}H]CHA. At all dissociation time points studied, both the mean levels for each cell line and all the individual observations showed a significant dependence of agonist-induced agonist dissociation on the level of receptor expression (Table 6.2). Figure 6.4 on page 172 illustrates this for four dissociation time points in the same manner as Figure 6.2. Table 6.2 provides strong evidence that agonist-induced agonist dissociation is dependent on the level of receptor expression, which suggests that the receptor environment and the factors that influence receptor behaviour depend on the level of receptor expression.

Tables 6.1 and 6.2 show little difference between the use of mean values for each cell line and all the individual observations. This provides evidence for a direct dependence on the level of receptor expression rather than differences due to the nature of individual cell lines.

If agonist-induced agonist dissociation is entirely dependent on receptor-receptor communication determined by the level of receptor expression, then the y-axis intercept of linear regression may be expected to correspond to dissociation with no agonist-induced agonist dissociation (i.e. dissociation by an antagonist chase). Table 6.3 on page 174 compares the mean levels of bound [^{3}H]CHA remaining after dissociation in the presence of DPCPX with the extrapolated y-axis intercept of the dependence of receptor expression on the level of agonist-induced agonist dissociation. It is difficult to subject the two parameters to statistical scrutiny especially as it is not known if the dependence of residual bound [^{3}H]CHA is linear (or not) with receptor expression level. However there does appear to be general similarity between dissociation by DPCPX chase and estimated dissociation by CHA in conditions with no receptor-receptor communication (at zero levels of receptor expression). Table 6.3 on page 174 provides strong evidence that agonist-induced agonist dissociation is entirely dependent on the level of receptor expression. At higher levels of receptor expression agonist is more effective at enhancing the dissociation of [^{3}H]agonist.

Figure 6.3 After 60 min agonist-induced agonist dissociation is dependent on the level of receptor expression.

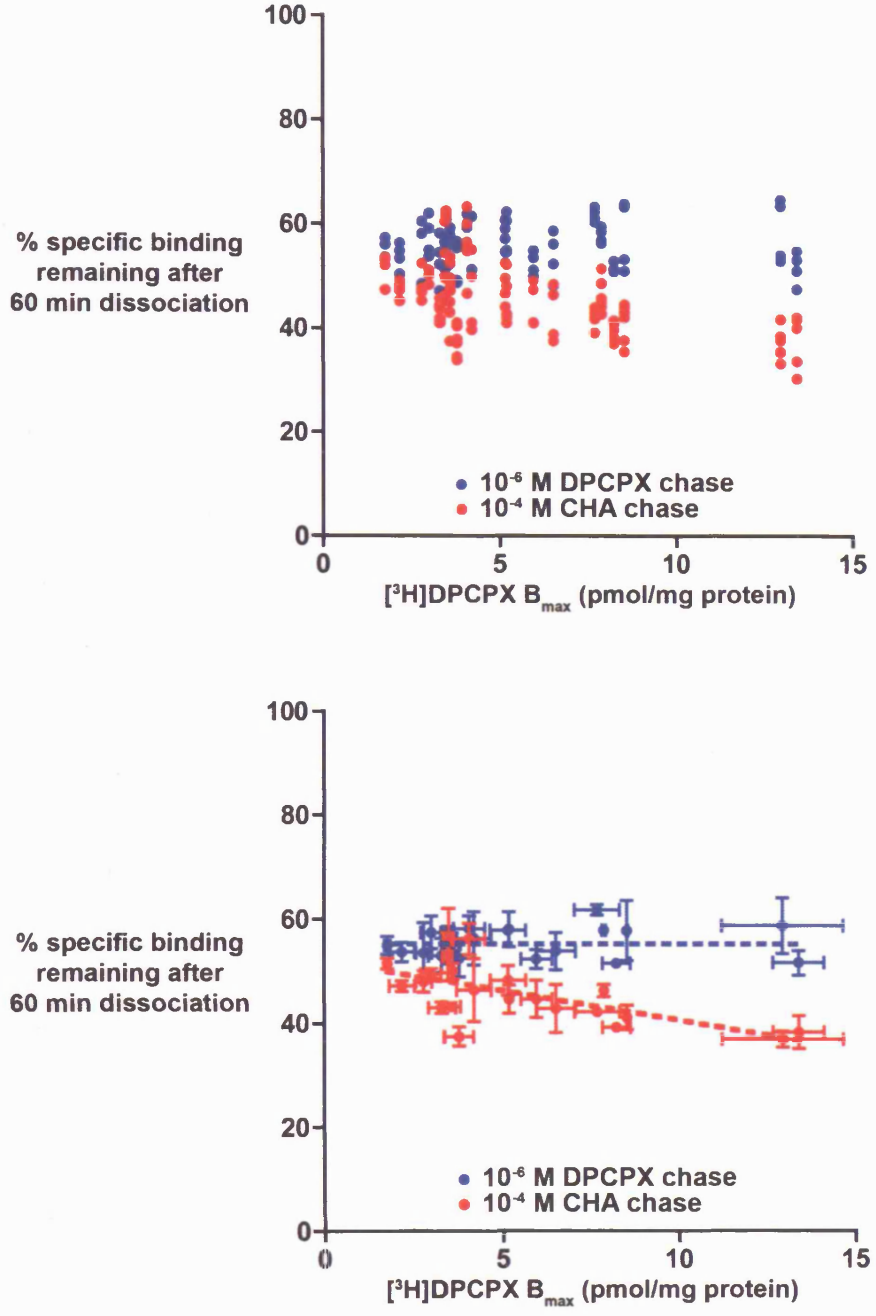

Figure 6.3: As for Figure 6.1 on page 167 the dependence of enhancement of [^{3}H]CHA dissociation after 60 min on the level of A_1R-GFP-Gα_i expression was investigated using individual observations and mean values for each cell line. Both approaches showed a significant dependence of agonist-induced agonist dissociation on the level of receptor expression (see Table 6.2 on page 173 for P values). Linear regression of the CHA chase data is indicated by the red line, and the mean level of bound [^{3}H]CHA remaining in the presence of DPCPX is indicated by the blue line.

Figure 6.4 The enhancement of [^{3}H]CHA dissociation by CHA was dependent on the level of A_1R-GFP-Gα_i expression at all dissociation time points studied.

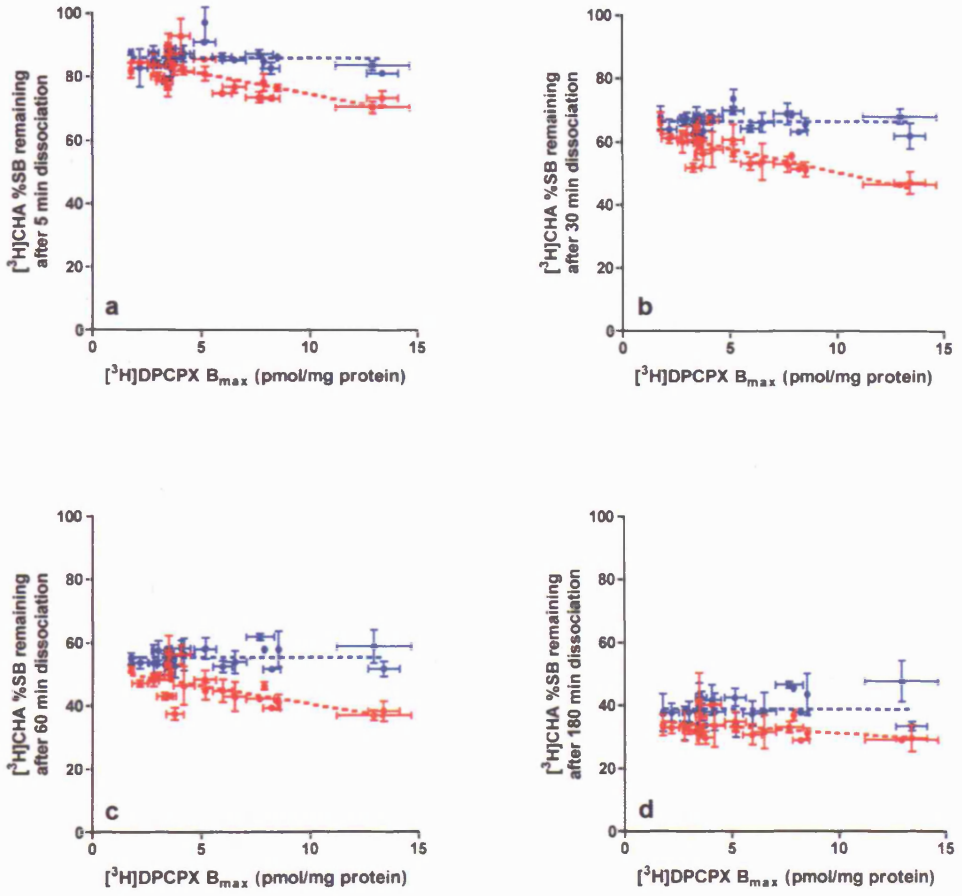

Figure 6.4: At all dissociation time points the enhancement of [^{3}H]CHA dissociation by CHA (●) was dependent on the level of A_1R-GFP-Gα_i expression. DPCPX data (●) from Figure 6.1 is shown for comparison. Linear regression of the CHA chase data is shown by the red line, as for Figure 6.3. The four dissociation times shown are 5, 30, 60 and 180 min (a, b, c and d respectively).

Table 6.2 Statistical analysis of the dependence of CHA-enhanced [^{3}H]CHA dissociation on the level of A_1R-GFP-Gα_i expression.

Dissociation time (min)	Significantly non-zero slope?	P value	Slope	y-intercept
Linear regression of all individual observations (n = 112)				
5	Significant	< 0.0001	-1.28	87.6
10	Significant	< 0.0001	-1.58	80.7
17	Significant	< 0.0001	-1.34	71.6
30	Significant	< 0.0001	-1.40	64.8
45	Significant	< 0.0001	-1.33	58.0
60	Significant	< 0.0001	-1.10	51.6
95	Significant	< 0.0001	-0.92	45.8
125	Significant	< 0.0001	-0.70	39.9
180	Significant	0.004	-0.41	35.4
Linear regression of mean values from each A_1R-GFP-Gα_i cell line (n = 22)				
5	Significant	0.0003	-1.27	87.4
10	Significant	< 0.0001	-1.60	80.9
17	Significant	< 0.0001	-1.39	72.1
30	Significant	< 0.0001	-1.47	65.3
45	Significant	< 0.0001	-1.38	58.4
60	Significant	0.0009	-1.14	52.0
95	Significant	0.001	-0.98	46.3
125	Significant	0.008	-0.73	40.1
180	Significant	0.049	-0.43	35.6

Table 6.2: At all dissociation time points agonist-induced agonist dissociation was dependent on the level of receptor expression. As illustrated in Figure 6.1 on page 167, the relationship was investigated using the mean for each cell line and all the individual observations. As for all statistical significance presented in this study, the dependence was significant if $P < 0.05$ (see Chapter 2.3.3 on page 59).

Table 6.3 Agonist-induced agonist dissociation is absent at very low levels of A_1R-GFP-Gα_i expression.

Dissociation time (min)	Mean [^{3}H]CHA %SB remaining in 10^{-6} M DPCPX (n = 22)	10^{-4} M CHA chase y-axis intercept (from Table 6.2)	Difference (DPCPX mean - CHA y-intercept)
5	86.0 ± 0.8	87.4	-1.4
10	80.0 ± 0.8	80.9	-0.9
17	73.9 ± 0.8	72.1	1.8
30	66.8 ± 0.6	65.3	1.5
45	60.8 ± 0.6	58.4	2.4
60	55.7 ± 0.6	52.0	3.7
95	48.4 ± 0.7	46.3	2.1
125	44.1 ± 0.8	40.1	4.0
180	39.4 ± 0.9	35.6	3.8

Table 6.3: The mean level of bound [^{3}H]CHA remaining after 20-fold dilution in the presence of 10^{-6} M DPCPX compared to the extrapolated level in the presence of 10^{-4} M CHA at zero A_1R-GFP-Gα_i expression.

6.2.3 The effect of the level of A_1R-GFP-Gα_i expression on the kinetics of dissociation of [^{3}H]CHA in the presence of chase ligand.

It has been shown previously that agonist-induced agonist dissociation at A_1HE membranes is manifest largely as an increase in the amplitude of the fast component of dissociation rather than a change in the rate constants of dissociation (Table 5.4 on page 130). The ability of CHA to enhance the dissociation of [^{3}H]CHA from the adenosine A_1 receptor has now been examined in detail and the kinetic data can be analysed to test whether the same parameter associated with [^{3}H]CHA dissociation is dependent on the level of receptor expression. Table 6.4 on the following page clearly shows that the increase in CHA-induced [^{3}H]CHA dissociation at greater levels of receptor expression is the consequence of an increase in the amplitude of the fast component of [^{3}H]CHA dissociation. Both the fast and slow rate constants of [^{3}H]CHA dissociation in the presence of CHA were not dependent on the level of receptor expression. These observations provide further evidence of two populations of [^{3}H]CHA both bound with high affinity at nM concentrations, which show 100-fold different rate constants of [^{3}H]CHA dissociation. The relative abundance of each population is dependent on the level of receptor expression.

The kinetics of [^{3}H]CHA dissociation by DPCPX chase were entirely independent of the level of A_1R-GFP-Gα_i expression (Table 6.4). This would be predicted from the insensitivity of the extent of [^{3}H]CHA dissociation by DPCPX chase on the level of A_1R-GFP-Gα_i expression.

6.3 The effect of the level of A_1R-GFP expression on the enhancement of [^{3}H]CHA dissociation by DPCPX and CHA.

The effect of the level of receptor expression on the dissociation kinetics of [^{3}H]CHA from membranes expressing the A_1R-GFP fusion construct at different levels was also investigated. Six A_1R-GFP membrane preparations were chosen which expressed the fusion construct over a range of densities. The cell lines were 5E4, 6H3, 6F12, 5C6, 6E5 and 5E10 (see Table 4.3 on page 95 for equilibrium binding properties). The effect of the level of receptor expression on the extent of [^{3}H]CHA dissociation in the presence of 10^{-6} M DPCPX or 10^{-4} M CHA was investigated in the same manner as for A_1R-GFP-Gα_i described above. Figure 6.5 on page 178 shows the effect of A_1R-GFP expression on agonist-induced agonist dissociation at four of the dissociation time points investigated. This can be directly compared to Figure 6.4 showing the greater number of A_1R-GFP-Gα_i membranes used. In general the six A_1R-GFP membranes showed [^{3}H]CHA

Table 6.4a Statistical analysis of the dependence of the kinetics of [^{3}H]CHA dissociation on the level of A_1R-GFP-Gα_i expression.

Parameter of dissociation	Significantly non-zero slope?	P value	Slope	y-intercept
10^{-4} M CHA chase (n = 22)				
$k_{-1,FAST}$	Not Significant	-	-	-
$span_{FAST}$	Significant	0.0007	1.4	34.0
$k_{-1,SLOW}$	Not Significant	-	-	-
$span_{SLOW}$	Significant	0.0007	-1.4	65.8
10^{-6} M DPCPX chase (n = 22)				
$k_{-1,FAST}$	Not Significant	-	-	-
$span_{FAST}$	Not Significant	-	-	-
$k_{-1,SLOW}$	Not Significant	-	-	-
$span_{SLOW}$	Not Significant	-	-	-

Table 6.4b Mean parameters describing two-phase exponential dissociation of [^{3}H]CHA from A_1R-GFP-Gα_i membranes.

Two-phase exponential dissociation	Fast		Slow	
Rate (k_{-1}) and amplitude (span)	k_{-1} (min^{-1})	span (%SB)	k_{-1} (min^{-1})	span (%SB)
10^{-4} M CHA chase (n = 22)	0.10 ± 0.01	-	3.5 ± 0.1 x10^{-3}	-
10^{-6} M DPCPX chase (n = 22)	0.10 ± 0.01	31.2 ± 0.8	3.4 ± 0.1 x10^{-3}	68.5 ± 0.8

Table 6.4: The effect of the level of A_1R-GFP-Gα_i expression on the four parameters describing two-phase exponential dissociation of [^{3}H]CHA was investigated by linear regression of the relationship. The P value, slope and y-axis intercept (i.e. the behaviour extrapolated to the absence of agonist-induced agonist dissociation) are reported where the best fit linear regression line had a significantly non-zero slope. The mean of each parameter is reported when no significant slope was found.

dissociation properties very similar to A_1R-GFP-Gα_i. However the absolute independence of the dissociation of [^{3}H]CHA in the presence of DPCPX was less clear for A_1R-GFP membranes than it was for A_1R-GFP-Gα_i. This appeared to be largely due to the reduced number of A_1R-GFP membrane preparations used (6 A_1R-GFP compared to 22 A_1R-GFP-Gα_i) and the reduced range of receptor expression levels.

Agonist-induced agonist dissociation at A_1R-GFP membranes was similar to that characterised in detail at A_1R-GFP-Gα_i membranes. CHA chase was more effective than DPCPX chase at membranes expressing the A_1R-GFP construct at higher densities. Unfortunately the data was not amenable to the same thorough statistical examination of any dependence on the level of receptor expression as was performed for the A_1R-GFP-Gα_i membranes presented in Tables 6.1 and 6.2. The mean levels of [^{3}H]CHA remaining at A_1R-GFP membranes after 10, 60 and 180 min dissociation in the presence of DPCPX is similar to those observed at A_1R-GFP-Gα_i membranes (Tables 6.3 and 6.5 on pages 174 and 179).

6.4 Comparison of the enhancement of [^{3}H]agonist dissociation from the A_1R alone and the A_1R-GFP and A_1R-GFP-Gα_i constructs.

Following detailed characterisation using A_1HE membranes (Chapter 5) membranes from the series of A_1R-GFP and A_1R-GFP-Gα_i cell lines were chosen in preference to A_1LE membranes to investigate the effect of receptor expression level on the kinetics of [^{3}H]CHA dissociation for a number of reasons. Equilibrium binding at both fusion constructs was essentially indistinguishable from A_1HE membranes and generally independent of the level of receptor expression (Chapter 4). The large number of A_1R-GFP and A_1R-GFP-Gα_i cell lines provided a greater resolution, or detail, with which to investigate any dependence on the level of receptor expression. Also, experiments investigating the dissociation of [^{3}H]CHA from A_1LE membranes were very noisy, variable and consequently difficult to analyse quantitatively. A_1LE membranes were in general difficult to obtain clean data with both equilibrium and kinetic binding experiments. Agonist-induced agonist dissociation was observed at A_1LE membranes in some experiments although the poor quality of the data prevented thorough examination. Figure 6.7 on page 182 shows the dissociation of [^{3}H]CHA at A_1LE membranes with large overlapping error bars at most dissociation time points. However there does appear to be a tendency for CHA chase to slightly enhance the dissociation of [^{3}H]CHA relative to DPCPX chase. With the detailed characterisation of the A_1R-GFP-Gα_i

Figure 6.5 The dependence of agonist-induced agonist dissociation on the level of A_1R-GFP expression.

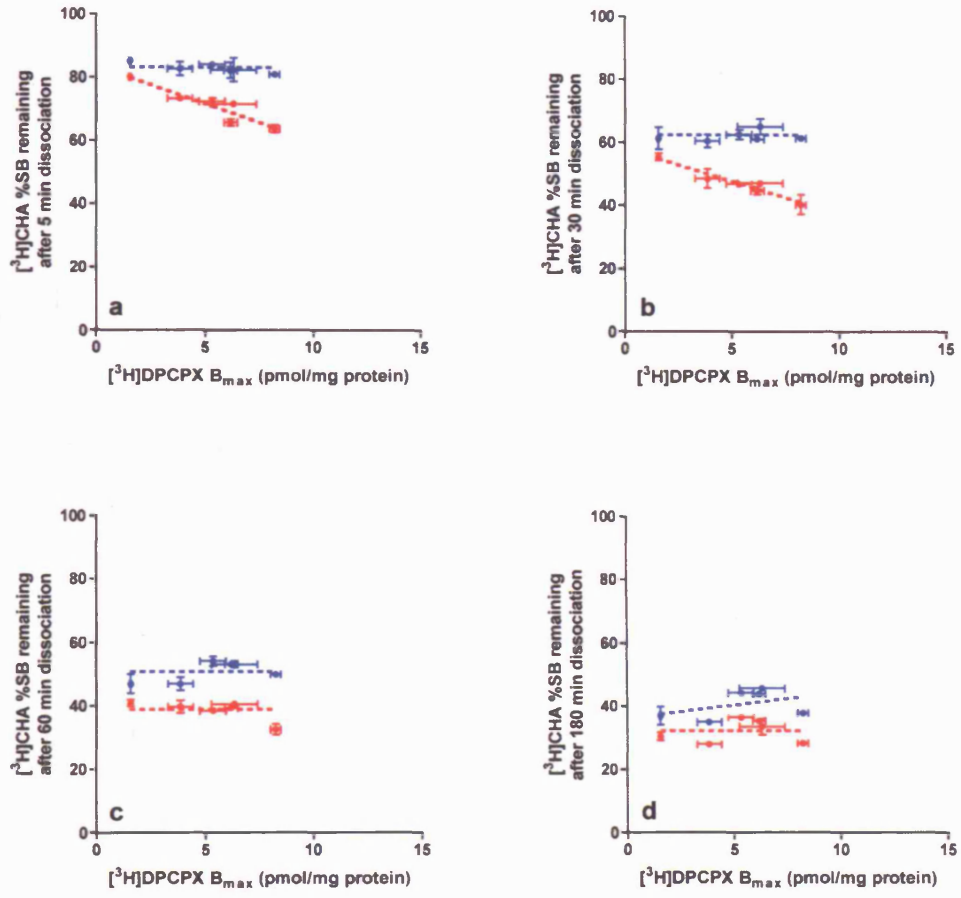

Figure 6.5: The dependence of the enhancement of [^{3}H]CHA dissociation on the level of receptor expression was investigated with a reduced number of A_1R-GFP cell lines compared to A_1R-GFP-Gα_i. Shown above are the levels of bound [^{3}H]CHA remaining after dissociation by 20-fold dilution in the presence of 10^{-6} M DPCPX (●) or 10^{-4} M CHA (●). The six A_1R-GFP cell lines were 5E4, 6H3, 6F12, 5C6, 6E5 and 5E10 (see Table 4.3 on page 95 for equilibrium binding properties). Where the level of bound [^{3}H]CHA remaining was not dependent on the level of A_1R-GFP expression a horizontal line is shown. Where a significant dependence was observed the best fit line from linear regression is shown. The four dissociation times shown are 5, 30, 60 and 180 min (a, b, c and d respectively).

Table 6.5 [^{3}H]CHA binding remaining after dissociation from A_1R-GFP membranes in the presence of DPCPX.

Dissociation time (min)	10	60	180
A_1R-GFP membranes			
% [^{3}H]CHA specific binding remaining after dissociation by 20-fold dilution with 10^{-6} M DPCPX chase (n = 12)	77.0 ± 0.6	50.8 ± 1.0	40.7 ± 1.3
A_1R-GFP-Gα_i membranes			
% [^{3}H]CHA specific binding remaining after dissociation by 20-fold dilution with 10^{-6} M DPCPX chase (n = 22)	80.0 ± 0.8	55.7 ± 0.6	39.4 ± 0.9
A_1HE membranes			
% [^{3}H]CHA specific binding remaining after dissociation by 20-fold dilution with 10^{-6} M DPCPX chase (n = 28)	86.1 ± 1.6	64.0 ± 1.7	46.6 ± 1.6

Table 6.5: Mean levels of bound [^{3}H]CHA remaining at A_1HE, A_1R-GFP and A_1R-GFP-Gα_i membranes after dissociation by 20-fold dilution in the presence of 10^{-6} M DPCPX. Data shown is the mean of all individual observations (performed in duplicate) at each time point. Figure 6.5 on the preceding page shows the same A_1R-GFP data (at 60 and 180 min) expressed as a mean for each cell line used. A_1HE and A_1R-GFP-Gα_i data are reproduced from Tables 5.3 and 6.3 (pages 130 and 174) respectively.

membranes, and to a lesser extent the A_1R-GFP membranes, the kinetics of the dissociation of [^{3}H]CHA from A_1LE membranes was not investigated further. Previous attempts to characterise the dissociation of [^{3}H]CHA from A_1LE membranes could not be fit to an equation describing monophasic exponential decay and showed no enhancement of [^{3}H]CHA dissociation by CHA chase relative to DPCPX chase (Browning 2003).

Figure 6.6 on the following page provides a visual comparison of individual [^{3}H]CHA dissociation experiments at A_1HE, A_1R-GFP and A_1R-GFP-Gα_i membranes. The extent of [^{3}H]CHA dissociation in the presence of DPCPX chase has been shown above to be essentially independent of the level of receptor expression and therefore mean levels can be compared between A_1HE, A_1R-GFP and A_1R-GFP-Gα_i membranes. Table 6.5 on the previous page lists the levels of bound [^{3}H]CHA remaining after 10, 60 and 180 min for A_1HE, A_1R-GFP and A_1R-GFP-Gα_i membranes. While the levels are not identical, there does not appear to be a sufficient difference between membrane types that could markedly impact on proposed mechanisms of DPCPX-enhanced [^{3}H]CHA dissociation. In general, the nature of the dissociation of [^{3}H]CHA from A_1HE, A_1R-GFP and A_1R-GFP-Gα_i membranes was similar.

6.5 Discussion.

Chapter 4 showed the equilibrium binding properties of membranes prepared from the series of A_1R-GFP and A_1R-GFP-Gα_i cell lines were very similar to A_1HE membranes which express the human adenosine A_1 receptor alone. The adenosine A_1 receptor fusion constructs appear to be representative of the A_1 receptor alone and are therefore of considerable interest as models of the effect of receptor expression level on receptor behaviour. Chapter 5 described "agonist-induced agonist dissociation" at A_1HE, A_1R-GFP and A_1R-GFP-Gα_i membranes. The dissociation of [^{3}H]CHA in the presence of excess unlabelled competing ligand was described by a two-phase exponential decay to non-specific levels. The agonist CHA was able to enhance the dissociation of [^{3}H]CHA to a greater extent than the antagonist DPCPX, and this was manifest as an increase in the amplitude of the fast component of [^{3}H]CHA and not a change in the rate constants of dissociation. Using membranes prepared from the series of A_1R-GFP and A_1R-GFP-Gα_i cell lines the work presented in this chapter investigated in detail the effect of receptor expression level on agonist-induced agonist dissociation. Chapter 8 debates in greater detail possible mechanisms for the results presented in this Chapter and throughout this study. A more simple summary of the results presented in this Chapter is given below.

Detailed characterisation of the kinetics and extent of dissociation showed the mechanism by

Figure 6.6 Visual comparison of the enhancement of [^{3}H]CHA dissociation from A_1HE, A_1R-GFP-Gα_i and A_1R-GFP membranes.

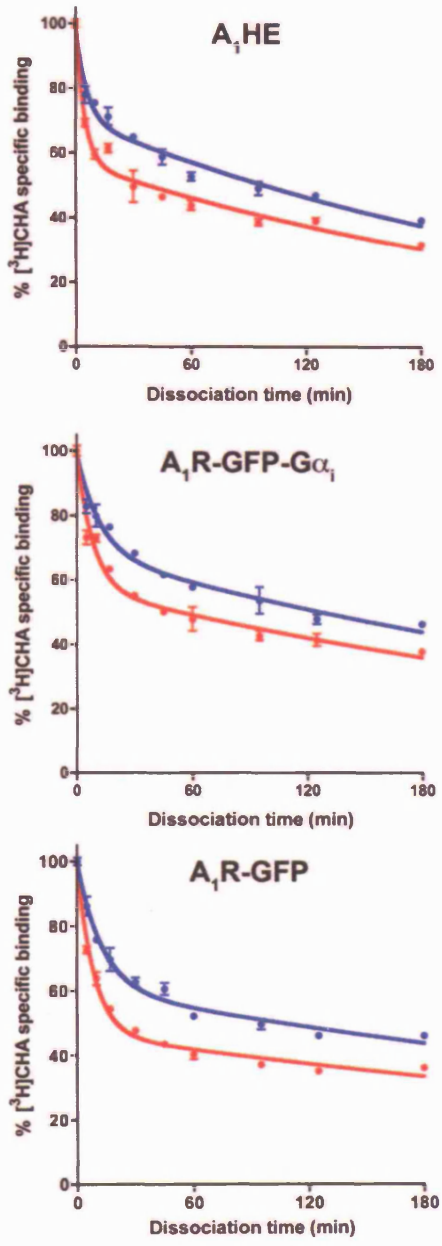

Figure 6.6: The dissociation of [^{3}H]CHA from A_1HE, A_1R-GFP-Gα_i and A_1R-GFP membranes. As usual, all three membranes were incubated for 60 min at RT in a volume of 100 μl before initiation of dissociation by addition of 2 ml buffer containing either 10^{-6} M DPCPX (●) or 10^{-4} M CHA (●). The concentrations of [^{3}H]CHA during the 60 min incubation before dissociation were 5.5, 5.0 and 5.7 nM (a, b and c respectively). The A_1R-GFP-Gα_i membranes were prepared from cell line 3F2 and A_1R-GFP from cell line 6E5 (see Table 4.3 on page 95 for details on each).

Figure 6.7 The dissociation of [^{3}H]CHA from A_1LE membranes in the presence of DPCPX or CHA chase.

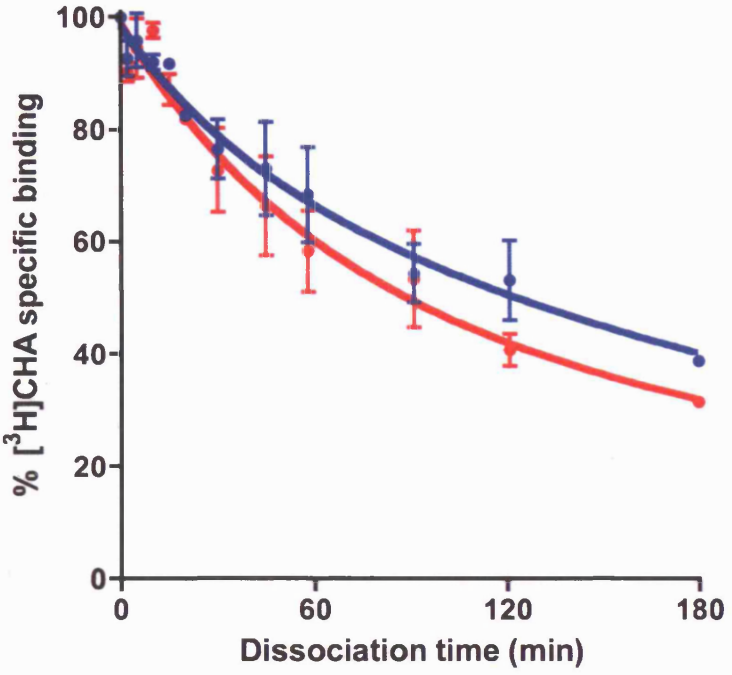

Figure 6.7: [^{3}H]CHA dissociation experiments at A_1LE membranes were performed in the same manner as described above. Membranes were incubated in a small volume (100 μl) for 60 min with [^{3}H]CHA before dilution with 2 ml buffer containing either 10^{-6} M DPCPX (●) or 10^{-4} M CHA (●). The data shown are the mean of two experiments (except 20 and 180 min where n = 1), each experiment measured in quadruplicate at all time points. The mean concentration of [^{3}H]CHA before dilution was 5.4 ± 0.1 nM (n = 2). The curves shown are non-linear regression using a two-phase model of exponential decay constrained to a plateau of non-specific binding.

which DPCPX enhances the dissociation of [^{3}H]CHA from the adenosine A_1 receptor is almost entirely independent of the level of receptor expression (Figure 6.2 and Table 6.1). The lack of any notable dependence on receptor density may favour a more "passive" mechanism by which DPCPX enhances the dissociation of [^{3}H]CHA. DPCPX binds at the adenosine A_1 receptor after [^{3}H]CHA has dissociated and so prevents the re-association of [^{3}H]CHA. The ability of DPCPX to enhance the dissociation of [^{3}H]CHA relative to the plateau of dilution only suggests "agonist locking" encompasses a degree of dissociation and re-association of [^{3}H]CHA.

The ability of CHA to enhance the dissociation of [^{3}H]CHA to an even greater extent than DPCPX (agonist-induced agonist dissociation) was more pronounced at greater levels of receptor expression (Figure 6.4). This dependence on receptor expression level was clearly significant at all dissociation time points investigated (Table 6.2). Agonist-induced agonist dissociation was confirmed as a mechanism manifest as an increase in the amplitude of the fast component of dissociation and not a change in either of the rate constants of dissociation (Table 6.4b on page 176). This is the property of the adenosine A_1 receptor's response to the binding of CHA which is dependent on the level of receptor expression. Although linear regression is used here to determine the relationship, the nature of this dependence is not known. Indeed one might expect the relationship to be dependent on $[R]^2$ if receptor dimers are being formed. This is discussed further in Chapter 8.

In summary, the work presented in this Chapter shows the extent of agonist-induced agonist dissociation at the human adenosine A_1 receptor is dependent on the level of receptor expression. This implies that the response of the A_1 receptor to the binding of agonist is different at different levels of receptor density. At greater levels of receptor expression there appears to be communication between high affinity agonist binding sites. Conceivably this may be conveyed between receptors by direct receptor-receptor interaction, possibly by receptor dimers, or by other components of the receptor signalling complex. These ideas are discussed further in Chapter 8.

Chapter 7

The localisation of the human adenosine A_1 receptor and its GFP fusion constructs in cell membrane fractions separated by their buoyant density.

7.1 Introduction.

The results presented in Chapters 5 and 6 provide evidence for receptor-receptor communication between high affinity agonist binding sites at the human adenosine A_1 receptor. Agonist stimulation of the adenosine A_1 receptor has been shown to stimulate the accumulation of the receptor into cell membrane "raft" domains characterised by their elevated level of the protein caveolin (Escriche *et al.* 2003 and Gines *et al.* 2001). Selective localisation of proteins in and out of cell membrane domains has the potential to alter the repertoire of proteins available for interaction and a change in the local receptor density may influence aspects of receptor behaviour. The aim of the work presented in this Chapter was to establish whether the human adenosine A_1 receptor membrane preparations used throughout this study were selectively localised in or out of "raft" domains.

Cell membrane "raft" domains are typically isolated by means of a density gradient formed by

high speed centrifugation of a solution of sucrose or a similar compound such as iodixanol. In this study iodixanol was chosen as the density gradient medium due to the number of published reports of its use including density gradient fractionation of CHO cell membranes (Abrami *et al.* 2001, Abrami *et al.* 2003, Frenzel & Falls 2001). The viscosity of solutions of iodixanol is lower than that of sucrose and the required density range of iodixanol gradients is also lower than for sucrose. Consequently iodixanol gradients are typically smaller in volume, show lower viscosity and thus require centrifugation for shorter periods of time. Smaller gradient volumes are important as they increase the likelihood of obtaining a clear Western blot directly from the gradient fraction without manipulations to increase the protein concentration. The systematic name for iodixanol is 5,5 -[(2-hydroxy-1,3-propanediyl)-bis(acetylimino)]bis-[*N*,*N* bis(2,3-dihydroxypropyl)-2,4,6-triiodo-benzenedicarboxamide] and it is essentially a dimer of iohexol. Iohexol is commonly employed as a radiopaque contrast agent for X-ray imaging of vascular systems within the body. The molecular structure of iodixanol and iohexol is shown in Figure 7.1 on the following page. The high density of iodixanol is the result of the substituted triiodobenzene rings which are linked to a number of hydrophilic groups.

Here, iodixanol density gradients were used to isolate membrane fractions of different density from membranes used for the radioligand binding studies presented in Chapters 4, 5 and 6. The molecular composition of these fractions were then characterised by Western blots using antibodies against A_1R, GFP, $G\alpha_i$, $G\alpha_{13}$, Fyn and caveolin. Table 2.1 on page 57 lists details of the antibodies used throughout this study.

7.2 Density gradient fractionation of membranes expressing the human adenosine A_1 receptor.

Following density gradient fractionation, as described in Chapter 2.2.7 on page 54, gradients were harvested from top (fraction 1) to bottom (fraction 7), and any remaining pellet resuspended in TNET buffer. The self-generated iodixanol gradient does not form a linear gradient, rather a profile with a shallow middle as shown in Figure 7.2 on page 187. The gradients were created by centrifugation of layers of 35% (1.2 ml), 30% (3 ml) and 5% (900 μl) iodixanol. The density profile of the harvested fractions (Figure 7.2a) generally agrees with the manufacturer's information showing a gradient generated from the centrifugation of 30% iodixanol (Figure 7.2b) although the observed densities were somewhat greater.

A_1HE and A_1LE membranes were fractionated by iodixanol density gradient fractionation and characterised by Western blots. Figure 7.3 on page 190 shows Western blots of A_1HE and

Figure 7.1 The molecular structures of iodixanol and iohexol.

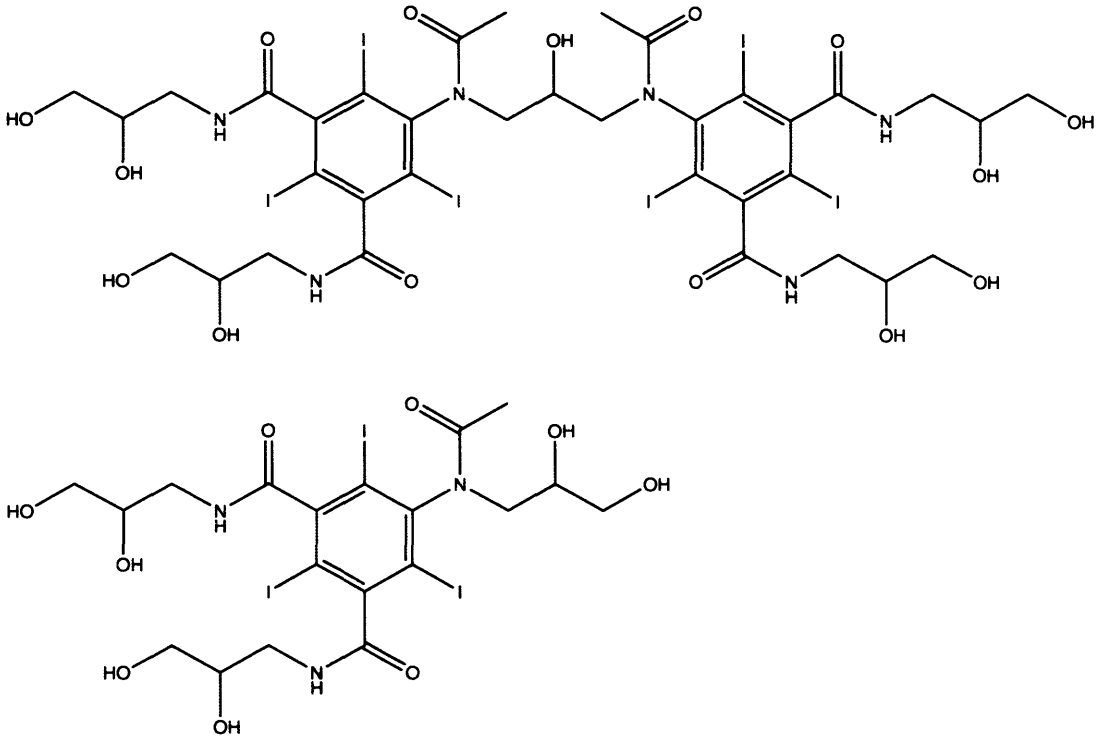

Figure 7.1: **(upper)** The molecular structure of iodixanol (molecular weight 1550) used in this study for density gradient fractionation. **(lower)** The molecular structure of iohexol (molecular weight 820) typically used as a medium to provide contrast for X-ray examination of vascular systems or body cavities.

Figure 7.2 Mean density of density gradient fractions.

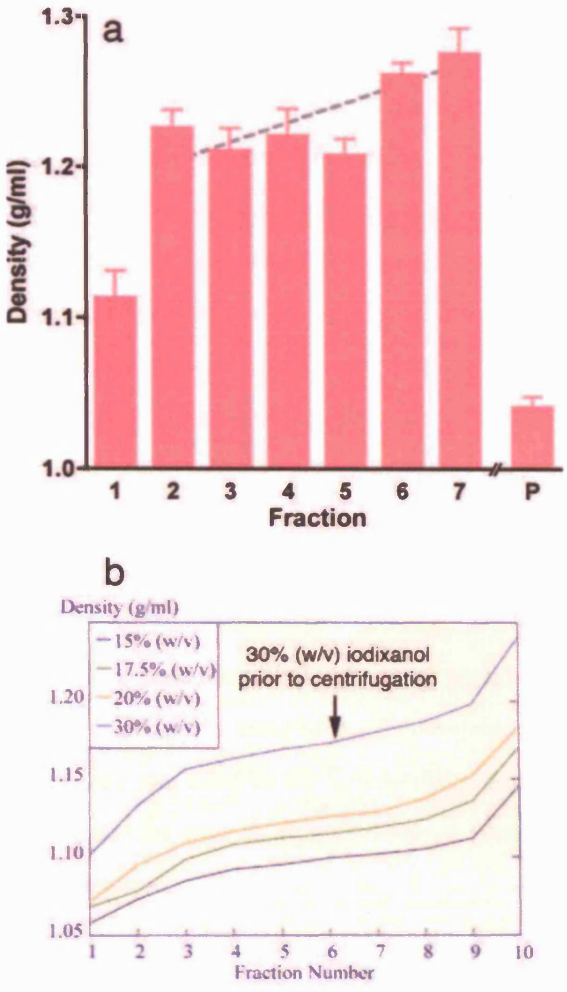

Figure 7.2: **(a)** Mean density (g/ml) of density gradient fractions (1 - 7) from A_1HE, A_1LE, A_1R-GFP and A_1R-GFP-Gα_i membrane fractionations. Data shown represents the mean density of the four different fractionations (n = 4 ± s.e.m.). The measurements of each fraction from each gradient were performed in duplicate. Samples from each fraction were diluted 1:1 twice in series in 0.85% NaCl before measurement of absorbance at 340 nm referenced against 0.85% NaCl alone. P = pellet resuspended in TNET buffer. The broken line indicates linear regression showing a significant (P = 0.007, slope = 0.01) increase in density from fraction 2 through to 7. Fraction 1 and the resuspended pellet were not included in the linear regression. **(b)** Information from the OptiPrep documentation showing self-generated iodixanol gradient formation following centrifugation at 353,000 *g* for 1 hr at 4°C. The gradient formed from 30% iodixanol is the top curve, as indicated.

A_1LE density gradient fractions using antibodies for A_1R, $G\alpha_i$, $G\alpha_{13}$ and caveolin. Caveolin is commonly employed as a marker of cell membrane domains of lower density, such as rafts. Although caveolin is found throughout the cell membrane, it is generally believed to be more concentrated in rafts (Waheed & Jones 2002). In Figure 7.3 the A_1HE gradient clearly shows an accumulation of caveolin, and by implication lipid rafts, in fractions 2 and 3. This is strong evidence for the successful isolation of caveolin-enriched lipid rafts. The A_1LE gradient in Figure 7.3 shows a less distinct distribution of caveolin throughout the gradients although fractions 3 and 4 show the greatest level of caveolin. In both the A_1HE and A_1LE gradients, longer exposure of autoradiography film identified the presence of caveolin in all fractions excluding the resuspended pellet.

Fyn (a member of the Src family of non-receptor tyrosine kinases) is also frequently employed as a marker for cell membrane raft domains, in the same manner as caveolin (see Figure 7.5 on page 191). Neither the A_1HE or A_1LE density gradients showed evidence of Fyn accumulation in any of the fractions. Figure 7.4 on page 191 shows a Western blot using an antibody for Fyn against unfractionated and fractionated A_1HE membranes. The expected Fyn band (approximately 59 kDa) is possibly faintly visible in unfractionated membranes, indicated by the red arrow, but it is not possible to identify accumulation of this band in any density gradient fractions. The molecular composition of the additional bands identified by the Fyn antibody were not investigated. Repeated attempts using altered blot conditions were unable to detect evidence of Fyn distribution across A_1HE and A_1LE density gradients.

$G\alpha_i$ exhibits a characteristic distribution across membrane density gradients. Figure 7.5 on page 191 shows a typical localisation of $G\alpha_i$ following fractionation of COS-7 cell membranes on an iodixanol density gradient (Waheed & Jones 2002). $G\alpha_i$ is observed in both "light" and "heavy" membrane fractions, with lower signals in the intermediate fractions. This can be seen in both the A_1HE and A_1LE gradients in Figure 7.3.

$G\alpha_{13}$ has been shown to not associate with lighter raft membrane fractions, for example as shown in Figure 7.5. In agreement with these observations, the A_1HE gradient fractions in Figure 7.3 show a strong localisation of $G\alpha_{13}$ in "heavy" fractions 6 and 7. Studies have shown $G\alpha_{12}$ to be localised differently from $G\alpha_{13}$, with $G\alpha_{12}$ being found in light raft membrane fractions (Figure 7.5). Western blots for $G\alpha_{12}$ of the A_1HE gradient were inconclusive, failing to show the presence of $G\alpha_{12}$ in any of the A_1HE fractions (results not shown).

The distribution of caveolin, $G\alpha_i$ and $G\alpha_{13}$ all seem to indicate that iodixanol density gradient fractionation of A_1HE and A_1LE membranes has successfully separated more dense "heavy" membrane fractions (containing $G\alpha_{13}$) from the less dense "raft" fractions (containing caveolin).

However, with uncertainty remaining over the specificity of the A_1R antibodies used in this study (shown by the presence of an A_1R-sized band in M_1R membranes in Figure 3.5 on page 71), it is not possible from Figure 7.3 alone to conclude whether the A_1R receptor is localised selectively into "light" or "heavy" domains of the cell membrane. In both the A_1HE and A_1LE gradients, the A_1R antibody identifies strong bands in fractions 6 and 7 (Figure 7.3). The A_1HE gradient shows a greater level of A_1R in the lighter fractions and especially fractions 2 and 3. Without proof of the specificity of the A_1R antibodies, it is difficult to conclude whether Figure 7.3 describes a difference in A_1R membrane localisation dependent on the level of receptor expression.

7.3 Density gradient fractionation of membranes expressing A_1R-GFP and A_1R-GFP-Gα_i fusion constructs.

The A_1R-GFP and A_1R-GFP-Gα_i fusion constructs are clearly identifiable from A_1R by their increased molecular size. With seemingly indistinguishable radioligand binding properties from the A_1R alone, it is interesting to speculate whether the localisation of the A_1R-GFP and A_1R-GFP-Gα_i fusion constructs may be similar to that of A_1R. Alternatively, if the localisation of A_1R and the fusion constructs is different, then it suggests that localisation has an insignificant influence on receptor behaviour in the conditions used in this study.

Density gradient fractionation of membranes expressing A_1R-GFP and A_1R-GFP-Gα_i fusion constructs was performed in order to investigate whether the constructs were selectively localised into components of the cell membrane. The attempts described above investigating the distribution of A_1R in membrane fractions were inconclusive due to uncertainty over the specificity of the antibodies against A_1R. Iodixanol density gradient fractionations of membranes expressing A_1R-GFP and A_1R-GFP-Gα_i constructs were performed and their molecular composition characterised by means of Western blots, shown in Figure 7.6 on page 193. Each of the blots shown in Figure 7.6 (apart from caveolin) is a separate gel and blot, rather than the same PVDF membrane stripped and re-probed with a different antibody. In both the A_1R-GFP and A_1R-GFP-Gα_i gradients caveolin shows a greater accumulation in the lighter fractions, suggesting successful fractionation. The membranes used for the fractionations shown in Figure 7.6 were 2G3 (A_1R-GFP-Gα_i) and 5F4 (A_1R-GFP) which have a [^{3}H]DPCPX B_{max} of 3.77±0.41 and 3.97±0.30 pmol/mg respectively prior to fractionation. More equilibrium binding properties are described in Table 4.3 on page 95.

The antibodies for A_1R and GFP show clearly that both fusion constructs are found predominantly in the "heavy" fractions 6 and 7, in Figure 7.6. The molecular weight of the A_1R-GFP and A_1R-GFP-Gα_i bands observed agrees with those observed in Figure 3.5. The antibody for GFP

Figure 7.3 Density gradient fractionation of A_1HE and A_1LE membranes.

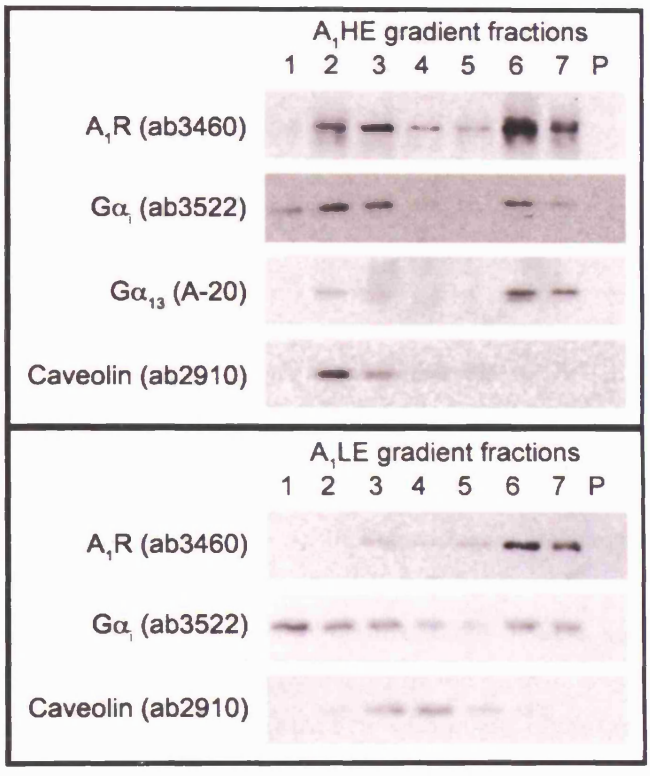

Figure 7.3: A_1HE and A_1LE membrane density gradient fractions probed for A_1R, Gα_i, Gα_{13} and the raft marker protein caveolin. Fraction 1 is the lightest, harvested first from the top of the centrifuge tube, and fraction 7 the most dense. Following removal of all the fractions, any remaining pellet (P) was resuspended in TNET buffer. The mean density of all iodixanol density gradients is shown in Figure 7.2 on page 187.

Figure 7.4 Western blot of A_1HE density gradient fractions for Fyn.

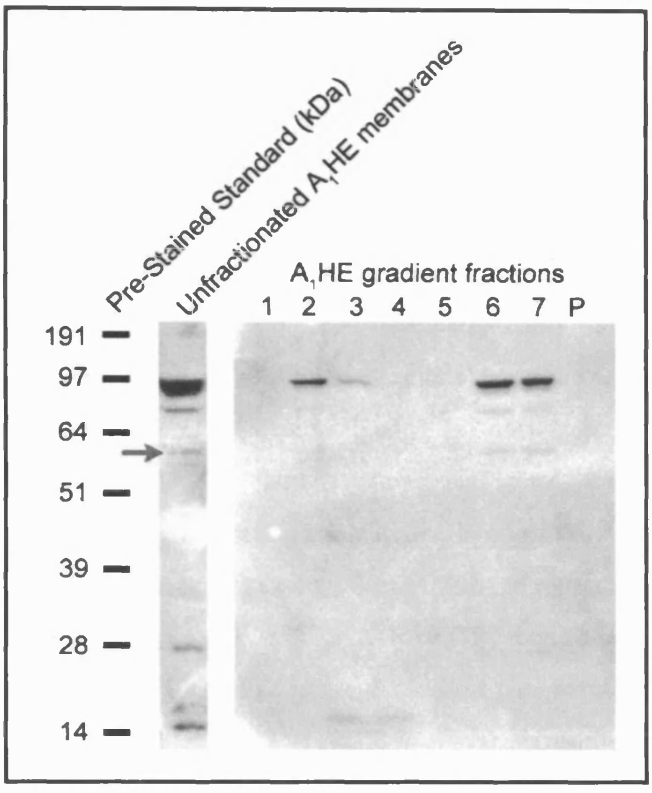

Figure 7.4: The A_1HE density gradient shown in Figure 7.3 on the preceding page was probed with an antibody for Fyn, often employed as an indicator of lighter membrane fractions along with caveolin. Fyn is expected to appear as a band of approximately 59 kDa, and is possibly present in the A_1HE membranes prior to fractionation (indicated by red arrow). However there is not strong evidence of differential localisation of the 59 kDa Fyn band in any of the gradient fractions (1 to 7) or pellet (P). The identity of the other bands identified by the Fyn antibody was not investigated.

Figure 7.5 Example of G protein and raft marker protein distribution following density gradient membrane fractionation.

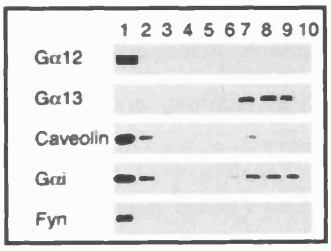

Figure 7.5: Figure showing distribution of $G\alpha_{12}$, $G\alpha_{13}$, caveolin, $G\alpha_i$ and Fyn from COS-7 cells following flotation and fractionation on an iodixanol density gradient (taken from Waheed & Jones, 2002).

detects a very faint presence of the fusion constructs in the other fractions, but these are negligible relative to the strong bands observed in fractions 6 and 7. These observations strongly indicate that in the absence of agonist treatment both the A_1R-GFP and A_1R-GFP-Gα_i fusion constructs are not concentrated into less dense domains of the cell membrane such as lipid rafts.

In Figure 7.6 endogenous human Gα_i shows the characteristic gradient distribution also observed in Figures 7.3 and 7.5. Human Gα_i is expected to show a molecular weight of approximately 40 kDa, as observed in Figure 7.6. Using the antibody for Gα_i, the A_1R-GFP-Gα_i construct appears to be identified in the same location in fractions 6 and 7 as by the antibodies for A_1R and GFP. However, the A_1R-GFP gradient also faintly shows these same "A_1R-GFP-Gα_i" bands in fractions 6 and 7, which is not expected. Western blot of the unfractionated A_1R-GFP and A_1R-GFP-Gα_i membranes using this Gα_i antibody is shown in Figure 7.7 on page 196. Figure 7.7 clearly shows the presence of a high molecular weight Gα_i band in the A_1R-GFP membranes, as observed in the A_1R-GFP gradient in Figure 7.6. What this band represents was not investigated, although it was not observed using antibodies for A_1R or GFP and therefore appears unlikely to be the A_1R-GFP-Gα_i construct. This high molecular weight Gα_i band, using antibody ab3522, was also observed in unfractionated A_1HE and A_1LE membranes (results not shown), so does not appear to be contamination of A_1R-GFP membranes or cells with A_1R-GFP-Gα_i membranes or cells especially as the A_1R and GFP antibodies do not identify the band.

These complications with the Gα_i antibody ab3522 are not particularly significant, bearing in mind that both the A_1R and GFP antibodies clearly show the fusion constructs are not present to any significant degree in "light" raft membrane fractions. Also, Chapters 4 and 6 failed to determine any effect of the tethered Gα subunit on either binding at equilibrium or the kinetics of binding.

7.4 Discussion.

The work presented in this Chapter provides novel evidence describing differential localisation of human adenosine A_1 receptor-GFP fusion proteins in domains of the cell membrane. The human adenosine A_1 receptor when covalently fused to GFP was not observed to any significant degree in cell membrane domains of low buoyant density including lipid rafts. Unfortunately direct characterisation of membranes expressing the adenosine A_1 receptor alone were inconclusive due to failure to prove the specificity of the A_1R antibodies for the A_1R alone. However, the antibodies were specific for the A_1R fusion constructs A_1R-GFP and A_1R-GFP-Gα_i due to their increased molecular size and was further supported by an antibody for GFP.

Figure 7.6 Density gradient fractionation of membranes expressing A_1R-GFP and A_1R-GFP-Gα_i fusion constructs.

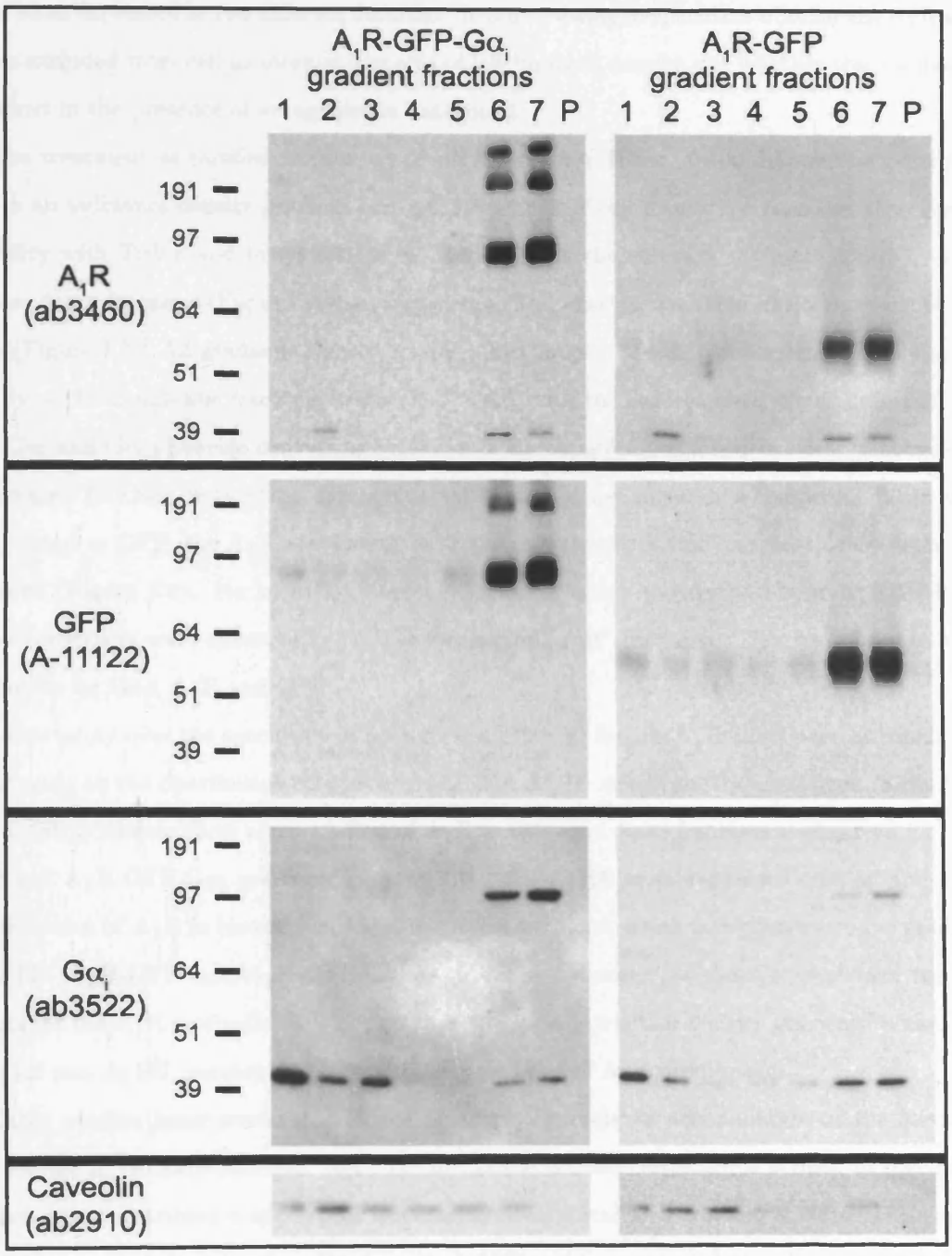

Figure 7.6: Density gradient fractionation of A_1R-GFP and A_1R-GFP-Gα_i membranes, characterised by Western blots using antibodies for A_1R, GFP, Gα_i and caveolin. As before, gradient fractions were harvested from lightest (fraction 1) to most dense (fraction 7), and any remaining pellet (P) resuspended in TNET buffer. See Figure 7.7 on page 196 for Western blot using Gα_i (ab3522) of the unfractionated A_1R-GFP and A_1R-GFP-Gα_i membranes presented in this figure.

Chapters 4 and 6 observed the binding of ligands at equilibrium and the kinetics of binding to the A_1R-GFP and A_1R-GFP-Gα_i constructs to be essentially indistinguishable from the A_1R alone when expressed at two different densities. It is interesting to speculate whether the A_1R alone is also excluded from cell membrane domains of low buoyant density and whether this localisation is altered in the presence of an agonist or antagonist.

The treatment of purified membrane preparations with Triton X-100 followed by centrifugation in an iodixanol density gradient separated fractions of cell membrane based on their level of solubility with Triton and buoyant density. Caveolin was characteristically more concentrated in the less dense fractions (Figures 7.3 and 7.6), while Gα_{13} was accumulated in the most dense fractions (Figure 7.3). All gradients showed a typical distribution of Gα_i. Measurement of the optical density of the membrane fractions (Figure 7.2) along with the characteristic distributions of caveolin, Gα_i and Gα_{13} provide convincing evidence for the separation of less dense detergent-resistant membranes (DRMs) from other detergent-soluble more dense membrane fractions. When covalently fused to GFP, the A_1R was almost entirely concentrated within the most dense membrane fractions (Figure 7.6). No appreciable accumulation of either the A_1R-GFP or A_1R-GFP-Gα_i fusion constructs were observed in the less dense "lipid raft" fractions. This was observed using antibodies for both A_1R and GFP.

Uncertainty over the specificity of both A_1R antibodies for the A_1R alone prevent conclusions being made on the distribution of A_1R in A_1LE and A_1HE membrane fractionations. Both A_1LE and A_1HE gradients show accumulation of A_1R in the same dense fractions as observed for A_1R-GFP and A_1R-GFP-Gα_i gradients (Figure 7.3). The A_1HE membrane fractionation also shows accumulation of A_1R in caveolin-enriched less dense fractions, which is in contrast to the gradients of A_1LE, A_1R-GFP and A_1R-GFP-Gα_i membranes. However, without a confirmed negative control for the A_1R antibodies it is not possible to conclude whether density gradient fractionation of A_1LE and A_1HE membranes shows different patterns of A_1R distribution.

Other studies have provided evidence of agonist stimulated accumulation of the adenosine A_1 receptor in caveolin enriched "raft" cell membrane domains although it is open to speculation whether this redistribution of receptor has functional significance or whether it is part of the mechanism of receptor internalisation (Escriche *et al.* 2003 and Gines *et al.* 2001). Unfortunately in the present study there was not sufficient time in which to investigate the effect of agonist or antagonist treatment on density gradient fractionation of A_1R-GFP and A_1R-GFP-Gα_i membranes. However the A_1R-GFP and A_1R-GFP-Gα_i gradients presented here in the absence of agonist treatment are entirely consistent with similar studies using non-fusion adenosine A_1 receptor. This provides further evidence that the A_1R-GFP and A_1R-GFP-Gα_i fusion constructs exhibit behaviour indis-

tinguishable from the adenosine A_1 receptor alone and further validates their use as models of the effect of receptor expression level.

Figure 7.7 Western blot of A_1R-GFP and A_1R-GFP-Gα_i membranes for Gα_i.

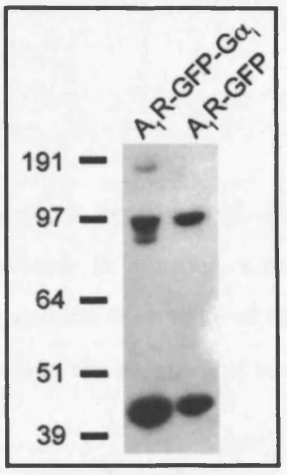

Figure 7.7: Western blot for Gα_i (ab3522) of unfractionated A_1R-GFP (2G3) and A_1R-GFP-Gα_i (5F4) membranes prior to density gradient fractionation shown in Figure 7.6 on page 193.

Chapter 8

Overall conclusions and future directions.

8.1 Summary.

In this section the findings of the previous experimental chapters are drawn together and some tentative molecular explanations provided. In addition, a number of suggestions are provided of future directions for this work. It is notable that some of the measured parameters are complex with 1:1 stoichiometries. This may reflect the presence of receptor dimers.

8.2 The effect of receptor density on equilibrium binding at the human adenosine A_1 receptor.

Membranes prepared from the A_1LE, A_1HE, A_1R-GFP and A_1R-GFP-Gα_i cell lines all showed essentially the same affinity constants for the G protein-coupled and uncoupled adenosine A_1 receptor. This consistency, especially of high affinity agonist binding at the G protein-coupled receptor, shows that the GFP of the fusion constructs does not substantially interfere with the binding of G protein to the receptor and formation of the high affinity agonist–receptor–G protein ternary complex. Also, there is little (if any) evidence that the covalently-attached Gα_i subunit binds with notable affinity to its attached receptor. The adenosine A_1 receptor of the A_1R-GFP-Gα_i fusion construct appears to bind exogenous G protein in a manner indistinguishable from the adenosine A_1 receptor expressed alone (A_1LE and A_1HE) and the A_1R-GFP construct. The kinetics of [^{3}H]CHA dissociation are essentially indistinguishable at A_1LE, A_1HE, A_1R-GFP and

A_1R-GFP-Gα_i membranes, further supporting identical binding and activation mechanisms at all the membrane types studied (the kinetics of binding are considered in more detail in Section 8.3 below).

Correspondingly the results for these different adenosine A_1 receptor membrane preparation types and fusion constructs are considered together, and it is assumed that there are common molecular explanations for the observed results.

It should be noted that all the processes involved in the interpretation of these complex results are observed in membrane preparations, and therefore occur in the absence of chemical or metabolic energy input. The only processes involved are binding events. While considering possible mechanisms it is important to realise that there may be background molecular events occurring in the membranes that are not being detected directly. These changes can be the evolution or abolition with time of molecular binding processes.

The effect of receptor density on fr_H.

In all cases the fraction of agonist binding which was of high affinity (fr_H) was less than one. From the ternary complex model, this implies the receptor is limited in the amount of G protein available with which to form high affinity agonist–receptor–G protein complexes. As the total amount of Gα_i is generally believed to be in excess of the total amount of receptor, fr_H of less than one implies there is segregation between G proteins and receptors. That is, the receptors and/or G proteins are substantially clustered away from each other and some receptors may not be in the vicinity of G protein at all. An alternative analysis may be that some receptor-G protein complexes may not have a 1:1 stoichiometry. fr_H extrapolates to between 0.7 and 0.8 at low concentrations of receptor (Figure 4.12 on page 102). This may show that 20-30% of receptors do not interact with G protein and 70-80% interact to form a complex with 1:1 (or 2:2) receptor-to-G protein stoichiometry at very low levels of receptor expression. As the level of receptor expression increases, fr_H is reduced, which may be the consequence of a change in the system to a 2:1 stoichiometry with equal proportions of high and low affinity agonist binding sites. Although a straight line is shown in Figure 4.12 to illustrate the the dependence of receptor density on fr_H, the nature of this dependence is not known and may not be linear. Figure 8.1 on page 204 plots the dependence of fr_H on log [^{3}H]DPCPX B_{max} in order to try and obtain a more even distribution of B_{max} data points. The non-linear regression curve shown was constrained to fr_H values of 0.70 and 0.35, showing the results obtained are consistent with the levelling-off of fr_H at high levels of receptor expression at values approximately 50% of those at very low levels of receptor expression. It is plausible this reduction in fr_H at high levels of receptor expression to half of that observed at very

low levels of receptor expression is the manifestation of adenosine A_1 receptor dimerisation where only one G protein is bound to each receptor dimer. Further evidence of A_1 receptor dimerisation from the kinetics of agonist binding, is discussed below.

8.3 The kinetics of agonist binding at the human adenosine A_1 receptor.

The association of [^{3}H]CHA at the adenosine A_1 receptor was biphasic and the rate constant of association of the fast component was dependent on the concentration of [^{3}H]CHA (Figures 5.5a & 5.5c on page 122). This is consistent with a simple bimolecular association at readily available high affinity agonist binding sites. Figure 4.3 (page 84) suggests there is a slow recruitment of additional G protein to form further high affinity agonist binding sites, with a rate constant of approximately 0.016 min^{-1}. By extrapolation there is a doubling of the number of high affinity agonist binding sites from $t = 0$ to $t = \infty$ in Figure 4.3. It appears a fraction of the total adenosine A_1 receptor population exists pre-coupled with G protein, and a further fraction is able to slowly form additional high affinity ternary complexes. The mechanism of this slow increase in high affinity agonist binding is unknown, and may be the result of the diffusion of additional G protein into the receptor environment or a change in the stoichiometry of agonist, receptor and G protein in high affinity complexes.

Agonist locking.

Following association for 60 min, the dissociation of [^{3}H]CHA at the adenosine A_1 receptor by 20-fold dilution was incomplete (Figure 5.6 on page 126). This pseudo-irreversible binding is termed "agonist locking." Approximately 35% of specific [^{3}H]CHA binding was reversible (Table 5.2 on page 126), and both the reversible and irreversible components were rapidly released by GTP. Sensitivity to GTP indicates both the "locked" and "unlocked" components represent agonist–receptor–G protein complexes. The relative amplitudes of the two components were not dependent on the concentration of [^{3}H]CHA used to label the receptor, suggesting this behaviour is an intrinsic property of the system and not due to labelling of more than one molecular species with slightly different affinities for [^{3}H]CHA. The observation that the off-rate of the reversible component of [^{3}H]CHA binding was dependent on the concentration of [^{3}H]CHA used to label the receptor (and therefore the concentration of [^{3}H]CHA following 20-fold dilution) may be explained by the onset of agonist-induced agonist dissociation at the higher concentrations of [^{3}H]CHA.

The phenomenon of agonist locking might be explained by the re-binding of [^{3}H]CHA following

dissociation and/or the time-dependent recruitment of additional G protein into the receptor environment. The assumption of [^{3}H]agonist re-binding implies the receptors are clustered together with a dissociated [^{3}H]agonist molecule binding to an unoccupied receptor before it can diffuse out of the membrane environment. However agonist locking is observed at membranes expressing both high and low levels of the adenosine A_1 receptor, and is not observed in the dissociation of [^{3}H]DPCPX. It is possible the receptors only cluster in the presence of agonist, or that the mode of access and exit of DPCPX from the receptor is different from that of agonists, disfavouring re-binding of [^{3}H]DPCPX.

The effect of DPCPX on the dissociation of [^{3}H]CHA.

DPCPX appears to prevent or abolish agonist locking. The ability of DPCPX to enhance the dissociation of [^{3}H]CHA from the adenosine A_1 receptor is independent of the level of receptor expression (for example see Figure 6.2 on page 168), is essentially absent during the rapid dissociation phase of [^{3}H]CHA dissociation (Figure 5.8 on page 129) and only becomes significant relative to dilution alone at longer times of 60 min or more (Table 5.3). This behaviour suggests the action of DPCPX is manifest by the prevention of [^{3}H]CHA re-binding and/or the recruitment of additional G protein, and not by the more active mechanism of agonist-induced agonist dissociation. The effect of DPCPX is of nanomolar potency, as might be expected from such an interpretation.

Agonist-induced agonist dissociation.

Unlabelled agonists rapidly enhanced the dissociation of [^{3}H]agonists, relative to that shown by DPCPX, from the adenosine A_1 receptor (for example see Figure 5.8 on page 129). This "agonist-induced agonist dissociation" is manifest as an increase in the amplitude of the fast component of [^{3}H]agonist dissociation, and possibly also the rate constant of dissociation (Tables 5.4 & 5.11, Figures 5.9, 5.11 & 5.21). The [^{3}H]CHA dissociation curves are essentially independent of the concentration of [^{3}H]CHA used to label the receptors (i.e. the initial receptor occupancy) (Figures 5.9, 5.11 & 5.13). As this agonist-induced agonist dissociation is dependent on the level of receptor expression (Figures 6.4 & 6.5) and is essentially absent at very low levels of expression (Table 6.3 & Figure 6.7), it appears as if there is communication between high affinity agonist binding sites in receptor–G protein complexes when the receptors are present at high concentrations.

It should be noted that no evidence is presented here of receptor–receptor interactions in the absence of coupled G protein, such as when the receptors were labelled with the inverse agonist [^{3}H]DPCPX. Also, all the unlabelled chase agonists examined are very potent at enhancing the dissociation of [^{3}H]agonist, relative to DPCPX chase or dilution alone, and these potencies are

comparable to those for the high affinity receptor (G protein-coupled) rather than the uncoupled receptor (see Figure 4.6 & Table 5.7). This again strongly suggests that this receptor–receptor communication occurs by means of high affinity agonist binding at receptor–G protein complexes and that receptors uncoupled to G protein do not influence agonist-induced agonist dissociation.

One possible mechanism driving agonist-induced agonist dissociation may be the the reversible formation of dimers or receptor–G protein complexes through which agonist-induced agonist dissociation is mediated through intra-oligomer interactions. These dimers may have a 2:1 stoichiometry or 1:1 stoichiometry of receptor to G protein. Agonists may modulate agonist dissociation by means of communication between the two high affinity agonist binding sites of dimeric receptor complexes. This communication may occur directly between receptors, or it may be mediated by another component of the receptor signalling complex, such as G protein.

The magnitude of agonist-induced agonist dissociation is related to the efficacy of the unlabelled chase agonist. Agonists of reduced efficacy showed a reduced ability to promote the dissociation of [^{3}H]agonist (Tables 5.6 & 5.7). This provides evidence that the transmission of binding information between the two receptors (R) is mediated by the magnitude of the efficacy induced conformational changes at the receptor that drives receptor activation. That is, the A-R*-R§-B G protein complex has communication between the binding sites for two agonist molecules, A and B, which may have the same or different efficacies and induce different conformational changes. The binding of B induces an efficacy related conformational change on the receptor molecule to which it binds and this change is transmitted to the receptor molecule that has A bound and thereby affects the dissociation of A. Equally in this description, the binding of A should affect the dissociation of B.

Agonist-induced agonist dissociation is found in the presence and absence of GTP (Figures 5.15, 5.16 & Table 5.8) indicating that the receptor–receptor interactions may be retained at least for a short time after the consequences of receptor activation. This finding holds the promise that some of these interactions may be present in whole cells.

The preliminary experiments reported in Section 5.6.6 combine the complexities associated with the [^{3}H]agonist association time courses with the complexities of [^{3}H]agonist dissociation outlined above and the effects of temperature. The initial aim was to provide the maximum "window" by which agonist-induced agonist dissociation can be detected. The largest window was detected at short incubation times and at 10-60 minutes dissociation (Figure 5.19 on page 154). The effect became attenuated with longer pre-incubation times, especially at higher temperatures but the deleterious temperature effect on binding (Figure 5.17 on page 150) may compromise this conclusion. It was also noticeable that the amplitude of the slowly dissociating component increased with pre-incubation time (Figure 5.19 on page 154), reflecting slow changes in the kinetics of the

system that are occurring during the experiment. These kinetic changes were also detected in the estimates of the rate constant of the fast dissociating component with length of pre-incubation (Figure 5.21 on page 156).

In summary, considerable qualitative and quantitative information on this complex system has been obtained. The results provide evidence of complex mechanisms by which the level of receptor activation is controlled. Further kinetic and biophysical experiments are required to elaborate the molecular details of the phenomena that have been uncovered.

8.4 Future Directions.

There are several interesting avenues along which the work presented here could be taken. Hopefully it would be relatively straightforward to continue the membrane domain fractionation experiments in order to investigate the effect of agonist or inverse agonist treatment on the distribution of receptor. Other studies have shown accumulation of the A_1 receptor in lighter membrane fractions following agonist treatment, although the functional significance of this is not known (Escriche *et al.* 2003 and Gines *et al.* 2001). It would be of interest to perform further density gradient fractionations of membranes expressing the fusion constructs at several different densities, to investigate the effect of expression level on the density gradient profile of the A_1 receptor. Without an antibody shown to be specific for the A_1 receptor alone, it is not possible to use the A_1LE and A_1HE membranes to investigate the effect of receptor expression level on the density gradient fractionation profile of the A_1 receptor. It may also be interesting to fractionate the membranes of live cells expressing the A_1 receptor, possibly also following agonist or inverse agonist treatment, to compare the distribution of the A_1 receptor in live cells and the membrane preparations used throughout this study.

Further experiments could employ techniques studying the A_1 receptor in living cells. Confocal microscopy of cells expressing the A_1-GFP fusion construct could be used to investigate general changes in receptor localisation throughout the whole cell, and may provide an interesting insight into changes in the cellular distribution of the A_1 receptor with agonist stimulation. At the other end of the scale, technologies such as fluorescence correlation spectroscopy (FCS) have begun providing insights into the behaviour of the A_1 receptor at the level of individual receptors and molecules. FCS has been used to investigate the effect of binding of the fluorescently labelled A_1 receptor antagonist XAC-BY630 on the distribution and diffusional properties of the A_1 receptor expressed in living CHO cells (Briddon *et al.* 2004). It would be extremely interesting to use these techniques, along with confocal microscopy, to investigate other labelled ligands such as

other antagonists and possibly even agonists on the diffusion, clustering, internalisation and even signalling of the A_1 receptor.

Peptides based on the proposed transmembrane helices of the adenosine A_1 receptor were synthesised, however there was insufficient time remaining to perform experiments utilising them. Studies have proposed that transmembrane helix peptides can disrupt GPCR oligomerisation, such as for the dopamine D_2 receptor (Ng *et al.* 1996). It would be interesting to investigate the effect of these peptides on agonist-induced agonist dissociation which may be mediated through direct receptor-receptor communication. Specific inhibition of agonist-induced agonist dissociation by a peptide of one of the transmembrane helices would provide compelling evidence supporting communication mediated by direct receptor-receptor interaction.

The adenosine A_1 receptor has been proposed to form oligomeric complexes with other GPCRs including the dopamine D_1 receptor (Gines *et al.* 2000), metabotropic glutamate receptor (Ciruela *et al.* 2001), and the $P2Y_1$ receptor (Yoshioka *et al.* 2001). The co-expression at high levels of one of these receptors with the adenosine A_1 receptor would enable the investigation of receptor-receptor communication within hetero-oligomeric complexes. It would be interesting to test whether an unlabelled agonist at the co-expressed receptor could induce the dissociation of [^{3}H]agonist in the same manner as A_1 receptor agonists can. Such an observation would provide credible evidence of functional implications to A_1 receptor hetero-oligomerisation.

Previous work here used the A_1LE and A_1HE cell lines to investigate the effect of receptor density on the functional properties of the adenosine A_1 receptor using a [^{35}S]GTPγS binding assay. Novel biphasic dose response curves were observed for high efficacy agonists at A_1HE membranes but not A_1LE membranes (Browning 2003, Browning *et al.* 2000c). Membranes prepared from the A_1R-GFP and A_1R-GFP-Gα_i cell lines may enable detailed characterisation of the dependence of this biphasic dose response curve on the level of receptor expression. Functional studies may be more sensitive in detecting the coupling of the A_1 receptor to the covalently attached G protein of the A_1R-GFP-Gα_i construct in the presence of pertussis toxin. The experiments presented in Chapter 4 showed no detectable high affinity agonist binding at the A_1R-GFP-Gα_i construct following incubation with pertussis toxin. Bevan *et al.* (1999) showed NECA stimulation of [^{35}S]GTPγS accumulation at the A_1R-GFP-Gα_i construct following incubation with pertussis toxin, however this was much reduced in amplitude and potency relative to [^{35}S]GTPγS binding in the absence of pertussis toxin.

Of course a high-resolution X-ray structure of the human adenosine A_1 receptor would be useful!

Figure 8.1 Speculation on the nature of the change in CHA fr_H with $[^3H]$DPCPX B_{max}.

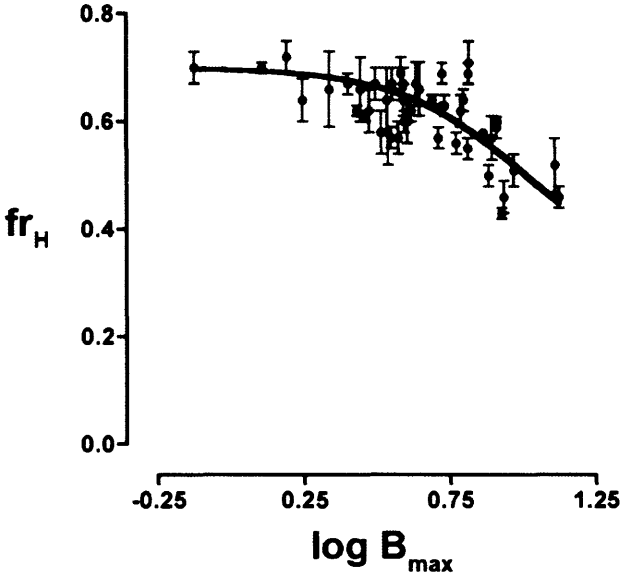

Figure 8.1: The data presented in Figure 4.12 on page 102 was transformed to illustrate the dependence of fr_H on log receptor density ($[^3H]$DPCPX B_{max}). The curve illustrated above was constrained to a maximum fr_H of 0.70 and minimum of 0.35. Data from cell line 4F2 was removed.

Chapter 9

References

AbdAlla S, Lother H and Quitterer U (2000) AT1-receptor heterodimers show enhanced G-protein activation and altered receptor sequestration. *Nature* 407:94-8.

Abrami L, Fivaz M, Kobayashi T, Kinoshita T, Parton RG and van der Goot FG (2001) Cross-talk between Caveolae and Glycosylphosphatidylinositol-rich Domains. *J. Biol. Chem.* 276:30729-30736.

Abrami L, Liu S, Cosson P, Leppla SH and van der Goot FG (2003) Anthrax toxin triggers endocytosis of its receptor via a lipid raft-mediated clathrin-dependent process. *J. Cell Biol.* 160:321-328.

Albert PR and Robillard L (2002) G protein specificity: Traffic direction required. *Cellular Signalling* 14:407-418.

Angers S, Salahpour A, Joly E, Hilairet S, Chelsky D, Dennis M and Bouvier M (2000) Detection of beta 2-adrenergic receptor dimerization in living cells using bioluminescence resonance energy transfer (BRET). *Proc. Natl. Acad. Sci. USA* 97:3684-9.

Baneres J-L, Martin A, Hullot P, Girard J-P, Rossi J-C and Parello J (2003) Structure-based Analysis of GPCR Function: Conformational Adaptation of both Agonist and Receptor upon Leukotriene B_4 Binding to Recombinant BLT1. *J. Mol. Biol.* 329:801-814.

Baneres J-L and Parello J (2003) Structure-based Analysis of GPCR Function: Evidence for a Novel Pentameric Assembly between the Dimeric Leukotriene B_4 Receptor BLT1 and the G-protein. *J. Mol. Biol.* 329:815-829.

Barrington W, Jacobson K and Stiles G (1990) Glycoprotein nature of the A_2-adenosine receptor binding subunit. *Mol. Pharmacol.* 38:177-183.

Bertin B, Freissmuth M, Jockers R, Strosberg AD and Marullo S (1994) Cellular signaling by an agonist-activated receptor/Gs alpha fusion protein. *Proc. Natl. Acad. Sci. USA* 91:8827-31.

Bevan N, Palmer T, Drmota T, Wise A, Coote J, Milligan G and Rees S (1999) Functional analysis of a human A_1 adenosine receptor/green fluorescent protein/$G_{i1}\alpha$ fusion protein following stable expression in CHO cells. *FEBS Letters* 462:61-65.

Bhattacharya S and Linden J (1995) The allosteric enhancer, PD 81,723, stabilizes human A_1 adenosine receptor coupling to G proteins. *Biochimica et Biophysica Acta* 1265:15-21.

Birdsall NJM, Burgen AS and Hulme EC (1978) The binding of agonists to brain muscarinic receptors. *Mol. Pharmacol.* 14:723-36.

Birdsall NJM and Lazareno S (2005) Allosterism at Muscarinic Receptors: Ligands and Mechanisms. *Mini-Reviews in Medicinal Chemistry* 5:525-543.

Bissantz C, Bernard P, Hibert M and Rognan D (2003) Protein-based virtual screening of chemical databases. II. Are homology models of G-Protein Coupled Receptors suitable targets? *Proteins* 50:5-25.

Block GA, Martin KJ, de Francisco ALM, Turner SA, Avram MM, Suranyi MG, Hercz G, Cunningham J, Abu-Alfa AK, Messa P, Coyne DW, Locatelli F, Cohen RM, Evenepoel P, Moe SM, Fournier A, Braun J, McCary LC, Zani VJ, Olson KA, Drueke TB and Goodman WG (2004) Cinacalcet for Secondary Hyperparathyroidism in Patients Receiving Hemodialysis. *N. Engl. J. Med.* 350:1516-1525.

Bray P, Carter A, Guo V, Puckett C, Kamholz J, Spiegel A and Nirenberg M (1987) Human cDNA Clones for an alpha Subunit of G_i Signal-Transduction Protein. *Proc. Natl. Acad. Sci. USA* 84:5115-5119.

Briddon SJ, Middleton RJ, Cordeaux Y, Flavin FM, Weinstein JA, George MW, Kellam B and Hill SJ (2004) Quantitative analysis of the formation and diffusion of A_1-adenosine receptor-antagonist complexes in single living cells. *Proc. Natl. Acad. Sci. USA* 101:4673-4678.

Browning C (2003) The Effect of Receptor Density on the Binding and Functional Properties of the Human Adenosine A_1 Receptor: PhD thesis, University College London, London.

Browning C, Beresford IJM and Birdsall NJM (2000a) Biphasic [^{35}S]GTPγS responses of human adenosine A_1 receptors expressed in CHO cell membranes. *Br. J. Pharmacol.* 131:35P.

Browning C, Beresford IJM and Birdsall NJM (2000b) The effect of guanine nucleotides and receptor density on agonist binding to human recombinant adenosine A_1 receptors. *Br. J. Pharmacol.* 129:42P.

Browning C, Beresford IJM, Sheehan MJ and Birdsall NJM (2000c) Characterisation of biphasic [^{35}S]GTPγS responses of human adenosine A_1 receptors using partial agonists and the allosteric enhancer PD81,723. *Br. J. Pharmacol.* 131:36P.

Bruns R and Fergus J (1990) Allosteric enhancement of adenosine A_1 receptor binding and function by 2-amino-3-benzoylthiophenes. *Mol. Pharmacol.* 38:939-949.

Cerione R, Sibley D, Codina J, Benovic J, Winslow J, Neer E, Birnbaumer L, Caron M and Lefkowitz R (1984) Reconstitution of a hormone-sensitive adenylate cyclase system. The pure β-adrenergic receptor and guanine nucleotide regulatory protein confer hormone responsiveness on the resolved catalytic unit. *J. Biol. Chem.* 259:9979-9982.

Chalmers DT and Behan DP (2002) The use of constitutively active GPCRs in drug discovery and functional genomics. *Nat. Rev. Drug Discov.* 1:599-608.

Cheng Y and Prusoff WH (1973) Relationship between the inhibition constant (K_1) and the concentration of inhibitor which causes 50 per cent inhibition (I_{50}) of an enzymatic reaction. *Biochem. Pharmacol.* 22:3099-108.

Christopoulos A (1998) Assessing the distribution of parameters in models of ligand-receptor interaction: to log or not to log. *Trends Pharmacol. Sci.* 19:351-357.

Christopoulos A and Kenakin T (2002) G Protein-Coupled Receptor Allosterism and Complexing. *Pharmacol. Rev.* 54:323-374.

Ciruela F, Casado V, Mallol J, Canela EI, Lluis C and Franco R (1995) Immunological identification of A_1 adenosine receptors in brain cortex. *J. Neurosci. Res.* 42:818-28.

Ciruela F, Escriche M, Burgueno J, Angulo E, Casado V, Soloviev MM, Canela EI, Mallol J, Chan W-Y, Lluis C, McIlhinney RAJ and Franco R (2001) Metabotropic Glutamate 1alpha and Adenosine A1 Receptors Assemble into Functionally Interacting Complexes. *J. Biol. Chem.* 276:18345-18351.

Cohen FR (1995) The allosteric regulation of adenosine receptors: PhD thesis, University College London, London.

Cohen FR, Lazareno S and Birdsall NJM (1996a) The affinity of adenosine for the high- and low-affinity states of the human adenosine A_1 receptor. *Eur. J. Pharmacol.* 309:111-114.

Cohen FR, Lazareno S and Birdsall NJM (1996b) The effects of saponin on the binding and functional properties of the human adenosine A_1 receptor. *Br. J. Pharmacol.* 117:1521-9.

Cordeaux Y, Briddon SJ, Megson AE, McDonnell J, Dickenson JM and Hill SJ (2000) Influence of Receptor Number on Functional Responses Elicited by Agonists Acting at the Human Adenosine A_1 Receptor: Evidence for Signaling Pathway-Dependent Changes in Agonist Potency and Relative Intrinsic Activity. *Mol. Pharmacol.* 58:1075-1084.

Cordeaux Y, IJzerman AP and Hill SJ (2004) Coupling of the human A_1 adenosine receptor to different heterotrimeric G proteins: evidence for agonist-specific G protein activation. *Br. J. Pharmacol.* 143:705-714.

Cvejic S and Devi LA (1997) Dimerization of the delta opioid receptor: implication for a role in receptor internalization. *J. Biol. Chem.* 272:26959-64.

Daumas F, Destainville N, Millot C, Lopez A, Dean D and Salome L (2003) Interprotein interactions are responsible for the confined diffusion of a G-protein-coupled receptor at the cell surface. *Biochemical Society Transactions* 31:1001-5.

De Lean A, Stadel JM and Lefkowitz RJ (1980) A ternary complex model explains the agonist-specific binding properties of the adenylate cyclase-coupled beta-adrenergic receptor. *J. Biol. Chem.* 255:7108-17.

De Vries L, Zheng B, Fischer T, Elenko E and Farquhar MG (2000) The regulator of G protein signaling family. *Annu. Rev. Pharmacol. Toxicol.* 40:235-71.

Deussen A (2000) Metabolic flux rates of adenosine in the heart. *Naunyn-Schmiedebergs Archives of Pharmacology* 362:351-63.

Elenko E, Fischer T, Niesman I, Harding T, McQuistan T, Von Zastrow M and Farquhar MG (2003) Spatial Regulation of Gαi Protein Signaling in Clathrin-Coated Membrane Microdomains Containing GAIP. *Mol. Pharmacol.* 64:11-20.

Ellis C (2004) The state of GPCR research in 2004. *Nat. Rev. Drug Discov.* 3:577-626.

Eroglu C, Brugger B, Wieland F and Sinning I (2003) Glutamate-binding affinity of Drosophila metabotropic glutamate receptor is modulated by association with lipid rafts. *Proc. Natl. Acad. Sci. USA* 100:10219-10224.

Escriche M, Burgueno J, Ciruela F, Canela EI, Mallol J, Enrich C, Lluis C and Franco R (2003) Ligand-induced caveolae-mediated internalization of A_1 adenosine receptors: morphological evidence of endosomal sorting and receptor recycling. *Exp. Cell Res.* 285:72-90.

Ferguson G, Watterson KR and Palmer TM (2000) Subtype-Specific Kinetics of Inhibitory Adenosine Receptor Internalization Are Determined by Sensitivity to Phosphorylation by G Protein-Coupled Receptor Kinases. *Mol. Pharmacol.* 57:546-552.

Ferguson SSG (2001) Evolving Concepts in G Protein-Coupled Receptor Endocytosis: The Role in Receptor Desensitization and Signaling. *Pharmacol. Rev.* 53:1-24.

Ferguson SSG, Ménard L, Barak LS, Koch WJ, Colapietro A-M and Caron MG (1995) Role of Phosphorylation in Agonist-promoted β_2-Adrenergic Receptor Sequestration. *J. Biol. Chem.* 270:24782-24789.

Finlayson K, Maemoto T, Butcher SP, Sharkey J and Olverman HJ (2003) Comparison of effects of $MgCl_2$ and Gpp(NH)p on antagonist and agonist radioligand binding to adenosine A_1 receptors. *Acta Pharmacologica Sinica* 24:729-40.

Fong CW and Milligan G (1999) Analysis of agonist function at fusion proteins between the IP prostanoid receptor and cognate, unnatural and chimaeric G-proteins. *Biochemical Journal* 342:457-63.

Fredholm BB, Battig K, Holmen J, Nehlig A and Zvartau EE (1999) Actions of Caffeine in the Brain with Special Reference to Factors That Contribute to Its Widespread Use. *Pharmacol. Rev.* 51:83-133.

Fredholm BB, Arslan G, Halldner L, Kull B, Schulte G and Wasserman W (2000) Structure and function of adenosine receptors and their genes. *Naunyn-Schmiedebergs Archives of Pharmacology* 362:364-74.

Fredholm BB, IJzerman AP, Jacobson KA, Klotz K-N and Linden J (2001) International Union of Pharmacology. XXV. Nomenclature and Classification of Adenosine Receptors. *Pharmacol. Rev.* 53:527-552.

Fredriksson R and Schioth HB (2005) The Repertoire of G-Protein-Coupled Receptors in Fully Sequenced Genomes. *Mol. Pharmacol.* 67:1414-1425.

Frenzel KE and Falls DL (2001) Neuregulin-1 proteins in rat brain and transfected cells are localized to lipid rafts. *J. Neurochem.* 77:1-12.

Fukushima Y, Asano T, Saitoh T, Anai M, Funaki M, Ogihara T, Katagiri H, Matsuhashi N, Yazaki Y and Sugano K (1997) Oligomer formation of histamine H2 receptors expressed in Sf9 and COS7 cells. *FEBS Letters* 409:283-6.

George S, Ruoho A and Malbon C (1986) N-glycosylation in expression and function of beta-adrenergic receptors. *J. Biol. Chem.* 261:16559-16564.

George SR, Fan T, Xie Z, Tse R, Tam V, Varghese G and O'Dowd BF (2000) Oligomerization of mu- and delta-opioid receptors. Generation of novel functional properties. *J. Biol. Chem.* 275:26128-35.

Gerwins P, Nordstedt C and Fredholm BB (1990) Characterization of adenosine A_1 receptors in intact DDT1 MF-2 smooth muscle cells. *Mol. Pharmacol.* 38:660-6.

Gines S, Ciruela F, Burgueno J, Casado V, Canela EI, Mallol J, Lluis C and Franco R (2001) Involvement of Caveolin in Ligand-Induced Recruitment and Internalization of A_1 Adenosine Receptor and Adenosine Deaminase in an Epithelial Cell Line. *Mol. Pharmacol.* 59:1314-1323.

Gines S, Hillion J, Torvinen M, Le Crom S, Casado V, Canela EI, Rondin S, Lew JY, Watson S, Zoli M, Agnati LF, Verniera P, Lluis C, Ferre S, Fuxe K and Franco R (2000) Dopamine D_1 and adenosine A_1 receptors form functionally interacting heteromeric complexes. *Proc. Natl. Acad. Sci. USA* 97:8606-11.

Guo W, Shi L and Javitch JA (2003) The Fourth Transmembrane Segment Forms the Interface of the Dopamine D_2 Receptor Homodimer. *J. Biol. Chem.* 278:4385-4388.

Gurevich VV, Pals-Rylaarsdam R, Benovic JL, Hosey MM and Onorato JJ (1997) Agonist-Receptor-Arrestin, an Alternative Ternary Complex with High Agonist Affinity. *J. Biol. Chem.* 272:28849-28852.

Haas HL and Selbach O (2000) Functions of neuronal adenosine receptors. *Naunyn-Schmiedebergs Archives of Pharmacology* 362:375-81.

Hamm HE (2001) How activated receptors couple to G proteins. *Proc. Natl. Acad. Sci. USA* 98:4819-4821.

Hebert TE, Moffett S, Morello JP, Loisel TP, Bichet DG, Barret C and Bouvier M (1996) A peptide derived from a beta2-adrenergic receptor transmembrane domain inhibits both receptor dimerization and activation. *J. Biol. Chem.* 271:16384-92.

Heuss C and Gerber U (2000) G-protein-independent signaling by G-protein-coupled receptors. *Trends Neurosci.* 23:469-475.

Hoffman BB, Michel T, Brenneman TB and Lefkowitz RJ (1982) Interactions of agonists with platelet alpha 2-adrenergic receptors. *Endocrinology* 110:926-32.

Hulme EC and Birdsall NJM (1992) Strategy and tactics in receptor-binding studies., in *Receptor-Ligand Interactions: A Practical Approach* (Hulme EC ed) pp 63-176, IRL Press, Oxford.

Hulme EC, Birdsall NJM and Buckley NJ (1990) Muscarinic Receptor Subtypes. *Annu. Rev. Pharmacol. Toxicol.* 30:633-673.

Hulme EC, Lu ZL and Bee MS (2003) Scanning mutagenesis studies of the M_1 muscarinic acetylcholine receptor. *Receptors & Channels* 9:215-28.

Inglese J, Koch WJ, Touhara K and Lefkowitz RJ (1995) $G\beta\gamma$ interactions with PH domains and Ras-MAPK signaling pathways. *Trends Biochem. Sci.* 20:151-156.

Jackson VN, Bahia DS and Milligan G (1999) Modulation of Relative Intrinsic Activity of Agonists at the Alpha-2A Adrenoceptor by Mutation of Residue 351 of G Protein Gilalpha. *Mol. Pharmacol.* 55:195-201.

Johansson B, Halldner L, Dunwiddie TV, Masino SA, Poelchen W, Gimenez-Llort L, Escorihuela RM, Fernandez-Teruel A, Wiesenfeld-Hallin Z, Xu X-J, Hardemark A, Betsholtz C, Herlenius E and Fredholm BB (2001) Hyperalgesia, anxiety, and decreased hypoxic neuroprotection in mice lacking the adenosine A_1 receptor. *Proc. Natl. Acad. Sci. USA* 98:9407-9412.

Jones KA, Borowsky B, Tamm JA, Craig DA, Durkin MM, Dai M, Yao WJ, Johnson M, Gunwaldsen C, Huang LY, Tang C, Shen Q, Salon JA, Morse K, Laz T, Smith KE, Nagarathnam D, Noble SA, Branchek TA and Gerald C (1998) GABA(B) receptors function as a heteromeric assembly of the subunits GABA(B)R1 and GABA(B)R2. *Nature* 396:674-9.

Jordan BA and Devi LA (1999) G-protein-coupled receptor heterodimerization modulates receptor function. *Nature* 399:697-700.

Kaupmann K, Huggel K, Heid J, Flor PJ, Bischoff S, Mickel SJ, McMaster G, Angst C, Bittiger H, Froestl W and Bettler B (1997) Expression cloning of GABA(B) receptors uncovers similarity to metabotropic glutamate receptors. *Nature* 386:239-46.

Kaupmann K, Malitschek B, Schuler V, Heid J, Froestl W, Beck P, Mosbacher J, Bischoff S, Kulik A, Shigemoto R, Karschin A and Bettler B (1998) GABA(B)-receptor subtypes assemble into functional heteromeric complexes. *Nature* 396:683-7.

Kellett E, Carr IC and Milligan G (1999) Regulation of G protein activation and effector modulation by fusion proteins between the human 5-hydroxytryptamine(1A) receptor and the alpha subunit of G(i1): differences in receptor-constitutive activity imparted by single amino acid substitutions in G(i1)alpha. *Mol. Pharmacol.* 56:684-92.

Kenakin T (1995) Agonist-receptor efficacy II: agonist trafficking of receptor signals. *Trends Pharmacol. Sci.* 16:232-238.

Kenakin T (2002) Efficacy at G-protein-coupled receptors. *Nat. Rev. Drug Discov.* 1:103-10.

Kenakin T (2003) Ligand-selective receptor conformations revisited: the promise and the problem. *Trends Pharmacol. Sci.* 24:346-354.

Kent RS, De Lean A and Lefkowitz RJ (1980) A quantitative analysis of beta-adrenergic receptor interactions: resolution of high and low affinity states of the receptor by computer modeling of ligand binding data. *Mol. Pharmacol.* 17:14-23.

Klaasse E, de Ligt RAF, Roerink SF, Lorenzen A, Milligan G, Leurs R and IJzerman AP (2004) Allosteric modulation and constitutive activity of fusion proteins between the adenosine A_1 receptor and different ^{351}Cys-mutated G_1 α-subunits. *Eur. J. Pharmacol.* 499:91-98.

Klotz KN (2000) Adenosine receptors and their ligands. *Naunyn Schmiedebergs Archives of Pharmacology* 362:382-91.

Klotz KN, Hessling J, Hegler J, Owman C, Kull B, Fredholm BB and Lohse MJ (1998) Comparative pharmacology of human adenosine receptor subtypes - characterization of stably transfected receptors in CHO cells. *Naunyn Schmiedebergs Archives of Pharmacology* 357:1-9.

Klotz KN, Keil R, Zimmer FJ and Schwabe U (1990) Guanine nucleotide effects on 8-cyclopentyl-1,3-[3H]dipropylxanthine binding to membrane-bound and solubilized A_1 adenosine receptors of rat brain. *J. Neurochem.* 54:1988-94.

Kollias-Baker C, Ruble J, Dennis D, Bruns RF, Linden J and Belardinelli L (1994) Allosteric enhancer PD 81,723 acts by novel mechanism to potentiate cardiac actions of adenosine. *Circulation Research* 75:961-71.

Krupnick JG and Benovic JL (1998) The role of receptor kinases and arrestins in G protein-coupled receptor regulation. *Annu. Rev. Pharmacol. Toxicol.* 38:289-319.

Kuner R, Kohr G, Grunewald S, Eisenhardt G, Bach A and Kornau HC (1999) Role of Heteromer Formation in GABAB Receptor Function. *Science* 283:74-77.

Kunishima N, Shimada Y, Tsuji Y, Sato T, Yamamoto M, Kumasaka T, Nakanishi S, Jingami H and Morikawa K (2000) Structural basis of glutamate recognition by a dimeric metabotropic glutamate receptor. *Nature* 407:971-7.

Lander ES, Linton LM, Birren B, Nusbaum C, Zody MC, Baldwin J, Devon K, Dewar K, Doyle M, FitzHugh W, Funke R, Gage D, Harris K, Heaford A, Howland J, Kann L, Lehoczky J, LeVine R, McEwan P, McKernan K, Meldrim J, Mesirov JP, Miranda C, Morris W, Naylor J, Raymond C, Rosetti M, Santos R, Sheridan A, Sougnez C, Stange-Thomann N, Stojanovic N, Subramanian A, Wyman D, Rogers J, Sulston J, Ainscough R, Beck S, Bentley D, Burton J, Clee C, Carter N, Coulson A, Deadman R, Deloukas P, Dunham A, Dunham I, Durbin R, French L, Grafham D, Gregory S, Hubbard T, Humphray S, Hunt A, Jones M, Lloyd C, McMurray A, Matthews L, Mercer S, Milne S, Mullikin JC, Mungall A, Plumb R, Ross M, Shownkeen R, Sims S, Waterston RH, Wilson RK, Hillier LW, McPherson JD, Marra MA, Mardis ER, Fulton LA, Chinwalla AT, Pepin KH, Gish WR, Chissoe SL, Wendl MC, Delehaunty KD, Miner TL, Delehaunty A, Kramer JB, Cook LL, Fulton RS, Johnson DL, Minx PJ, Clifton SW, Hawkins T, Branscomb E, Predki P, Richardson P, Wenning S, Slezak T, Doggett N, Cheng JF, Olsen A, Lucas S, Elkin C, Uberbacher E, Frazier M, Gibbs RA, Muzny DM, Scherer SE, Bouck JB, Sodergren EJ, Worley KC, Rives CM, Gorrell JH, Metzker ML, Naylor SL, Kucherlapati RS, Nelson DL, Weinstock GM, Sakaki Y, Fujiyama A, Hattori M, Yada T, Toyoda A, Itoh T, Kawagoe C, Watanabe H, Totoki Y, Taylor T, Weissenbach J, Heilig R, Saurin W, Artiguenave F, Brottier P, Bruls

T, Pelletier E, Robert C, Wincker P, Smith DR, Doucette-Stamm L, Rubenfield M, Weinstock K, Lee HM, Dubois J, Rosenthal A, Platzer M, Nyakatura G, Taudien S, Rump A, Yang H, Yu J, Wang J, Huang G, Gu J, Hood L, Rowen L, Madan A, Qin S, Davis RW, Federspiel NA, Abola AP, Proctor MJ, Myers RM, Schmutz J, Dickson M, Grimwood J, Cox DR, Olson MV, Kaul R, Shimizu N, Kawasaki K, Minoshima S, Evans GA, Athanasiou M, Schultz R, Roe BA, Chen F, Pan H, Ramser J, Lehrach H, Reinhardt R, McCombie WR, de la Bastide M, Dedhia N, Blocker H, Hornischer K, Nordsiek G, Agarwala R, Aravind L, Bailey JA, Bateman A, Batzoglou S, Birney E, Bork P, Brown DG, Burge CB, Cerutti L, Chen HC, Church D, Clamp M, Copley RR, Doerks T, Eddy SR, Eichler EE, Furey TS, Galagan J, Gilbert JG, Harmon C, Hayashizaki Y, Haussler D, Hermjakob H, Hokamp K, Jang W, Johnson LS, Jones TA, Kasif S, Kaspryzk A, Kennedy S, Kent WJ, Kitts P, Koonin EV, Korf I, Kulp D, Lancet D, Lowe TM, McLysaght A, Mikkelsen T, Moran JV, Mulder N, Pollara VJ, Ponting CP, Schuler G, Schultz J, Slater G, Smit AF, Stupka E, Szustakowski J, Thierry-Mieg D, Thierry-Mieg J, Wagner L, Wallis J, Wheeler R, Williams A, Wolf YI, Wolfe KH, Yang SP, Yeh RF, Collins F, Guyer MS, Peterson J, Felsenfeld A, Wetterstrand KA, Patrinos A, Morgan MJ, de Jong P, Catanese JJ, Osoegawa K, Shizuya H, Choi S, Chen YJ and International Human Genome Sequencing C (2001) Initial sequencing and analysis of the human genome. [erratum appears in Nature 2001 Aug 2;412(6846):565 Note: Szustakowki, J [corrected to Szustakowski, J]]. *Nature* 409:860-921.

Latif R, Ando T, Daniel S and Davies TF (2003) Localization and Regulation of Thyrotropin Receptors within Lipid Rafts. *Endocrinology* 144:4725-4728.

Latini S, Bordoni F, Pedata F and Corradetti R (1999) Extracellular adenosine concentrations during in vitro ischaemia in rat hippocampal slices. *Br. J. Pharmacol.* 127:729-39.

Lazareno S, Dolezal V, Popham A and Birdsall NJM (2004) Thiochrome Enhances Acetylcholine Affinity at Muscarinic M_4 Receptors: Receptor Subtype Selectivity via Cooperativity Rather than Affinity. *Mol. Pharmacol.* 65:257-266.

Lefkowitz RJ (2004) Historical review: A brief history and personal retrospective of seven-transmembrane receptors. *Trends Pharmacol. Sci.* 25:413-422.

Leid M, Schimerlik M and Murray T (1988) Characterization of agonist radioligand inter-

actions with porcine atrial A_1 adenosine receptors. *Mol. Pharmacol.* 34:334-339.

Libert F, Van Sande J, Lefort A, Czernilofsky A, Dumont JE, Vassart G, Ensinger HA and Mendla KD (1992) Cloning and functional characterization of a human A_1 adenosine receptor. *Biochemical & Biophysical Research Communications* 187:919-26.

Limbird LE (1986) Chapter 1: Historical perspective., in *Cell Surface Receptors: A Short Course on Theory and Methods* (Limbird LE ed) pp 1-21, Kluwer Academic Publishers, Lancaster.

Liu X, Liu T, Slusarski DC, Yang-Snyder J, Malbon CC, Moon RT and Wang H-y (1999) Activation of a Frizzled-2/β-adrenergic receptor chimera promotes Wnt signaling and differentiation of mouse F9 teratocarcinoma cells via Gαo and Gαt. *Proc. Natl. Acad. Sci. USA* 96:14383-14388.

Lorenzen A, Fuss M, Vogt H and Schwabe U (1993) Measurement of guanine nucleotide-binding protein activation by A_1 adenosine receptor agonists in bovine brain membranes: stimulation of guanosine-5'-O-(3-[35S]thio)triphosphate binding. *Mol. Pharmacol.* 44:115-123.

Lorenzen A, Guerra L, Vogt H and Schwabe U (1996) Interaction of full and partial agonists of the A_1 adenosine receptor with receptor/G protein complexes in rat brain membranes. *Mol. Pharmacol.* 49:915-26.

Mahan L, McVittie L, Smyk-Randall E, Nakata H, Monsma FJ, Gerfen C and Sibley D (1991) Cloning and expression of an A_1 adenosine receptor from rat brain. *Mol. Pharmacol.* 40:1-7.

Mahle C, Wiener H, Yocca F and Maayani S (1992) Allosteric interactions between the binding sites of receptor agonists and guanine nucleotides: a comparative study of the 5- hydroxytryptamine1A and adenosine A1 receptor systems in rat hippocampal membranes. *J. Pharmacol. Exp. Ther.* 263:1275-1284.

Martin SC, Russek SJ and Farb DH (1999) Molecular identification of the human GABABR2: cell surface expression and coupling to adenylyl cyclase in the absence of GABABR1. *Mol. Cell. Neurosci.* 13:180-91.

McVey M, Ramsay D, Kellett E, Rees S, Wilson S, Pope AJ and Milligan G (2001) Monitoring receptor oligomerization using time-resolved fluorescence resonance energy transfer and bioluminescence resonance energy transfer. The human delta -opioid receptor displays

constitutive oligomerization at the cell surface, which is not regulated by receptor occupancy. *J. Biol. Chem.* 276:14092-9.

Monnot C, Bihoreau C, Conchon S, Curnow KM, Corvol P and Clauser E (1996) Polar Residues in the Transmembrane Domains of the Type 1 Angiotensin II Receptor Are Required for Binding and Coupling. *J. Biol. Chem.* 271:1507-1513.

Motulsky HJ (2003) *Prism 4 statistics guide - statistical analyses for laboratory and clinical researchers.* GraphPad Software Inc, San Diego (http://www.graphpad.com).

Neubig RR and Siderovski DP (2002) Regulators of G-protein signalling as new central nervous system drug targets. *Nat. Rev. Drug Discov.* 1:187-97.

Ng GY, O'Dowd BF, Lee SP, Chung HT, Brann MR, Seeman P and George SR (1996) Dopamine D_2 receptor dimers and receptor-blocking peptides. *Biochemical & Biophysical Research Communications* 227:200-4.

Ng GY, Clark J, Coulombe N, Ethier N, Hebert TE, Sullivan R, Kargman S, Chateauneuf A, Tsukamoto N, McDonald T, Whiting P, Mezey E, Johnson MP, Liu Q, Kolakowski LF, Jr., Evans JF, Bonner TI and O'Neill GP (1999) Identification of a $GABA_B$ Receptor Subunit, gb2, Required for Functional $GABA_B$ Receptor Activity. *J. Biol. Chem.* 274:7607-7610.

Novi F, Scarselli M, Corsini GU and Maggio R (2003) An Unusual Form of the Association Binding Kinetics of N-[^{3}H]Methylscopolamine to the Split Muscarinic M_2trunk/M_2tail Receptor. *J. Pharmacol. Exp. Ther.* 305:786-795.

Palczewski K, Kumasaka T, Hori T, Behnke CA, Motoshima H, Fox BA, Le Trong I, Teller DC, Okada T, Stenkamp RE, Yamamoto M and Miyano M (2000) Crystal structure of rhodopsin: A G protein-coupled receptor. *Science* 289:739-45.

Palmer TM, Benovic JL and Stiles GL (1996) Molecular Basis for Subtype-specific Desensitization of Inhibitory Adenosine Receptors. ANALYSIS OF A CHIMERIC A_1-A_3 ADENOSINE RECEPTOR. *J. Biol. Chem.* 271:15272-15278.

Phillips W, Wong S and Cerione R (1992) Rhodopsin/transducin interactions. II. Influence of the transducin-beta gamma subunit complex on the coupling of the transducin-alpha subunit to rhodopsin. *J. Biol. Chem.* 267:17040-17046.

Pierce KL and Lefkowitz RJ (2001) Classical and new roles of β-arrestins in the regulation of G-protein-coupled receptors. *Nat. Rev. Neurosci.* 2:727-33.

Pierce KL, Premont RT and Lefkowitz RJ (2002) Seven-transmembrane receptors. *Nat. Rev. Mol. Cell Biol.* 3:639-50.

Pike LJ (2004) Lipid rafts: heterogeneity on the high seas. *Biochem. J.* 378:281-92.

Pitcher JA, Freedman NJ and Lefkowitz RJ (1998) G PROTEIN COUPLED RECEPTOR KINASES. *Annu. Rev. Biochem.* 67:653-692.

Porkka-Heiskanen T, Strecker RE, Thakkar M, Bjorkum AA, Greene RW and McCarley RW (1997) Adenosine: A Mediator of the Sleep-Inducing Effects of Prolonged Wakefulness. *Science* 276:1265-1268.

Ralevic V and Burnstock G (1998) Receptors for Purines and Pyrimidines. *Pharmacol. Rev.* 50:413-492.

Schoneberg T, Schulz A and Gudermann T (2002) The structural basis of G-protein-coupled receptor function and dysfunction in human diseases. *Rev. Physiol. Biochem. Pharmacol.* 144:143-227.

Sheehan MJ, Wilson DJ, Cousins R, Giles H (2000) Relative intrinsic efficacy of adenosine A_1 receptor agonists measured using functional and radioligand binding assays. *Br. J. Pharmacol.* 131 Suppl:34P.

Schwabe U and Trost T (1980) Characterization of adenosine receptors in rat brain by (-)[3H]N6-phenylisopropyladenosine. *Naunyn Schmiedebergs Archives of Pharmacology* 313:179-87.

Smith PK, Krohn RI, Hermanson GT, Mallia AK, Gartner FH, Provenzano MD, Fujimoto EK, Goeke NM, Olson BJ and Klenk DC (1985) Measurement of protein using bicinchoninic acid. [erratum appears in Anal Biochem 1987 May 15;163(1):279]. *Analytical Biochemistry.* 150:76-85.

Stiles G (1986) Photoaffinity cross-linked A_1 adenosine receptor-binding subunits. Homologous glycoprotein expression by different tissues. *J. Biol. Chem.* 261:10839-10843.

Stiles GL (1988) A_1 adenosine receptor-G protein coupling in bovine brain membranes: effects of guanine nucleotides, salt, and solubilization. *J. Neurochem.* 51:1592-8.

Teller DC, Okada T, Behnke CA, Palczewski K and Stenkamp RE (2001) Advances in determination of a high-resolution three-dimensional structure of rhodopsin, a model of G-protein-coupled receptors (GPCRs). *Biochemistry* 40:7761-72.

Trincavelli ML, Tuscano D, Marroni M, Falleni A, Gremigni V, Ceruti S, Abbracchio MP, Jacobson KA, Cattabeni F and Martini C (2002) A_3 Adenosine Receptors in Human Astrocytoma Cells: Agonist-Mediated Desensitization, Internalization, and Down-Regulation. *Mol. Pharmacol.* 62:1373-1384.

Tsien RY (1998) The green fluorescent protein. *Annu. Rev. Biochem.* 67:509-44.

Ukena D, Padgett WL, Hong O, Daly JW, Daly DT and Olsson RA (1987) N6-substituted 9-methyladenines: a new class of adenosine receptor antagonists. *FEBS Letters* 215:203-8.

van Koppen C and Nathanson N (1990) Site-directed mutagenesis of the M_2 muscarinic acetylcholine receptor. Analysis of the role of N-glycosylation in receptor expression and function. *J. Biol. Chem.* 265:20887-20892.

Vassilatis DK, Hohmann JG, Zeng H, Li F, Ranchalis JE, Mortrud MT, Brown A, Rodriguez SS, Weller JR, Wright AC, Bergmann JE and Gaitanaris GA (2003) The G protein-coupled receptor repertoires of human and mouse. *Proc. Natl. Acad. Sci. USA* 100:4903-4908.

Vial C, Roberts JA and Evans RJ (2004) Molecular properties of ATP-gated P_2X receptor ion channels. *Trends Pharmacol. Sci.* 25:487-493.

von Kugelgen I and Wetter A (2000) Molecular pharmacology of P_2Y-receptors. *Naunyn Schmiedebergs Archives of Pharmacology* 362:310-23.

Waheed AA and Jones TLZ (2002) Hsp90 Interactions and Acylation Target the G Protein $G\alpha_{12}$ but Not $G\alpha_{13}$ to Lipid Rafts. *J. Biol. Chem.* 277:32409-32412.

Waldhoer M, Wise A, Milligan G, Freissmuth M and Nanoff C (1999) Kinetics of Ternary Complex Formation with Fusion Proteins Composed of the A_1-Adenosine Receptor and G Protein alpha -Subunits. *J. Biol. Chem.* 274:30571-30579.

Wedegaertner PB, Wilson PT and Bourne HR (1995) Lipid Modifications of Trimeric G Proteins. *J. Biol. Chem.* 270:503-506.

Wenzel-Seifert K and Seifert R (2000) Molecular Analysis of beta 2-Adrenoceptor Coupling to G_s-, G_i-, and G_q-Proteins. *Mol. Pharmacol.* 58:954-966.

Wetherington JP and Lambert NA (2002) Differential Desensitization of Responses Mediated by Presynaptic and Postsynaptic A_1 Adenosine Receptors. *J. Neurosci.* 22:1248-1255.

White JH, Wise A, Main MJ, Green A, Fraser NJ, Disney GH, Barnes AA, Emson P, Foord SM and Marshall FH (1998) Heterodimerization is required for the formation of a functional GABA(B) receptor. *Nature* 396:679-82.

Wise A, Carr IC and Milligan G (1997) Measurement of agonist-induced guanine nucleotide turnover by the G-protein G_{i1}alpha when constrained within an $alpha_{2A}$-adrenoceptor-G_{i1}alpha fusion protein. *Biochem. J.* 325:17-21.

Wise A, Sheehan M, Rees S, Lee M and Milligan G (1999) Comparative analysis of the efficacy of A_1 adenosine receptor activation of $G_{i/o}$ alpha G proteins following coexpression of receptor and G protein and expression of A_1 adenosine receptor-$G_{i/o}$ alpha fusion proteins. *Biochemistry* 38:2272-8.

Yin D, Gavi S, Wang HY and Malbon CC (2004) Probing receptor structure/function with chimeric G protein-coupled receptors.[erratum appears in Mol. Pharmacol. 2004 Jul;66(1):198]. *Mol. Pharmacol.* 65:1323-32.

Yoshioka K, Saitoh O and Nakata H (2001) Heteromeric association creates a P_2Y-like adenosine receptor. *Proc. Natl. Acad. Sci. USA* 98:7617-7622.

Zamah AM, Delahunty M, Luttrell LM and Lefkowitz RJ (2002) Protein Kinase A-mediated Phosphorylation of the β_2-Adrenergic Receptor Regulates Its Coupling to G_s and G_i. DEMONSTRATION IN A RECONSTITUTED SYSTEM. *J. Biol. Chem.* 277:31249-31256.

Zeng FY and Wess J (1999) Identification and molecular characterization of M_3 muscarinic receptor dimers. *J. Biol. Chem.* 274:19487-97.

Zhang Z, Austin SC and Smyth EM (2001) Glycosylation of the Human Prostacyclin Receptor: Role in Ligand Binding and Signal Transduction. *Mol. Pharmacol.* 60:480-487.

Chapter 10

Acknowledgements

First and foremost I would like to thank my supervisor, Dr Nigel Birdsall, for his limitless patience, guidance, tuition, and invaluable help in the preparation of this document.

I would also like to thank Dr Ed Hulme for his informed input and experience, and lab members (past and present) Carol Curtis, Ray Leppik, Chris Browning, Mark Bee, Jan Lloyd, Chris Wilson, Alex Goodwin and Asma Baig for their help, suggestions, tuition and general friendliness throughout this project. Thanks also to Dr Sebastian Lazareno and Dr John Eccleston for their critical evaluation of my Mid-term report and their constructive suggestions. Thanks to Chris Atkins and Graham Preece for their expert help with all the FACS selection and analysis. Thanks to Rina Sorathia for experienced help when designing my Western blotting protocol. Thanks to Nigel Douglas (no longer at NIMR) for his immensely knowledgeable tuition and support with all kinds of random Linux questions. Thanks to our super-efficient and friendly head technician Karen Grover. And a huge thanks in general to everyone at NIMR who made the last three years such an educational, interesting and fun experience!

I would like to thank Prof John Kelly for his enormous help in giving me my Wellcome Trust Vacation Scholarship in the summer before my final year at university and a job for 9 months working in the Fujisawa Institute for Neuroscience Edinburgh for which he was director at the time. Without either of those positions I would not have had the opportunity of the last three years and the work presented in this thesis.

Thanks Kat for all your patience, feeding and gardening! It's your turn at thesis-writing next!

But above all I would like to express my heartfelt gratitude to my parents for their unfailing support.

My enormous gratitude to everyone contributing to the development of LyX (http://www.lyx.org). A phenomenal document processor for writing everything from single page letters to this thesis; and it's free! A donation will be on it's way once I've been paid. Huge thanks to everyone porting and developing the Mac version of LyX. Arguably the best version of all, and integrated seamlessly into Mac OS X and all the other applications used in the preparation of this document (GraphPad Prism, Microsoft Excel, Endnote, Adobe Photoshop and Acrobat Professional). Big credit should also go to Gerben Wierda's teTeX implementation for Mac OS X (http://www.rna.nl/tex.html) without which LyX would have been of no use whatsoever.

Respect to Apple Computer for developing an operating system as sweet as OS X, and thoroughly converting me to 100% OS X from an existence caught between Linux and Windows at the start of my PhD. There is no other operating system (not counting the use of VMWare which is really running two operating systems at the same time) that enables me to run all the applications I need at the same time. Whilst writing my thesis I can happily report no crashes or the slightest hint of instability of OS X or any application. It was a totally trouble-free experience especially with the joyous LyX. Thanks Apple!

Finally, some trivial properties of this document; 63607 words, 69 Figures (47 in colour), and 19 Tables.

Occurrence of the following words in this document; receptor (923), adenosine (462), agonist (446), NIMR (9), dog (4) & sheep (2).

Autumn at The National Institute for Medical Research, Mill Hill, London.